PLASTIC FLOW, PRESSURE MELTING AND OTHER MECHANISMS IN THE DEFORMATION OF ICE I

by

Paul Barnes

A dissertation submitted for the Degree of
Doctor of Philosophy in the University of Cambridge

Short Title:

Mechanisms of
Deformation in Ice I.

Gonville and Caius College,
Cambridge.

January 1968

"Hast thou entered into the treasures of the snow?"

- Job 38.22.

PREFACE

The work described in this dissertation was carried out during the period October 1963 to September 1967 in the Sub-department of Surface Physics, Cavendish Laboratory, in the University of Cambridge, under the supervision of Dr D. Tabor, F.R.S.

The experimental work, reviews, discussion and figures are, unless otherwise stated, the original work of the writer. This dissertation has not been submitted for a degree at any other university.

I wish to thank the Scientific Research Council for a maintenance grant, and the support of Professor F. P. Bowden, F.R.S., C.B.E., who accepted me into his laboratory and has always shown an interest in the work.

The success of this work owes much to the inspiration and advice of Dr Tabor. In addition, Dr G. de Q. Robin and Mr J. C. F. Walker have given much of their time in the many discussions which have proved so helpful. In the course of this work I have benefited from many other sources of discussion, data and unpublished work. For this I thank Professors J. Weertman, B. Kamb, Drs. S. Evans, J. W. Glen, J. F. Nye, G. Swinzow, P. V. Hobbs, M. Murray, E. LaChapelle, V. Schytt, Messrs R. O. Ramseier, J. Paren, and other colleagues.

I would also like to express my gratitude to the staff of the machine shop for their expert assistance and to Mrs V. Cole and Mr A. Peck for their part in the preparation of this dissertation.

David Barnes.

CONTENTS

CONTENTS (continued)

CONTENTS (continued)

CHAPTER I

INTRODUCTION

This introduction deals with the reasons for the research carried out by the author rather than the results. These are summarised in each chapter and also in the final chapters.

It has long been recognised that while ice is one of the most common of terrestial materials, it is also one of the most unusual. Its peculiarities not only exist at the more widely appreciated macroscopic level, but also extend to such microscopic features as its hydrogen bonding and nature of crystal defects. Explaining these qualities presents problems which have occupied the minds of eminent scientists for over a hundred years. Against this background it usually comes as a considerable surprise to discover that in some particular physical aspect, ice behaves like a "typical solid". Indeed it is in these "well behaved" fields that the study of ice may become particularly rewarding. This is because it is often the unusual properties of ice that can be used as tools for observing the more orthodox behaviour of ice. Examples of this sort of situation are evident in the study of the deformation of ice discussed in this thesis. To compare the results of this research with that of other work on ice, Chapter III has been written to present some of the unusual physical properties of ice that are relevant to this work.

Apart from being a useful medium for general research into the physics of the Solid and Liquid State, ice has a number of industrial and civil applications. The possible use of ice for water desalination and maritime airports (in the form of icebergs) is widely appreciated. Not so well known, for example, are its potentialities as an electrical semiconductor-rectifier etc. [see Runnels (292)] and as a glass or crystal polishing agent [- being used in U.S.S.R., see Belyshkin (293)].

The physical properties of ice also figure strongly in Geophysical-Glaciological studies. This is a field of great importance. One aspect is the behaviour of glaciers and polar ice sheets and their effect on the future weather. In this connection it is necessary to understand the flow laws and general physical properties of ice very close to the melting point. Again the behaviour of ice close to the melting point largely governs the movement of terrestrial ice masses. In this light it is somewhat surprising how little work has been directed towards the study of ice in this temperature range.

This laboratory has a long-standing interest in the deformation, friction and adhesion of ice. In addition it has had considerable experience in the study of hardness, friction, internal friction, and the creep of solids at elevated temperatures. For these reasons a meeting was held at this laboratory on the 29th November 1963 between Professor F. P. Bowden, Dr D. Tabor, Dr G. de Q. Robin, Dr J. F. Nye, Dr W. H. Ward, and the writer, to discuss the possibilities of studying the bulk and surface flow of ice near its melting point.

The work described in this thesis makes a contribution to our understanding of the physical processes involved in the deformation and flow of ice. Some of these results, particularly those associated with melting phenomena, resolve some of the anomalies in previous research.

Apart from the purely physical aspects, this study (especially Chapters IV and V) has a bearing on the movement of glaciers at their beds. These implications are discussed more fully in Chapter VII.

CHAPTER II

A. APPARATUS

2.1 The Apparatus Requirements

To carry out the proposed study on the mechanical properties of Ice I, it was necessary to design and construct an apparatus which possessed the following features:

a. A means of producing and measuring steady horizontal velocities for constant creep rate and friction experiments. The velocity range required was from about 10^{-5} to 1 cm/sec; the lower speeds are comparable to those at which most temperate glaciers slide over their beds.

b. It was necessary to measure the horizontal forces (or stresses) required to produce this movement. The range of forces required was about 0.1 to 100 Kgs. Thus the longitudinal shear stresses present at the bed of glaciers (about ½-5 bars) can be easily achieved with this apparatus on specimens with dimensions of the order of centimetres.

c. A means of producing and measuring constant vertical forces (or stresses) of up to 500 Kgs. or more for hardness, friction and creep experiments. These large forces are required to simulate the pressures reached at the bottom of glaciers, say 500 atmospheres, over easily measurable areas (of the order of sq. cms.).

d. It was necessary to measure the vertical velocities (or strain rates) produced under the action of the above forces. The range required is a little less than that in (a).

e. A temperature range of about +5 to -15°C with a constancy and accuracy of measurement of at least $\pm$ 0.1°C was required.

This versatile apparatus is capable of providing for a wide and interesting combination of experiments. A considerable part of the research time was spent in trying to achieve the above aims. However only the essential features of the apparatus are dealt with in the following section.

2.2 The General Features of the Apparatus

The mechanical part of the apparatus was made in two sections; the first section was rigidly attached to a steel table and housed in a medium sized (4' x 4' x 7', internal dimensions) refrigerator. This section was comprised of those parts necessary for the application of stresses to the ice specimens. The second section (the main drive unit) was positioned outside the refrigerator.

To avoid rusting up of the moving parts by condensation inside the refrigerator, the first section was made mainly of brass. This section of the apparatus is similar in principle to an "Eldredge Friction apparatus" i.e. a horizontal cantilever arrangement in which the cantilever can be rotated about a vertical axis passing through the cantilever fulchrum. This section is shown in Fig.II.I. The horizontal brass "double strip" beam acts as the cantilever. It is attached near one end to the main stainless steel vertical rod (1 inch diameter) by means of two stainless steel "Hoffman" ball bearings on the sides of the central brass block. This ball bearing attachment acts as the horizontal axis fulchrum. Thus by varying the distance between the indenter (shown in Fig.II.I) and this fulchrum, and by adding weights to various parts of the brass beam, the required range of vertical forces (or load) could be easily attained. The central brass block is attached to the main vertical rod by two "Hoffman" stainless steel ball bearings. (The main vertical rod is rigidly attached to the steel table). This ball bearing assembly provides for rotation of the beam about a vertical axis coincident with the main vertical rod. The two sets of ball bearings effectively act as a universal joint for the general movement of the beam. Two separate drive units are used for the movements of the beam about these two axis. These are discussed separately.

2.3 The Vertical Movement (or Lowering) of the Beam

It is essential that the experimenter can apply the beam load from outside the refrigerator so that the temperature conditions remain undisturbed during an experiment. Therefore the car jack, which normally supported the beam,

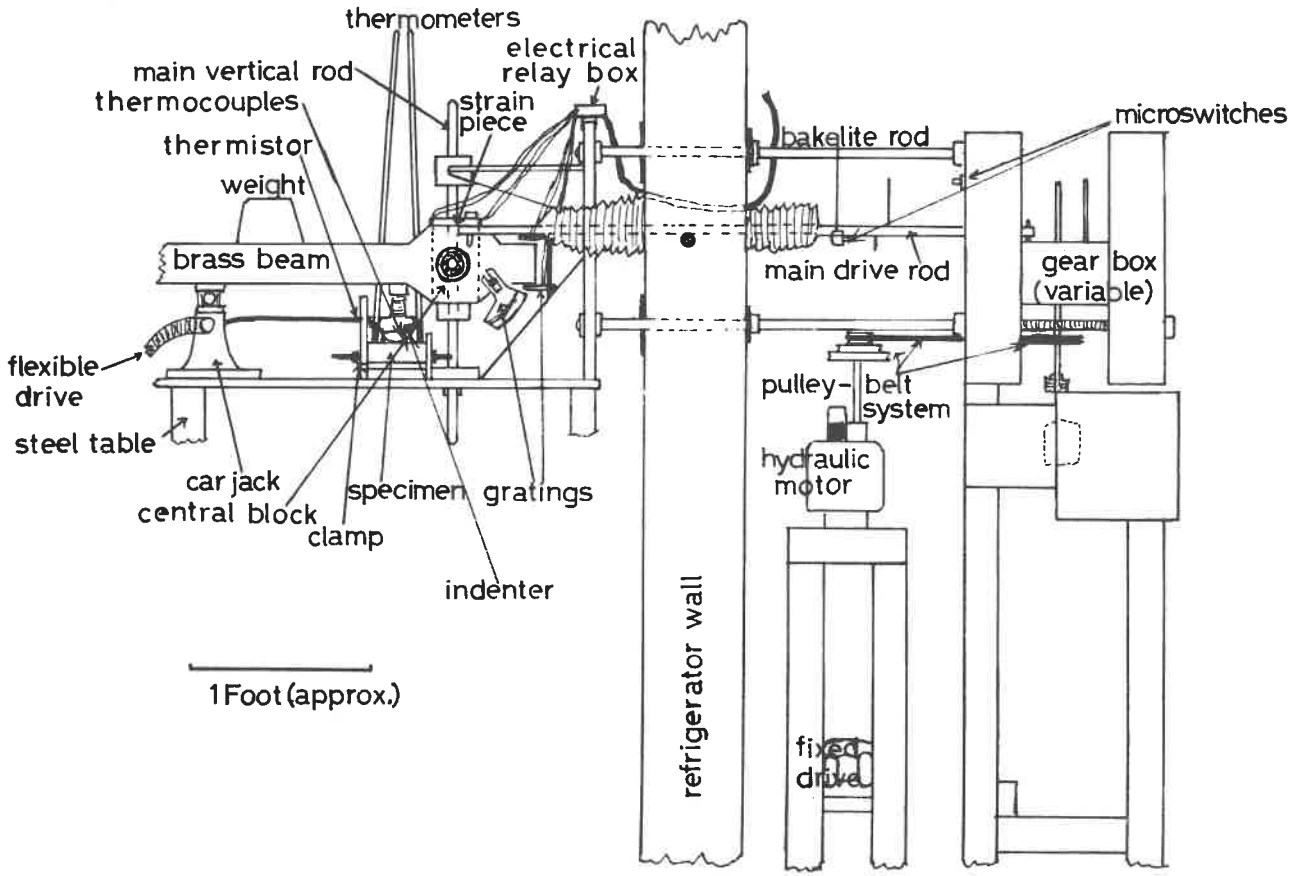

Plan for Figs. II.I and II.II.

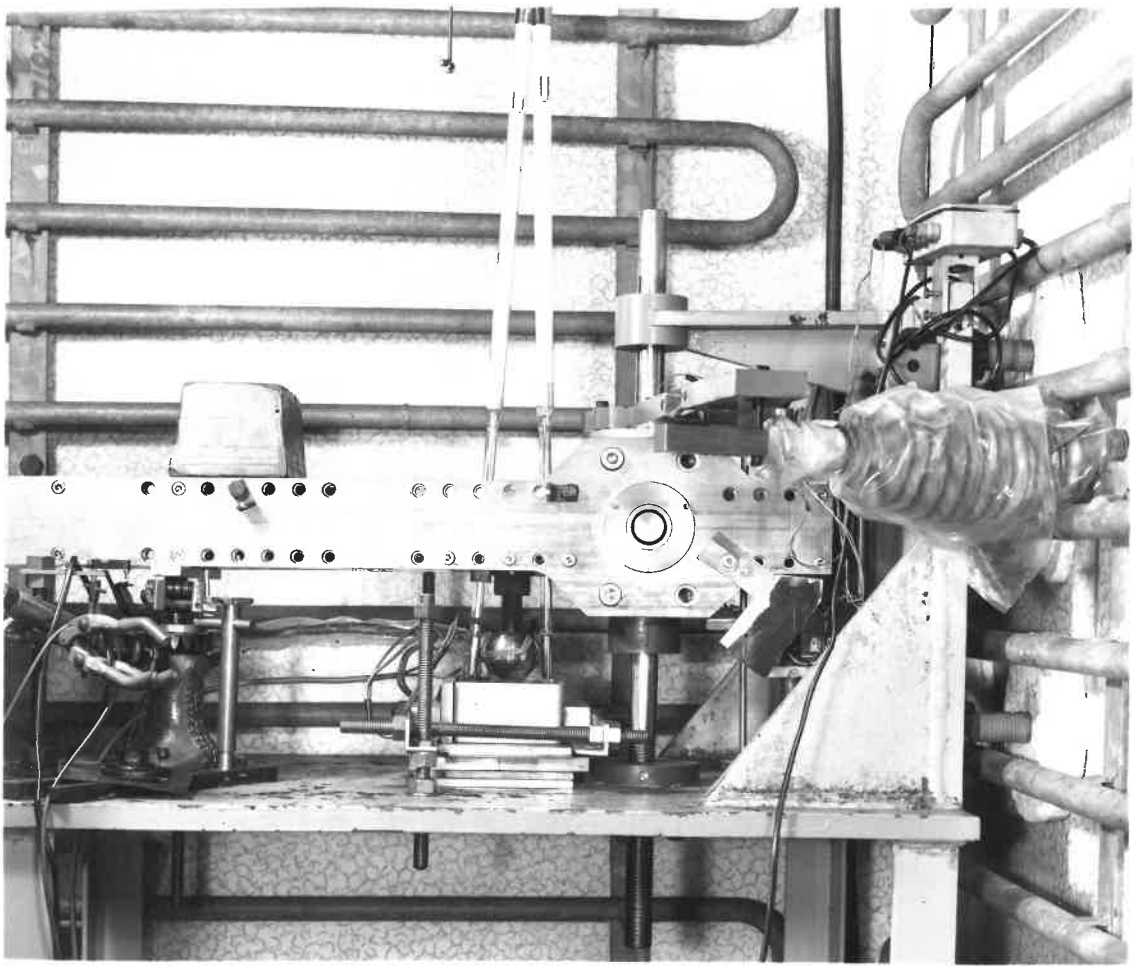

Fig. II.I Apparatus - Brass Section (Sec. 2.2)

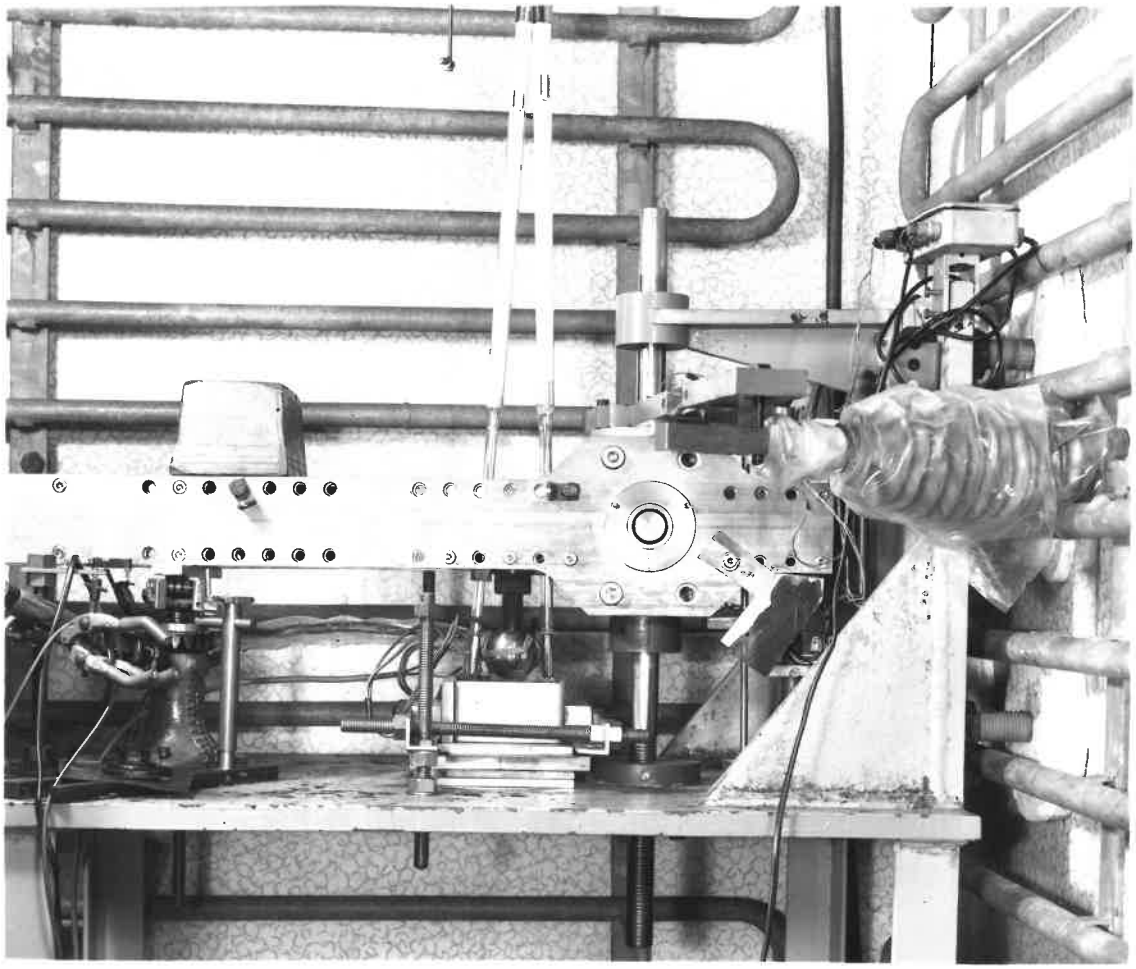

Fig. II.I Apparatus - Brass Section (Sec. 2.2)

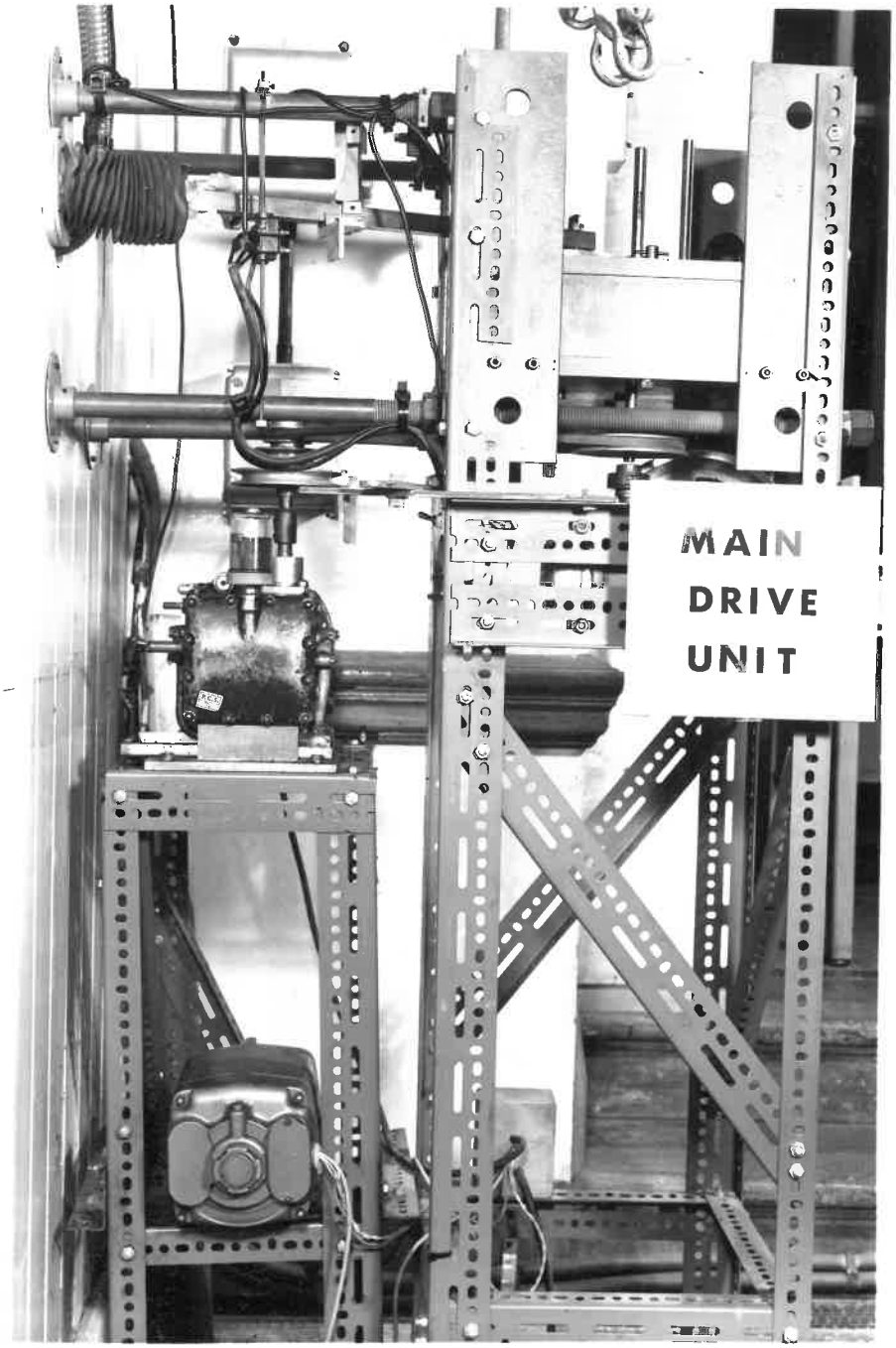

Fig. II.II Apparatus - Main Drive Unit (Sec. 2.4)

was linked to a flexible drive and this was led outside the refrigerator. In this way the beam and the indenter could be lowered onto the ice specimen at the required moment from outside the refrigerator.

The vertical movements can be measured by means of a diffraction-photocell arrangement which is described in Section 2.4. Fig.II.IV gives a typical trace obtained during a hardness test, using this technique.

2.4 The Horizontal Movement of the Beam

The main drive unit for the horizontal movement is housed outside the refrigerator Fig.II.II. It is rigidly attached to the steel table (and hence also the first section) by means of four 1 inch diameter bakelite rods passing through the refrigerator wall. The drive unit contains two gearboxes. One has a fixed (2,800:1) ratio. The other is a specially made "Class A" six speed gear box (ratios between 5 and 15,625) which delivers the output. To reduce vibration the two drive motors were housed separately and connected to the gearboxes by a system of belts and pulleys. The two motors are of the reversible type. One is a fixed speed type while the other has a continuously variable hydraulic drive. The output of the final gearbox is delivered to the brass beam by means of a 3/4" square brass rod supported over its length by ball bearings. This rod is connected (by ball bearings) to the horizontal arm on the central block. In this way, operation of the drive unit results in the rotation of the beam about the vertical axis. The indenter thus moves in a horizontal circular fashion. By using different combinations of motor speeds, pulley wheels and gearboxes, a range of "indenter speeds" of about 0.5×10^{-5} to 1 cm./sec. is obtainable.

The horizontal force (or torque) producing this motion is measured by means of a variable "strain piece" inserted in the horizontal arm. During movement the strain-piece produces a differential strain between the two resistance strain gauges cemented to its sides. The resistance strain gauges are connected electrically to two arms of an A.C. Wheatstone bridge which is housed in the electronics section in another room. With this arrangement, the balance point of the bridge is automatically compensated against temperature changes in the refrigerator. Using different strain-pieces, forces in

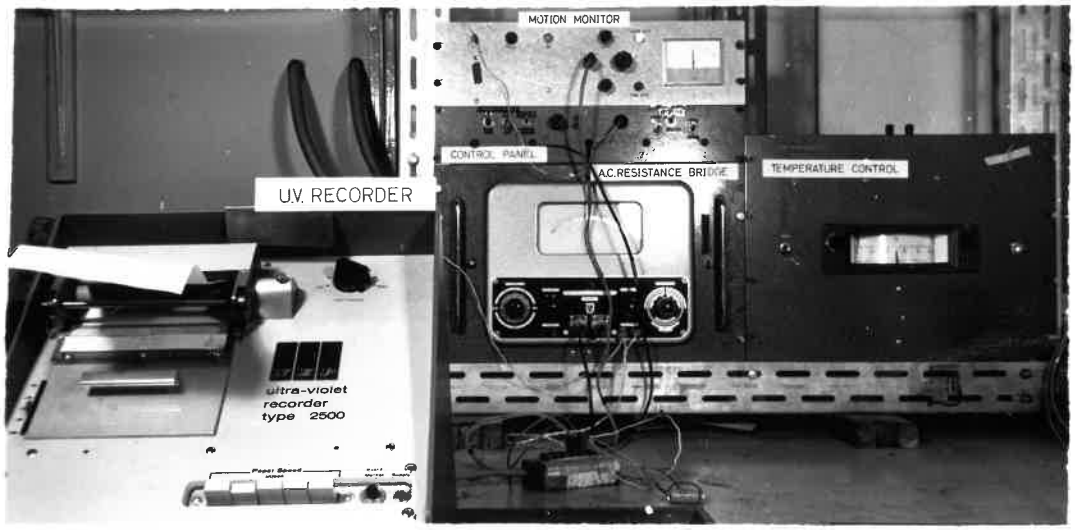

Fig. II.III Apparatus - Electronics Section (Secs. 2.3 to 2.7)

the range of about 0.05 - 200 Kgs. can be continuously measured during an experiment to an accuracy of about 2 per cent.

The speed of the indenter is accurately measured by using pairs of precision optical diffraction gratings (radial type). One grating is kept stationary while the other moves with the brass beam. The light passing through these two gratings from a suitable source, is detected by a photocell. The small electrical output is "pre-amplified" and then relayed electrically to the electronics section room where it is further amplified for continuous recording. The sinusoidal type of time variation of this output is used to determine the vertical and horizontal velocities. The accuracy of this measurement may be varied by using diffraction gratings with different resolutions. Typically, for the friction experiments; the diffraction grating resolution used was about 31 lines/inch, the speed of sliding was about 3×10^{-2} cms/sec with an accuracy of measurement of $\pm \frac{1}{2}$ per cent. This accuracy was more than adequate for these experiments. The horizontal force and sliding speed readings are recorded simultaneously on a moving strip U.V. recorder. The electronics section and U.V. recorder are shown in Fig.II.III. Typical traces obtained from the recorder are shown in Fig.II.IV and are discussed later.

It was a little difficult eliminating the mechanical resonant frequencies at the lower speeds. It was eventually achieved by choosing the correct stiffness characteristics of the driving components.

2.5 The Specimen Temperature

Temperature is one of the most important parameters in these investigations, so a considerable time was spent in temperature probe tests throughout the refrigerator. An optimum combination of controlling and working points was found. A bimetallic thermostat was placed at the optimum controlling point. This operates a three phase relay - (methyl chloride) refrigerant motor system. The specimen is always located near the optimum working point. Its temperature is measured independently by (a) a resistance thermometer located near the specimen, with thermocouple attachments to the indenter (the electrical output is relayed to the electronics section), (b) a system

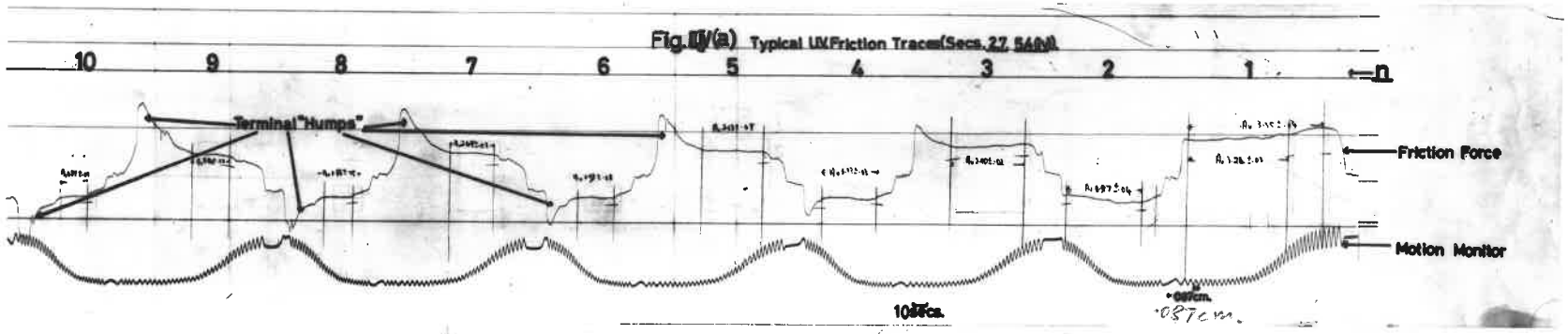

Fig. II(a) Typical UX Friction Trace (Secs. 27, 54 (a))

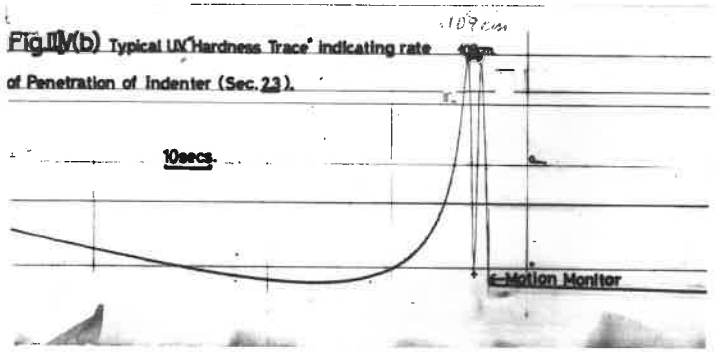

Fig. II(b) Typical UX 'Hardness Trace' indicating rate of Penetration of Indenter (Sec. 23).

of two or three "Beckmann" thermometers which are lowered onto the specimen surface (these were read from outside the refrigerator using a telescope). Using these two systems the air temperature, around a specimen, is found to have a near sinusoidal variation of about $\pm$ 0.07°C with a period of 15-30 minutes. The temperature variations in the ice specimen are less than this. About 12 hours after setting the temperature control, the temperature constancy of the specimen is about $\pm$ 0.1°C. If however the refrigerator is left to "settle down" for a day or so, the specimen temperature constancy usually approaches a value of about $\pm$ 0.03°C over several hours.

The thermometers are restandardised against the ice point after every series of experiments to within an accuracy of about $\pm$ 0.02°C. This means that the absolute accuracy of specimen temperature measurement is better than $\pm$ 0.05°C, while the relative accuracies between different experiments in one series is better still, about $\pm$ 0.03°C.

2.6 The Arrangement used for Hardness Measurements

For hardness experiments, the ice specimen is contained in a steel box and held in the table clamping system. The general arrangement is as in Fig. II. I. The loads used in hardness experiments usually lay in the range 90-140 Kgs. The accuracy of its measurement is approximately $\pm$ 3 per cent. It should be pointed out that the path traced out by the indenter during indentation of the specimen is a small arc of a circle about the ball bearing axis. However the length of this arc is < 0.3 cms., and this is very small compared to the diameter (about 35 cms.) of the circle - so for these purposes the movement of the indenter can be considered as a vertical line. A ball bearing support fixed to the car jack allows the beam to be driven in the horizontal direction while being supported by the car jack. In this way the indenter can be moved above different regions of the specimen between indentations so that three or four indentations can be made on one specimen without interrupting the experiment.

2.7 The Arrangement used for Friction Measurements

The arrangement used here is an extension of that used in the hardness measurements. After the indenter is lowered onto the specimen in the usual way, the main drive unit is switched on. The indenter then moves over the specimen. The speed of sliding is calculated from the output of the optical grating-photocell system. The horizontal force is calculated from the strain-piece-A.C. bridge-system output. Dividing the value of this force by the vertical load one obtains a value for the coefficient of friction μ of the indenter on the specimen. In order to minimise errors, the strain-piece-A.C. bridge-system is calibrated (using standard weights) after every experiment. In addition a small correction is made for the friction of the ball bearings. This is determined by removing the indenter and specimen and supporting the beam using a smooth 4" steel ball held between two steel flat plates. With the beam supported by this system (placed approximately at the position previously occupied by the indenter), the horizontal drive is activated. The "strain-piece-output" then gives a measure of the friction of the ball bearings for the same conditions of loading and temperature as in the friction experiment. It can be shown theoretically that the friction of the "large sphere and flat plates" system is negligible in this determination. The effect of this correction is to reduce the coefficient of frictions by about 15 per cent. The final "inherent accuracy" of the apparatus for measuring μ is $\pm$ 2-5 per cent.

The path of the friction track is an arc about the vertical rod axis. However the length of this arc is small (about 2 cms.) compared to the diameter (about 28 cms.) of the circle; the friction track path can therefore be considered to be a straight line.

A system of micro-switches activates the reversing mechanism of the drive motor. This enables one to perform repeated traversals over the same friction track length.

A typical continous recording of the friction force and motion data on U.V. photographic paper is shown in Fig.II.IVa Its characteristics are discussed later (Sec.5.4, (iv)).

This account concludes the description of the main apparatus. The apparatus worked extremely satisfactorily during the whole of the research project. The somewhat large dimensions of the apparatus were found to be fully justifiable in view of the results of the experiments; the recrystallisation effects described in Chapters IV and V would have been considerably smaller and possibly unnoticed had smaller dimensions been used. Furthermore because of the general robustness of the apparatus the unwanted "stick slip motion", so common with other slow speed friction apparatus, was avoided. The temperature control proved to be more than adequate in that its errors were always negligible in comparison with the other variable parameters.

The other minor apparati used in this research are described in the appropriate chapters.

B. SPECIMEN PREPARATION

2.8 Purity of Specimen

Two methods for the preparation of ice specimens were used in this work. The water used was double distilled and passed through a "Bio-deminrolit" positive and negative ion exchange column. This water was then boiled in a flask in order to get rid of the dissolved air. The flask stop was closed while still boiling. When ready for use, the water was partially frozen and the flask stop then opened for pouring.

Ionic impurities can affect the mechanical properties of ice (see Sec. 3.6, (a)). It is therefore necessary to have some idea of the electrical conductivity of the water used in these preparations. For this purpose a cell containing two-platinised-platinum-electrodes was adapted. About 1½ volts D.C. was applied across the electrodes of the cell containing the water, and the current was measured using a spot galvonometer (capable of measuring down to 1 nano-amp). Continual voltage reversal prevented hydrolysis-build-up on the electrodes.

Using this system, it was found that the water used had a conductivity of the order of 10^{-6} $(ohm.cms.)^{-1}$. However other investigations showed that these conductivities approximated to the lower limit of measurement of this conductivity-cell. Hence the water used may have had lower conductivities than this value.

However the "Frost crystals" used in Glen's method (Sec.2.9) collected impurities on the refrigerator pipes and after melting they showed increased conductivities of up to $10^{-5}(ohm.cms.)^{-1}$. The final mixture had a melted conductivity of 10^{-5} to $10^{-6}(ohm.cms.)^{-1}$.

2.9 Highly Polycrystalline Specimens

The method used here is similar to that used by Glen ((1),(2)) for his creep experiments. A cold steel (or aluminium) mould was filled with frost crystals collected from the cold refrigerator pipes. The compacted frost particles acted as randomly orientated seed crystals. The distilled water was cooled to $0^{o}C$ and allowed to percolate slowly through the frost crystals until the mould volume was almost completely occupied, and the outermost frost crystals were only just beginning to melt. In general this process was not done under vacuum as in Glen's method.

The ice produced in this way was always a little "cloudy" mainly because of the vacuum or air bubbles formed in the ice. It was found desirable, in some of the later experiments, to produce more cloudy ice with higher bubble concentrations. This was achieved by using a slightly smaller volume of water in the percolation process.

No detailed studies were made of the orientation of the grains produced in these specimens. However it is reasonable to assume that no strong preferred orientation existed since Glen did not observe any strong preferred orientation in his specimens.

The grain sizes produced by this method were 1-3 mms. Glen showed that if left for about a weeek at temperatures warmer than $-10^{o}C$, considerable grain growth could occur. Roos (3) has also shown that grain growth in thin ice sections near $0^{o}C$, can be as large as 50% in 10 hours. However in this work

the specimens were stored below - 10°C and used as soon as possible after their preparation. No measurable grain growth was observed.

The surfaces of these specimens were polished with a warm(about +10°C) smooth brass plate. At first the excess water was removed with filter papers. As the surface became smoother, colder (about +3°C.) brass plates were used. With care smooth looking surfaces could be produced.

2.10 Clear, Columnar Grained Specimens

The apparatus used here was developed during this work as a means of growing specimens with properties contrasting strongly to that of the highly polycrystalline ice. The apparatus (shown schematically in Fig.II.V) is a relatively simple one but capable of producing high quality ice specimens.

When in use, the apparatus was set up as in Fig.II.V with the top of the overflow tube level with the top of the specimen mould. Before growing the system was flushed with the pure water a few times and then filled to capacity. The heater (5-15 watts) and insulation system produced equilibrium temperature gradients indicated by the arrows. The temperature of the surrounding air was maintained at about -7°C. The coldest part of the apparatus was the top surface of the water. Hence the nucleation of the ice began by forming a thin surface layer. The output of the heaters was very slowly reduced so that the horizontal 0°C isotherm dropped slowly through the mould. Thus each successive layer of ice formed was seeded by the crystals above. As a result long columnar grains (of the type A and E) were usually formed. During growth the extra volume produced (since $\rho_{ice} < \rho_{water}$) was removed by a flow of water through the overflow tube and spilling into the reservoir. The overflow system is the novel feature of this apparatus as it avoids the build up of hydrostatic pressure during growth. Therefore strain free ice specimens were produced provided the growth was terminated before the lower ice level reached the overflow neck. The duration of growth was about 4 days. The ice specimens were removed by gentle warming of the mould, and transferred to similar moulds for further use in the main apparatus.

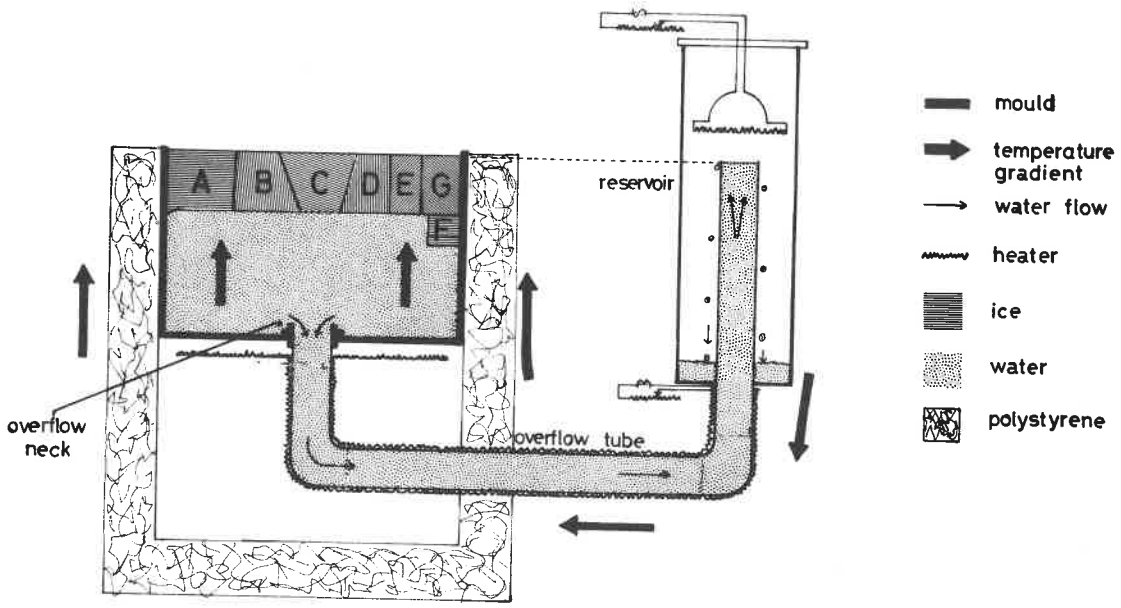

Fig. II.V Schematic Diagram of Crystal Grower (Sec. 2.10).

The specimens produced by this method measured about (11 x 9 x 5) cms. They were nearly always completely bubble free and extremely clear. In fact they were usually so clear optically after surface polishing, that when held in front of a suitable background, they were almost impossible to see. The columnar grains were usually about 1 cm. square and up to 5 cms. long - if the growth was performed very slowly, some of the grains would be larger than this (up to 4 cms. square). Sometimes certain grains (such as B and D) would grow at the expense of another (such as C). Hobbs (4) has shown that this sort of growth is governed by certain conditions of orientation of the individual grains. Nucleation and growth of grains (such as F) from the sides was rare and only possible when the temperature gradients were different from those indicated in Fig.II.V. No systematic study was made of the orientation of these grains. However it was noticed that there was a tendency for grains near the top ice surface to have their C-axis vertical; this was particularly so for the larger grains. The orientation fabric diagram for these specimens must have been very similar to those for the surface of lake ice as, for example, in (5) .

Typical grain structures for these specimens can be seen in the undisturbed regions of Figs.IV.II, V. III, and V.IV.

The procedure for surface polishing was the same as in Section 2.9.

2.11 Sectioning of Specimens

For optical examination of the ice (usually after deformation), it was necessary to section the specimens. This was done using a cold saw similar to that described by Bader (6). These sections were about 1 cm. thick. The cut regions (which were disturbed) were removed by gentle melting on a smooth brass plate. For optical observation and photography of bubble layers in ice, the optimum thickness of the sections was found to be 0.5-1 cm.

However for polarised light examination, the optimum thickness is about ½-1½ mms. This further thinning was performed in a similar fashion using a colder (about +2°C.) brass plate. The excess water was removed mainly by the use of filter papers. When the specimens became rather thin, it was found useful to remove the water by sliding the section from the brass plate on to a small

plate of 0.007" thick bakelite. With a slight bending of these plates, most of the water ran away from under the section. The sections were frozen on to perspex slides for viewing in polarised light.

Two directions of sectioning were used. The most common was vertical (perpendicular to the surface). For an indentation experiment, the vertical section was usually made through the centre of the indentation. In this way the disturbed region beneath the surface could be studied. It was sometimes found useful to cut (horizontal) sections parallel and close to the surface of the ice containing an indentation. In this way one obtained a "plan view" of the surface disturbance.

2.12 The Crossed-Polaroid Viewer

Ice has a birefringence of 0.0014. Hence the path difference between white light rays when the electric vectors point along the C axis and in the basal plane respectively, is ½-1 wavelengths for a 0.3 mm thick crystal. However there is no path difference when both electric vectors are in the basal plane (i.e. when the light ray is coincident with the C axis). This principle is used for orientation work with the Crossed-Polaroid Viewer.

The Crossed-Polaroid Viewer made for this work is shown in Fig.II.VI. By using a special gearing system, the polar and azimuthal angles of the specimen stage could be varied simultaneously by controls at the top of the instrument. Using a systematic method outlined by Bader (6), the C axis of an individual grain could be made to "optically stand up" using these controls. With the specimen in this position, the path differences for all the polarised white light rays travelling vertically up through this grain to the viewer, is zero. Hence such a grain appears black when viewed above the second polariser because these two polarisers were geared so as to remain at 90° to each other. Using this technique, the orientation of the C axes of different grains in a section could be determined. The thickness of the specimen and refraction effectslimited these determinations to those grains with C axes within about 45° of the perpendicular to the section surface. Effectively, this meas that the technique was more useful for sections parallel to the surface of the columnar grained specimens (Sec.2.10).

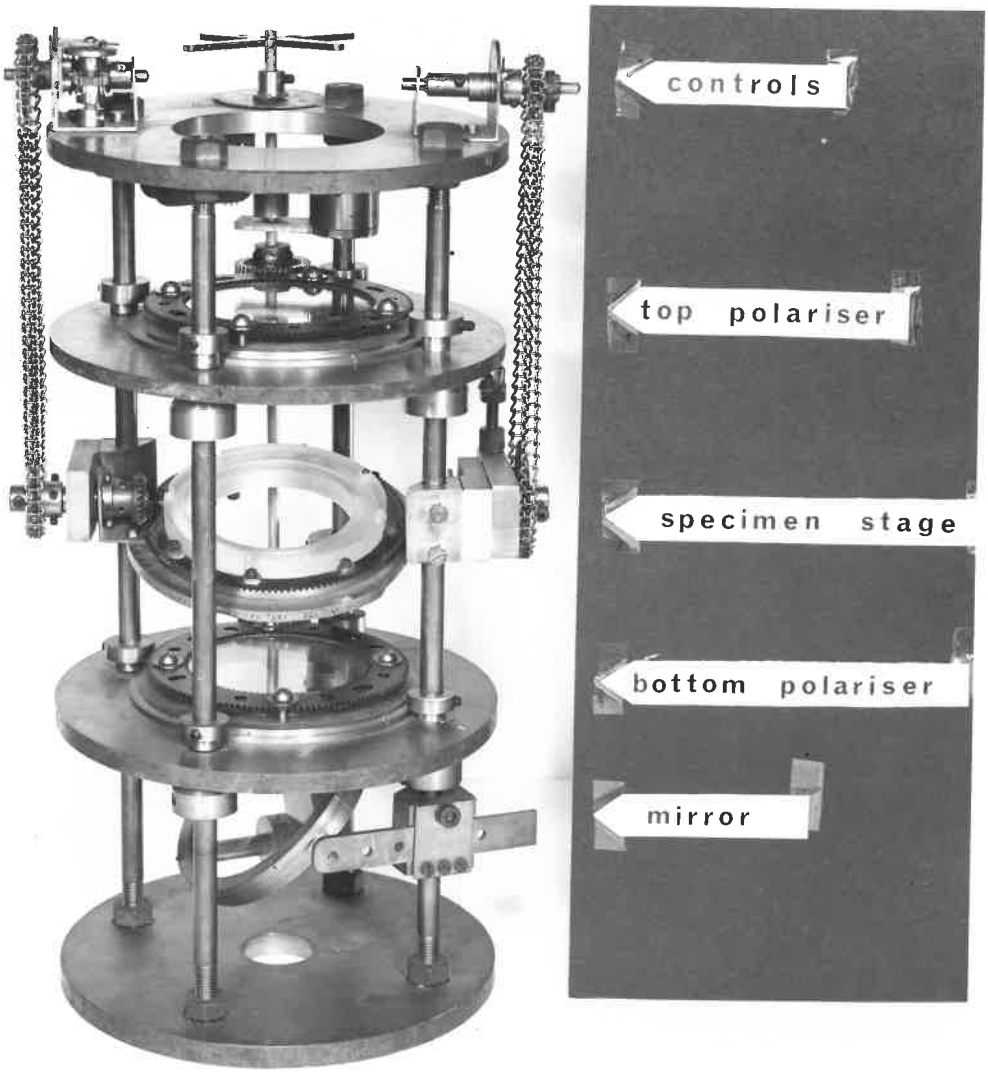

Fig. II.VI Apparatus - The Crossed Polaroid Viewer (Sec. 2.12)

By using a camera fixed above the top polariser, photographs could be taken; the various grains were revealed by their different colour responses to the white light. For this reason it was often found more revealing to use colour rather than "black and white" photographs.

Because small (less than ½ mm) recrystallised grains were common in this work, the sections had to be thinned to at least ½ mm. for clarity to be preserved.

On freezing the section to the perspex slide, the thin film of water did not always extend over the whole section. Therefore after complete freezing, the section often had a very small step running across it. Sometimes this could at first sight be mistaken for a grain boundary. It could however be easily distinguished by noting that it ran across several grains sometimes with fringe effects near its edge.

CHAPTER III

A REVIEW OF CERTAIN PHYSICAL PROPERTIES OF ICE

3.1 The Phase Diagram for Ice

Kamb (7) has determined the phase diagram for Ice and Water for a wide range of pressures and temperatures. This is an extension of the previous work by Bridgman (10) and Tamman (11) and is shown in Fig.III.I.

The low temperature cubic form (I_c) of ice (formed by vapour condensation) is formed at temperatures below about -105°C. A number of studies (for example, (8) and (9)) have been made of this form of ice, the values given for the transition temperature varying from about -80°C to -105°C. At lower temperatures still, an amorphous form of ice can be grown from the vapour.

The hydrogens are believed to occupy ordered positions in the lattice of certain phases of ice (possibly I_c, II, and VIII). This is not so with the ordinary hexagonal form of Ice I. The implications of hydrogen disorder in ordinary Ice I are discussed in Sections 3.2-3.4, 3.6.

One of the most striking features of the phase diagram of ice is the negative $\frac{dp}{dT}$ slope of the Ice I-Water phase boundary. This means (i) that water is denser than ice, and (ii) that ice can be made to melt under the application of a pressure; this effect is known as "pressure melting". The lowering of the melting point by pressure is given by:

$$\frac{\Delta T}{P} = 0.0074 \ ^{\circ}C \text{ per atmosphere at } 0^{\circ}C \qquad (3.1)$$

The phase diagram of ice shows that the Ice I, Ice III, Water triple point occurs at around -20°C. and 2 k.bars pressure. This leads to an important point viz., that pressure melting of ice cannot occur below -20°C.

In the hardness and friction experiments (described in Sections 3.4 and 3.5) the temperature range is in the region of 0°C to -14°C, and the effective pressure range is between 1-1,000 bars. Hence Ice I and Water are the only stable phases that can be present in these experiments.

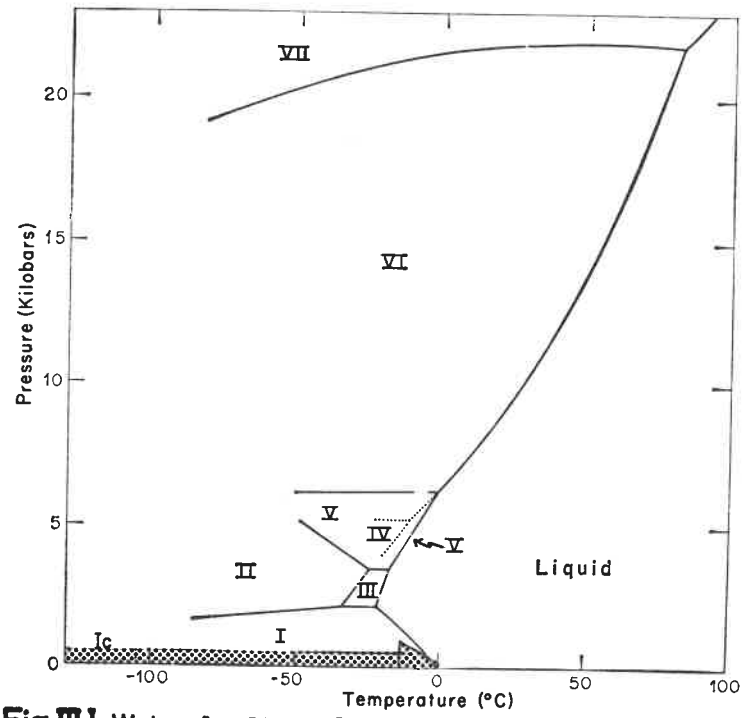

Fig.III.1 Water-Ice Phase Diagram-after Kamb (Sec. 3.1)

(▒ denotes phase space occupied by this research).

However in the rolling friction experiments (Chapter VI) the temperature range is about $0^{\circ}C$ to $-185^{\circ}C$. Here there is therefore a possibility of cubic (I_c) and amorphous ice being present. However the ice specimens were cooled from about $-10^{\circ}C$. to $-185^{\circ}C$. then warmed from $-185^{\circ}C$ to $-20^{\circ}C$ in less than half of a day. It is extremely unlikely that these two phases could be formed under these conditions.

3.2 Ice I - its Structure and Point Defects

Useful reviews of the crystal structure of Ice I have been given by Lonsdale (12) and Owston (13), (317) . We discuss here some of the more important features.

The structural arrangement of the oxygen atoms in the Ice I lattice was correctly deduced by Bragg (14) from X-ray data on ice. In this arrangement each oxygen atom is surrounded by its four nearest neighbours in a tetrahedral fashion. In Ice I this arrangement leads to a hexagonal symmetry (shown in Fig.III.II) for which the unit cell dimensions are approximately

$$\left.\begin{aligned} a &= 3.52\ \text{Å} \\ c &= 7.37\ \text{Å} \\ \text{O-O bond lengths} &= 2.76,\ 2.77\ \text{Å} \end{aligned}\right\} \text{ at } 0^{\circ}C$$

Because the X-ray scattering power of the hydrogen atoms (or protons) is so small, the location of their positions in the oxygen lattice remained uncertain for some considerable time. More recent work (for example, further X-ray work (13) and neutron diffraction studies heavy (D_2O) ice (15) confirms in general that:

(i) The hydrogen atoms occupy bond positions close to one of the oxygen atoms on the oxygen-oxygen bonds.

(ii) There is no preferred orientation of the hydrogen atoms (in contrast to Ice Ic, II, and VIII) in the lattice.

(iii) There is only one hydrogen for each oxygen-oxygen bond.

(iv) There are two hydrogens near each oxygen atom.

(v) The hydrogen atoms are continually moving about to different positions in this lattice.

We consider these points in more detail:

(i) This point was made by Bernal and Fowler (16). The O-H distance is about 1 Å compared to the O-O bond length of about 2.76 Å. The hydrogen imparts its electron to the resulting H_2O electronic structure. The resulting hydrogen then effectively becomes a proton. Sometimes in this connection the term "hydrogen atom" is used "loosely" but really meaning a proton.

(ii) This is known as Pauling's (17) disordered proton model. The specific heat determinations and resulting calculations of the zero point entropy of ice ((17)-(21)) confirm this model. If this rule were not obeyed, and provided one does not postulate an ordered-domain theory in ice such as that proposed by Eyring et al. (22) (and perhaps observed by Truby (23)), then one might expect Ice I to be piezo-electric and ferro-electric. It is therefore interesting to note that a temporary (about 5 days) piezo-electric effect has been reported (24) for freshly grown ice crystals (well-annealed crystals do not show this effect). This temporary effect may be a consequence of the ordering properties of the (moving) ice-water interface present in the original growth of the crystals from the melt (or vapour). The case for proton ordering at ice surfaces is discussed further in Section 3.4. Observations of ferroelectricity of ice at low temperatures (25) suggest that there may be appreciable proton ordering below $-170^{\circ}C$.

(iii) and (iv) are known as the Bernal-Fowler rules. The violation of these rules give rise to point defects in the ice structure.

A breach of rule (iii) produces the so-called Bjerrum defects ((26),(27)). These are commonly called the L-defect (no hydrogens on the O-O bond), and the D-defect (two hydrogen atoms on the O-O bond). These defects are illustrated in Fig.III.II.

Failure of rule (iv) produces ionic defects. An oxygen atom with three hydrogen atoms close to it is a positive ion, denoted as $(H_3O)^+$; with only one hydrogen atom is a negative ion $(OH)^-$. These defects are illustrated in Fig.III.II.

(v) The movement of the protons in the ice lattice implies that the orientations of the individual ice molecules are continually changing. This effect can be seen in the polarization response of the ice molecules to an applied

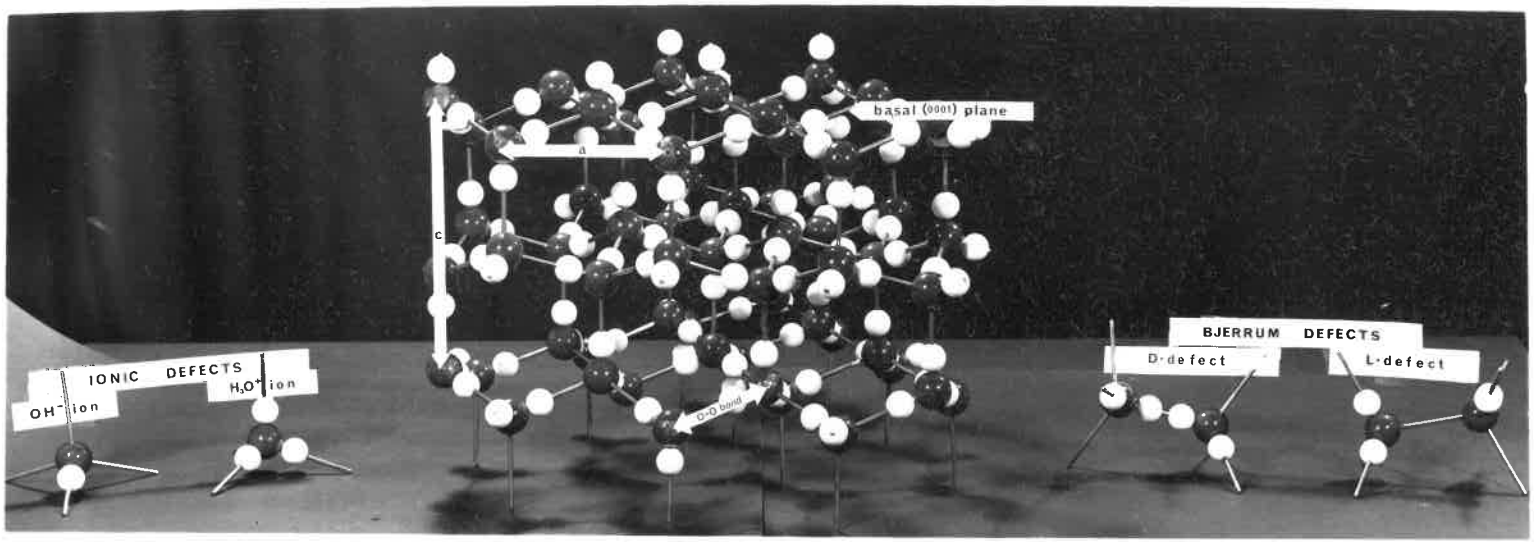
IONIC DEFECTS
OH^- ion
H_3O^+ ion
basal (0001) plane
a
c
O-O bond
BJERRUM DEFECTS
D-defect
L-defect

Fig.III.II Model illustrating the Structure of Ice I and its Point Defects. The large (dark) balls represent the Oxygen atoms and the small (light) balls represent the Hydrogen atoms.

alternating electric field. The time for the decay (or build up) of polarization can give some idea of the time taken for molecular re-orientations. Evans (28) has reviewed the experimental values of these relaxation times for ice. Whereas for ice near $0^{\circ}C$, the relaxation time is about 10^{-4} sec. or less, it increases exponentially with decreasing temperature to a value of 0.1 sec. at $-60^{\circ}C$.

It is clear that in order to accomodate these continual changes in molecular orientation, rules (iii) and (iv) have to be "momentarily" violated during the orientating procedure. The picture we have is one in which Bjerrum defects are rapidly migrating through the ice lattice. As they move through the lattice, these defects re-orientate the ice molecules. The Bjerrum defects necessary for this reorientation may be formed by thermal activation or by dissociation from other types of defects in ice such as a molecular vacancy. Kopp (91) has made a detailed study of this latter type of formation. The Bjerrum defects move by thermal activation and possibly by quantum mechanical tunnelling.

The ability of ice molecules to re-orient themselves in the presence and absence of external influences, plays an important part in the electrical and mechanical properties of Ice I (see Sec. 3.3, 3.4, 3.6).

3.3 Structure and Properties of Ordinary and Closely Confined Water

We wish to discuss some unusual physical properties of water when spatially confined. It is necessary to first consider the properties of ordinary water.

A large number of divergent theories have been proposed to describe the microscopic state of water; for example, see the following reviews ((29)-(38)). The "unstructured liquid" models for water ((39)-(41)) have proved useful but to satisfy detailed studies of its properties, the "structure models" of water are necessary. Such models require small clusters of structured water molecules continuously changing (or "flickering") in size and position about 10^{10}-10^{11} times per second. Estimates of these cluster sizes vary between 25 and 10,000 molecules. It is also estimated that about 13 per cent ((64), (92)) of the bonds in these water structures are broken.

Any structure model which approximates to reality, must account for the main properties of water. In view of the rather unusual properties of water, this is no easy task; among the foremost features that need to be explained are (a) the density of water being more than that of Ice I, (b) the density maximum at $+4^{o}C$, (c) the viscosity minimum of water in the k-bar pressure range (see for example, (38), (42)-(44)), and (d) the dielectric behaviour of water. We now outline some of these structure theories proposed for water:

It is assumed that two or more types of structure exist in water. Features such as the $+4^{o}C$ density maximum, may be accounted for by a suitable choice of structures and the variations of their proportions with temperature.

Some of the structures suggested are rather complex ((29),(33),(45)-(48)). They have arrangements of water molecules with different numbers of hydrogen bonds (that is; 0 (monomeric), 1,2, 3 and 4 hydrogen bonds per water molecule) and different energy levels of bonding. By analogy to the clathrate hydrate structures of some inert gasses, it has been suggested ((49)-(51)) that polyhedral-clathrate-hydrate-cage-structures may exist in water with a low concentration of monomeric water molecules.

Other models however only consider the (broken down) structures of the various Ice polymorphs. Thus Röntgen et al. ((52)-(55)) have considered water to be a mixture of Ice I (or some other Ice form) with the monomeric water molecules occupying interstitial spaces in the ice lattice. The significant structure theories of Eyring et al. ((37),(38)) consider a mixture of light and dense Ice structures with a certain amount of monomeric water molecules and fluidized vacancies. The latter theory (38), in particular, considers the Ice I (Light) and Ice III (dense) structures. This treatment gives good agreement with the experimental data for the variation of viscosity, specific heat and other properties of water.

In some of the following discussions it is assumed that, at temperatures very close to the melting point, water contains a considerable amount of Ice-I-like-structure. The observations by Jamin (56), Damien [(142),(143)] and Erréra (57) on the refractive index of water near $0^{o}C$ ("the water seemed to anticipate the ice values of refractive index a little before attaining ice-like-rigidity") may possibly be regarded as experimental confirmation of

this view. However some of the theories outlined above do not consider any Ice I-like-structure to be present in water at any temperature. The high-order phase transitions possibly manifested in the properties of water at warmer temperatures (known as "kinks", see (35), (58), (59)) do not necessarily require the presence of Ice I structure in water. However it would seem to the writer that the evidence suggests that water very close to the melting point contains a considerable amount of Ice I-like-structure.

In this connection, it is surprising that unconfined water supercools so readily in the absence of ice-nuclei (see for example (60)) to -40°C. There is insufficient space for a full discussion of this phenomenon but it is worth pointing out the implications of Morgan and Warren's X-ray diffraction studies on water (61). Extrapolation of their data from above 0°C implies that at about -40°C the number of next-nearest neighbours in supercooled water finally reduces to the same value, 4.0, as that for the perfect Ice I structure. We note that the physical properties of supercooled water (for example, density (62)) are in general a close extrapolation of those of cold water. The preliminary work of Narsingh Dass and Gilra (63) suggest that one exception is the refractive index; the extrapolation is smooth but non-monotonous. Otherwise, supercooled water can be considered as very cold water. This is in contrast to the properties of "confined water" at low temperatures described below.

We now compare the behaviour of confined water to that of ordinary water described above. In spite of some of the seemingly incredible properties reported so far, it is becoming increasingly clear, in view of the work by many different investigators, that water exhibits some unusual properties under closely confined conditions.

At this juncture, it is necessary to comment on some of the theoretical work of Fletcher (64). (For criticisms of this work, see (65), and Fletcher's reply (121)). Fletcher assumes that the surface layers of water consist mainly of Ice I-like-structures with c-axes perpendicular to the free surface. This is a reasonable starting assumption (95). Fletcher shows that because of the relatively high polarisability of the protons, the surface energy can be considerably lowered (by 10^{-13} to 10^{-12} ergs/molecule, or 1.5 to 15 k.cal/mole)

if there are no hydrogen atoms pointing vertically outwards from the surface layer of oxygens i.e. if all the surface hydrogen atoms point inwards. This decrease in surface energy offsets the decreased entropy due to this extra ordering. Because of the large number of defects in water (about 13 per cent of the bonds are broken, see above), this surface-ordered orientation is reduced to almost random after a relatively few numbers of molecular layers below the surface. By minimizing the thermodynamic Free Energy of these layers, Fletcher calculates that at $0^{\circ}C$, this ordering will have decayed exponentially to a value of 1/e in about δ = 13 molecular layers (about 26 Å). This calculation is specifically for water at $0^{\circ}C$, but there is no reason why this ordering should not exist for temperatures above (e.g. room temperature) and below (e.g. supercooled water temperatures) $0^{\circ}C$ with different values of δ .

It should be pointed out that hydrogen ordering on a water surface implies an electrostative potential jump across the surface (of the order of volts, see (64)). Several attempts have been made to measure this jump for both ice and water surfaces (see for example, (75), (76)). It is difficult however to make quantitative conclusions from such measurements because of the uncertain effects of a) the polarization of the surface oxygen ions, b) the polarization of water molecules close to the ends of the dangling bonds within the bulk liquid, and c) the ordering (of opposite sense) produced on the surface of the electrode introduced for this measurement. In fact the theory effectively assumes the water surface to be a saturated air-water interface. It is worth considering other experimental possibilities; substitution of a glass (or quartz)- water surface for the above, may possibly increase this ordering effect (and therefore δ) on account of the presence of the hydroxyl groups on the quartz surface. Conversely a metal surface (which has, on account of its "free electrons" effectively an infinite polarisability) may adjust better to the field emanating from the water dipoles, thus reducing δ. It may be that a microscopic description of water confined by a glass capillary, for example, is an extension of Fletcher's picture of a free water surface.

One of the most unusual properties of confined water is its "supercooling". While ordinary water can be supercooled in the absence of ice-nuclei down to

about -40°C, water contained in very fine glass capillaries can be supercooled far below this temperature sometimes in the presence of ice-nuclei. This phenomenon has been demonstrated rather elegantly by Hori (66) who investigated the maximum supercooling of water contained between two flat parallel glass (and quartz) plates (see Fig.III.III). He found that for plate separations of δ = 10-1,000 μ, the supercooled water froze at temperatures between -10°C and -40°C just like ordinary water. However for $\delta \ll 10\mu$, the water usually remained unfrozen even below 90°C (i.e. the water seemed to retain its optical and mechanical properties). A more surprising effect was discovered on substituting a convex lens for the top flat plate so as to produce a central region with $\delta < 1\mu$ say, and outer regions with increasing δ values (up to 3μ say) (see Fig.III.III.(b)). With this arrangement it seemed possible to freeze the outer annulus of water while the inner narrower regions remained liquid. This observation is significant; it suggests that for $\delta < 1\mu$ the water fails to freeze even in the presence of an ice-nucleating-source. The vapour pressure of water for $\delta < 4\mu$ was unmeasurably small, while that for $\delta > 4\mu$ was similar to bulk water. One could interpret these results as implying considerable hydrogen ordering present in water for $\delta < 1\mu$, while for δ = 1-10μ there is still sufficient ordering to hinder crystallisation. A similar phenomenon has been observed by Swinzow (67). By placing a glass capillary, with a constriction in its middle, in a temperature gradient directed along its length, Swinzow observed the water crystallising from the colder side of the constriction. The water in the constriction failed to freeze but seemed to act as a nucleus so that the water on the warmer side could crystallise (see Fig.III.III). This is of considerable interest as it would seem to imply that the water transmits some kind of nucleation for further crystallisation while failing to freeze itself. The Russian investigators Derjaguin et al. ((68)-(73)) have measured other physical properties of water in fine capillaries. They found that in 1-2 μ capillaries at room temperature, the water had a different density and thermal expansion to that of bulk water. In addition the viscosity of the water was found to be as much as ten times greater (0.19 poise) that that of bulk water. More recent work (73) shows that (like Hori's observation) this fine capillary water can be supercooled below

-key as in Fig. II.V

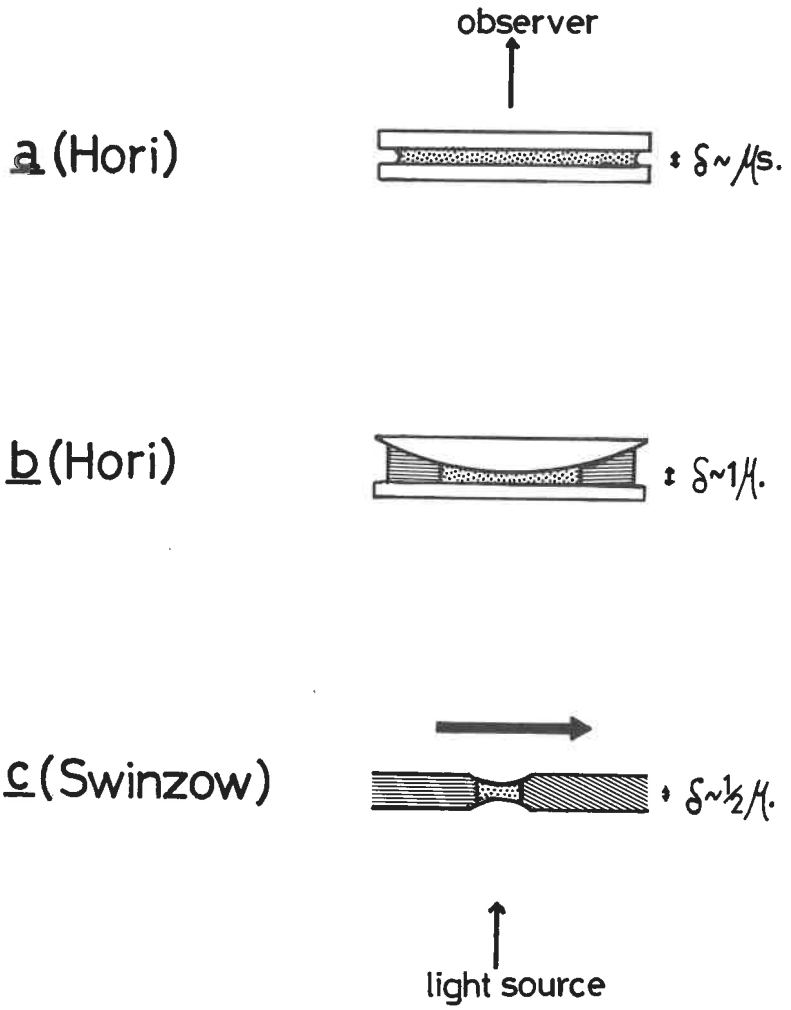

Fig. III.III Examples of Closely Confined Water (Sec. 33).

-key as in Fig. II.V

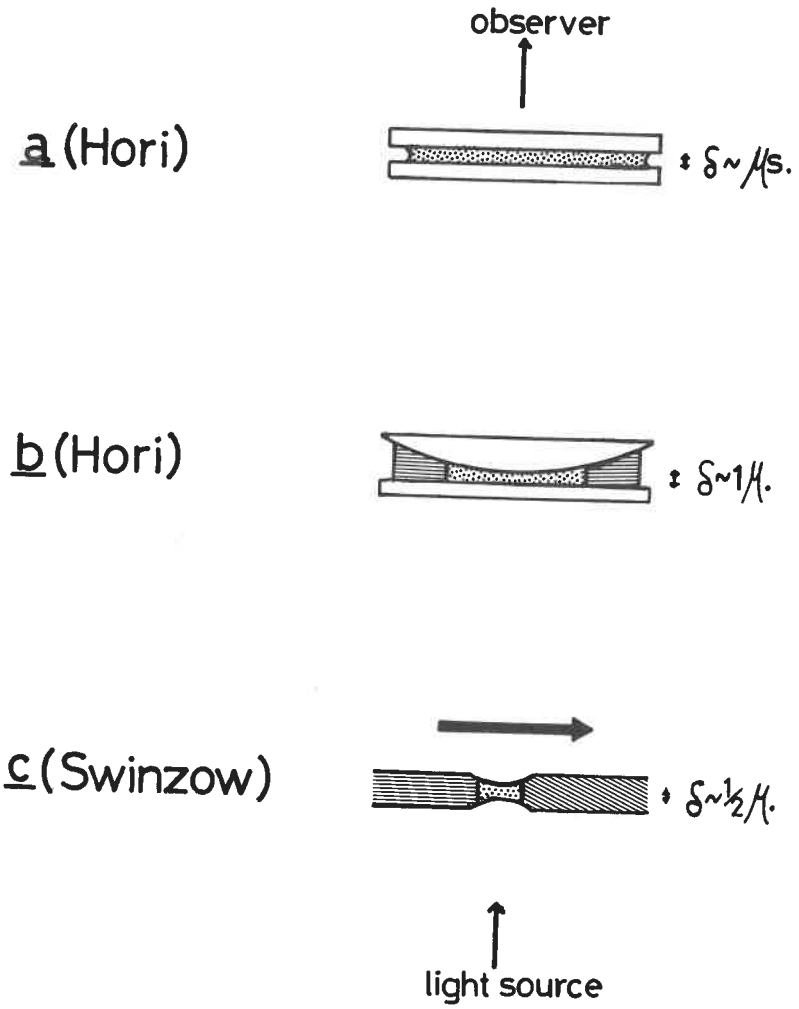

Fig.III.III Examples of Closely Confined Water (Sec.3.3).

-40°C. In addition it was found that when freezing finally occurred at -60°C, there was a smaller, 5 per cent, volume increase compared to the 8.3 per cent increase for the water-ice change at 0°C. Derjaguin calls this "quasi ice". On warming, this "quasi ice" melts at -30 to -15°C with an analogous 5 per cent volume decrease. The choice of the expression "quasi ice" seems to the writer to be rather unfortunate. What is implied is that the ice which has frozen from the ordered water may have some ordered structure. Derjaguin and Green-Kelly (72) have also reported that water under confined conditions can possess distinct birefringence values of 0.002-0.003. Palmer et al (74) have also shown that water contained between mica plates ($\delta < 5\mu$) possesses dielectric properties intermediate between that of water and ice. These two observations may infer some order in the confined water.

Among the names used for confined water which displays these unusual properties are: "special water", "ordered water", "quasi-liquid", "quasi-fluid", "quasi-crystalline-water".

3.4 Structure and Properties of Ice Surfaces

We now consider some unusual features of the ice surface and try to correlate them with those described for water in Sec.3.3. From as far back as the nineteenth century, discussions on sintering and regelation experiments ((77)-(82)) led some to propose the well known "surface liquid layer" theory for ice. There followed much controversy over which of the two processes, "liquid layer" or "pressure melting", was responsible for regelation. While it seems that for regelation experiments in ice near 0°C ((83)-(86)), pressure melting may be invoked (see for example, Nye (87)); for regelation at lower temperatures (i.e. below the pressure melting temperature), "liquid layer" theory may possibly apply (see (88)) - unfortunately the study of low temperature regelation is somewhat neglected. Considerable controversy still exists on the subject of the "surface liquid layer". While it is clear that ice surfaces (like water) definitely show some unusual effects, they are not assumed by all to be the result of a surface-liquid-layer. Before outlining these unusual effects, we consider the theoretical work of Fletcher (64) on the ice surface.

Fletcher extends his earlier arguments used for water (Sec.3.3) to the case of the ice surface. He points out that, unlike water, the ice lattice is sufficiently well behaved structurally (i.e. it has a low defect density) so as to seriously hinder the randomnisation of the hydrogen atoms below the surface. This means that any surface ordering would extend a considerable (macroscopic) distance into the bulk ice (compared to only 13 molecular layers with water). This would greatly decrease the bulk entropy of ice. Because the bulk entropy of ice is usually not small enough to allow bulk ordering of the hydrogen atoms (see Sec. 3.2), Fletcher concludes that surface ordering of a solid ice surface, in the manner described for the water surface, cannot permanently exist. (Temporary ordering may possibly occur, see for example Sec.3.2). However, developing an idea of Weyl (89), Fletcher shows that the surface energy of ice may still be lowered provided there is sufficient energy available for the latent heat needed for melting a thin water film on the ice surface. The hydrogen ordering in the water layer is then assumed to vary from near 100 per cent at the upper air-water interface to near 0 per cent at the lower water-ice interface. Hence by introducing this liquid layer concept, the surface energy may be reduced on account of the surface hydrogen ordering in the liquid layer; the impossible constraint of bulk ordering in the ice is avoided by allowing the order to relax in the liquid film. By minimising the Gibbs Surface Free Energy, Fletcher shows that such a film is thermodynamically stable between 0 and $-13^{\circ}C$ and probably to $-30^{\circ}C$. The calculated values of δ show an approximately exponential variation with temperature from $-24^{\circ}C$ ($\delta = 8$ Å = 4 molecular layers) to $-2^{\circ}C$ ($\delta = 200$ Å = 100 molecular layers), ($Q \simeq 15.6$ k.cal/mole), with a fairly sharp increase around $-9^{\circ}C$ to $-3^{\circ}C$. Experimentally, this means the theory predicts that the critical temperatures for film observation are $-30^{\circ}C$ to $-24^{\circ}C$ where the film begins to form, and $-9^{\circ}C$ to $-3^{\circ}C$ where the film thickness δ increases sharply. It is important to realise that in many of the experiments designed to demonstrate the presence of this liquid film, the ideal air-water film-ice interfaces assumed by Fletcher, are not present. For example (as pointed out in Sec.3.3), glass-water film-ice systems as used in optical and mechanical tests may increase ordering effects, while metal-water film-ice systems, as

used in electrical and mechanical tests, may possibly decrease the ordering effects. Other experimental variables which may affect δ are

a) the hydrostatic pressure of the system,

b) the vapour pressure of the air,

c) surface crystallographic orientations other than the basal plane. For example, the polarisation (and hence δ) is expected to be smaller for surfaces parallel to the c axis (see Kopp (92), p.8).

Reviews on the experiments concerned with the surface-liquid-film have been made by Kopp (92) and Barnes (95). The latter has made an extensive review of the present experimental situation, but space permits only a brief account here. Some of these experiments are discussed below under the appropriate sub-titles:

(i) Ellipsometry. Direct methods, such as ellipsometry, have not yet confirmed the presence (or absence) of a liquid layer. Kopp ((94), p.83) has shown that with the stringent requirements for transparent media, such as ice, ellipsometry results are inconclusive.

(ii) Electrical. Electrical conductivity results show a very definite surface effect. A number of investigators ((92)-(94),(96)-(99),(267)) have shown that there is an anomalous increase in the conductivity of certain ice samples at temperatures between about $-20^{\circ}C$ to $0^{\circ}C$. In particular (see for example (96), (267)) it has been shown that there is a direct correlation between this increase and the lengths of the paths taken by the surface currents. Noting that the conductivity of water is 100-1,000 times higher than ice, these anomalies may therefore be attributed to electrical conduction through the liquid film on the surface of the ice specimen. A complication inherent in these experiments is, of course, that two interfaces (ice-metal electrode, and ice-air) are present. Latham (100) has measured the charge transfer produced by temperature gradients in ice. Latham shows that above $-7^{\circ}C$, the charge transfer increases rapidly. This increase is directly proportional to the surface:volume ratio. It is therefore suggested that it is due to the increased ion mobility in a surface liquid-like-film.

(iii) Sintering of Ice Spheres. Several investigations ((101)-(109)) have been made of the rate of sintering (or neck growth) of small ice spheres with

radii considerably less than 1 mm. and for temperatures between $-25^{o}C$ to $0^{o}C$. Sintering is known to produce considerable changes in many of the physical properties (e.g. "strength") of snow ((122)-(128)). Unfortunately different theoretical interpretations of these results are possible, and so one cannot as yet deduce whether or not this neck growth can be attributed to a rapid surface diffusion in the liquid film. It may be that when computer techniques are used (as for example in (110)) for calculating the effects of evaporation, condensation, surface and volume diffusion in sintering processes, more definite conclusions will be drawn from these observations.

One important point that emerges here, is the dependence of the rate of neck growth on the vapour pressure of the air (Hosler et al. (106)). In a saturated atmosphere, the rate of sintering is appreciable down to $-25^{o}C$; however when the vapour pressure is less than saturation, no appreciable sintering occurs below $-4^{o}C$. Hosler et al. explain this effect in terms of rapid evaporation which is sufficient to hinder the formation of a stable liquid film below $-4^{o}C$.

(iv) Mechanical. Jellinek ((111)-(113)) has measured the tensile and shear adhesion of quartz and steel flat plates to ice. The value of the tensile strength was found to be about 15 times larger than the shear strength value. Jellinek interpreted these two values as indications of the surface tension and viscosity η respectively of a liquid film between the ice and the plates. On this interpretation, the following film characteristics were deduced:

ice/stainless steel:	η = 70-700 poise,	δ = 100-1,000 Å.
ice/quartz:	η = 15-150 poise,	δ = 100-1,000 Å.

While (like the capillary experiments, Sec.3.3) these viscosity values are rather high compared to bulk water (0.018 poise), they are far too low for comparison with ice ($\eta_{ice} > 10^{14}$ poise).

Nakaya and Matsumoto (108) have also interpreted their observations in terms of the "viscous water film". Two small suspended ice spheres in contact were mechanically constrained so that the couples acting on the spheres produced rotation of the spheres about their centres. This smooth rotation was observed down to $-7^{o}C$. This effect was interpreted by viscous-liquid-like shearing

between the surfaces of the spheres which were kept in contact by the surface tension forces of the film. With Sodium Chloride concentrated at the spheres' surfaces, the surface melting and rotation was increased. It has been pointed out (114) that electrical charging of the spheres (produced by temperature gradients) could also have been the cause of their attraction. However one still has to explain why the rotation only occurred between $-7^{o}C$ and $0^{o}C$. A possible explanation is that rapid electrical charge transfer occurs in the liquid film over this same temperature range, $-7^{o}C$ to $0^{o}C$ (see (ii) above). The concept of electrical attraction was introduced as an objection to the liquid layer idea in sphere rotation, but on closer examination it would seem, if anything to support it.

(v) Pressure Effect. By pressing a flat glass plate on an ice lens, Nakamura (115) has shown (optically and mechanically) that a thin liquid film is formed at the contact region. The pressures involved were 30 times less than that required by pressure melting and the film was observed down to $-30^{o}C$. As the triple point temperature is about $-20^{o}C$ (see Sec.3.1), this cannot be an ordinary pressure melting effect. Because no optical fringes were observed, it was deduced that $\delta > 5{,}000$ Å say.

(vi) Movement of Solids in Ice. We consider here the movement of a solid in ice at temperatures low enough to exclude pressure melting. For the two following cases the driving force is:

a) gravity, as in a regelation experiment (88)

b) a temperature gradient (116)

The results are shown to be consistent with a model comprising of a thin liquid film (of size comparable to Fletcher's value) between the solid and the ice.

(iii) Particle and Bubble Movement at Ice-Water Interfaces. Glass particles (Hoekstra and Miller (116))and air bubbles (Maeno (117)) in water do not appear to adhere to the ice surface, even when the ice surface is advancing (i.e. growing) upwards into the liquid zone. These effects are shown to be consistent with a model in which a thin film exists between the ice surface and the approaching bubble or particle.

(viii) Particle Movement at an Ice-Air Interface. Nakaya, Hanajima, and Muguruma (118) have observed the movement of dust particles on the edge of an evaporating snow crystal. As the edge recedes the particles move with it as if stuck to the edge by means of a liquid film surface tension effect. The "sticking power" or adhesion was noticeably high and observed below $-30^{\circ}C$. In addition, Itagaki (144) has recently reported the anomalous "Brownian type of motion" of glass beads on an ice surface which is exposed to an unsaturated atmosphere.

(ix) Surface Layers on Ice. We briefly consider here the properties of thin surface layers (or steps) on an ice surface. If a liquid film of thickness δ does exist on an ice surface, then all surface layers of thickness $\sim\delta$ must be expected to display the high mobility characteristics of a viscous liquid layer, rather than those of a solid. Three observations are described:

a) Optical observations by Hallet (119) have been made of the high mobility of the edge of an ice step (or layer). Such steps were 200-2,000 Å high and were observed down to $-17\frac{1}{2}^{\circ}C$.

b) Electron microscope studies (see discussion by Kopp (92), p.4) of replicated etch-pits on ice reveal time dependent microstructures 200-2,000 Å high at $-20^{\circ}C$.

c) Microcinematographical observations have been made by Nakaya et al. (118) of the ridge left on an ice surface after being impacted by a supercooled droplet. The heights of the ridges were about 7,000 Å at $-9^{\circ}C$.

(x) Density. Hobbs et al. (120) have measured the density of fine ice particles as a function of temperature and particle size. Changing the particle size produces changes in the surface: volume ratio; therefore if a surface liquid layer exists with a measurably different density to that of bulk ice, these measurements should be capable of detecting such a change. So far only preliminary measurements have been made, but they show indications of such a change.

In this discussion, the agreement between experimentally obtained activation energies has not been considered. There is often found a distrust for arguments based on comparisons of activation energy. . . . . .

. . . . . This may seem to be particularly so for the case of ice where a number of mechanisms seem to have comparable activation energies. Experimentally observed effects usually involve processes in addition to film formation. Kopp ((93),(94)) however has made a valuable contribution to this field by showing that the activation energies for these component processes are separable and indeed calculable.

Many objections to the theory of "surface films on ice and water" may be raised on the grounds of complications due to other unusual surface properties of ice (e.g. impurity migration to the surface). In addition experiments often introduce other surfaces (glass, metal etc.) which probably interact with the subject of examination - this may be an experimental advantage at times. Alternative ideas to "ordered liquid film theory" may be offered in order to provide better explanations for the above described effects. In fact the writer feels that the "film" theory may well not fully explain all the experiments described. However one can say that there are a large number of very unusual effects related to the surfaces of ice and water; in fact some 30-40 different phenomena have been covered in this summary. Any view disapproving entirely of an ordered film theory would therefore have to provide alternative explanations for a large number of effects. In contrast, Fletcher's description of ice and water surfaces shows remarkable agreement with most of the observations. But so far unfortunately, no <u>single</u> experiment has been devised which <u>by itself</u> convincingly confirms the ordered surface film theory.

Before leaving this interesting topic, it is worth discussing one other phenomenon which is regarded as not entirely unconnected with this field; the presence of a liquid film at large angle grain boundaries may be considered as a special case of the surface film effect. The grain boundary is thus technically regarded as the surface of one of the grains; the other grain effectively replacing the air, glass or metal medium present in the previous experiments. The problem is not just as simple as this, and of course may be treated from completely different physical standpoints; in addition the effect will depend strongly on the relative orientations of the grains. However this picture suggests that we should anticipate effects attributable to ordered-liquid-like-grain boundaries at temperatures considerably below the melting

point (to $-30^{o}C$, say). Such effects are indeed apparent in some of this research and are discussed more fully with the Internal Friction data in Chapter VI. It is most important however that one should differentiate between this effect and the liquid grain boundary process invoked in Chapter IV on the Hardness of Ice. The former effect is based on arguments concerning a gradual variation in size δ of the liquid grain boundaries over a wide range of temperatures; the latter involves a sudden increase in size of these liquid layers when their hydrostatic pressure reaches the critical pressure melting value. Thus this latter effect applies only to temperatures above the pressure melting temperature of the ice, while the former applies to temperatures lower than this as well.

3.5 Thermodynamic Theories of Hydrostatically and Nonhydrostatically Stressed Solids

In this thesis we are often concerned with pressure melting effects in ice (see Sec.3.1). Even though a full appreciation of the thermodynamic situation is far beyond the scope of this work, it is nevertheless essential that one is able to choose the correct thermodynamic formulae for each physical situation. We wish to calculate the melting point of ice for several cases involving different stress conditions imposed on the ice and the water produced by the melting. The melting point of the stressed ice is usually characterised by ΔT which is defined as the difference between this melting point and $0^{o}C$. The mechanical system and the ice specimen are assumed to be contained in an atmosphere at the standard 76 cm. of mercury pressure.

(a) Hydrostatically stressed Ice and Water. When a hydrostatic pressure (P) is applied to both the ice and water phases, the depression of the melting point is deduced from the Clausius-Clapeyron equation:

$$\left(\frac{\Delta T}{P}\right) = -\frac{\Delta V}{\Delta S} = -0.0074^{o}C/\text{atmosphere} \qquad (3.1)$$

where ΔV and ΔS are the ice-water changes in volume and entropy. In a direct experiment, Moser (129) found that for a pressure change of about

1 atmosphere this was very close to the observed value.

(b) Hydrostatically Stressed Ice, Unstressed Liquid. In a calculation due to Poynting (130) it is assumed that the melted ice is instantaneously released from the applied pressure. As a result, the lowering of the melting point is about 11 times greater than that indicated by equation (3.1).

(c) Ice under Uniaxial Strain. Riecke (131) considers the behaviour of ice under a uniaxial compression. He assumes that the external forces do no work and the only effect is due to release of elastic strain energy in the ice when melting occurs. The depression of the melting point is proportional to the square of the stress and is therefore always positive:

$$\frac{\Delta T}{\sigma^2} = \frac{-V_s}{2E.\Delta S} = -4.51 \times 10^{-7}\ {}^{o}C.bar^{-2} \qquad (3.2)$$

where E is the relevant elastic modulus, and V_s the specific volume of the ice phase. This lowering is minute: to illustrate this point, we consider the maximum pressure melting possible under the hydrostatic conditions of (a). As pointed out in Sec.3.1, the triple point limits this sort of pressure melting to $T \simeq -20^{o}C$, $P \sim 2{,}000$ atm. Using this high value of P for the stress in Riecke's formula, the value of ΔT is only $-1.8^{o}C$. Even for this extreme case, we see that the Riecke's formula predicts a lowering considerably smaller than that given by the integrated value obtained from equation (3.1). For smaller values of P, the difference becomes even grater.

(d) General Theory for Nonhydrostatically Stressed Bodies. The correct thermodynamic conditions for equilibrium of solids under non-hydrostatic stresses were first derived by Gibbs (132). Kamb ((133),(134)) has shown that there are difficult conceptual problems in formulating a Gibbs Free Energy (or chemical potential) for non-hydrostatically stressed solids. In accordance with Gibbs' formulation, Kamb (135) has avoided this ambiguity in developing his thermodynamic theories by defining a chemical potential for the liquid phase only. On the other hand Kamb ((133),(134)) contends that some of the once accepted thermodynamic theories (e.g. Goranson (136) and Verhoogen (137)) depart from Gibbs' formulation and are therefore incorrect. Kamb also shows that, for different reasons, MacDonald's theory (138) is incorrect.

In simple physical terms, this means that in order to determine the change in the melting point of a non-hydrostatically stressed solid, we have to first allow a small portion of the solid to melt, and then consider the hydrostatic pressure P of this liquid phase in the system. The pressure P as used in equation (3.1) must therefore refer to that of the liquid phase (which is equal to the particular stress component in the solid perpendicular to this solid-liquid interface). This gives a different value for the change in melting point to that obtained if one were to incorrectly use the mean stress component (defined as $P=(\sigma_x+\sigma_y+\sigma_z)/3$ as used in plasticity theory) in the solid. For example in the case of a uniaxial stress σ, the mean stress is $\sigma/3$; to use this incorrect value for P in equation (3.1) would predict a change in the melting point which is 3 times too small.

Unfortunately because of the confusion caused by the contemporary existence of these different formulae, some of the theories developed in studies of ice and glaciology (e.g.(139),(140)) are incorrect. Also in a preliminary study, Barnes and Tabor (141) compared the hardness of ice and Glen's((1),(2)) creep results for ice near the melting point. It was required to show that the ice specimens in Glen's $-0.02^{\circ}C$ experiments were at the melting point. Because of the confusion described above, Barnes and Tabor tried using both values for P (σ,$\sigma/3$) in their calculations. It was concluded, irrespective of which value for P was used, that the ice was very close to the pressure melting point. In the light of the above, we now consider only the correct ($P=\sigma$) value (i.e. the lower curve in Fig.8(141), or Fig.XXII in Ch.IV), which predicts the larger depression.

In Chapters IV and V we have calculated the pressure melting point of the ice using the hardness value for P in equation (3.1) rather than the mean stress in the ice which is about 2/3 of this value. Because the pressure of the thin water film formed beneath the indenter is given approximately by the value of the hardness, it is seen that our pressure melting calculations are in accordance with the Gibbs-Kamb formulation. The good agreement here between calculation and observation may be taken as confirmation of the Gibbs-Kamb formulation. It is worth noting that Nye also uses the Gibbs-Kamb formulation in his regelation theory (87). In this case it would appear that the

confirmation of the Gibbs-Kamb formulation (and therefore reasons for rejection of the alternative theories) is even stronger.

(e) Theory of Recrystallisation under Stress. Kamb (135) has used his non-hydrostatic stress thermodynamic theory to predict the type of preferred orientation obtained with glacier ice which has recrystallised after plastic flow. Two cases are treated; with and without the liquid phase at the grain boundaries. It would seem that the theory predicts little observable difference between the two cases. This is unfortunate for our purposes, because it suggests that the premiss used in Chapter IV (i.e. that the crystallisation and grain growth in the pressure melting regime is controlled by a liquid grain boundary effect) cannot really be checked from orientation studies on the deformed ice.

3.6 Mechanical Properties of Ice I

This section is not intended to be a complete review of the mechanical properties of Ice I. Such a review would be premature as there exist considerable disagreement between the flow laws obtained by different observers. It is hoped that the different results will be unified once a few critical experiments have been performed. Hence these different flow laws will only be discussed briefly here.

Considerable reference will be made to Glen's flow law for the steady state creep for polycrystalline ice:

$$\dot{\epsilon} = A' \sigma^{n} \exp\left(\frac{-Q}{RT}\right) \qquad (3.3)$$

The full meaning of this equation is discussed later. In view of the fact that Glen's stress and temperature conditions correspond roughly to our hardness data, we shall usually use Glen's flow for comparative studies although alternative flow laws are sometimes used. The steady state creep of single crystal and polycrystalline ice will be discussed separately. The concepts of single crystal flow can then be extended to polycrystalline flow. The interpretation of the flow laws involve dislocation mechanisms; these will be more fully explained later.

(a) Single Crystal, Easy Glide

A lot of work has been done since the early experiments of Glen ((1), (2), (145)) and Steinemann (146). It has long been realised (McConnel, (149)) that, for ice, easy glide occurs in the basal $\{0001\}$ plane. This basal slip takes place as intense deformation in thin layers known as "glide layers". Nakaya and Wakahama have observed glide layers of widths 0.1-0.5M separated by 10-60M. These layers have been shown rather beautifully by Nakaya ((150)-(152)) using shadow photography (see also (163), (179), (258)). Experiments designed to observe anisotropy of flow in the basal plane ((145), (157), (153), (146), (200), (201), (156)) show that there is only a little, if any, preference for slip in the $\langle 11\bar{2}0 \rangle$ direction. Also Kamb (154) has shown theoretically that this anisotropy must be small for ice. It will be seen that the creep of ice single crystals is distinctly different to that for polycrystals. Basically, two types of experiments are used; (i) the variation (with time) of the creep rate $\dot{\varepsilon}$ for a constant stress σ, and (ii) the variation (with time) of the stress required to maintain a constant strain rate. It is found that for easy glide in single crystals, the exponent m is lower (usually 1.3-2.5) than for polycrystals (usually about 3-4). A summary of some of the activation energies obtained from mechanical, electrical, diffusion and other experiments on ice has been given by Itagaki (165). Walker (155) however has pointed out that there are indications in many of these experiments that Q is not single valued over a temperature T range of say $0^{\circ}C$ to $-30^{\circ}C$. It would seem that there is a continual variation of Q with T, with a fairly rapid change (called a "kink") at transition temperatures (T_c) somewhere between $-6^{\circ}C$ to $-11^{\circ}C$, say.

The writer has therefore reviewed some of the data on the mechanical properties of ice (single and polycrystals) and has tabulated them in the following Tables III.I-III. Table III.I. below considers the experiments concerned mainly with the basal plane properties of single crystals.

Table III.I, Activation Energies Q and Stress Exponents m concerned with Deformation in the Basal {0001} Plane of Ice.

No.	Reference Method	Stresses Temperatures	Q (k.cal/mole)	m	Comments
1	Jones & Glen (156)	above 10 bars	9½(-90°C)	2.2±.3(-50°C)	(i) m varies with stress.
	Tension, constant $\dot{\sigma}$ and constant $\dot{\epsilon}$.	-90°C to -10°C	15.6(-50°C to -10°C)	-2.3±.3(-70°C)	(ii) Definite variation of Q with T.
2	Readey and Kingery (157)	few bars	14.3±1½	2.5-1.5 as $\dot{\epsilon}$ increases	The Q given is an averaged one, but inspection shows there is a definite "kink tendency" at about -7°C.
	Tension, constant $\dot{\epsilon}$	-42°C to 0°C			
3	Higashi, Koinuma, and Mae (158)	½-5 bars	10.4	1.53	(i) Temperatures too low to indicate any real kink.
	Tension, constant $\dot{\epsilon}$	-40°C to -15°C			
4	Higashi et al.(158) (159), (189)	few bars	15.8	1.58	
	Tension constant $\dot{\epsilon}$				
5	Steinemann (146),(148)	~ bars	about (10- > 20	1.3-1.8, early 2.3-4, later	(i) 2 ranges defined for m; (1) early - $\dot{\epsilon}$=10 to 20%, (2) late-high σ and $\dot{\epsilon}$ values.
	Shear constant σ	-2°C to -20°C			(ii) the scatter in Q values too large for analysing variation with T.

Table III.I CONTINUED

No.	Reference Method	Stresses Temperatures	Q (k.cal/mole)	m	Comments
6	Griggs and Coles (160)	1.45-14 bars	Large variations†	2*	*(i) Used an unusual analysis. However it can be shown that m ≃ 2. †(ii) Results admitted to be rather unreproducible.
	Compression, constant σ	-1°C to -18°C			
7	Butkovich and Landauer (161), (162)	about ½-2½ bars	-	2.49	
	Shear, constant σ	-5°C			
8	Higashi and Sakai (163)	-	12-17	-	
	grain boundary movement in stressed ice beams.	-5°C to -21°C			
9	Butkovich (164)	about 30-200 bars	Only relative Q values	-	(i) Definite kink at about -7°C. (ii) These indentations must also produce a certain amount of non basal glide
	Hardness	-5°C to -50°C			

Except for No.1 in the above Table, the activation energy values Q are averaged over the whole Temperature range and therefore do not individually demonstrate any variation. However even using these averaged values and inspecting their relevant temperature ranges, it can be seen that Q is some sort of function of temperature and stress. However in addition to No.1, if one looks carefully at the curves presented in the papers listed (e.g., Nos.2, 3, 5, 6, 8, and 9), it can be seen that there is a general trend of higher Q's at the higher temperatures. In particular, some of the curves are not inconsistent with a sharpish increase above $T_c = -6^{\circ}C$ to $-10^{\circ}C$. The writer makes a tentative description of the variation of Q: Q varies from about 9½ k.cal/mole (at $-90^{\circ}C$) to values up to 30 k.cal/mole (at $0^{\circ}C$), with a sharp increase above $T_c = -6^{\circ}C$ to $-10^{\circ}C$. This variation is complicated by other factors i.e. Q also increases with the stress σ, and T_c may be a function of σ. It is possible that this description may partly explain why the activation energies obtained in these experiments are so different. Impurity effects may be another reason for these differences (for example, see the effect of ionic impurities on Q as shown by Jones and Glen (156).

There are discrepancies in the values of the exponent m. However it is true that the different analyses used may partly account for these variations. Generally speaking the m values for single crystal easy glide are lower than those for the flow of polycrystalline ice.

Accurate values of Q and m are of importance in choosing the correct microscopic models for the flow of ice. For example, a model involving dislocation climb would require $Q_{creep} \simeq Q_{self\ diffusion}$. It is interesting to note that the self diffusion experiments on ice (using a variety of tracers; H.F, O_{18}, D_2, Tr_3) give values for Qs.d which are usually between 11 and 18 k.cal/mole (see for example (165)-(171), (296)). However one should note that these Q values are somewhat time dependent (for example, Itagaki's (165) curves show that Q can be more than doubled for $t < 30$ hours).

It is clear that an important future experiment would be to make accurate Q determinations (and possibly m as well) over a wide range (at least $-30^{\circ}C$ to $0^{\circ}C$) of temperature. (An investigation of its stress variation would also be useful.) The different ranges of Q may then be representative of distinctly different creep mechanisms. This sort of behaviour has been

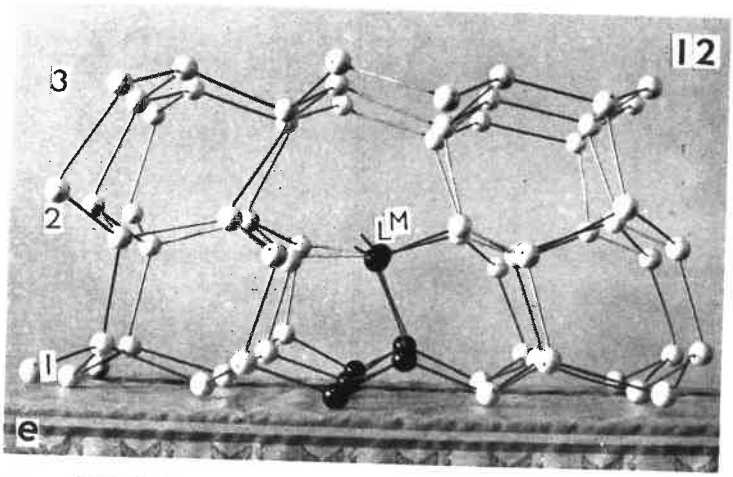

Fig.III.IV Horizontal (mixed) dislocation in Ice I - after Wakahama (Secs. 3.3, 3.6).

observed in other materials; for example Lytton, Shepard and Dorn (172) have shown 3 distinctly separate Q ranges in the easy glide of Aluminium Single Crystals over the (0.1 to 1).* Tm temperature range. Similar effects are observable with polycrystalline creep in other materials (e.g., Atkins and Tabor (173)), and in particular Flinn and Munson (174) have shown that the transition temperature (Tc) for polycrystalline Zinc is stress dependent. (For a general discussion of these effects, see for example Garofalo (175)).

We shall now consider some of the mechanisms proposed for the basal glide of ice. The results of experiments on the basal glide of ice have led the investigators to propose a number of mechanisms:

Wakahama ((176)-(179)) has shown that the yield point curves for ice in easy glide are consistent with an explanation based on a system of basal dislocations generated from Frank-Read sources of lengths between 3.2 μ - 54 μ (stress range, 0.3 bars - 20 bars). In particular Yosida and Wakahama (180) have shown, using three dimensional models (see Fig.III.IV), that partial dislocations and stacking faults can be easily constructed with minimal local lattice distortion (their existence however is questionable). Higashi et al. (158) note that the absence of work hardening in ice, as seen from their yield point curves, indicate that the initial number of dislocations and their rate of increase must be low. Higashi (159) also shows that the velocity of the dislocations should be stress dependent. Etch pit and X-ray diffraction studies (discussed later) suggest that the relevant basal dislocation is the $\langle 11\bar{2}0 \rangle$ type and is capable of cross-slipping between basal planes on pyramidal and possibly prismatic planes.

A number of theoretical treatments on the dislocation movement in ice are summarised below:

(i) Glen (181) has made a valuable contribution in showing the importance of hydrogen disorder and Bjerrum defect production (see Sec.3.2) in the motion of dislocations. Glen argues that if dislocations were to move through an ice lattice without reorientation of the hydrogen atoms, Bjerrum defects would be generated behind the dislocation (see Fig.III.V). The stresses required to produce this sort of dislocation movement could be as high as 4,300 bars. (The implications of this sort of movement are discussed in Chapter IV). Because

(i) Defect Free Lattice

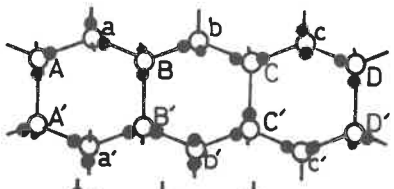

(ii) Dislocation at B

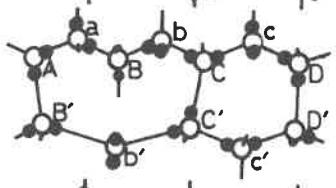

(iii) D-defect (BC') and
L-defect (CD') produced
by Dislocation Movement

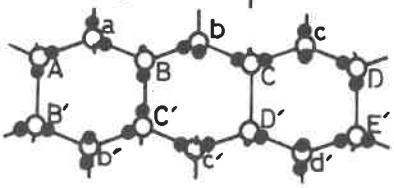

(iv) H^+ atoms move so as
to prevent the formation
of Bjerrum Defects

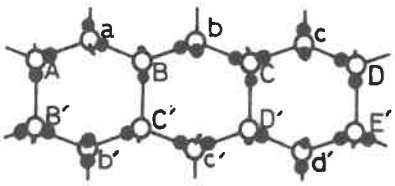

Fig.III.V Alternative Models of Dislocation Movement - after Glen (181).

it is known that ice deforms under stresses far smaller than this, Glen concludes that at low stresses a dislocation only moves when the lattice hydrogen bonds ahead of it have become correctly oriented. The thermal motion of Bjerrum defects in the lattice help to produce these re-orientations (as described in Sec.3.2). It is believed that the dislocation velocity is limited by the rate at which these Bjerrum defects can migrate and re-orient the hydrogen atoms ahead of the dislocation. At low temperatures, the number of thermally activated Bjerrum defects is low and this process is therefore severely limited. However the number of defects can be greatly increased by hydrogen fluoride doping of the ice. In fact the increased flow rate observed in hydrogen fluoride doped ice (Jones and Glen (156)) led Glen to propose this theory. At higher temperatures, the number of thermally activated Bjerrum defects increases, and it is then expected that hydrogen fluoride will have less effect on the creep rate of ice. In fact it was observed by Jones and Glen that the hydrogen doping was not so effective at $-20^{\circ}C$. These experiments serve to show that ordinary dislocation movement is the rate controlling mechanism in the basal glide of ice at low temperatures. The fact that a little softening was still observed at $-20^{\circ}C$, shows that while at these higher temperatures, dislocation movement may not be so slow as to be the rate controlling process in basal glide, it is nevertheless still slow enough to limit the rate of basal glide.

(ii) Weertman (182) has proposed the well known "dislocation climb" model for non-hexagonal metals. Under the action of the applied stress the dislocations climb over immobile-dislocation-obstacles. The climb is considered to be the slowest part of the dislocation movement and is therefore the rate controlling process. The activation energy for creep should on these grounds therefore be close to that of self diffusion (for ice, $Q_{s.d.} \approx$ 15 k.cal/mole). Weertman then using this model, calculates the creep rate and derives formulae similar in form to Glen's law (equation (3.3)). It is interesting to note that these formulae break down when the applied stress is so large that the dislocations pass over the obstacle after only a small (comparable with lattice unit) distance of climb. In this event the climb process is presumably no longer rate controlling because the time spent during

the climb process is so small. Weertman has calculated that for aluminium the formulae becomes invalid for $\sigma > (10^{-3}-10^{-2})$ x theoretical yield stress. For aluminium this occurs at $\sigma \sim 10^{2}-10^{3}$ bars. In agreement with this estimate, the creep data of Servi and Grant (186) on aluminium shows departure from Weertmans formulae at $\sigma > 10^{2}-10^{3}$ bars. (There are alternative explanations for this.) The creep rate above these stresses is faster than that calculated from Weertman's formulae. Mathematically, this means the exponent m is no longer constant but increases with stress. For ice, the value of $(10^{-3}-10^{-2})$ x theoretical yield stress is about 30-300 bars. Even though one should not necessarily expect this estimate to also hold for ice, it is worthwhile noticing that Chapter IV discusses departures from Glen's law for stresses comparable with the above value.

Weertman has noted that immobile dislocations cannot be formed with hexagonal systems like ice. He therefore extended the theory by proposing a model in which the dislocations pile up on neighbouring slip planes (183). This model predicts $m = 4.5$ and $Q = Q$ s.d. Weertman's Peierl's Stress model (184), which predicts $m = 2\frac{1}{2}$, is not thought to be applicable to ice.

(iii) Another theory due to Weertman (185) that merits consideration, because it bears resemblance to Glen's model, is the "Eshelby-Schoeck Viscous Dislocating Damping" model ((187),(188)). The theory predicts that the exponent $m = 3$. Weertman argues that if the dislocation glide velocity is limited by the rate of hydrogen (or proton, to be more correct) ordering in the lattice, then one can use relaxation time data from Internal Friction-proton reorientation-peaks (see Chapter VI.) to calculate the dislocation glide velocity. Weertman suggests that for temperatures up to $-2^{\circ}C$ (with a relaxation time of $1\frac{1}{2} \times 10^{-5}$ sec.) the dislocation glide could be rate controlling. This is surprising because in general the Eshelby-Schoeck mechanism is not usually considered to be important near the melting points of solids. However similar conclusions could be drawn from the data of Jones and Glen above.

Obviously there is plenty of scope for conjecture on the mechanisms of basal glide in ice. A tentative account is offered; at low temperatures, Glen's "hydrogen re-orientation" model (or the somewhat equivalent Weertman's

"viscous glide" model) accounts for the rate of basal glide. At slightly higher temperatures, dislocation climb becomes more important, with increasing cross-slip at still higher temperatures (up to the melting point). However at high stresses, because of the breakdown of the dislocation climb model (when $\sigma \sim$ 30-300 bars, say), dislocation glide may become important again.

In order that one may properly test any overall description of basal glide in ice (such as above), it is really necessary that more detailed and direct observations be made of dislocations in ice deformed at these temperatures. It is also required that accurate basal glide experiments be carried out on ice samples using, as close as possible, identical techniques and samples over the whole temperature range.

(b) Single Crystal, Hard Glide

We now consider the experiments in which the specimens were so oriented as to exclude the possibility of basal glide taking place during deformation. The results from three such experiments are shown in Table III.II. It is clear that non basal slip is very different to the above considered basal slip in ice; the creep rates are orders of magnitude slower and the exponent m is somewhat higher (about 3-7).

We now consider some of the mechanisms proposed more specifically for non basal glide, as opposed to the more general mechanisms described in "easy glide" above.

Higashi (159) has drawn attention to the rows of minute voids in the basal plane which appeared after non basal glide. He interpreted these observations in terms of interactions between dislocations climbing on primary slip planes (of type $\{10\bar{1}0\}$) and producing excess vacancies leading to voids in the crystal.

Bartlett and Readings (190) have made polarised light observations indicating $1/4^{\circ}$ to 1° misorientations between thin lamellae in compressed single crystals of ice. These misorientations can apparently be only explained in terms of dislocations whose Burgers vectors have a non basal component.

Tegart (191) has considered the non basal slip of ice by analogy with data on other materials (zinc, cadmium, magnesium). In particular, he

Table III.II, Activation Energies Q and Stress Exponents m concerned with the Non-Basal Deformation of Ice

No.	Reference Method	Stresses Temperatures	Q (k.cal/mole)	m	Comments
1	Butkovich and Landauer (161), (162)	about ½-4 bars	-	m=2.96 *-see 1)	1)* for minimum creep rate, averaged value.
	Shear constant σ	-5°C			2) the strain rates (for a given stress) were about 100-1,000 times slower than the easy glide experiments (Table III.I, No.7).
2	Jellinek and Brill (220)	½ bar	-	-	1) ½° "misallignement" from perfect hard glide. 2) Only one "hard glide experiment". 3) No quantitative treatment but an inspection of their curves shows that hard glide is 20-30 times slower than easy glide.
	Tension, constant σ	-5°C			
3	Higashi et al (158), (159), (189)	100-200 bars	14	7	1) Formation of voids. 2) Yield Stress 10-20 times higher than for easy glide (Table III.I, No.4).
	Tension constant $\dot{\epsilon}$	-10°C to -20°C			

considers the Peierl's Stress mechanism (184) and Friedel's mechanism (192) of thermally activated cross slip from the basal into the prismatic plane. Tegart considers that, in view of the etch pit studies of ice, the latter is the more likely explanation for the non-basal slip in ice.

To further this discussion, we need now to consider direct observations of dislocations in deformed ice.

(c) Observations of Dislocations in Ice

Etch pit studies have for some time been regarded as a potentially useful tool in the studies of dislocations in ice. In addition Higuchi (193) has shown that the etch pits may be used as a means of determining the orientation of the c and a axis in an ice crystal. It has not always been certain that surface etch-pits correspond to the direction of emergence of a dislocation at the surface. However the identification of etch pits with dislocations was suggested by the marked dependence of etch pit densities on the mechanical workening of ice. The effect of vibration (Bryant and Mason (194)), mechanical polishing (Muguruma (195)), or shear stresses of the order of bars (Muguruma and Higashi (196)) on an ice crystal is to increase the density of etch pits from 10^5-$10^6/cm^2$ to 10^6-$10^7/cm^2$. (A particularly striking example of this effect was obtained in the hardness studies (Fig.IV.XI).) It is believed that this increase is an indication of dislocation multiplication caused by the applied stresses during mechanical treatment.

Studies of etch pits (i) in the base of large thermal etch pits (Muguruma and Higashi (197)), (ii) on the prism planes of plastically deformed ice crystals (Muguruma (258)), have been interpreted as evidence for a) the cross gliding of dislocations on (non basal) prismatic $\{10\bar{1}0\}$ and possibly pyramidal $\{11\bar{2}2\}$, and b) the cross slip between basal planes. Even more specifically:

1) the etch pit-channel effects on the basal planes of deformed (0.1 bars) ice (196) have been interpreted as arising from vacancy trails and indicate the directions of motion of dislocations. Their characteristics suggest the following dislocation movements:

screw dislocations; $\{10\bar{1}0\}\langle\bar{1}\bar{1}23\rangle$, and $\{11\bar{2}2\}\langle\bar{1}\bar{1}23\rangle$ glide systems

mixed dislocations; $\{10\bar{1}0\}\langle11\bar{2}0\rangle$ glide system.

2) the spiral etch pits observed in ice crystals ((198),(199)) have been interpreted as suggesting screw $\langle0001\rangle$ non basal dislocations.

However the "Lang X-ray diffraction topography technique" as used by Hayes and Webb ((200),(201)) show only basal $\langle11\bar{2}0\rangle$ dislocations. Observations were made of basal plane loops, cross-slip (of $\langle11\bar{2}0\rangle$ dislocations)

on probably $\{1\bar{1}01\}$ pyramidal planes, dislocation reactions, and prismatic punching; however there was no evidence for widely separated partial dislocations (in contrast to Wakahama's models, mentioned earlier) or for dislocations with Burgers vectors not lying in the basal plane.

Hayes and Webb give alternative explanations for the etch pit observations, which do not involve the concept of non basal dislocations. However Muguruma (199) argues that non basal dislocations, if they existed, would not be very noticeable in Hayes and Webb's diffraction pictures. It is important to note that the Lang technique is only useful for lightly strained ice crystals. However we have already seen that non basal glide is much harder than basal glide. It is therefore reasonable to say that the "Lang technique", while an extremely useful tool for studying low densities of basal dislocations in ice, is not really suited for studies on ice samples which have been highly stressed in order to initiate non basal glide.

We note therefore that there are different ideas on how ice undergoes non-basal glide. It is apparent from the above discussion ((a)-(c)), that while a certain amount is known about the general properties of ice single crystals, there also remains a number of problems to be explained. In addition, the unusual glide behaviour described by Tamman and Salge (153), and rare occurrences of "easy bending of ice crystals", are strange effects which will require better understanding.

Bearing all this in mind, we now turn to the more complicated creep of polycrystalline ice.

(d) The Creep of Polycrystalline Ice

Considerable reference will be made, in this thesis, to the flow law of polycrystalline ice as described by Glen (equation (3.3)). The reason for this is that apart from its general usage in glaciology, there is a general similarity between the ice specimens (see Sec.2.9) and the stress-temperature ranges used in Glen's experiments and some of the experiments described in this thesis (Chapters IV, V). In order to understand the concept of steady state creep in ice, we consider typical strain-time curves from Glen's ((1),(2)) and Steinemann's ((147),(148)) uniaxial compressional and tension tests (Fig.III.VI). It is seen that for stresses of about 6 bars, three very

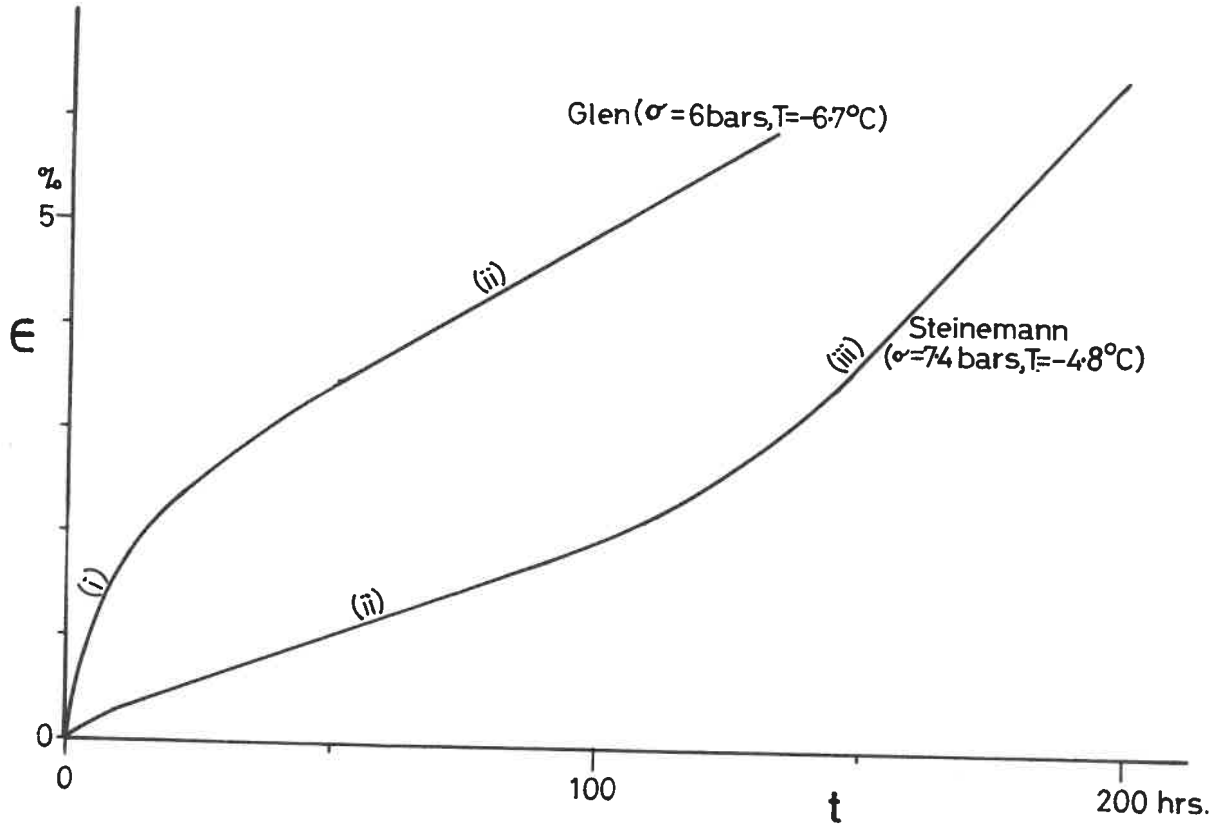

Fig.III.VI Typical Creep curves for Polycrystalline Ice illustrating the 3 stages (Sec.3.6,d).

distinct regions of creep behaviour are apparent. These are referred to, in order of occurrence, as:

(i) Transient Creep (curve, cubic form),
(ii) Steady State Creep (straight line),
(iii) Accelerating Creep (straight line but with slope greater than that in (ii)).

Andrade ((202),(203)) has shown that for many polycrystalline substances, the strain is proportional to the cube root of the time in the transient creep regime. Glen found that reasonable agreement with this law was obtained from his tests on polycrystalline ice. More specifically, Mott (204) has related the constant of proportionality to the steady state creep rate (see Sec.4.10). The steady state creep region is characterised by the straight line portion of the creep curve after the transient creep effects have died away. The slope of this straight line is known as the steady-state-creep-rate $\dot{\epsilon}$ and its variation with temperature and stress is given by Glen's law (equation (3.3)). The accelerated creep region is seen in the creep curves as a region of increased creep rate which supersedes the steady state creep. The time period to the onset of this accelerated stage is clearly very stress dependent. The reason for this acceleration is believed to be a recrystallisation effect producing grains with their basal planes preferentially oriented in the plane of maximum shear. We have seen that the basal plane in ice is one of easy glide, and therefore a preferred orientation such as this would produce accelerating creep. In fact Steinemann showed that a preferred orientation, such as that described above, was present in his ice crystals which were deformed at $-4.8^{\circ}C$. In addition he showed that the recrystallisation coincided with the onset of accelerated creep. In the absence of any contrary observations one can reasonably assume this explanation to hold good.

Glen made two types of analysis of his creep curves by

(i) calculating the minimum creep rate on each curve,

(ii) using Andrade's law, calculating $\dot{\epsilon}_{\text{steady state}}$. In this way the effects of transient and accelerated creep could be eliminated.

Using these two analyses, Glen obtained the parameters:

m = 3.2, using analysis (i)

m = 4.2, using analysis (ii)

Q = 31.8 k.cal/mole (excluding the -0.02°C results)

$A_1 = 7 \times 10^{24}$ years^{-1}. bar^{-m}.

Clearly as there is an earlier onset of accelerated creep with the larger stresses, the two analyses will give similar $\dot{\epsilon}$ values for the lower stresses only. Analysis (ii) is obviously more meaningful.

We now consider other work on ice over a wider range of experimental conditions. We must first note that flow laws other than that given by Glen (Equation (3.3)) have been used by other workers, viz.

(i) $\dot{\epsilon} = a\sigma + b\sigma^m$ (3.4)

(ii) $\dot{\epsilon} = A''.\sinh(\alpha\sigma)^{m'}.\exp\left(\frac{-Q}{RT}\right)$ (3.5)

where A'', α, m', a, b are suitable constants, a and b being temperature dependent. The reasons for these alternative flow laws are (i) that at low stresses it is to be expected that a viscous shearing of grain boundaries will predominate the deformation (see for example Cottrell (205) and Garofalo (175) for more detailed discussions of this effect), (ii) that at higher stresses, deviations from Glen's law are apparent in that m is shown to increase with increasing stress. McQueen, Wong and Jonas (206) for example have shown that for aluminium, flow law (ii) gives a far better fit than Glen's type of law to their data. (Flow law (ii) of course has more arbitrarily adjustable constants than Glen's flow law). It is the writer's opinion that the only physically meaningful use of these laws is to use (i) to allow for deviations from Equation (3.3) at low stresses due to the viscous effect, and (ii) to allow for deviations from Equation (3.3) at higher stresses where Equation (3.3) would indicate that m is stress dependent.

The results of several workers show wide variations in the critical parameters A', A'', m, m', and Q using these analyses. However it can be stated that while there are large variations in the A values (an order or so difference in magnitude), the differences in the m and Q parameters are not so large. Apart from the obvious reasons, such as different grain sizes, sample purity and preferred orientations for the wide scatter of results, the writer believes that part of the discrepancy lies in the different analyses used. The different stress systems present in many of the experiments have been related using an "octahedral flow law" defined by Nye in his analysis

of glacier flow ((207),(208)). It is therefore essential that we briefly consider the implications of this octahedral representation.

Glen (209) has discussed this problem at some length. His tensor analysis is briefly outlined here. (The usual conventions for tensor suffixes are used). Using relations between second rank tensors (such as stress and strain), the generalised flow law becomes somewhat complex but includes three invariants of the stress tensor. The first of these Σ_1 is defined as:

$$\Sigma_1 = \sigma_x + \sigma_y + \sigma_z = 3P \qquad (3.6)$$

where $\sigma_x, \sigma_y, \sigma_z$ are the principle stresses, and P the hydrostatic pressure thus defined.

However it is known that provided temperatures are measured relative to the pressure melting point, hydrostatic pressure has little or no effect on the flow law of ice ((210)-(212),(148)). Hence Σ_1 must not enter the flow law and this is ensured by defining the stress deviator σ'_{ij}:

$$\sigma'_{ij} = \sigma_{ij} - P = \sigma_{ij} - \frac{1}{3}\Sigma_1 \qquad (3.7)$$

However, because of the lack of experimental data, it is difficult to know what are the exact effects of the second and third stress invariants on the flow law. In order to use Glen's flow law for the different stress systems present in glaciers, Nye assumed that (i) the flow law was independent of the third invariant, (ii) the ice deformed as an incompressible solid, and (iii) that the components of the stress deviator and strain rate were related in a simple way:

$$\dot{\epsilon}_{ij} = \lambda \sigma'_{ij} \qquad (3.8)$$

Equations (3.3), (3.6)-(3.8), can be combined to give the sort of octahedral relation used by Nye, viz:

$$\dot{\gamma} = A''.\tau^{n}.\exp\left(\frac{-Q}{RT}\right) \qquad (3.9)$$

where (i) the octahedral strain rate is defined as:

$$2\dot{\delta}^2 = \dot{\epsilon}_{ij}\dot{\epsilon}_{ij} \qquad (3.10)$$

which for three mutually perpendicular linear strain rates $(\dot{\epsilon}_x, \dot{\epsilon}_y, \dot{\epsilon}_z)$ becomes: $2\dot{\delta}^2 = \dot{\epsilon}_x^2 + \dot{\epsilon}_y^2 + \dot{\epsilon}_z^2$ (3.11)

(ii) the octahedral stress is defined as:

$$2\tau^2 = \sigma'_{ij}\cdot\sigma'_{ij} \qquad (3.12a)$$

which for three mutually perpendicular stress deviators $(\sigma'_x, \sigma'_y, \sigma'_z)$ becomes:

$$2\tau^2 = \sigma'^2_x + \sigma'^2_y + \sigma'^2_z \qquad (3.12b)$$

Using equations (3.6) and (3.7) for σ'_x etc., a little algebra will show that equation (3.12a) becomes

$$\tau^2 = \frac{1}{2}\sqrt{(\sigma_x - \sigma_y)^2 + (\sigma_y - \sigma_z)^2 + (\sigma_z - \sigma_x)^2} \qquad (3.12c)$$

This is the form of equation that is used in many of the papers to be discussed below.

Glen shows that using Nye's assumptions leads to a flow law of the form:

$$\dot{\epsilon}_{ij} = B.(\Sigma'_2)\sigma'_{ij} \qquad (3.13)$$

where B is the particular flow law function used, and Σ'_2 is the second invariant of the stress deviator tensor defined as

$$\Sigma'_2 = \tfrac{1}{2}\sigma'_{ij}\sigma'_{ij} = -(\sigma'_x\sigma'_y + \sigma'_y\sigma'_z + \sigma'_z\sigma'_x) \qquad (3.14)$$

The validity of equation (3.13) (or the equivalent equations (3.8)-(3.12)) may be tested in two ways:

(i) By comparing the results obtained (Steinemann (148)) for shear and uniaxial stress respectively,

(ii) comparing shear and compression strain rates for an experiment in which the specimen is subjected to simultaneous shear and compression (Steinemann (148)).

Glen shows that Nye's equations do not really show agreement with the results obtained in either (i) or (ii). These two tests however illustrate two ways in which the octahedral law can fail:

(i) Nye (207) has shown, using the octahedral representation to compare the results of uniaxial compression with those of uniaxial shear, that the compressive stresses and strain rates should be divided and multiplied respectively by $\sqrt{3}$. It can be shown (using Nye's equations) that this is equivalent to saying that for the same values of compressive stress and shear stress, the values of strain rates for compression and shear should differ by a factor of $(3)^{n+1/2}$ (shear strain rates being the higher value). In fact the results of Steinemann suggest that this difference is smaller than the $(3)^{n+1/2}$ factor predicted using Nye's equations. However for this case where octahedral comparison is made between two simple stress systems (shear and compression), the failure of the octahedral representation to predict the correct numerical factor can in principle be easily circumvented; by performing a series of experiments in which compression and shear stresses are applied consecutively to the same specimen under the same experimental conditions, a new empirical factor could be determined. By performing such experiments over wide ranges of temperature, stress, and type of specimen, the new empirical factor could be obtained. It is the writer's opinion that much better agreement could be achieved between the shear and compressive tests using this empirical approach rather than the octahedral representation. Furthermore, it seems somewhat pointless continuing the common practice of reviewing the results of shear and compressive stress experiments by different workers until this has been tried.

(ii) Whereas case (i) illustrates how the octahedral representation can be "wrong by a constant factor", the more complex stress systems are seen to produce much greater difficulties of treatment. Glen shows that the difference between experiment and octahedral theory cannot be expressed as a simple correction

factor when the more complex stress systems, such as Steinemann's simultaneous shear and compression, are considered. Complex stress systems are present in Glaciers and therefore the use of the octahedral treatment (for example Nye, Weertman et al. (207), (208), (213), (140)) cannot always be strictly correct here. (Glen discusses these examples in more detail.) Hence the values for the "absolute rate factor" (A' as in Equation (3.3)) derived from Glaciological and hole closure observations cannot be really relied upon. However the values obtained for the parameters m and Q will probably be more reliable.

Bearing in mind all these complications, Table III.III gives a summary of some of the creep experiments on polycrystalline ice. For reasons which should be readily apparent from the discussion above, the absolute rate parameter A' will not be considered.

In Table III.III, the data in Nos.5) - 9) show deviations from Glen's law ($\sigma < 1$ bar) presumably because at low stresses the viscous-grain-boundary-sliding mechanism becomes important. The interpretations of the data in Nos. 9) - 13) depend, either in part or whole, on the octahedral type of representation.

Table III.III makes it clear that there are many different ideas on the correct values for Q and m. However as with the data in Table III.I for easy glide in single crystals, it can be seen that there are similar definite general trends showing variations in Q and m over the different stress and temperature T ranges. (This was first pointed out to the writer by Walker (155).) However the trends here are much more definite than those in Table III.I. Particularly pertinent in this respect are the results of Steinemann (No.2) on polycrystalline ice. The general trend is one in which Q increases from about 10 k.cal/mole below - 30°C., to above 30 k.cal/mole near 0°C. If instead of a general consideration of the data in Table III.III, one examines each set of data separately, it is found that there are suggestions of a sharp change in the rate of increase of Q (i.e. a temperature "kink") at a temperature T_c between -7°C and -15°C, say. (For similar kinks with other polycrystalline materials, see for example Atkins and Tabor (173)). The

Table III.III. Activation Energies Q and Stress Exponents m concerned with the Deformation of Polycrystalline Ice

No.	Reference Method	Stresses Temperature	Q (k.cal/mole)	m	(i) Analysis Used Comments
1	Glen (1), (2)	1-11 bars	31.8 §(ii)	4.2 § (iii)	(i) Equation (3.3) used. (ii) For 3 temperatures: 1.5°C, -6.7°C, -12.8°C. (the -0.02°C results are excluded. (iii) Using Andrade's law.
	Compression, constant σ. Grain size, ~ mms.	-0.02°C to -13°C. (4 temperatures)			
2	Steinemann (147), (148)	0.7-20 bars	Variation: 13.8-38.5 with σ and T § (ii), (iii)	Variation: 1.85-4.16 with σ § (iv)	(i) Essentially Glen's Equation (3.3) used. (ii) See Fig.IV.X. (iii) For example, σ = 10 bars, variation: Q = 13.8 (at T = -22°C) - 33.8 (at T = -1.9°C). (iv) See Fig.IV.VIII
	" and " tension	-1.9°C to -22°C			
3	Nayar (215)	6.47 bars	"kink": 15, 105 §(ii)		(ii) Curves show a definite kink at about -10°C: Q = 15 (-10° to -27°C), Q = 105 (-10°C to -3°C).
	Tension, constant σ.				
4	Raraty and Tabor (216)	about 10-20 bars	12 §(ii)	-	(i) Essentially Glen's Equation (3.3) used. (ii) These experiments do not really measure the flow rate of ice - Sec.5.4 shows rather, that the friction and adhesion experiments reflect the flow characteristics of the surface layers of ice.
	Adhesion strength	about -3°C to -30°C			

Table III.III (Continued)

No.	Reference Method	Stresses Temperature	Q(k.cal/mole	m	(i)	Analysis Used Comments
5	Butkovich and Landauer (217)	10^{-2}-10^{-1} bar	14.3	1 §(ii)	(i)	Equations (3.4) and (3.5) used.
					(ii)	Results therefore imply that the "viscous sliding" effect predominates at these low stresses
	Compression, constant σ. Two grain sizes, 3 mms. and ~ cms.	-1.3°C to -18.9°C.				
6	Mellor and Smith (218)	½-20 bars	11.3 §(ii)	3.5	(i)	Equation (3.4) used.
					(ii)	Some of the curves give a "hint of kinking" at about -15°C.
	Compression, constant σ. Grain size ~ 1/mm.	-½°C to -34½°C				
7	Landauer (219)	0.002-5 bars	14 §(ii)	1(.002 - .1 bars), ~3 (1-5 bars) §(iii)	(i)	Essentially Equation (3.4) used.
					(ii)	Q averaged over 3 temperatures, error ± 20 %
	Compression, constant σ and constant $\dot{\epsilon}$, Compressed SNOW.	-5°C, -10°C, -20°C.			(iii)	Results therefore imply that the "viscous sliding" effect predominates at these low stresses.
8	Jellinek and Brill (220)	0.35-2½ bars	16.1 §(iv)	1 §(ii), (iii)	(i)	A viso-elastic formula was used.
					(ii)	Results show that a certain "viscous effect" predominated at these stresses.
	Tension, constant σ. Grain size 1-2 mms.	-5°C, -10°C, -15°C.			(iii)	It was found that $\dot{\epsilon} \propto t^{-\frac{1}{2}}$.
					(iv)	Averaged over the 3 temperatures.

Table III.III (continued)

No.	Reference Method	Stresses Temperature	Q(k.cal/mole	m	(i)	Analysis Used Comments
9	Dillon and Anderland (221)	about 6-15 bars §(ii)	11.4 §(iii)	4.6-6.8 §(iv)	(i)	Equations (3.3) and (3.5) used.
					(ii)	Octahedral stress values.
					(iii)	Averaged over 3 temperatures (-10°C to -1½°C).
	Compression constant σ, Grain size 1-2 mms or less	-1½°C to -14°C (4 temperatures)			(iv)	Results show better fit to Equation (3.5) at these high stresses - but see preceeding discussion on octahedral analysis; Equation (3.3) analysis gives varying m for T= -4°C to -14°C.
10	Butkovich and Landauer (161), (162)	-½ - 10 bars	-	2.96 §(ii)	(i)	Glen's Equation (3.3) used.
					(ii)	Minimum $\dot{\epsilon}$ used, therefore m is really higher than 2.96.
	Shear, constant σ.	-5°C			(iii)	Important feature: $\dot{\epsilon}$ polycrystal $\simeq \dot{\epsilon}$, hard glide - single crystal $\simeq$ (100-1,000) $\dot{\epsilon}$, easy glide - single crystal.
11	Higashi (222)	2-6 bars §(iii)	37.8 §(iv)	~3 §(ii), (v)	(i)	Glen's Equation (3.3) used, but see (v).
					(ii)	Analysis uses octahedral representation for this shear system.
	Hydrostatic collapse of hollow ice cylinddrs. 2 Grain sizes, several mms and ~ cms.	-1.9°C, -4.2°C, -10.8°C.			(iii)	Circumferential stress.
					(iv)	Only 3 temperatures, but it can be seen that there is a "hint of kinking" of Q at above -10°C.
					(v)	Indications of m increasing with stress.

Table III.III (continued)

No.	Reference Method	Stresses Temperature	Q(k.cal/mole	m	(i) Analysis Used Comments
12	Jellinek (223)	1-3 bars §(ii)	14.1 §(iii)	- §(i)	(i) Equation (3.5) used. (ii) Circumferential stress. (iii) Only 4 temperatures, but it can be seen that there is a "hint of kinking" at -10 ± 5°C. (iv) Analysis uses octahedral representation for this shear stress system.
/of thick wall	Hydrostatic collapse/ cylinders. Snow-ice, grain sizes 1-2 cms.	-5½°C -20°C			
13	Nye (207)	0.1-5 bars §(ii)	-	3.07 §(iii)	(i) Glen's Equation (3.3) used. (ii) Octahedral stress values. (iii) Octahedral representation used for this shear stress system - however additional longitudinal stresses may be of importance. (iv) Presumably temperatures close to the melting point - see Sec.7.2, (i)(3).
	Analysis of data on contraction of horizontal tunnels in glaciers.	§(iv)			

effect of increased stress σ is also to increase Q, but not so markedly as with temperature (see Fig.IV.X). Further experiments may also show that T_c is a function of the stress as has also been found for polycrystalline zinc (174).

These variations of Q (and m) with stress and temperature may partly account for the large differences in the creep parameters for ice, as measured by different experimenters. It is believed by the writer that these variations, together with the uncertainties involved in the use of the octahedral law, would explain much of the disagreement in the creep parameters (particularly A) deduced from the different experiments. More experiments of a unifying nature are needed.

It is now necessary to consider what are the controlling mechanisms of deformation in polycrystalline ice. Taylor (224) has shown that an individual grain in a polycrystalline material can be deformed at constant volume into any arbitrary shape as long as slip can occur in five independent directions. If the number of independent directions is less than five, certain grains will oppose the deformation more strongly than others; the rate of slip in these "badly oriented" grains will in general limit the rate of deformation of the aggregate. As ice has only one "easy" slip plane (i.e. the $\{0001\}$ basal plane), this means that the rate of deformation of polycrystalline ice will be limited by the grains which are not favourably oriented for basal slip. A complete description of the processes in the creep of polycrystalline ice would include non basal glide, diffusion of grain boundaries leading to grain growth, viscous-inter-crystalline-sliding and rotation, recrystallisation, and eventually cracking (see for example, Gold (225), Shoumsky (226), Ivanov and Lavrov (229), and Glen (227), (228)). Statistically grain boundary cracking accounts for about one quarter of the number of cracks formed; however crack formation is a process which in general is more important in high stress experiments (above 10-70 bars - see Gold (230) - (234), Jellinek (111), Raraty and Tabor (216), and Butkovich (235)). The low stress experiments (Nos. 5, 7, 8 in Table III.III, see also Meier (236)) suggest that "viscous-grain-boundary-sliding" only becomes really important when the stresses are very low - (0.002-0.1) bars, say. For medium stresses it would seem, to the writer, that one of the most crucial experiments performed was that of Butkovich and Landauer (Table III.III, No.10). They showed that there is close agreement between the creep rate value for polycrystals and single crystals oriented for hard-non-basal glide. However the creep rates for single crystal easy glide was 100-1,000 times faster. Thus while the other processes described above may play a part in the deformation of polycrystalline ice, it would seem that the rate controlling factor is the hard-non-basal slip in the grains which are unfavourably oriented for basal glide. The writer believes that this is a more likely explanation than the treatment by Weertman (185) which involves the resolving of stresses onto the basal planes of the individual grains.

In concluding this Section, we note that there are many difficulties in generalising Glen's flow law for different temperature and stress ranges, and

for the more complex stress systems. Using the octahedral representation to overcome these difficulties, Nye has made much fruitful use of the flow law. However in view of the limitations and uncertainties of this representation, it would seem to the writer that it is in the interests of Glaciology (and the physics of ice) that further complex stress system experiments should be performed in the near future. This would provide for a more generalised flow law and would relate the laboratory experiments more closely to the stress conditions occurring in glaciers.

CHAPTER IV

THE HARDNESS OF ICE

A. General Account

4.1 Introduction

(i) The Meaning of Hardness.

This chapter concerns the main bulk of this research. Because it involves the results of many experiments, it would not be practical to deal fully with all these experiments. For this reason these experiments will be grouped together in a more convenient order. However a list of all the hardness experiments is given in Sec. 4.2.

In order to facilitate the understanding of these experiments, a brief discussion is given here on the physical meaning of "hardness" and how meaningful this concept is when applied to ice within, say, 15°C of its melting point.

In these hardness experiments, a hard indenter (of some regular geometrical shape) is pressed into the surface of the ice with a known load L for a specific time t. After removal of the indenter, the projected area A of the permanent indentation is measured. The diameter d of the indentation does not change considerably (due to elastic recovery effects) during removal of the indenter. Hence it is assumed that:

$$A = \frac{\pi d^2}{4} \tag{4.1}$$

The Hardness p (or H) is defined as the ratio of the load to the projected area of the permanent indentation, i.e.,

$$H = p = \frac{L}{A} \tag{4.2}$$

It is usually measured in units of kgs./mm^2 or bars and has the same dimensions as a pressure. Clearly a large indentation area (for a given load) would imply

that the ice is flowing readily. Hence low hardness values indicate large flow rates while large hardness values indicate small flow rates. Now, in particular Tabor ((237) - (243)) has applied these ideas to the case of an ideal plastic material (i.e. $n \to \infty$ in a flow law like equation (3.3)). However nearly two-thirds of the mean pressure of contact is in the form of a hydrostatic pressure and only one-third remains effective in producing plastic flow. Tabor shows that because, in general, hydrostatic pressure itself plays no part in producing plastic flow of metals (this is also approximately true for ice, see Sec.3.6 (d)), then

$$\frac{1}{3} p \simeq Y \quad \text{or} \quad P \simeq 3Y \qquad (4.3)$$

This equation is seen to be approximately true for a wide variety of indenter geometries. However it is found, for example, that deviations occur when a spherical indenter (with radius R) is used and $d \sim 2R$. This is because the geometry of the indentation changes with $\frac{d}{2R}$.

But for a non-ideal plastic, the Yield stress Y is not a single valued parameter, but varies with strain rate (i.e. m is finite, as in equation (3.3)). In terms of a hardness experiment, this means that the indenter is continually sinking into the material, and therefore the hardness p decreases with time t. The time parameter t can therefore be regarded as a measure of the effective strain rate. In a more recent kinematic treatment of hardness, Tabor et al. (244) extend these ideas to non-ideal plastics with a flow law form analogous to that of ice (equation (3.3)). It is seen that the parameter $\frac{1}{t}$ can be considered as proportional to the effective strain rates present in the hardness experiments. These ideas are considered in a little more detail in Section 4.10.

(ii) Two Regimes of Hardness with Ice.

Fig.IV.I shows a set of preliminary results on the hardness of ice. It will be shown in Section 4.4 that these particular results are not very accurate, but they are only used here to illustrate the main points. The deformation can be divided into two distinct regimes:

Firstly for temperatures below about $-1.5^{\circ}C$ (for these particular results), the hardness values for a given loading time decrease exponentially with

increasing temperature, and at a constant temperature decrease with loading time in a power law form. This behaviour resembles that of metals at elevated temperatures and may, in a similar way, be explained in terms of Glen's Creep law. For this reason, this sort of deformation will be called the (colder) "creep regime" deformation.

Secondly at above about $-1.5^{\circ}C$ (for these particular results), the hardness drops off markedly. It appears that this transition temperature ($-1.2^{\circ}C$, here) corresponds to the pressure melting temperature of the ice under the hydrostatic pressure imposed by the indenter (see Sec.3.5 (d)); i.e. the hardness curves intersect the pressure melting curve at approximately this same temperature ($-1.2^{\circ}C$). Correspondingly this "hardness drop" is interpreted in terms of pressure melting phenomena. There are complications in understanding the exact mechanisms involved, but by varying the experimental parameters in these hardness tests, a clearer picture is gained. It will be shown that the thermal conductivities of the ice and the indenter, the loading time t, the motion of water films, and the presence of liquid like grain boundaries are relevant factors.

In parallel with the two regimes of hardness behaviour, it is found that there is a correspondingly marked change in the general nature of the deformed ice: (1) Polarised light and etchant-replica techniques reveal the grain structure of these deformed zones. It is found that in these zones, the indentation initiates recrystallization of the ice. Now, whereas the ice deformed in the creep regime (temperatures below $-1.2^{\circ}C$) shows recrystallized grain sizes of about 0.5 mm, with the ice deformed in the pressure melting range (above $-1.2^{\circ}C$) the recrystallized grains are consistently larger and usually about 0.2 - 0.4 mms size. (2) Optical examination and etchant-replica studies also show two types of behaviour of the air bubbles in the deformed ice. In the cold-creep-regime, the deformation zones become "cloudy", whereas in the warm-pressure melting-regime the bubbles disappear producing a region of optically clear ice beneath the indenter. These features are also explained in terms of specific mechanisms operating in the creep and pressure melting regimes. A general picture of these features is shown in Fig.IV.I.

4.2 List of Experiments

Table IV.I Hardness Experiments

Code No.	Nature of Experiment	Time Range / Loads	Indenter Geometry / No. of Indentations	Nature of Specimen / Temperature		Comments
2A	STATIC HARDNESS Preliminary experiment. Motion monitor used for determining rate of "sink in" of indenter, Sec.4.4 (i).	Up to 10^4 secs.	1" diam. sphere, 135° Cone. (steel), (brass).	Highly polycrystalline ice.	(i)	Elastic Recovery considered.
					(ii)	Concluded equation (4.3) approximately independent of indenter geometry.
		84,54 kgs.	8 indentations	-0.57°C to -10.36°C	(iii)	Recrystallization effects noticed.
5B	STATIC HARDNESS Semi-preliminary experiment. Large grain specimens show the recrystallization habits very clearly, Sec.4.4(ii).	$10, 10^2, 10^3$ secs.	2½" diam. sphere. 60°, 105°, 135° cones. (steel), (brass)	Clear columnar grained ice.	(i)	Pressure melting treatment.
					(ii)	Creep regime interpreted in terms of Glen's law.
					(iii)	Recrystallization effects systematically observed.
		95 kgs.	33 indentations.	-0.02°C to -11.93°C		
6C	STATIC HARDNESS More accurate experiment, particularly in the pressure melting regime. Wide range of loading times, Sec.4.5.	1½.10, $10^3, 10^4$ secs.	Standard Vickers 136° Pyramid. (steel)	Highly polycrystalline ice	(i)	Concluded transition temperature varies with time of loading t_f.
					(ii)	Deduced m as a function of stress.
		92 kgs.	38 indentations	-0.08°C to -11.26°C		

TABLE IV.I (Continued)

Code No.	Nature of Experiment	Time Range / Loads	Indenter Geometry / No. of Indentations	Nature of Specimen / Temperature	Comments
8D	STATIC HARDNESS Low thermal conductivity indenter used, Sec.4.6.	$1\frac{1}{2}$.10,10^2 10^3 secs.	Standard Pyramid (ebonite)	Highly polycrystalline ice	(i) Concluded that pressure melting effect not so pronounced as with steel indenters.
		89 kgs.	24 indentations.	-0.11° to -11.48°	
7E	DYNAMIC HARDNESS Preliminary experiment (IMPACT EXPERIMENT) Sec.4.7.	about 10^{-4}sec.	Variety of spheres (steel)	Highly polycrystalline ice	(i) Concluded "rebound velocity" for impact on ice was negligible.
				approx. -5°C	
7F	DYNAMIC HARDNESS (IMPACT EXPERIMENT) Sec.4.7.	(2.5-11.4) x 10^{-4}sec.	Spheres (steel)	Highly polycrystalline ice.	(i) Concluded that there is a pressure melting effect at -3°C or above,
		0.53,2.04 lb.spheres.	30 indentations	-0.32°C to -11.87°C	
9G	DYNAMIC HARDNESS (IMPACT EXPERIMENT) Sec.4.7.	(1.0-8.9) x 10^{-4}sec.	Spheres (steel)	Highly polycrystalline ice.	(i) Confirmed (i) in 7F. (ii) Failed to differentiate between results with different spheres.
		0.02195, 0.496, 1.98 lb spheres.	100 indentations	-0.12°C to	

TABLE IV.I (Continued)

Code No.	Nature of Experiment	Time Range / Loads	Indenter Geometry / No. of Indentations	Nature of Specimen / Temperature	Comments
10H	STATIC HARDNESS Observations on the movement of bubble layers in deformed ice, Sec.4.9.	10,30,100, 300,10^3 10^4 secs.	2" diam. sphere (steel)	Highly polycrystalline ice	(i) Concluded "bubble loss" is not a temperature gradient effect.
		128 kgs.	6 indentations.	0^oC	
10I	STATIC HARDNESS Measurement of "lip volumes", Sec.4.8 (i).	10,30,100, 10^3,10^4 secs.	2" diam. sphere (steel)	Highly polycrystalline layers sandwiched in clear columnar grained ice.	(i) Made quantitative estimates of importance of regelation effect. (ii) Observed that the "viscous water layers" are very small at $t = 10^3$, 10^4 secs.
		128 kgs.	5 indentations	0^oC.	
11J	STATIC HARDNESS Observation of bubbles during indentation using a "remote control camera", Sec.4.9.	up to 3,300 secs.	2" diam. sphere (steel)	Columnar grained ice	(i) Concluded "bubble loss" was very small in single crystals.
		approx. 80 kgs.	3 indentations	0^oC.	

TABLE IV.I (Continued)

Code No.	Nature of Experiment	Time Range Loads	Indenter Geometry No. of Indentations	Nature of Specimen Temperature	Comments
10K	(Subsidiary Experiment) Measurement of densities of bubbly ice specimens, Sec.4.8 (ii)	-	-	Highly polycrystalline ice	(i) Typical density value of 0.86 ± 0.02 gm/cc.
13L	(Subsidiary Experiment) Measurements of electrical conductivities of melted ice from 2A-10K samples.	-	-	Ice from experiments 2A-10K.	(i) Results given in Chapter II.

TABLE IV.II Examination of Deformed Ice

Technique of Observation	Experiment No.	Nos. of Observations
(i) Crossed Polaroid viewing of thin sections.	2A	9
(ii) Ordinary optical examination of sections	"	
	"	
	5B	
	6C	34
	7F	3
	10H	8
	11J	6
(iii) Etchant-Replica examination	8D	1
	9G	61
	10H	32
		18

Table IV.III List of extra apparatus constructed for the hardness experiments

Experiment No.	Constructions
5B	Variety of conical and spherical indenters.
6C	Pyramidal indenter (steel).
8D	(i) Pyramidal indenter (ebonite), (ii) General thermal insulation of the specimen clamping system and brass beam.
7F	(i) Construction of "pendulum type apparatus" for impact experiments with 2 different spheres, (ii) Reconstruction of the temperature-measuring system so as to be suitable for this apparatus.
9G	(i) Construction of "sphere dropping apparatus" for impact experiments with 3 different spheres, (ii) Reconstruction of the temperature-measuring system so as to be suitable for this apparatus.
10K, 10I, 11J	Increase load range and "penetration depth" of the loading system.
11J	(i) Make (and test) a Remote Control Camera for bubble observations on specimens - operatable from outside the refrigerator, (ii) Make "perspex surround" for optical viewing of the ice specimens while held in the clamping system.

Table IV.IV List of Ice Specimens Used

Experiment No.	Type of Specimen
2A, 6C, 8D, 7E, 7F, 7G, 9G, 10I, 10K	Highly polycrystalline (described in Sec.2.9).
5B	Clear columnar grained ice (described in Sec.2.10).
10H	Clear columnar grained ice with 2 horizontal layers of bubbly polycrystalline ice "sandwiched in".
11J	Clear columnar grained ice with bubbles introduced by (i) concentration of mercury lamp rays, (ii) introduction of bubbly polycrystalline sections of ice, (iii) variation of growth method.

4.3 Accuracy of the Hardness Measurements

In the hardness experiments, the errors in temperature T and loading time t may be neglected in comparison with others.

One of the important features of these experiments is that while the hardness values are not accurate in an absolute sense, the "relative accuracies" of the hardness values in one set of experiments are much higher. This effectively means that there are substantial systematic errors common to each set of experiments in which the random errors are not so large. The resultant random errors in each set of experiments can be estimated by considering the scatter of points in the Hardness curves of Figs. IV.I or Fig.IV.VII. This is seen to be about ± 10 per cent on average but considerably less in the pressure melting region. The resultant systematic errors may be estimated by comparing the hardness curves from different sets of experiments. For example by comparing the hardness curves in Figs.IV.I, IV.III, and IV.IV, it is seen that there are systematic shifts in the hardness values of about 20-60 per cent.

The possible sources for these random and "systematic" errors are given:

Table IV.V Sources of Errors in Static Hardness Measurements

No.	Estimated Error	Source
§ (i)	~10%	Error in determining projected area of indentation. These areas are large in the pressure melting regime but small at low temperatures. This means that the fractional errors will be smaller at the former, and larger at the latter temperatures.
* (ii)	0 - 7 %	Errors due to general preferred orientation in the ice specimens. Butkovich (164) has shown that, except near -10°C, the hardness of differently oriented crystals may vary by as much as 7 % over the temperature range of these experiments. These errors will be more dominant in large grain specimens (Sec.4.4) than highly polycrystalline specimens (Sec.4.5).
§(iii)	?	In addition, the grains beneath the indenter will show some scatter in orientation about the mean preferred orientation discussed in (ii). These effects are also greater for large grain ice specimens (Fig.IV.I) than highly polycrystalline specimens (Fig.IV.VII).

Table IV.V (continued)

No.	Estimated Error	Source
* (iv)	?	Grain size may also be important.
* (v)	?	It has already been pointed out (Secs.2.8, 3.6, and Table III.III(4)) that ionic impurities may affect the mechanical properties of ice at all temperatures. In one set of experiments, the same water is used for different specimens. This means that impurity effects should be constant throughout one set of experiments.
* (vi)	2 %	The same load is usually used for each set of experiments. Estimates of its error of determination are made by normal methods.
*(vii)	10 %	Different indenter geometries are used. However the indenter geometry is usually kept the same through a particular set of experiments (e.g. sphere, Sec.4.4. Fig.IV.I; pyramid Secs.4.5, 4.6, Figs.IV.III,IV.IV.). The effect of indenter geometry on hardness has already been discussed (Sec.4.1). It is noted that the geometrical effects with a spherical indenter also vary with the relative indentation size $\frac{d}{D}$.

§ These sources produce random errors, and probably account for the scatter (average of about 10 %) obtained in the hardness curves.

* These sources produce systematic errors, and probably account for some of the "relative shifts" between hardness curves in different experiments.

It is important to remember that the relative accuracy in one set of experiments is an important parameter in this work. The credibility of the pressure melting phenomena (change of slope of each curve at the pressure melting point), and the accuracies in the determinations of Q and m both depend on these random errors. It is therefore fortunate that these random errors are much smaller than the systematic errors. Furthermore, by making a fairly large number of observations, the final errors in the Q and m computations are much smaller than those for an individual hardness value.

Equally fortunate, the absolute accuracy of these experiments is not important for this work. The only need for accurate absolute determinations would be for a determination of the constant A' in the flow law given by equation (3.3). However it has already been pointed out (Sec.3.6) that for a number of reasons, such a pursuit at present would not be very useful. In addition, the "theory of hardness" does not at present provide for accurate determinations of A' from hardness data.

These remarks have been made in general for Static Hardness tests. However the same are also generally valid for impact experiments where, if anything, the random and systematic errors are believed to be a little larger still.

B Experimental Observations

4.4 Preliminary Results on the Hardness of (i) Highly Polycrystalline and (ii) Columnar Grained Ice

This section summarises some of the results from the preliminary experiments Numbers 2A and 5K (see Table IV.I).

A variety of indenter geometries were used, viz., 1" and 2½" diameter steel spheres, and 60°, 105°, 135° brass cones. It was concluded that these different indenters gave approximately the same values for the hardness of ice when similar specimens and experimental conditions were used.

(i) Highly Polycrystalline Ice (Experiment No.2A). In this set of experiments preliminary investigations were made on the hardness, elastic recovery and structure of deformed ice in hardness experiments using a 1" diameter sphere and 135° cone indenter. The results on hardness were not very accurate and are not discussed. A rough investigation was made of the elastic recovery of the indentation after removal of the indenter. This was done by using the "vertical movement optical grating system" to determine the rate of vertical penetration of the indenter into the ice surface (see Fig.II.IV). The recovery of the indentation was determined by using a specially made micrometer system which could measure the difference in levels of the ice surface and the bottom of the indentation after recovery. These results are discussed a little further in Sec.4.15.

A crossed-polaroid study was made of the grain structure of sections cut horizontally through the indentation. It was immediately apparent that the ice in the deformed zone near the indenter had undergone recrystallisation, and that the exact nature of this recrystallization was strongly dependent on the temperature during indentation. Because the grain size of the undeformed ice was also fairly small (0.1-0.3 mms), the recrystallization zone did not contrast strongly with the undeformed ice. In addition the horizontal sections did not show very much of the recrystallized zone. For these reasons it was decided that it was necessary to do hardness experiments using large (columnar) grained ice specimens, and to cut vertical sections through the indentations for the crossed-polaroid examination. In this way a clear picture of the deformed zone and its recrystallization habits was obtainable. Such methods were used with the columnar grained ice experiments described below.

(ii) Large (Columnar) Grained Ice (Experiment No.5B) Some of the quantitative aspects of these hardness results are not as good as those in Sec.4.5 mainly because of the reasons discussed in Table IV.V ((ii), (iii), (iv) and (vii)). An additional difficulty with a spherical indenter is the measuring of the indentation diameter. This is inaccurate because the indentation edge is not so well defined as with, for example, a pyramidal indenter.

The results are shown in Fig.IV.I. A vertical line indicates the transition of the two regimes (i) the creep regime below the pressure melting temperature, and (ii) the pressure melting regime above the pressure melting temperature. The different natures of the deformed ice in these two regimes are also indicated. The most pronounced difference between the structures of the deformed ice in these two regimes is obtained from the Friction results (Figs.V.III - V.VI). This is because in the Friction experiments the resultant stresses on the ice beneath the indenter are higher and therefore the stress-induced recrystallization effects are better developed. However some individual examples of the sort of recrystallisation effects produced in these hardness experiments are shown in Figs.IV.II.

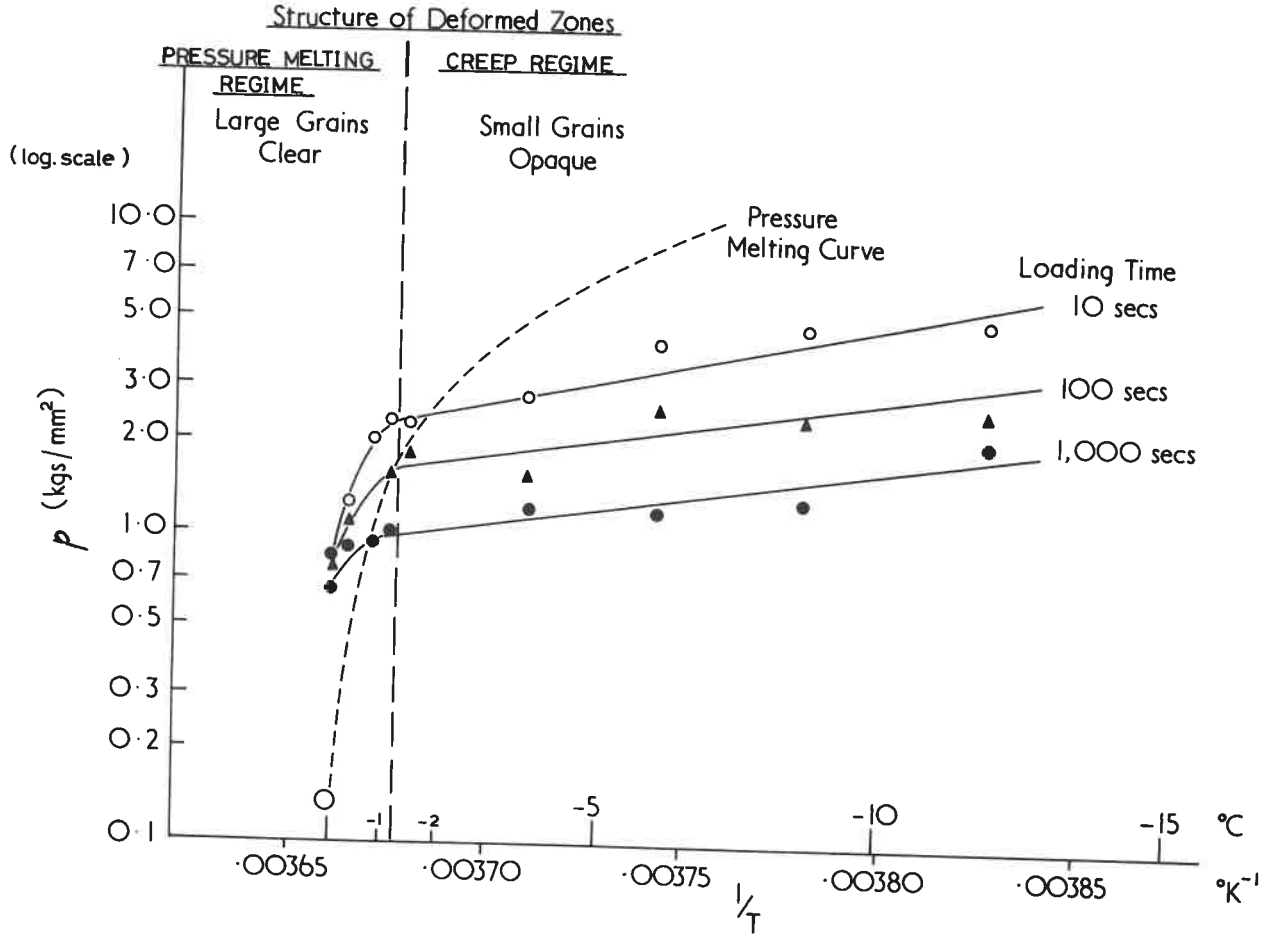

Fig. IV.I Preliminary Hardness Results (Large Grain Ice, Sec. 4.4).

Fig.IV.II.a. The Recrystallisation produced after Indentation at -1.4°C for 1,000 sec using a 2½" diameter Spherical Indenter (Secs.4.4, 4.11). x 2.5, approx.

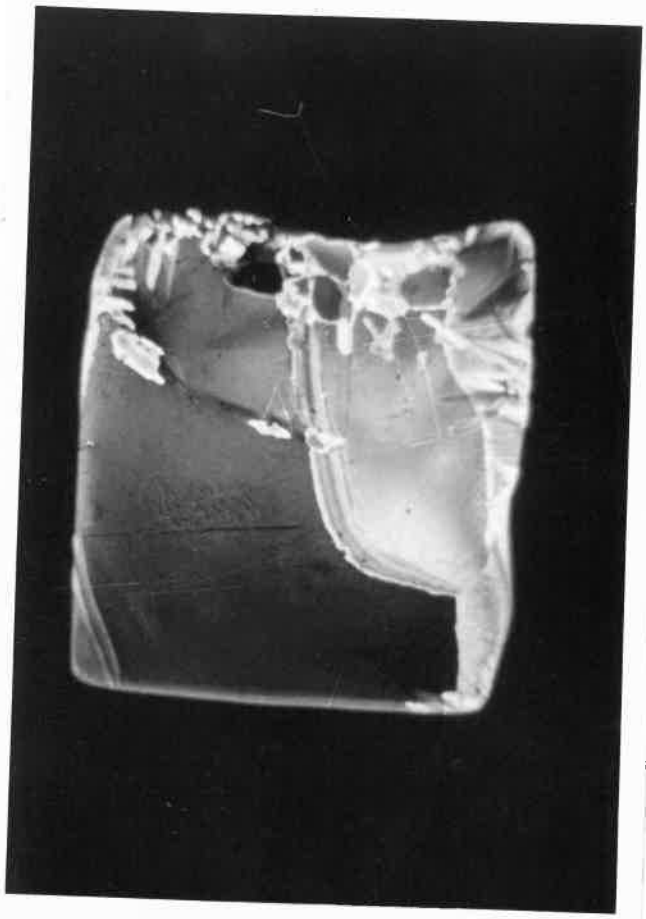

Fig.IV.II.b. The Recrystallisation produced after Indentation at -1.4°C for 1,000 sec using a 135° Conical Indenter (Secs. 4.4, 4.11).
x 2.5, approx.

The quantitative results on the hardness results yield:

$$Q = 29.7 \pm 4 \text{ kcal/mole}$$
$$m = 3.85 \pm 0.3$$

The method of determination of these constants is shown in Sec.4.10. The above results compare well with those obtained by Glen:

$$Q = 31.8 \text{ k.cal/mole}$$
$$m = 3.2 \text{ or } 4.2, \text{ the latter value being preferred}$$

(see Sec.3.6). However the results of Sec.4.5 are always used for further quantitative treatments on the hardness of ice. This is because the results in Sec.4.5 are more accurate. A particular shortcoming of these results (Fig.IV.I) is that they give the impression that the hardness curves converge in the pressure-melting regime. However the more accurate experiments of Sec.4.5 (Fig.IV.III) (performed over a wider loading time range) show that this is certainly not the case.

4.5 The Hardness of Highly Polycrystalline Ice when using a Steel Pyramidal Indenter and a Wide Range of Loading Times

These results comprise the most accurate set of hardness data in this research. Because of the sharp edges formed in a pyramidal indentation, the accuracy of measurement of the indentation area is improved. Because the grains in the highly polycrystalline ice specimens are small, orientation effects are reduced. These specimens are similar to those used by Glen (1) and therefore comparisons between his results and these is logical.

Some details of this experiment are given in Table IV.I (No.6C). The hardness curves are given in Fig.IV.III. One important feature of these results is the wide range of loading times ($1\frac{1}{2}$ sec. to 10^4 sec.) and hardness values (14 bars to 300 bars). This implies a range of pressure melting temperatures; i.e. the t = 1.5 secs curve is seen to intersect the pressure curve at $-1.8^{\circ}C$, whereas the $t = 10^4$ curve intersects at $-0.8^{\circ}C$. (This is in

Fig.IV.III Hardness of Ice; Steel Pyramidal Indenter, Wide Range of Loading Times (Secs.4.5, 4.11, 4.12).

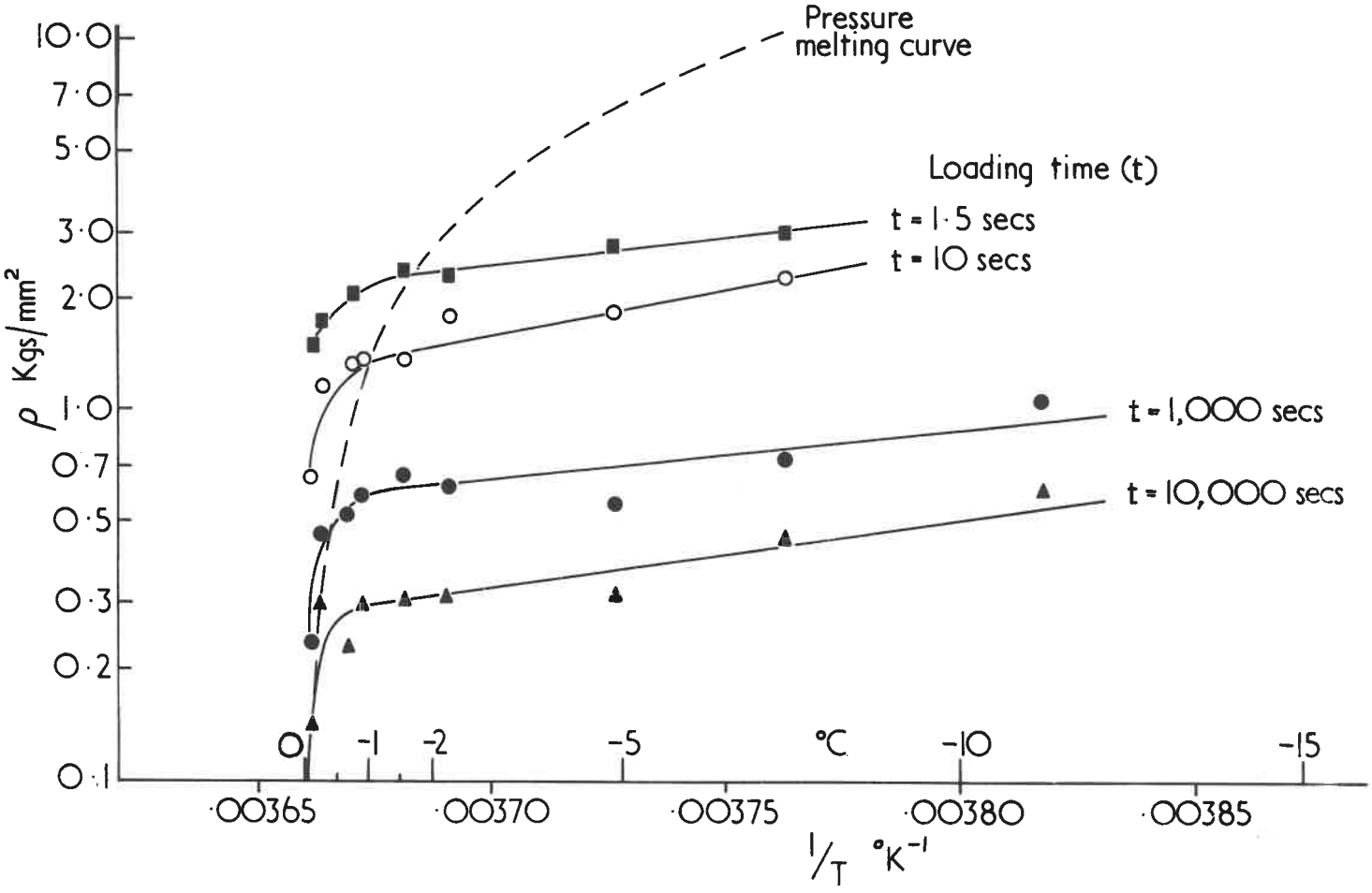
Pressure melting curve
Loading time (t)
t = 1·5 secs
t = 10 secs
t = 1,000 secs
t = 10,000 secs
10·0
7·0
5·0
3·0
2·0
1·0
0·7
0·5
0·3
0·2
0·1
p Kgs/mm²
0
-1
-2
-5
°C
-10
-15
·00365
·00370
·00375
·00380
·00385
1/T °K⁻¹

contrast to the results of Sec.4.4 where the range of pressure melting temperatures is virtually zero over the loading time range, $t = 10 - 10^3$ secs, used.) However it can be seen that on each curve the drop in hardness begins just above its particular pressure melting temperature. Thus we have identified the "hardness drop transition temperature" with the pressure melting temperature over a range ($-0.8^{\circ}C$ $-1.8^{\circ}C$) of temperatures. This therefore considerably strengthens our contention that the "hardness drop" must be interpreted in terms of pressure melting phenomena. While one could argue that this correlation in Sec.4.4 was coincidental, it is unlikely to be the case for these results.

It is seen that the hardness curves do not converge in the pressure melting regime. In fact it turns out that the exponent m derived from these curves is a good measure of the relative proximity of these curves. The averaged values obtained for the creep ($m = 4.44$) and pressure melting ($m = 4.22$) regimes are almost identical and indicate that, if anything, the hardness curves diverge slightly in the pressure melting regime.

The determination of the creep parameters Q and m is discussed more fully in Sec.4.10. The averaged values are given here:

Table IV.VI Comparison of Values for Q and m obtained from hardness and creep results

Hardness Results (Fig.IV.III)	Glen's (1) Results
$Q = 35 \pm 5$ k.cal/mole	$Q = 31.8$ k.cal/mole
$m \quad 4.4 \pm 0.5$	$m = 3.2$ or 4.2 (latter value preferred).

These results compare well with those obtained from Glen's Flow Law. The most important difference between these two determinations of Q and m is that the stress range in these hardness tests is higher than that in Glen's creep experiments. That the values for Q and m, obtained for our high stress hardness experiments, are a little higher than those of Glen is seen to be in accordance with the personal belief (expressed in Sec.3.6(d)) that both Q and m increase slightly with increasing stress.

4.6 The Hardness of Ice when using an Ebonite Pyramidal Indenter

These hardness experiments were similar in principle to those in Section 4.5 and were performed on highly polycrystalline ice specimens. The important difference in this set of experiments was that the ice specimen was thermally insulated from the surrounding apparatus. This was done by (i) placing insulating material between the ice specimen and the clamping system, and (ii) using an ebonite indenter. Some further details of this arrangement is given in Tables IV.I. No.8D and IV.III No.8D.

The purpose of these alterations was to gain further information on the pressure melting effects described in the previous sections. Insulation of the ice specimen in this way, effectively provided a "thermal block" between all the possible sources of heat (such as the brass beam, steel indenter etc.) and the ice specimen. In order to get a good idea of the behaviour of this system in the pressure melting regime, most of the hardness experiments were performed at, near, or above the pressure melting point. The hardness curves are shown in Fig.IV.IV.

Fig.IV.V gives a comparison between these hardness curves and those obtained using the steel pyramid (Sec.4.5). For reasons already discussed in Section 4.3, it is to be expected these two sets of results show systematic differences in the hardness values. Therefore in Fig.IV.V the ebonite indenter hardness curves have been shifted a little in a vertical direction so that the straight line (creep regime) portions approximately coincide. In this way easy comparison can be made between the steel and ebonite indenter hardnesses in the pressure melting regime. While there is a definite drop in the ebonite indenter values above the pressure melting temperature, it is not nearly so dramatic as with the steel indenter. This drop is interpreted in terms of a liquid-grain-boundary process which is active only above the pressure melting temperature. The difference between the steel and ebonite indenter hardness values is attributed to a regelation process which is active only with the steel indenter. These arguments are discussed more fully in Section 4.12.

Etchant-replica studies were made of ice sections cut parallel and perpendicular to the indentations. These revealed the grain boundaries, etch pits,

4.6 The Hardness of Ice when using an Ebonite Pyramidal Indenter

These hardness experiments were similar in principle to those in Section 4.5 and were performed on highly polycrystalline ice specimens. The important difference in this set of experiments was that the ice specimen was thermally insulated from the surrounding apparatus. This was done by (i) placing insulating material between the ice specimen and the clamping system, and (ii) using an ebonite indenter. Some further details of this arrangement is given in Tables IV.I. No.8D and IV.III No.8D.

The purpose of these alterations was to gain further infomation on the pressure melting effects described in the previous sections. Insulation of the ice specimen in this way, effectively provided a "thermal block" between all the possible sources of heat (such as the brass beam, steel indenter etc.) and the ice specimen. In order to get a good idea of the behaviour of this system in the pressure melting regime, most of the hardness experiments were performed at, near, or above the pressure melting point. The hardness curves are shown in Fig.IV.IV.

Fig.IV.V gives a comparison between these hardness curves and those obtained using the steel pyramid (Sec.4.5). For reasons already discussed in Section 4.3, it is to be expected these two sets of results show systematic differences in the hardness values. Therefore in Fig.IV.V the ebonite indenter hardness curves have been shifted a little in a vertical direction so that the straight line (creep regime) portions approximately coincide. In this way easy comparison can be made between the steel and ebonite indenter hardnesses in the pressure melting regime. While there is a definite drop in the ebonite indenter values above the pressure melting temperature, it is not nearly so dramatic as with the steel indenter. This drop is interpreted in terms of a liquid-grain-boundary process which is active only above the pressure melting temperature. The difference between the steel and ebonite indenter hardness values is attributed to a regelation process which is active only with the steel indenter. These arguments are discussed more fully in Section 4.12.

Etchant-replica studies were made of ice sections cut parallel and perpendicular to the indentations. These revealed the grain boundaries, etch pits,

Fig.IV.IV Hardness of Ice; Ebonite Pyramidal Indenter
(Details, Sec.4.6)

Fig.IV.V Figure showing the comparison between the hardness (p) results of Fig.IV.III and the hardness results obtained using an ebonite indenter (Fig.IV.IV). The latter curves have been shifted slightly in a vertical direction so the straight line portions approximately coincide. In this way easy comparisons can be made between the steel and ebonite indenter hardnesses in the pressure melting regime. While there is a definite drop in the ebonite indenter values, it is not nearly so dramatic as with the steel indenter (Sec.4.12).

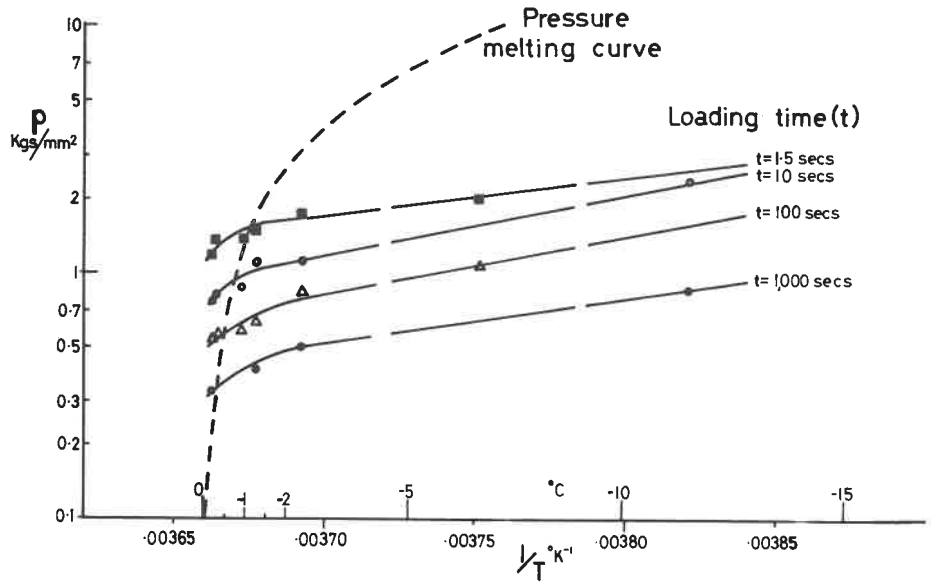
Pressure
melting curve
Loading time (t)
t=1·5 secs
t=10 secs
t=100 secs
t=1,000 secs
p
Kgs/mm²
10
7
5
2
1
0·7
0·5
0·3
0·2
0·1
0
-1
-2
-5
°C
-10
-15
·00365
·00370
·00375
·00380
·00385
1/T °K⁻¹

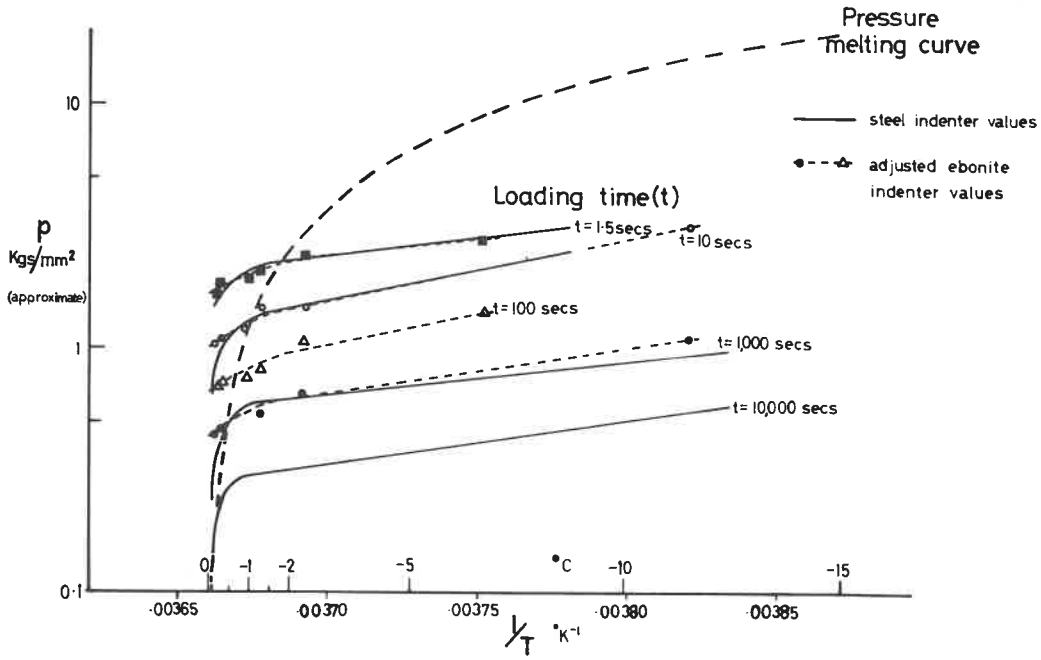
Pressure
melting curve
steel indenter values
adjusted ebonite
indenter values
Loading time (t)
t=1·5secs
t=10 secs
t=100 secs
t=1,000 secs
t=10,000 secs
p
Kgs/mm²
(approximate)
10
1
0·1
0
-1
-2
-5
°C
-10
-15
·00365
·00370
·00375
·00380
·00385
1/T °K⁻¹

micro-bubbles and other characteristics of the deformed ice. These will be dscussed in more detail later. One important feature however that merits mention here is that of the grain size observations. It was found that etchant-replicas laid on the indentation surfaces indicated that these surface layers exhibited similar recrystallization habits as those found in the crossed-polaroid sections for ice deformed in both the creep and pressure melting regimes. This is important because it demonstrates that the recrystallization effects, described for the crossed-polaroid sections, were in no way a result of the cutting processes necessary for obtaining the vertical sections.

4.7 The Dynamic (or Impact) Hardness of Ice

Tabor ((237)-(239)) has derived equations for the effective hardness values involved in an impact hardness experiment. If a hard spherical ball of mass M, radius R is impacted on a surface with an initial impact energy E', then it is found that the effective hardness p and impact time t are given by

$$p = \frac{E'}{Va} \tag{4.4}$$

$$t = \frac{\pi}{2}\sqrt{\frac{M}{2\pi pR}} \tag{4.5}$$

where Va is the apparent volume of the indentation. These equations assume that the rebound energy of the sphere is negligible. It is also assumed that the indentation recovers elastically. This means that one may use Va, the apparent volume that is calculated from the radius a of the indentation assuming the indentation to have the same curvature as the indenter. Provided $a \ll R$, one may make the approximation:

$$Va = \frac{\pi a^4}{4R} \tag{4.6}$$

Substituting this in (4.4) gives

$$p = \frac{4R.E'}{\pi a^4} \qquad (4.7)$$

These equations are used for calculating the dynamic hardness and impact times involved in these experiments.

The impact experiments were performed on highly polycrystalline ice specimens. Altogether 3 sets of experiments were performed - some of the experimental details are given in Table IV.I (Nos.7E,7F,9G). The first experiment was a preliminary one: It was found that the rebound energies of the spheres after impact were negligible - this means that equation (4.4) is valid for ice.

The other two experiments yielded data on the dynamic hardness and impact times for ice. The range of results obtained lie in the approximate ranges:

$$d = 0.3 - 1 \text{ cm}$$
$$p = 100 - 1{,}000 \text{ bars}$$
$$t = 10^{-4} - 10^{-3} \text{ sec.}$$

These results are shown in Fig.IV.VI. It is seen that each curve is an approximate straight line below about $-3^{\circ}C$ with similar slopes to those of the static hardness curves. One important difference is that whereas the static hardness curves are constant loading time curves, the impact time varies along each impact hardness curve even though the sphere (mass, M) and energy of impact E' are constant for each curve. This variation in t is given by equation (4.5):

$$t \propto p^{-\frac{1}{2}} \qquad (4.8)$$

It is shown in Section 4.10 that the slopes of the constant loading time-hardness curves may be used for calculating Q, the activation energy for creep. It is necessary therefore to consider what effect this t variation has on the values of Q calculated from dynamic hardness results. For this reason, the writer has developed the following equations:

The dynamic hardness is assumed to be given by:

$$p' = k'.t^{-\frac{1}{m'}}. \exp \frac{+Q'}{M'RT} \qquad (4.9)$$

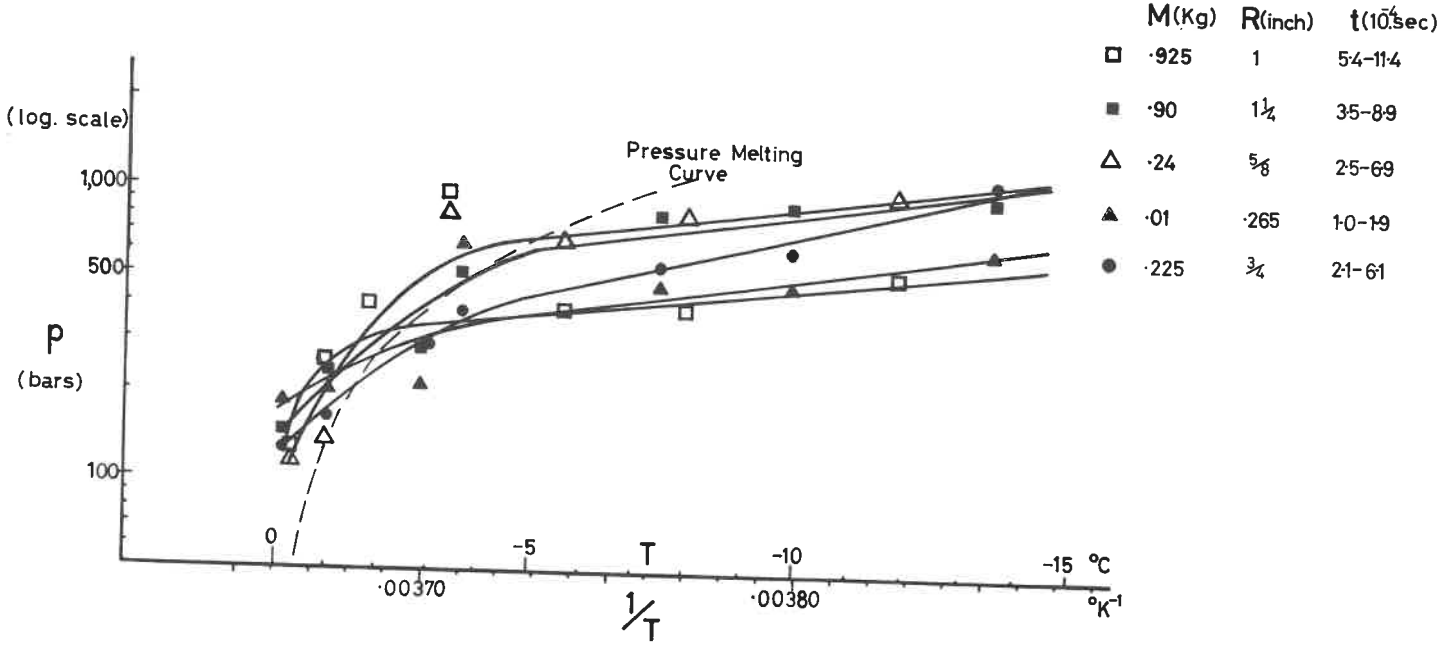

Fig.IV.VI Dynamic Hardness of Ice – some individual curves (Secs.4.7, 4.11, 4.12).

(These types of equations are discussed in Sec.4.10, the constants k', m' and Q' are assumed to be those for dynamic hardness and not necessarily the same as those for static hardness).

Differentiating equations (4.9) and (4.5) gives

$$\frac{\partial t}{\partial T} = \frac{-Q'}{2m'RT^2} \cdot t \cdot \frac{m'}{m' + \frac{1}{2}} \qquad (4.10)$$

Using this equation, it can be shown that the slope $\frac{\partial (\log p)'}{\partial \left(\frac{1}{T}\right)}$ of the dynamic hardness curve becomes

$$\frac{\partial (\log p)'}{\partial \left(\frac{1}{T}\right)} = \frac{Q'}{m'R} \left\{ 1 + \frac{1}{1 + 2m'} \right\} \qquad (4.11)$$

For static hardness curves the slope is given by

$$\frac{\partial (\log p)}{\partial \left(\frac{1}{T}\right)} = \frac{Q}{mR} \qquad (4.12)$$

This means that the activation energies Q' estimated from the impact experiments are over-estimated by a fraction $\frac{\Delta Q'}{Q'}$ given by:

$$\frac{\Delta Q'}{Q'} = \frac{1}{1 + 2m'} \qquad (4.13)$$

It will be shown in Sec.4.11 that typical values of m' for dynamic hardness are greater than 10. Using equation (4.13), this shows that a correction factor of less than 5 per cent should be applied. This is small enough to be ignored in these results.

Because the stresses are generally much higher in these impact experiments (compared to the static experiments), the pressure melting temperature is depressed further to about $-3^{\circ}C$. It is seen that on each of the 5 curves there is a definite drop in hardness above the pressure melting temperature. It is surprising that at these high rates of strain (or small impact times) a small but definite pressure melting effect is still present. However it confirms even more strongly the contention that the hardness drop is a pressure melting effect.

In order to compare these results with those of the static hardness curves the 5 dynamic hardness curves are smoothed into one average curve. The comparison is seen in Fig.IV.VII. It must be remembered that this single curve is, statistically speaking, very representative of the dynamic hardness results of ice - it has been averaged from 130 different indentations!

It was originally hoped that by performing 5 sets of experiments (using 5 different spheres) it would be possible to calculate the exponent m' from the different dynamic hardness curves. However because the value of m' is high for impact experiments, the hardness curves for different spheres lie very close to each other. It turns out that in order to get an accuracy of m' of 10 per cent say, the dynamic hardness values would have to be accurate to $< \frac{1}{2}$ per cent. This sort of accuracy cannot be achieved for dynamic hardness experiments, at present. However a rough value for m' may be calculated by comparing dynamic and static hardness curves. These calculations are discussed in Sec.4.11.

Some etchant-replica and polarised light studies were made of the indentations formed by impact. However because the indentations and deformed zones were small, it was not possible to observe the recrystallization features using 1/4-1/2 mm sections in the crossed-polaroid viewer. It is on occasions such as these that one realises how useful etchant-replica techniques can be. By laying a replica on the etched surface of an indentation, observations of the topmost grains were made using an optical microscope. It was found that, as with the static indentations, two different types of recrystallization were initiated in the deformed ice. Below the pressure melting temperature, small ($< \frac{1}{2}$ mm) grains were produced while above the pressure melting temperature, larger (0.5 - 3 mm) grains were produced. Again it seems somewhat suprising that two such well-defined regimes of recrystallization are present in these high strain rate experiments.

The writer did not expect to obtain such a close comparison between the effects of pressure melting on the hardness and recrystallization habits in static and dynamic tests. That such good comparison does exist is encouraging; even though it was unexpected for these high strain rates, the close agreement is now considered as further confirmation of the pressure melting theories proposed in this Chapter.

4.8 Additional Experiments

(i) Measurement of Regelated Lip Volume.

In order to fully develop the quantitative theory of hardness in the pressure melting regime (Sec.4.12) it was first necessary to have some means of estimating the amount of ice which "regelates" to the side of the indenter during a hardness experiment.

The formation of a lip at the edge of an indentation is common in hardness experiments. Similar small lips were also produced with the low temperature (creep regime) hardness tests on ice. However the nature of an indentation lip produced in the pressure melting regime is entirely different; it is found to be clear, well defined, with sharp apex and with its innermost face possessing curvature which is almost identical to that of the indenter. These features are in contrast to those formed by plastic flow and are believed to be produced by the refreezing of water which has melted under the indenter - hence the name "regelated lip".

Using a steel spherical indenter, indentations were made at $0^{\circ}C$ (the details are given in Table IV,Im No.10I). On removal of the indenter, the dimensions of the lips were measured using callipers. A schematic picture of these regelated lips is given in Fig.IV.XIV.

(ii) Density of Bubbly, Highly Polycrystalline Ice.

It was required to determine the density of bubbly, highly polycrystalline ice in order to make certain small corrections in the quantitative theory of hardness (Sec.4.12). This was done by cutting out a number of small cubes from some bubbly highly polycrystalline specimens. The cube was shaped by gentle melting with a brass block, and its dimensions determined using callipers. The cubes were weighed in the normal way, and the densities values were averaged giving 0.86 ± 0.02 gm/cc. This value is about 6 per cent lower than the value for pure ice (0.9168 gm/cc). It is interesting to note that Bader (245) has obtained similar values (0.894-0.86 gm/cc) for bubbly ice in glaciers.

4.9 The Bubble Loss in Single and Poly Crystals of Ice

This section deals with those experiments (and their results) listed as Nos.10H and 11J in Table IV.I. In general these may be divided into two categories:

(i) Examination after indentation. In this experiment (No.10H) the bubbles were observed after indentation using etchant-replica, crossed-polaroid, and ordinary optical techniques. The bubble behaviour in the ice beneath the indenter was compared to that away from the indenter.

A method was devised for incorproating horizontal layers of bubbles in clear ice. This was achieved by the alternate sandwiching of layers of clear large grained ice and bubbly highly polycrystalline ice. The method was tricky and all in all the two specimens used took many weeks of preparation. Only one of these two specimens gave successful results. The results of the optical examination of a vertical section from this specimen after three separate indentations is illustrated in Fig.IV.XVIII. It is seen that nearly all the bubble loss occurs when the indentation time lies between 10 and 1,000 secs. From this the rate of bubble loss can be estimated.

This experiment was originally designed in order to investigate the effect if any of temperature gradients on the movement of the bubbles. The temperature during these indentations remained constant to within a few hundredths of a degree during the period in which the bubble loss took place ($t = 10 - 10^3$ secs). Sometimes after longer loading times ($t \rightarrow 10^4$ secs), the temperature began to show signs of changing a little, but by this time most of the bubble loss had occurred. The conclusions drawn from these experiments are discussed in Sec.4.12.

(ii) Examination during indentation. The techniques used in these investigations were extremely difficult. During the many weeks of experimentation only one experiment (out of several attempted) was successful.

The experiment involved the observation of the bubbles through the side of the specimen during indentation. In order that the bubbles might remain visible, only very clear ice specimens were used. In order to prevent cracking during indentation the specimens had to be held firmly in a surround.

However, in order to be able to see the bubbles the surround obviously needed to be transparent. For this reason flat strips of perspex were used. The ice specimen then had to be carefully polished and shaped so that it fitted the perspex surround tightly - any air gaps present would have obscured the visibility of the bubbles. The first picture (-1 day)of Fig.IV.XX illustrates the experimental arrangement showing the spherical steel indenter, thermometers and ice specimen surrounded by strips of perspex.

The bubbles were observed during indentation by means of a specially made remote control camera. By using flexible connections the "wind on" and shutter mechanisms of the camera could be operated from outside the refrigerator - human observation inside the refrigerator would not have been any use since the temperature conditions would have been altered too much by the body heat.

Several methods were tried for the implantation of bubbles into clear ice viz. laser beam, mercury lamp beam, growth bubble, and mechanical insertion techniques. All except the laser beam technique were successful to a point but the only completely successful experiment turned out to be that with the growth bubble specimen. It also turned out that this specimen was a single crystal. The photographs taken during indentation (at $0^{\circ}C$) of this specimen are shown in Fig.IV.XX and discussed in Sec.4.12. Some of the experimental details are given in Table III.I (No.11J).

C Discussion of Results

4.10 Kinematic Theory of Hardness

Section 4.1 gives the equations of hardness for a perfectly plastic solid. This treatment effectively assumed that the hardness values are not time-dependent. This is equivalent to assuming that the yield stress (as measured in a stress-strain experiment) is independent of strain rate.

In general solids, including ice, do not behave as a perfect plastic; it is necessary to consider how the hardness equations transform when more realistic equations of flow are used.

One way to treat non-ideal plastic flow is to consider the yield stress to be strain rate dependent. From equation (4.3) it can be seen that this implies that the hardness should also be strain rate dependent - this is equivalent to saying that the hardness varies with loading time.

Atkins, Silvério, and Tabor (244) however have developed a more rigorous kinematic treatment of this problem. They assume that the solid obeys a creep process - flow law like that of ice i.e.

$$\dot{\epsilon} = A' . \sigma^m . \exp\left(\frac{-Q}{RT}\right) \qquad (3.3)$$

where $\dot{\epsilon}$ is the steady state creep rate.

Tabor et al. argue that the strain rates involved in an indentation test, must not be associated with the indenter geometry but with the rate at which the plastic-elastic boundary diffuses into the undeformed (or "virgin") material ahead. For this reason they use a transient (rather than steady state) creep law in the kinematic theory of hardness. Mott (204) (see also Sec.3.6,(d)) has given a relationship between transient creep rate ($\dot{\epsilon}_{tr}$) and steady state creep rate ($\dot{\epsilon}$) based on a model of dislocation climb:

$$\dot{\epsilon}_{tr} = A_2 . \dot{\epsilon}^{1/3} . t^{-2/3} \qquad (4.14)$$

A_2 being a constant and $\dot{\epsilon}$ given by equation (3.3). Combining equations (3.3) and (4.14) gives:

$$\dot{\epsilon}_{tr} = A_3 . \sigma^{m/3} . t^{-2/3} . \exp\left(\frac{Q}{3RT}\right) \qquad (4.15)$$

where A_3 is a new constant.

By analysing the kinematics of a spherical indentation, and assuming equation (4.15) can be applied to a system of "plastically" expanding concentric shells beneath the indenter, the following hardness equation is derived:

$$p^{-m/3} - p_o^{-m/3} = A_4 . (t^{1/3} - t_o^{1/3}) . \exp\left(\frac{-Q}{3RT}\right) \qquad (4.16)$$

where p_o is the hardness immediately after attaining the full load L

at time t_o. This equation may be simplified by neglecting $p_o^{-m/3}$ and $t_o^{-1/3}$ - this is obviously a good approximation when fast loading rates $\left(\frac{L}{t_o}\right)$ are used. Equation (4.16) then becomes

$$p = A_o\left(\frac{1}{t}\right)^{1/m} \cdot \exp\left(\frac{Q}{mRT}\right) \qquad (4.17)$$

This hardness equation is the one that is used for the analysis of the hardness of ice in this chapter. This equation assumes the presence of transient creep; however it appears that the final conclusions are not greatly dependent on which creep equation is used.

The writer has found it useful when comparing hardness and creep data to rewrite equation (3.3) in terms of the stress for direct comparison with equation (4.17):

$$\sigma = A_5 \cdot (\dot{\epsilon})^{1/m} \cdot \exp\left(\frac{Q}{mRT}\right) \qquad (4.18)$$

$$p = A_o \left(\frac{1}{t}\right)^{1/m} \cdot \exp\left(\frac{Q}{mRT}\right) \qquad (4.17)$$

Using these forms, both hardness and creep data may be plotted on the same log (stress/hardness) - reciprocal temperature plots with slopes equal to $\frac{Q}{mR}$ in each case. The hardness results and Glen's creep data have been compared in this way in Sec.4.11.

It is now necessary to consider how the hardness depends on the loading period (0 - t_o sec). It was noted above that equation (4.17) is an approximation for which the loading period t_o is small compared to the time period for which the load is at its full value - i.e. $t_o \ll t$ (the loading time). For short loading time experiments (e.g. $t = 1\frac{1}{2}$ secs ,or impact experiments $t \sim 10^{-4}$ sec) this is obviously not such a good approximation. Silvério (246) however has made a study of how the initial hardness p_o depends on the rate at which the load is applied (i.e. $\frac{L}{t_o}$). It is found that if the load is applied at a constant rate $\dot{L}$ for a given time t_o and then immediately removed, the diameter d of the resulting indentation is given by

$$d = A_6 \cdot \dot{L}^y \cdot t_o^{\,x} \cdot \exp\left(\frac{-q}{RT}\right) \qquad (4.19)$$

where $$q \simeq \frac{Q}{15} \simeq \frac{Q}{2m} \qquad (4.20)$$

$$y \simeq 0.38 \qquad (4.21)$$

and $$x \simeq 0.44 \qquad (4.22)$$

These four equations seem to hold over a wide range of single crystal and polycrystal materials and over a wide range of temperatures. In order to find out the range of loading rates $\dot{L}$ for which equations (4.18)-(4.22) are valid, Tabor et al. applied the equations to the results on the dynamic hardness of tin, assuming that the impaction can be approximated to a constant-loading-rate experiment. They found that very good agreement is obtained - the dynamic hardness results calculated using equations (4.19)-(4.22), gave values about 25-30 per cent higher than those calculated from equation (4.7).

It appears therefore that equations (4.19)-(4.22) are valid over a wide range of materials, temperatures, and loading rates. For these reasons the equations are considered to be important and their validity in describing the low temperature hardness of ice is discussed here and in Sec.4.11.

Tabor et al. also show that equations like (4.19)-(4.22) can also be derived from their kinematic theory. One important feature of this derivation is that the factor 15 in equation (4.20) arises in the theory from the value $\sim 2m$, where $m \simeq 10$. Now it is common (see Mclean(247)) for m to be $\simeq 5$ for low ($\sigma < 10^{-4}E$) stresses but increasing to ~ 10 for the high stresses ($\sigma > 10^{-3}E$) experienced in static and dynamic hardness experiments. However Section 4.10 shows that for ice, the low m value ($m = 3.2$-5) persists for creep and static hardness tests (i.e. $\sigma \lesssim 3 \times 10^{-3}.E$); it is only in dynamic hardness tests (i.e. $\sigma > 5 \times 10^{-3}.E$, say) that the exponent m for ice begins to increase to values >10. This may therefore imply that equation (4.20) only holds for dynamic hardness (i.e. not for static tests) tests on ice. If this is so, this reservation somewhat complicates the analysis used for the low temperature hardness of ice in Section 4.11.

Fig.IV.VII Figure showing the indentation hardness (p) of ice (logarithmic scale) for different loading times and temperatures (T) (reciprocal scale). The crosses indicate the averaged impact hardness results of Fig.IV.VI while the other points show the static hardness results of Fig.IV.III. The dotted line is a phase transition curve indicating $p \sim \frac{1}{T}$ co-ordinates at which pressure melting is expected to occur. It is calculated here assuming the hydrostatic pressure of the potential liquid phase to be given by the hardness (p). It is seen to cut the hardness plots at temperatures varying between about $-0.8^{\circ}C$ and $-3^{\circ}C$. It is seen that below the pressure melting temperatures (that is, to the right of the broken line), the curves are approximately straight in accordance with the expected exponential variation. Above the pressure melting temperatures (that is, to the left of the broken line) the hardness falls rapidly. (Secs. 4.11.4.12).

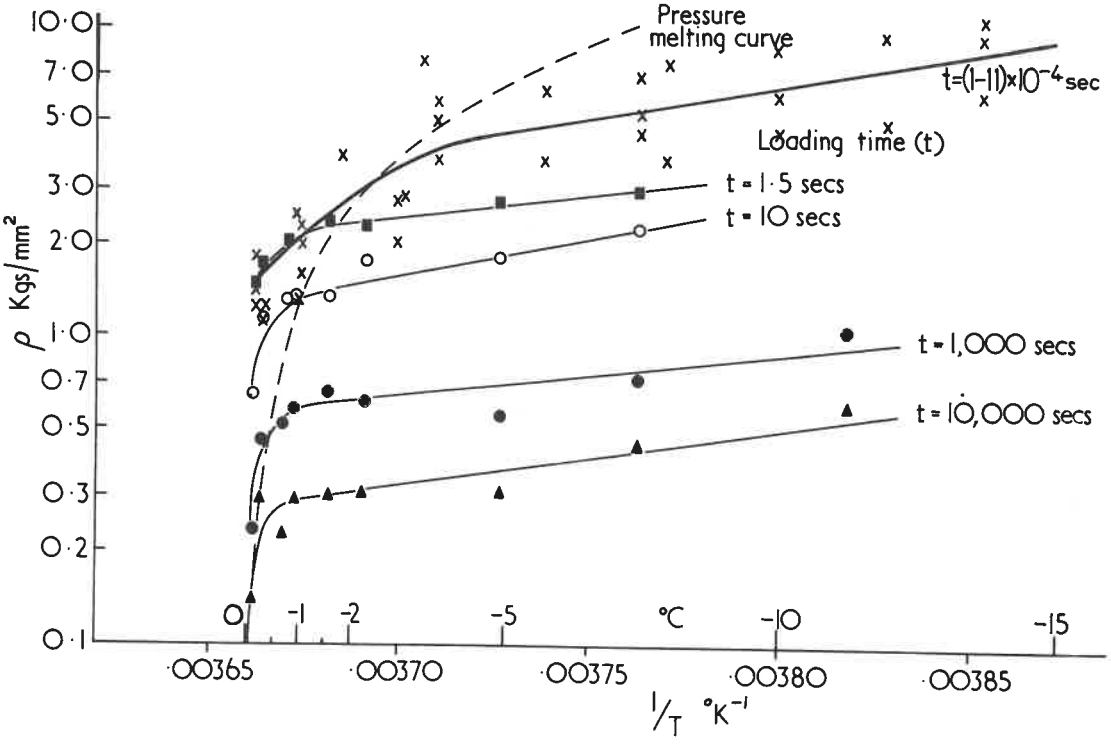
Pressure melting curve
t=(1-11)×10⁻⁴sec
Loading time (t)
t = 1·5 secs
t = 10 secs
t = 1,000 secs
t = 10,000 secs
ρ Kgs/mm²
10·0
7·0
5·0
3·0
2·0
1·0
0·7
0·5
0·3
0·2
0·1
0
-1
-2
-5
°C
-10
-15
·00365
·00370
·00375
·00380
·00385
1/T °K⁻¹

4.11 The Interpretation of the Hardness of Ice in the Creep Regime

In Section 4.1 it was shown that, phenomenologically, the hardness of ice may be divided into two distinct regions over the temperature range $0^{\circ}C$ to $-12^{\circ}C$. We discuss here in more detail the lower temperature (below about $-1.8^{\circ}C$ for static hardness, $-3^{\circ}C$ for dynamic hardness) "creep regime" hardness.

Fig.IV.VII shows the summarised results for both the static (Sec.4.5) and dynamic (Sec.4.7) hardness of highly polycrystalline ice (plotted on a log. hardness - reciprocal temperature scale). It can be seen from equations (4.17) and (4.18) that the slopes of these curves yield values for $\frac{Q}{m}$ where Q (the activation energy) and m (the stress exponent) are the same parameters as those used in the creep law for ice. The average values for m and Q for the static hardness are in good agreement with those obtained from creep measurement by Glen (1) (see Table IV.VI, Sec.4.5). We now however discuss the variations in these parameters.

(i) Variation of m with stress

It can be seen from equation (4.17) that by considering, at a particular temperature, the two values of hardness (p_1, p_2) for two different loading times (t_1, t_2), one may calculate m from the relation:

$$\frac{p_1}{p_2} = \left(\frac{t_2}{t_1}\right)^{1/m} \qquad (4.23)$$

The value of m determined in this way is then deemed as the value for the particular temperature chosen and for the stress given by the mean of p_1 and p_2. In this thesis the possible variations of m with temperature are not considered. Therefore by averaging the values of m over the whole creep-regime temperature range, one can plot these averaged values for m against the effective stress (taken as the mean of p_1 and p_2). Fig.IV.VIII shows this variation (on logarithmic scales) of m as obtained from the static and dynamic hardness results. One shortcoming of these results is that the last point on the graph ($m = 13.4$) represents a value averaged

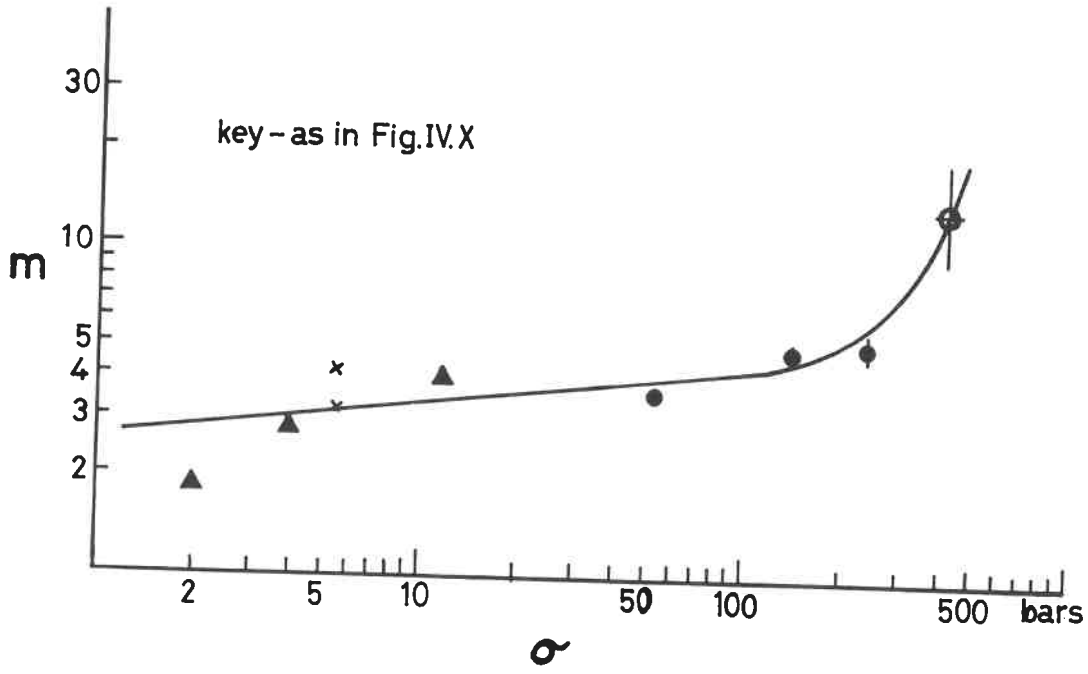

Fig.IV.VIII Variation of Stress Exponent with Stress (log. scales).

between the dynamic and static (t = 1½ secs) hardness curves. There are obvious disadvantages involved in combining results from two different types of experiments - it would have been better if two dynamic hardness curves (for different spheres) had been combined but, as explained in Sec.4.7, for reasons of accuracy this was not possible. However, in spite of this obvious failing, Fig.IV.VIII gives a fairly reliable picture of the stress variation of m. Apart from the general increase of m with stress, the outstanding feature of Fig.IV.VIII is the rapid increase of m above stresses of about 300 bars. It must be decided however whether this increase in m is a true increase or whether it merely illustrates the fact that equations such as (4.23) are not valid for impact experiments where the load is continually changing. In order to investigate this possibility it was decided to try and use equations (4.19)-(4.22) to predict the dynamic hardness of ice. Because these equations are concerned with the effects of a changing load (i.e. a rate of change of load $\dot{L}$), it should in principle be possible to determine what effect the load rate effect has on the dynamic hardness of ice. However the results of these investigations merely implied that the "load rate effect" is responsible for only a small part of the increase in m. It now appears that the use of equations (4.19)-(4.22) in this connection was invalid. This was so because in order to put a numerical value to the constant A_6 in equation (4.19), the loading rate results for the "static" hardness (t = 1½ secs) experiments were used. However because m appears to vary rapidly at these stresses, the use of equations (4.19) - (4.22) in a situation like this is meaningless; this point was also made in Sec.4.9 in fact this complication does not arise with most other materials because, for them, m does not increase rapidly for the range of stresses involved in hardness experiments. Bearing in mind all these complications, the writer considers that this rapid increase in m is a genuine effect.

It is necessary to consider some of the many possible physical explanations for this rapid increase in m. Physically this increase means that the ice at these stresses is beginning to flow at creep rates which are much greater than those predicted by Glen's flow law or the static hardness results.

This interpretation is illustrated in Fig.IV.IX where the stresses required to produce given strain rates (or inverse of loading times) are plotted. It is seen that the strain rate increases so rapidly as to appear almost independent of the stress for stresses greater than about 1,000 bars, say. It would appear that this stress level is critical for a number of reasons:

(1) It is shown in Sec.3.6 (a), that Weertman's dislocation climb model breaks down for stresses above $(10^{-3}-10^{-2})$ x theoretical yield stress because at these stresses the "climb distance" becomes small (compared with the lattice unit). For ice this value is ~30-300 bars - this is very close to the values for dynamic hardness.

(2) Many other materials also show rapid increases in m at these sort of stresses.

(3) The theoretical yield stress of ice is ~30,000 bars. Theoretically these sort of stresses should be capable of producing shear without requiring the help of dislocations that are necessary for slip at lower stresses.

(4) Glen has shown (see Sec.3.6(a)) that stresses of 4,300 bars are sufficient to produce dislocation movement without re-orientation of the hydrogen atoms in the ice lattice. At low stresses, this re-orientation process is necessary and slows up the rate of dislocation movement and therefore also the creep rate in ice. Hence the permitted absence of hydrogen reorientation at these high stresses provides a possible explanation for the rapid strain rates encountered. Clearly, stresses which are just a little less than 4,300 bars should also produce rapid strain rates because thermal activation may help the stress in forcing the dislocations to move without proton reorientation.

The above list shows that a number of unusual effects are expected to take place almost simultaneously. It is obviously quite easy to propose a number of explanations (based on these 4 effects) for the increase in m. A tentative explanation is offered by the writer: At stresses of about 300 bars the processes of dislocation climb or cross slip are no longer rate controlling (see (1) above). This means that ordinary slip may become the rate controlling processes. However these stresses are perhaps

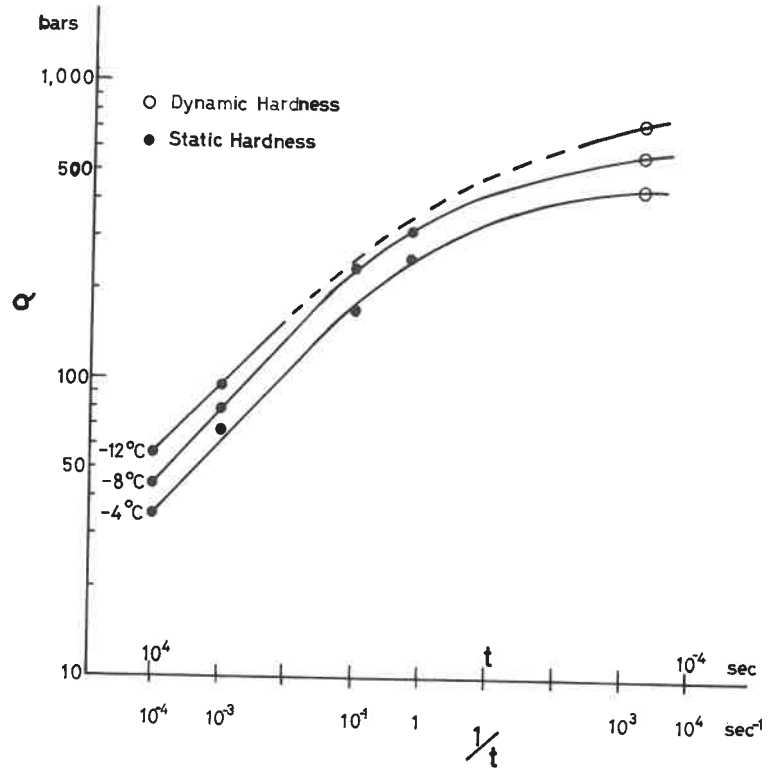

Fig.IV.IX Stress required for a given strain rate (inverse loading time).
(log. scales)

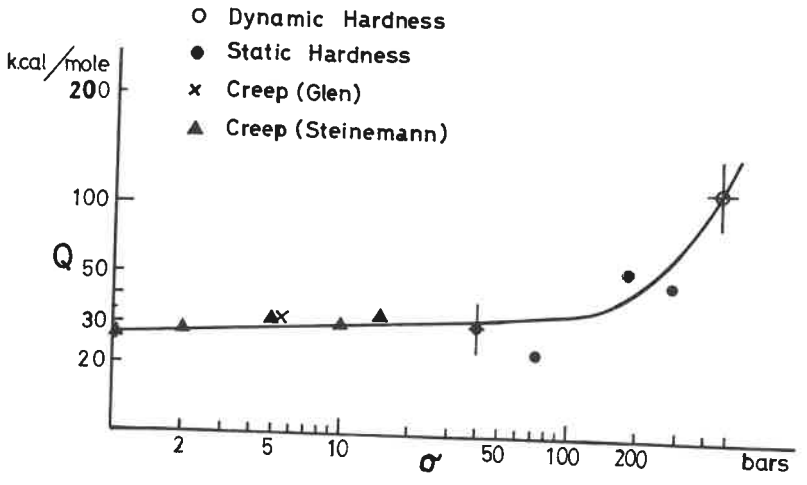

Fig.IV.X Variation of Activation Energy with stress (log. scales).

large enough to force the dislocations to move without re-orientation of the hydrogen atoms. The partial removal of this delaying process causes the strain rates to increase rapidly to the kind of values observed in dynamic hardness measurements. At even higher stresses, shear may possibly occur without the presence of dislocations.

Before leaving this topic we compare these results to those obtained by other workers on the creep of polycrystalline ice. Steinemann's results (Table III.III.(2)) also show an increase of m with stress. Fig.IV.IX also shows the variation of m with stress using the values of Steinemann and Glen and those obtained from the static and dynamic results. Glen (227) has criticised Steinemann's results on the grounds that some of Steinemann's results were not fully compensated for transient creep effects. However Fig.IV.IX shows good agreement between Steinemann's results (for lower stresses) and the hardness results.

(ii) Variation of Q with stress.

It is shown in Section 4.7 that the slopes of the hardness curves yield values for $\frac{Q}{m}$. Hence knowing m, the activation energy Q for creep may be calculated. It is somewhat surprising that the slope values of $\frac{Q}{m}$ for dynamic and static hardness results are approximately the same, viz:

Average STATIC hardness value; $\frac{Q}{m} = 8 \pm 1$ k.cal/mole
Average DYNAMIC hardness value; $\frac{Q}{m} = 8.7 \pm 1$ k.cal/mole

However one important difference here is that the values of m are considerably different (see (i) above). Using the average values for m obtained for the static and dynamic (respectively) hardness results yields:

Average STATIC hardness value; $m = 4.44 \pm 0.4$, $Q = 35.7 \pm 5$ k.cal/mole
Average DYNAMIC hardness value; $m = 13.4 \pm 5$, $Q = 120 \pm 50$ k.cal/mole

This shows an enormous increase in Q for these high stresses. As in (i) above it is necessary to consider whether the above value represents a genuine increase in Q or whether the increase merely illustrates that this method for determining Q was invalid for dynamic hardness measurements. For this reason it was again decided to consider the application of the load rate equations

(4.19) - (4.22) to both the static and dynamic determinations of Q.

The writer has therefore attempted to examine a little further the equations (4.19) - (4.22): we note that for a static hardness test, equations (4.1) and (4.2) show, that for a given load and temperature,

$$P_{stat.} \propto d^{-2} \tag{4.24}$$

Inserting this into the loading rate (r.1) equation (4.19) gives:

$$P_{stat.l.r.} \propto \dot{L}^{-2y} . t^{-2x} . \exp\left(\frac{Q}{mRT}\right) \tag{4.25}$$

Comparing this with:

$$P_{stat.} \propto \left(\frac{1}{t}\right)^{1/m} . \exp\left(\frac{Q}{mRT}\right) \tag{4.17}$$

we see that the temperature variations in these two equations is the same. The conclusion drawn from this is the following: if one were to calculate Q from a hardness experiment which involved a gradual rather than a spontaneous application of the load, one would obtain the correct value even if equation (4.17) was mistakenly used instead of equation (4.25).

We now use a similar argument for the equations of dynamic hardness. We note that for a dynamic hardness test, equations (4.7) shows that, for a given impact energy and temperature,

$$P_{dyn.} \propto d^{-4} \tag{4.26}$$

Inserting this into the loading rate equation (4.19) would give:

$$P_{dyn.l.r.} \propto \dot{L}^{-4y} . t^{-4x} . \exp\left(\frac{2Q}{mRT}\right) \tag{4.27}$$

This would indicate that the exponential temperature variation in equation (4.27) was twice as fast as that in equation (4.17). However this conclusion is an incorrect one - this arises because we have ignored the variations in $\dot{L}$ and t. We overcome this difficulty by noting that for a dynamic experiment $\dot{L}$ may be written as

$$\dot{L} = \frac{P_{dyn.l.r.} \times A}{t} \propto \frac{P_{dyn.l.r.} \times d^2}{t} \tag{4.28}$$

and from equation (4.5)

$$t \propto P_{dyn.l.r}^{-\frac{1}{2}} \tag{4.29}$$

Using this relation for $\mathring{L}$ and t in equation (4.27) yields:

$$P_{dyn.l.r} \propto \exp\left(\frac{Q}{mRT}\right) \tag{4.30}$$

Hence it is seen that a correct interpretation of the dynamic hardness equations shows that an identical temperature variation is obtained for calculations using the instantaneous load equation (4.19) and the load rate equations (4.19) and (4.30). A similar conclusion was drawn with the static hardness equations. The overall conclusions to be drawn from these arguments is that load rate effects cannot account for the large variations in the activation energy Q obtained from static or dynamic hardness results.

Even though the activation energy obtained for the dynamic results is unusually large, the writer is forced to conclude that in view of the arguments presented above, this activation energy (120 ± 50 k.cal/mole) must be a genuine value. A curve has therefore been constructed (Fig.IV.X) showing the variation of Q with stress: the curve shows the individual static hardness values, the averaged dynamic hardness value, and the values obtained by Glen and Steinemann for polycrystalline creep.

Even though a certain amount of scatter is seen in Fig.IV.X, the general trend of Q increasing with stress is evident. It is interesting to note that in the review on the creep of polycrystalline ice (Sec.3.6,(d)) it is stated that there is evidence in some of the literature for an increase of Q with stress. It is fair to point out that the writer had made this statement without knowing that it was to be confirmed later by the hardness results.

Before leaving this subject it must be pointed out that there is considerable difficulty in explaining what sort of deformation mechanism requires such a high activation energy. If "dislocation movement without hydrogen orientation" is the only controlling mechanism (as suggested in (i) above) then one would not expect the activation energy to be so high. The only other large activation energies known to the writer are (i) 105 k.cal/mole quoted by

Nayar (Table III.III(3)) for the creep of polycrystalline ice under a tension of 6½ bars, and (ii) values of 30-75 k.cal/mole quoted by Kuroiwa (274) for the grain boundary internal friction peak of ice. The deformation and piling up of dislocations at grain boundaries is known to be important at high stresses in many other materials. Whether this mechanism is responsible for the high activation energy here is debatable. It is regretted that this problem must, for the moment, remain unanswered.

(iii) Recrystallisation effects in the Creep Regime.

It was pointed out in Section 4.1 that the recrystallisation effects in the Creep Regime differed considerably from those observed in the Pressure Melting Regime. Examples of these sort of effects are given in Sections 4.2, 4.4, 4.5, 4.7, and Chapter V. It is found that the sizes of the recrystallised grains are about 0.1 - 0.7 mm. The depth of the recrystallised zone is a maximum for ice indented at the warmest temperatures of the creep regime i.e. just below the pressure melting temperature (-1.5°C, say). At about -10°C, the zone becomes so small as to be only just perceptible. This recrystallisation is interpreted as a stress-enhanced recrystallisation effect.

Steinemann has shown (see Sec.3.6,(d)) that recrystallisation effects provide a physical explanation for the accelerated creep of ice; the recrystallisation produces grains with a preferred orientation favourable for easy glide along the basal plane. It is interesting to compare Steinemann's results at low stresses (~ bars) and a temperature of -4.8°C to the hardness results. The writer has extrapolated (logarithmically) Steinemann's recrystallisation curves up to stresses of 50-500 bars. This extrapolation shows that recrystallisation, with a grain size of about 0.5 mm, is to be expected after about 1-1,000 secs of indentation. This shows remarkable agreement with the time scale and grain sizes involved in the hardness experiments. This almost certainly indicates that the recrystallised ice, beneath the indenter in the hardness experiments, must have been in a condition suitable for accelerated creep - no attempt was made to show that this preferred orientation actually existed in the recrystallisation zone. However, even if the material near the contact zone is in a condition suitable for accelerated creep, the creep process as a whole is governed by the diffusion of the plastic zone into the

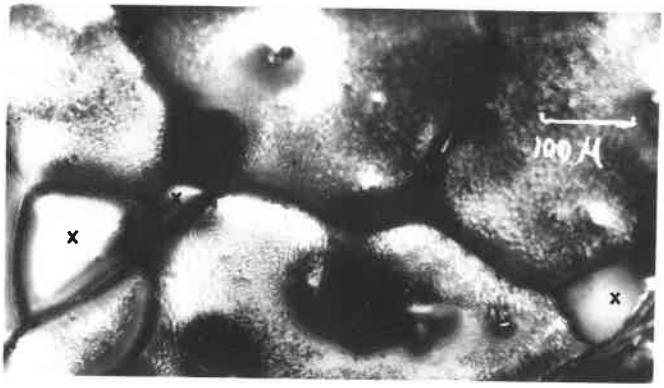

Fig.IV.XIa Replica of an Etched Ice Surface after Indentation at -1·55°C for 12 secs. The Large (>5mm) grains have high etch pit densities, but the 3 new grains (<·2mm, marked with x) are etch pit free.

Fig.IV.XIb 10^3 secs Indentation. The grains are less than 3mm and are all etch pit free.

virgin ice below it. This is apparently the rate-limiting part of the process and for this reason hardness results are explicable in terms of the transient creep process occurring in this region.

In addition, the recrystallised grains in the deformation zone scatter light strongly and appear "white" in contrast to the relatively transparent ice (examples given in Chapter V).

The etched-replica pictures also reveal some interesting features of these recrystallised grains. Space permits a description of only one observation here. Fig.IV.XI shows the etch pit characteristics of the recrystallized grains. It is immediately apparent that the larger grains show heavy etching while the smallest grains are completely free of etch pits. This phenomena is interpreted as an increase in the number of dislocations in the larger grains due to their growth under the imposed stress. The smallest grains are presumably the most recently nucleated grains and are therefore relatively strain free and relatively dislocation free.

It must be remembered that the general features of recrystallisation outlined here are evident in both the static and the dynamic hardness results. They are however in complete contrast to those for recrystallisation in the pressure melting regime; the latter recrystallisation is discussed in the next Section.

4.12 The Interpretation of the Hardness of Ice in the Pressure Melting Regime

This section deals with some qualitative and quantitative aspects of the deformation of ice at (and above) its pressure melting temperature. Section 4.1 points out the anomalies in the deformation behaviour of ice above the pressure melting temperature viz., the drop in hardness values, the large grain sizes and bubble loss in the deformed ice. These anomalies were also presented in a previous paper by Barnes and Tabor (141). In both these accounts it was noted that these anomalies occurred above the pressure melting temperature and indicated that pressure melting must be playing an important role. However, no attempt was made to give a detailed quantitative account of the exact mechanisms involved in the pressure melting regime. It is the purpose of this section to try and give a fuller explanation of these observed effects.

(1) The Drop in Hardness.

Fig.IV.VII summarises the dynamic hardness (Sec.4.7) and static hardness (Sec.4.5) results for highly polycrystalline ice. Fig.IV.VII is particularly useful in that it covers extremely wide ranges of the experimental variables. It is noticed that the large stress range covered by this Figure implies a range of pressure melting temperatures of about $-0.08^{\circ}C$ to $-3^{\circ}C$. It can be seen that on every curve there is a definite drop in hardness values above the pressure melting temperature. It is perhaps somewhat surprising that this effect is so consistent for a loading time (or strain rate) range of nearly 10^8 in which the modes of cold temperature deformation differ considerably.

The drop in hardness, the bubble loss and large grain size might have been explained on the assumption that the whole of the region beneath the indenter undergoes pressure melting. This, however, is impossible as there is insufficient heat available from the surrounding ice or the indenter to provide the necessary latent heat.

The ebonite indenter (Sec.4.6) experiment, the bubble loss experiments (Sec.4.10) and the etchant-replica techniques give more insight into the different mechanisms involved. Table IV.VII, and Figs.IV.XII, IV.XIII, and IV.XXIII attempt to give a quantitative estimate, by volume, of the relative magnitudes of these mechanisms. In order to do this it was first necessary to measure the volume (V_{ind}) of the indentations. The magnitude of each mechanism was then considered to be the indentation volume it would produce in the absence of the other mechanisms, expressed as a percentage of (V_{ind}).

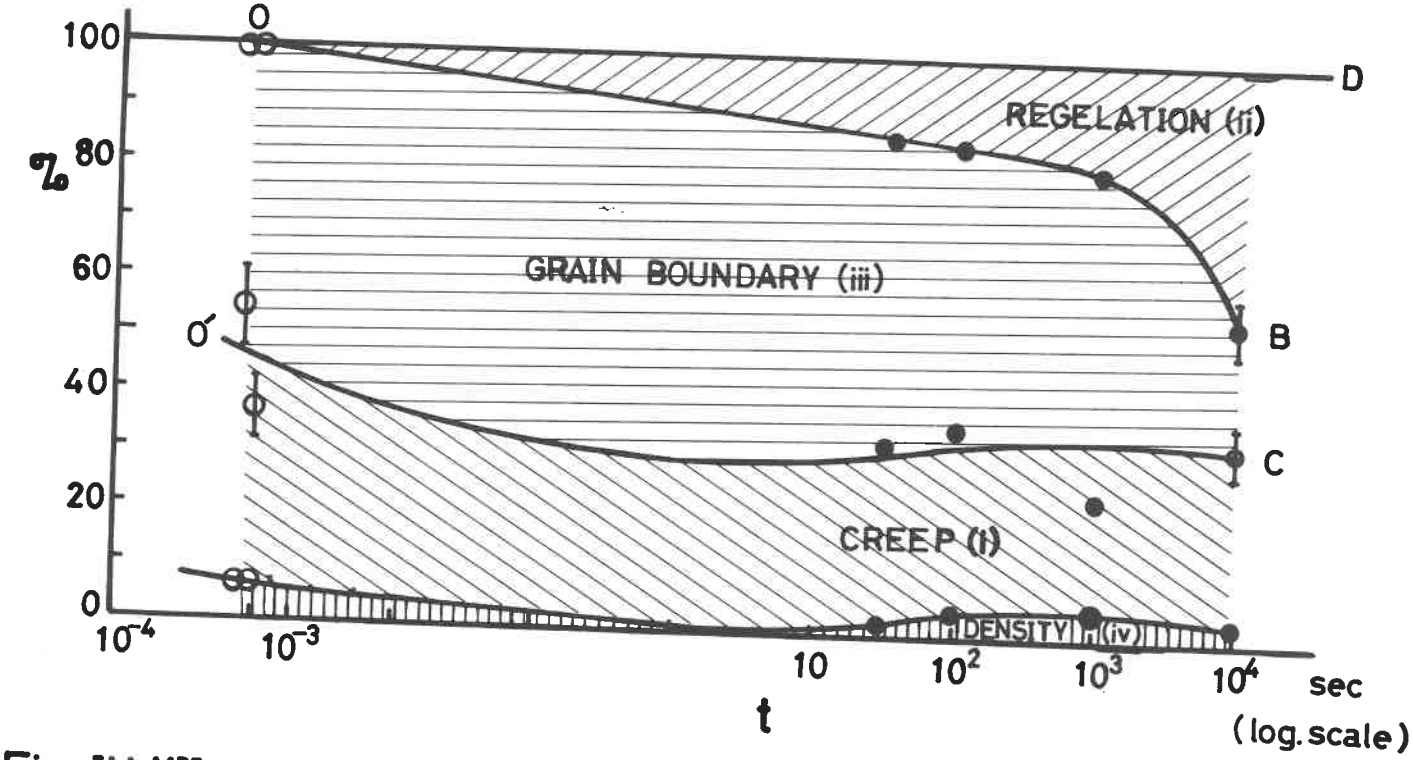

Fig. IV. XII Mechanisms of Deformation in Ice – see Table IV.VII.

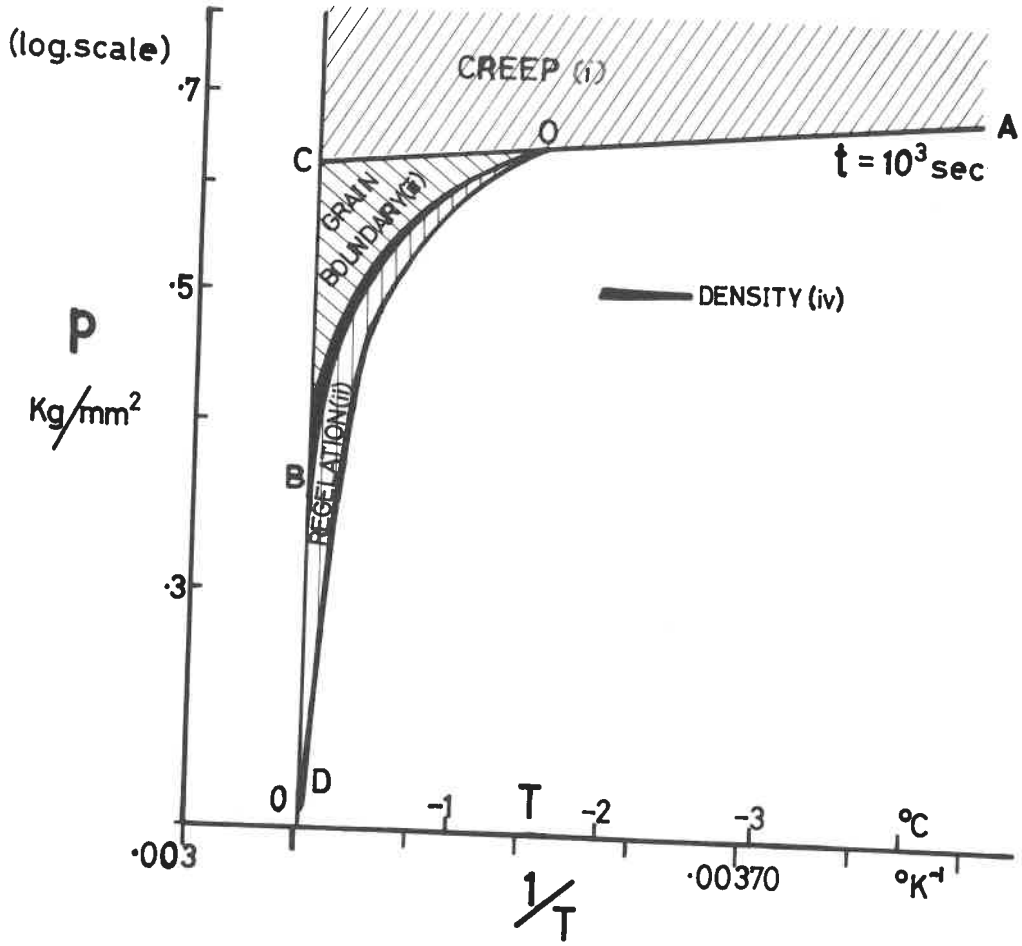

Fig.IV.XIII Contribution of each Mechanism to the Hardness - see Fig. IV.XII.

Table IV.VII Relative magnitudes of mechanisms involved in the indentation of Ice at 0°C (using a steel indenter)

Mechanism	$t=10^4$ secs. (10-18 bars)	$t=10^3$ secs. (19-27 bars)	$t=10^2$ secs. (35-43 bars)	$t=7.5\times10^{-4}$ sec. (110-190 bars)
(i) Creep	30	30	29	40
(ii) Regelation	45	19	14	-
(iii) Other Processes (grain boundaries)	22±6	46±7	52±8	54±15
(iv) Minor Processes (density changes)	3	5	4	6
V_{ind} (ccs)	2.7	0.9	0.25	0.025

The values given in Table IV.VII are also showed graphically (and more fully) in Figs.IV.XII and IV.XIII. We now consider these mechanisms in more detail:

(i) Creep. This refers to that part of the deformation still attributable to creep. It is easily estimated by extrapolating to 0°C the creep rate observed at lower temperatures. This extrapolation is also indicated by the line OC in Fig.IV.XIII.

(ii) Regelation. Here we consider the transport of ice which has melted under the indenter due to the high hydrostatic pressures. On reaching the side of the indenter the water refreezes as the hydrostatic pressure here is considerably lower (atmospheric). In this way a "regelated lip" is formed. Its appearance is readily characterised by its sharp well defined outline and relative transparency in contrast to the general cloudiness of the ice specimen. These points are discussed more fully in Sec.4.8. The volume is simply the measured volume of the lip (V_{lip}) as indicated in Fig.IV.XIV.

It is not possible to explain the formation of the regelated lip in terms of a rapid bulk melting and transfer of ice to the lip: this would demand far too large a rate of generation of heat. However, we can consider a continuous regelation type of heat cycle in which a thin film melts directly under the indenter and is then squeezed out to the sides of the indenter. On refreezing there, the liquid gives up its latent heat which is transported back, usually

Fig.IV.XIV Figure showing schematic representation of the terms: (V_{lip}) the volume of the regelated lip, and (V_{ind}), the volume of the indentation below the surface level of the ice. Part of (V_{ind}) includes plastic indentation of the ice. This produces some "pile up" of ice around the indentation. In general, this is very small and has been neglected in calculating (V_{lip}) (Sec.4.11(i))

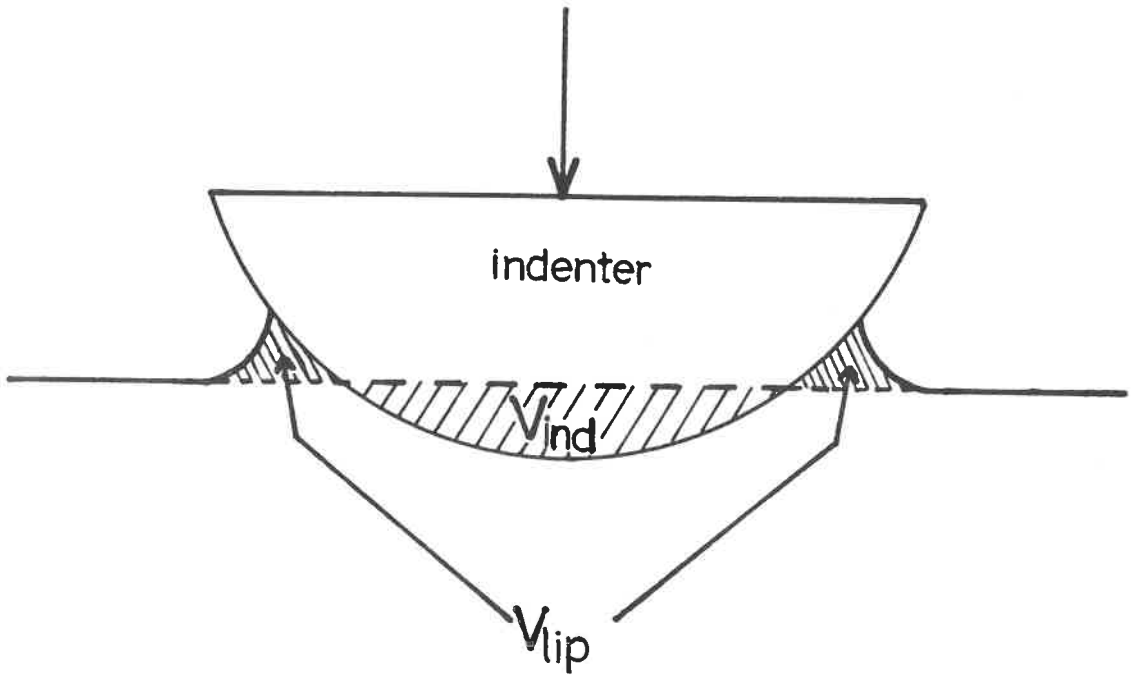
indenter
V_{ind}
V_{lip}

via the steel indenter, thus providing the latent heat for further melting under pressure. In this way the observed lip volumes can be produced within the observed loading times, using only a small recycling quantity of heat. A rough estimate shows that for a steel indenter, the temperature difference necessary for the observed transport in the time available, is less than $1/100^{o}C$. This is therefore consistent with the known conditions of temperature constancy present in these experiments - the temperatures in the steel indenter hardness experiments were constant to within a few hundredths of a degree for indentation times considerably longer than 1,000 seconds.

A few simple calculations have been performed in order to make a rough estimate of the thickness of the surface regelation film: it is assumed that the rate controlling part of the regelation process is the rate at which latent heat for melting is transferred through the steel indenter. This means that one can assume that the thickness of the regelation film adjusts itself so that it is extruded at a rate which is compatible to the rate of melting beneath the indenter. Using typical values for the indenter size, hardness, lip volume etc. and assuming the viscosity η of the water film is 2×10^{-2} poise one obtains a film thickness:

$$\delta \sim 1 \mu$$

This value indicates that it may be possible to detect the surface regelation film optically. No sophisticated attempts were made to observe this film, but the writer noticed that upon removal of the indenter after a loading time of 1,000 seconds at $0^{o}C$, there appeared to be an extremely thin water film covering about half of the indentation surface area (that is, the central portion). From its visual appearance, its mechanical response to stroking with a thin sheet-strip of bakelite, and its rate of freezing it was deduced that its thickness must have been extremely small (probably $\sim$ microns). However no such film was observed after the removal of the indenter after 10^{4} secs. Fig.IV.VII shows that for $t = 10^{4}$ secs., the hardness approaches the pressure melting point. This means that after $t = 10^{4}$secs., it is to be expected that the regelation process is diminishing.

Sections 3.3 and 3.4 present evidence for the increased viscosity values of water when confined spatially or to the mother ice surface. Values given for the viscosity are 0.2 poise ($\delta \sim$ microns) and 70-700 poise ($\delta \sim$ 10-100 Å). However it turns out that the thickness of the surface film is not very sensitive to changes in the viscosity ($\delta \propto \sqrt[3]{\eta}$); using these higher viscosity values gives values:

$$\delta = 2\mu \quad (\eta = 0.2 \text{ poise})$$
$$\delta = 30\mu \quad (\eta = 700 \text{ poise})$$

The conclusion drawn from these calculations is the following: even if a liquid layer exists on the surface of ice at 0°C the data from the experiments described in Sections 3.3 and 3.4 suggests that this layer should not greatly affect the flow characteristics of the surface regelation layer. In addition the "surface film on ice" theory is regarded as being more pertinent to stable surfaces. The indenter-ice surface however is always changing.

(iv) Minor Processes (density changes)

This term refers to an additional small effect which must also be considered, i.e. the change in density of the ice from its original bubbly to its final clear state. Using the density values obtained from the experiments described in Section 4.8, it it possible to estimate the change in indentation volume which arises from the bubble loss of the clear ice in the regelated lip and beneath the indenter.

(iii) Other Processes (or grain boundary processes)

This refers to the amount of deformation unaccountable by the processes considered above. Its magnitude is therefore calculated by subtracing the contributions of these processes ((i), (ii) and (iv)) from the total volume of the indentation (V_{ind}). It is suggested that a thin viscous water-like layer is formed at the grain boundaries above the pressure melting temperature. This facilitates rotation, movement and growth (and possibly preferred orientation) of the ice grains.* It is therefore considered that these factors, together

*There has been suggested (309) another mechanism by which the liquid grain boundary process may produce enhanced flow rates. This mechanism is called "intergranular-regelation". It is shown schematically in Fig.IV.XV. Liquid

footnote contd.

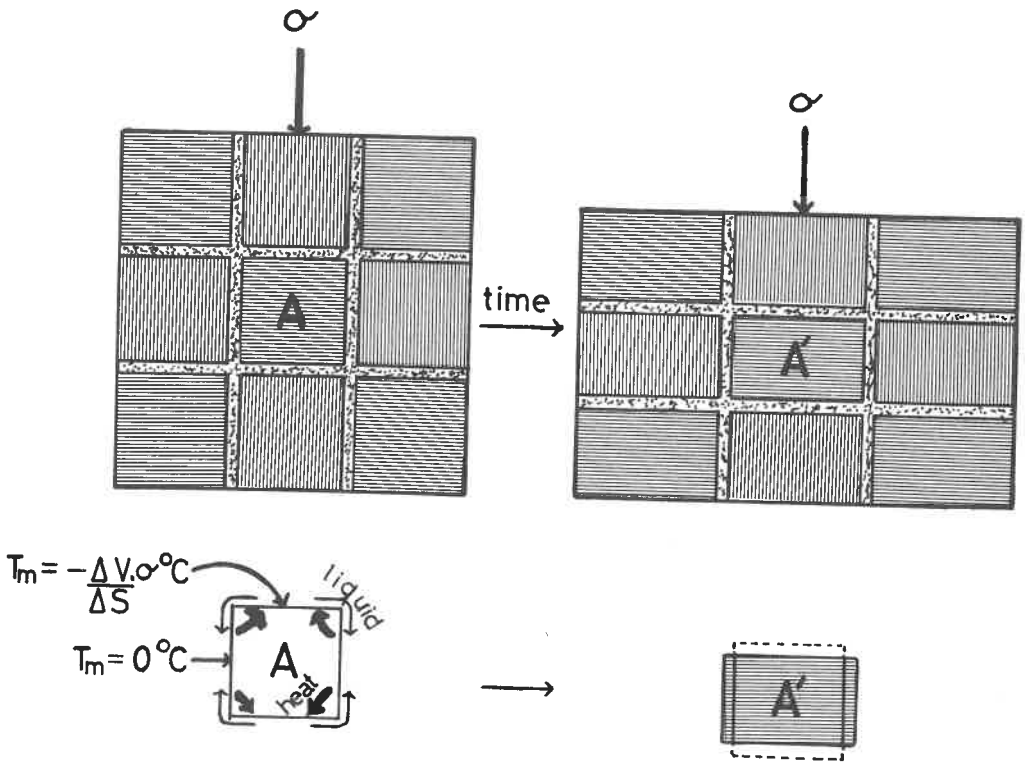

Fig.IV.XV Schematic —Strain produced by Intergranular Regelation (see Secs.3.5,4.12,4.13) — key as in Fig.II.V.

with the surface regelation (ii) and density change (iv) processes, account for the observed drop in hardness and the large grain size in the pressure melting regime. (The surface regelation and density change processes are not sufficient by themselves to fully account for the hardness drop.) It can be shown that the amount of heat required for such a film (say a few microns thick) is small - in fact about 150-500 times less than that which would be needed if bulk melting was invoked.

We now consider further evidence to show (a) that the surface regelation and density change processes are insufficient by themselves to account for the observed hardness drop, and (b) that grain boundary melting occurs.

(1) Evidence for the Grain Boundary Melting Process (No.(iii))

(a) The part of the indentation volume which we attribute to the grain boundary process does not depend on the thermal properties of the indenter or the ice; it is the result of some intrinsic property of the ice. This can be shown by considering the results of the hardness of ice using an ebonite indenter substituted for the steel indenter (Sec.4.6). We note that the thermal conductivities of steel, ice, ebonite are in the ration 260:12:1. This means that when a steel indenter is used and regelation occurs, the heat is transported primarily through the steel indenter. On the other hand with an ebonite indenter the main heat transport occurs through the ice. For the same temperature gradients, the rate of heat, transport would be $\frac{260}{12} \simeq 22$ times less with the ebonite indenter. The volumes of the regelated lips would therefore be negligible. Indeed a simple calculation shows that the temperature difference required for the heat transport necessary for a regelation process with an ebonite indenter is of the order of tenths of a degree (compared to $< \frac{1}{100}^{\circ}C$ for a steel indenter). No such large temperature differences occur in these experiments. In fact, while no attempt was made to measure the lip volumes produced by the ebonite indenter, they were noted to be extremely small. This means that lip formation is associated with a

---

footnote contd.
flows from the low melting point faces to the high melting point faces of the grains and thereby contributes to the total deformation. This process becomes more important as the grain size decreases. A simple calculation indicates that it could markedly affect the hardness results for $t > 100$ secs. If stress concentrations exist on certain grains, the effect will be considerably greater.

regelation process provided the rate at which heat can flow is appreciable. With the ebonite indenter, regelation under the conditions of these experiments is negligible. Fig.IV.V. shows a comparison between the ebonite and steel indentation hardness curves. It can be seen that there is still a drop in hardness as before, but not as dramatically as with the steel indenter. If the grain boundary process (iv) were not operative, one would expect little or no drop at all in the hardness values as the regelation process is not active in this case. Hence this experiment provides evidence to show that there must be processes other than regelation responsible for the increased flow of ice above the pressure melting temperature. Indeed a simple calculation shows that, within the experimental error, the magnitude of the "grain boundary" process for the ebonite indenter is almost identical with that for the steel indenter. This point may also be illustrated with the use of Figs.IV.XII and IV.XIII. In the absence of the surface regelation process, the ebonite indenter is expected to give hardness values corresponding to the other 3 processes only (i), (ii) and (iv)) in action. This means that the hardness values for the ebonite indenter, according to this theory, are expected to correspond to the lines OB and AOB in Figs.IV.XII and IV.XIII. The simple calculation (mentioned above) in fact shows that within the experimental error, this is exactly what happens. These results are encouraging - essentially they show that there is some other process (apart from (ii) and (iv)) responsible for the hardness drop and that the relative magnitude of this other process remains approximately the same in the absence of the surface regelation process.

(b) It is necessary now to consider evidence more directly related to the grain boundaries in ice. Kuroiwa (248) has noted that there is sometimes a lack of etch pits at ice grain boundaries and has suggested that this is a result of the liquid like state of the ice near the grain boundaries. Figs. IV.XVI and IV.XVII show two of the more striking examples of this effect obtained by etchant-replica techniques on ice which has undergone indentation near $0^{\circ}C$. It is interesting to note that these two photographs also show a similar effect around a bubble contained at a grain boundary for the two cases (a) when the bubble is much larger than the clear band as in Fig.IV.XVI(a),(c), and (b) when the bubble is comparable in size to the clear band as in Fig.IV.XVII. Numerous examples of this sort of effect were seen during this research. The

Fig.IV.XVI(a) Figure showing replica of an etched ice specimen which has undergone indentation near 0°C. The specimen was sectioned in the plane of the indentation (perpendicular to the ice surface). The arrow indicates the direction of the indentation. The clear bands, indicating regions of relatively etch pit free ice, are seen alongside the grain boundaries. A similar effect is also noticeable with the bubble contained on the grain boundary (at the lower middle part of the picture. The bubble is larger than the width of the clear band and the band is seen to follow the circumference of the bubble. See also the enlarged Figures (b) and (c) overleaf. (Sec.4.12(2)).

Fig.IV.XVII Figure showing replica of an etched ice specimen which has undergone indentation near 0°C. The specimen was sectioned perpendicular to the plane of the indentation (parallel to the ice surface). Clear bands similar to those in Fig.IV.XVI are seen. The effect of a bubble (of size comparable to the band width) contained on the grain boundary is seen. The bubble distorts the shape of the clear band. (Sec.4.12, (2)).

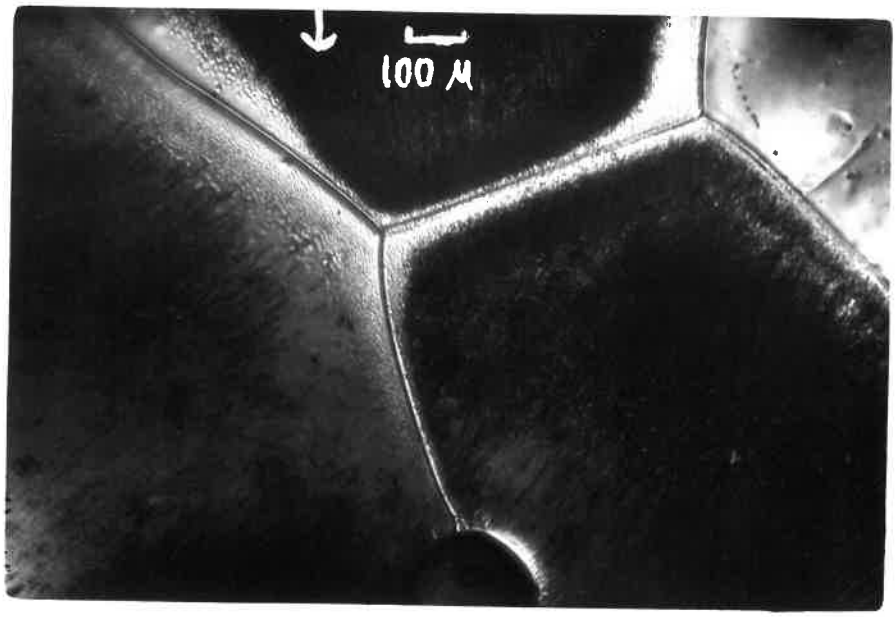
100 μ

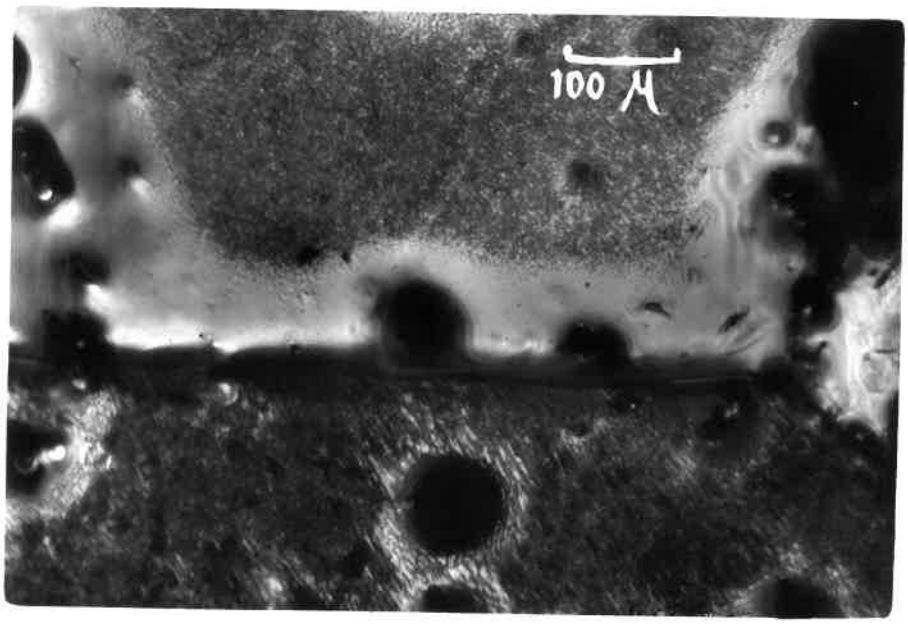
100 μ

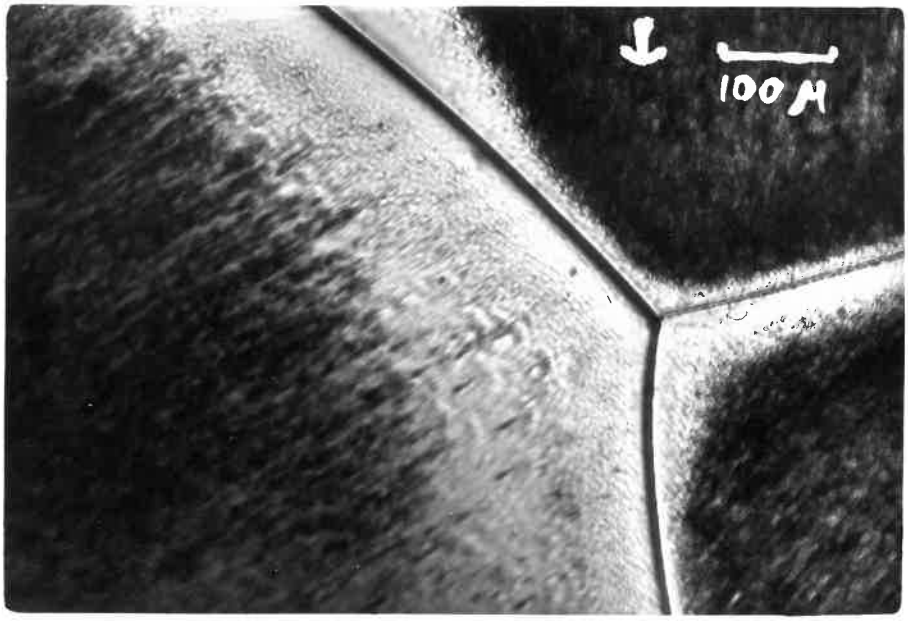
100 μ

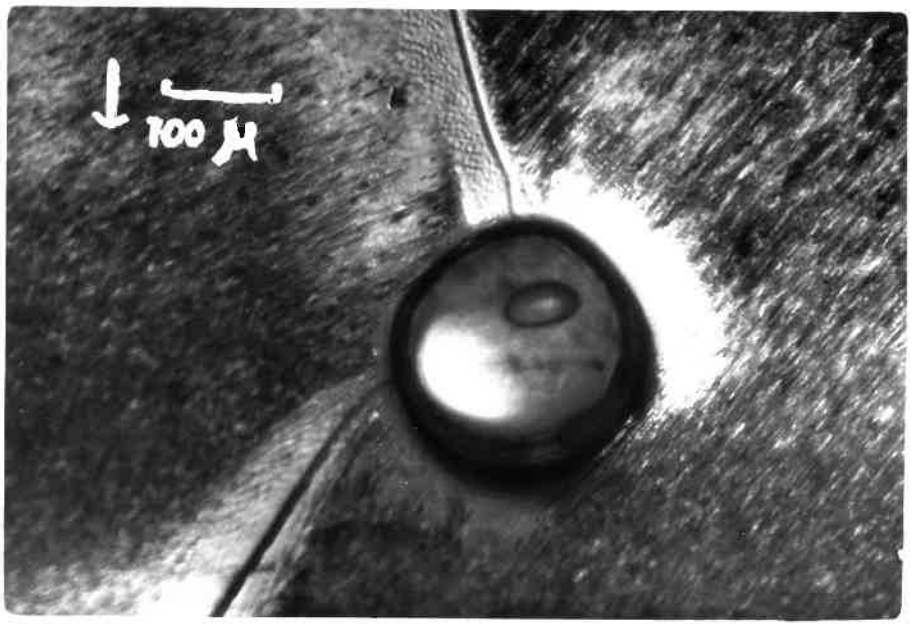
100 μ

Fig. IV. XVI(b) Enlargement of upper part of Fig. IV. XVI(a).

Fig. IV. XVI(c) Enlargement of lower part of Fig. IV. XVI(a).

Fig.IV.XVI(b) Enlargement of upper part of Fig.IV.XVI(a).

Fig.IV.XVI(c) Enlargement of lower part of Fig.IV.XVI(a).

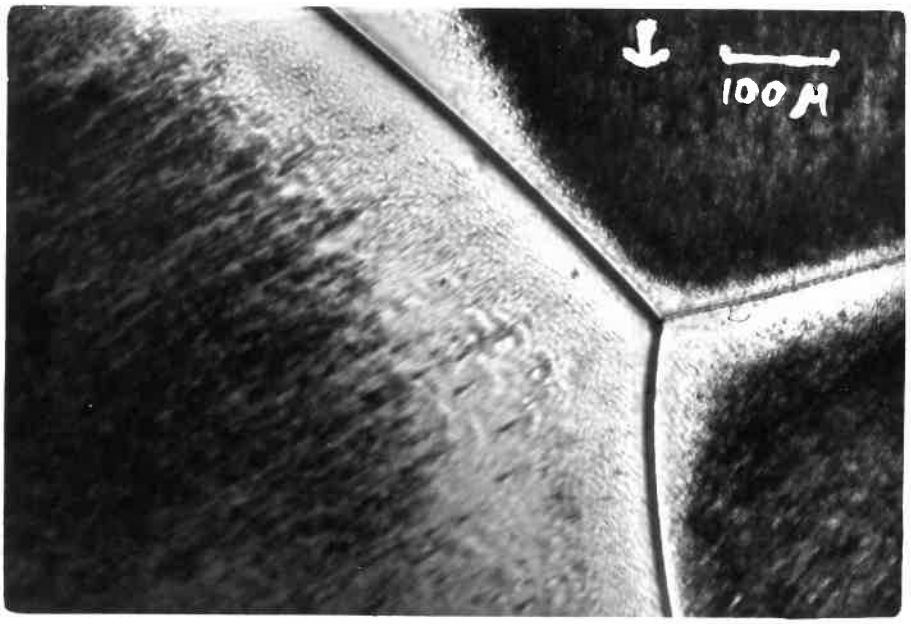
100 μ

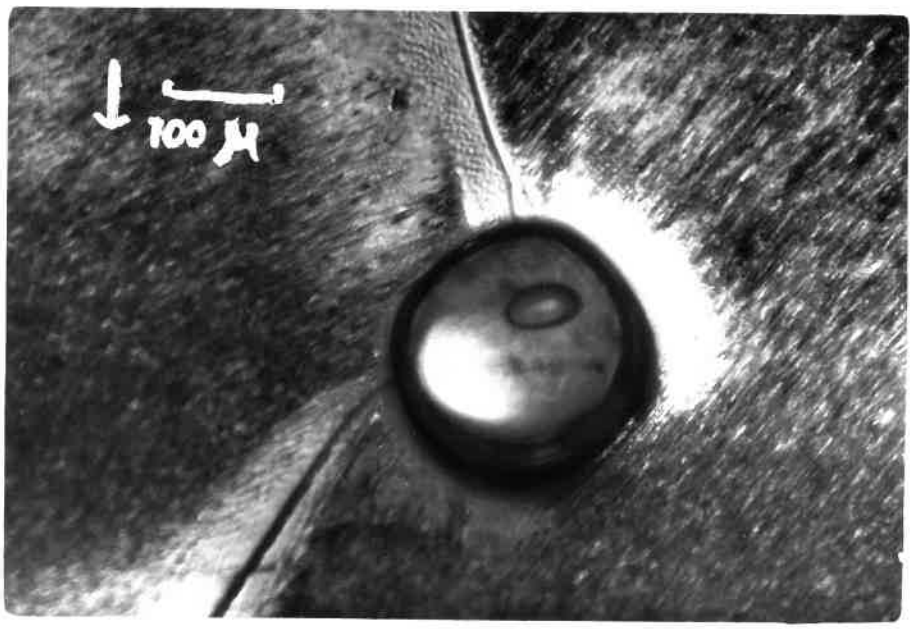
100 μ

width of the film varied considerably from grain to grain - this is of course to be expected since the angle of misfit between different grains also varies.

We see that the viscous grain boundary effect together with processes (ii) and (iv) so far adequately account for the above increase in flow rate and grain size of ice deformed above the pressure melting temperature. In particular we suppose that this viscous layer is liquid-like in nature for two reasons: (1) The etchant-replica result, and (2) that any explanations must include some melting phenomenon because the anomalous increase in flow rate always occurs above the pressure melting temperature.

(3) Grain Boundary Effects and Bubble Loss.

It now remains to see if the liquid grain boundary effects could also account for the anomalous bubble loss which is observed in the deformed zone at temperatures above the pressure-melting temperature. There are listed below six possible mechanisms which have been suggested in order to explain the observed rapid bubble loss:

(1) Bulk melting of the ice under the indenter.

(2) Fragmentation (and ultimate dispersion) due to regelation resulting from stress concentrations on the bubble.

(3) Coalescence in a strain rate-field.

(4) Migration in a stress gradient.

(5) Migration in a temperature gradient.

(6) Migration, annihilation or aggregation at a liquid type of grain boundary. We consider these in a little more detail:

(1) The possibility of bulk melting has already been discounted.

(2) No real evidence so far has been found to support this mechanism.

(3) Weertman (249) has made theoretical study of the rate of coalescence of bubbles in a strain rate (velocity gradient) field. It is concluded that a total strain of at least 800 per cent is required before appreciable coalescence occurs. The strains involved in an indentation test are typically $\sim$8 per cent, so clearly this effect cannot account for the bubble loss observed.

(4) No theoretical calculations have at present been performed to evaluate this. However, it is clear that this mechanism cannot be important since

Fig. IV. XVIII Optical examination of bubbles in ice which has undergone three separate indentations near $0^{\circ}C$. The specimen was sectioned in the plane of the indentation (perpendicular to the ice surface). The specimen was made with two layers of bubbly ice deliberately sandwiched between clear ice. It is seen that the bubble loss occurs when the indentation time lies between 10 and 1,000 seconds. From this, the rate of bubble loss can be estimated (Sec. 4.12, (3)).

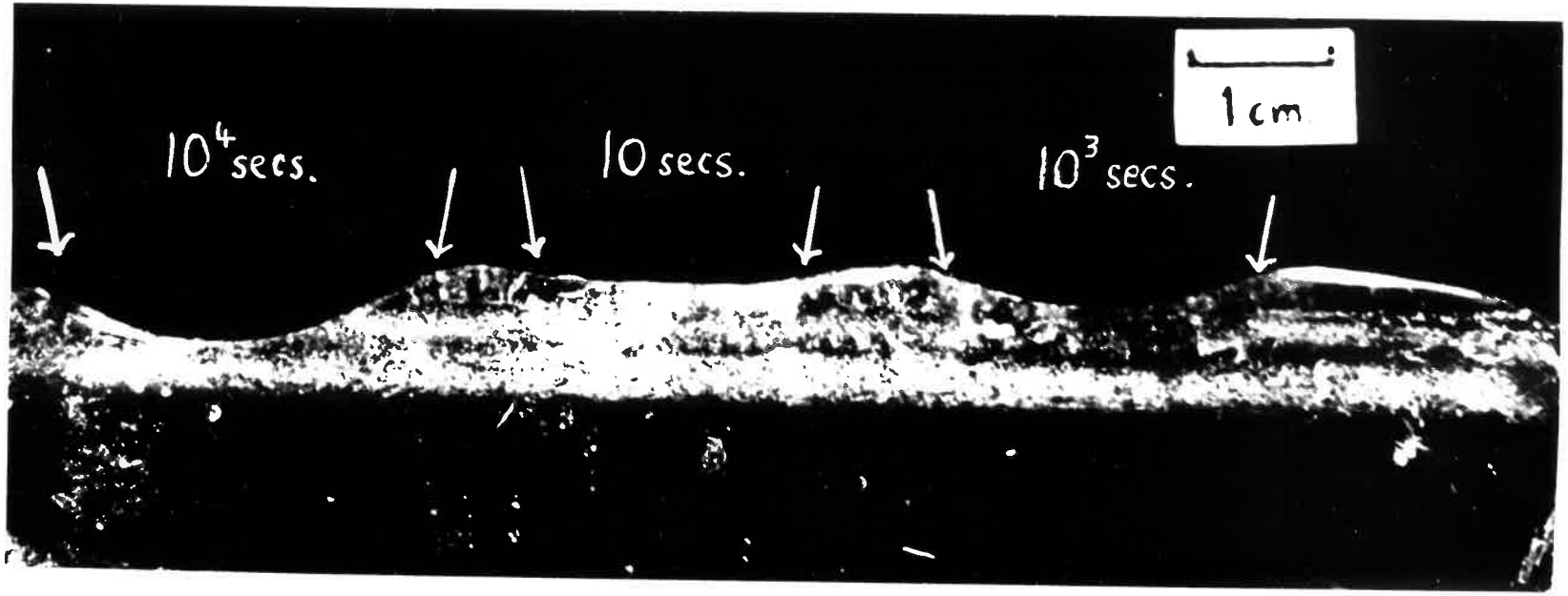
1cm
10^4 secs.
10 secs.
10^3 secs.

the stresses (and stress gradients) are their lowest for indentations at $0^{\circ}C$, whereas it is precisely at these temperatures that the bubble loss is at its greatest.

(5) The effective bubble velocity was estimated by examining indentations in an ice specimen in which two horizontal layers of bubbly ice were sandwiched between clear ice. This experiment is described in more detail in Section 4.9(i). From Fig.IV.XVIII it is seen that the bubble loss occurs between $t = 10$ and 10^3 secs. From this we estimate the effective bubble velocity as 10^{-4} - 10^{-2} cms/sec. However Nakaya (250) and Stehle (251), (252) obtained bubble velocities of 10^{-5}-10^{-6} cms/sec. for a unit temperature gradient in ice near $0^{\circ}C$ and bubble pressures of approximately 10^{-3} to 1 atmosphere. As the temperature gradients inherent in the hardness tests were small and the bubble pressures must have been near atmospheric, this means that the effective bubble velocities in the indentation tests are about 10^3-10^7 too high to be attributed to a temperature gradient effect. It should be noted that Stehle's experiments were done at temperatures up to about $-\frac{1}{2}^{\circ}C$ below the melting point. However it would be surprising if this 1-2$^{\circ}C$ difference in homologous temperature could increase the rate of bubble migration by a factor of 10^3-10^7.

In addition, the temperature gradient effect fails to explain why the bubble loss occurs only above the pressure melting temperature.

(6) All evidence so far suggests that the bubble loss is dependent on the presence of grain boundaries. Fig.IV.XIX shows a picture of a replica taken of a lightly etched vertical section of ice which has been indented at $0^{\circ}C$ for 10^4 secs. This shows how the micro-bubbles are often concentrated along or parallel and close to a grain boundary.

This view is also confirmed by an additional experiment in which a vertical line of bubbles in a single crystal was photographed (by a remote control camera) during the indentation. The experimentation is described in Section 4.9(ii). Fig.IV.XX shows the time sequence of photographs obtained - the bubble line was viewed through the bulk ice and the perspex surround and therefore because of refraction effects, the part of the indenter below the ice surface appears smaller. The crossed polaroid picture shows the whole of the indentation region to be a single crystal. It is clear that in this case

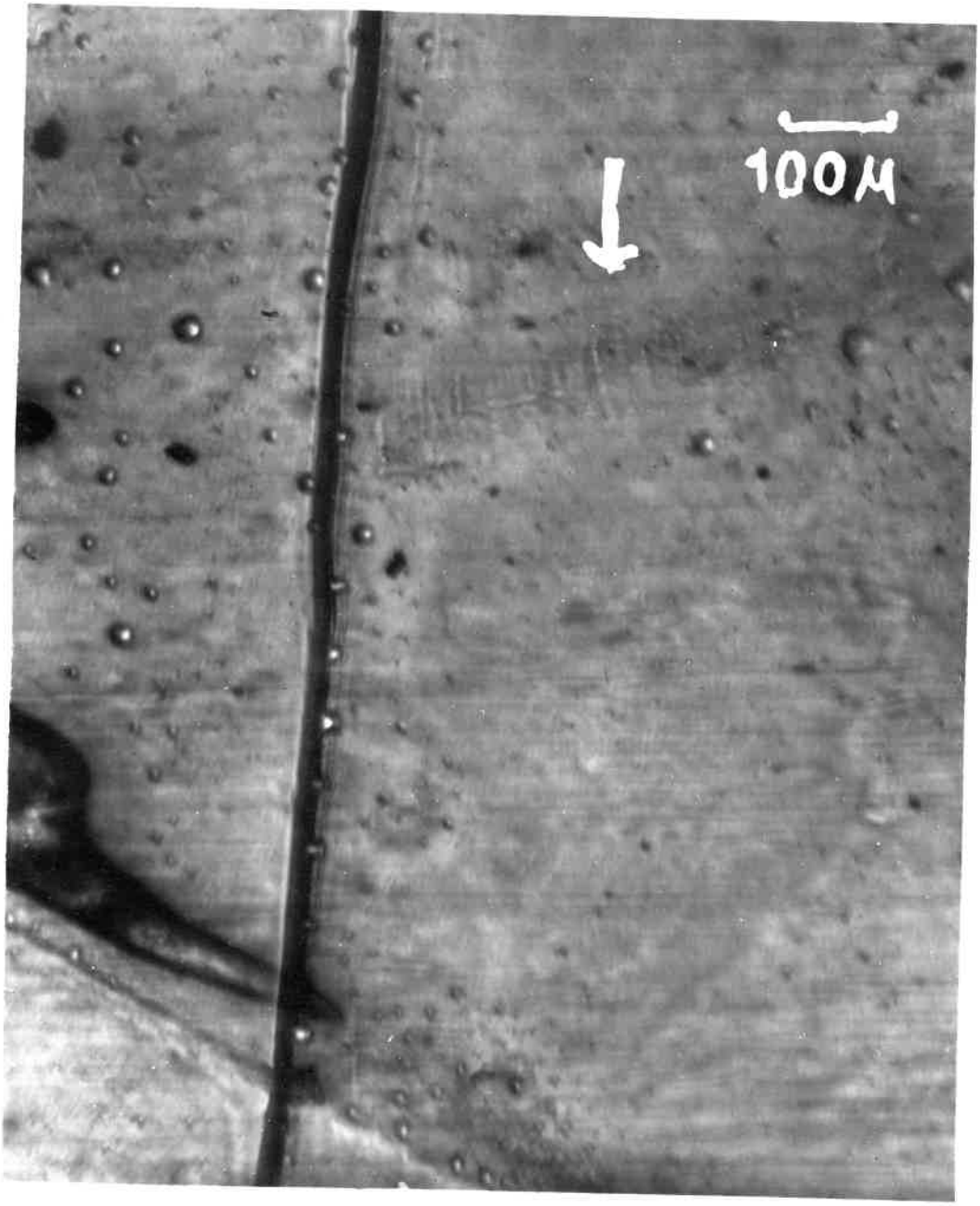
100 M

Fig.IV.XIX Figure showing a replica of lightly etched ice which has undergone indentation near $0^{\circ}C$. The specimen was sectioned in the plane of the indenter and the arrow indicates the direction of the indentation. The micro-bubbles are seen to be concentrated along or parallel and close to the grain boundary (Sec.4.12,(3)).

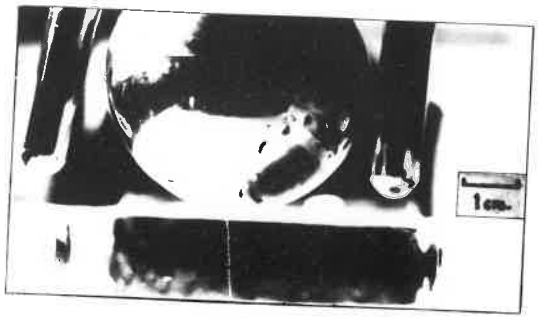

-1 day

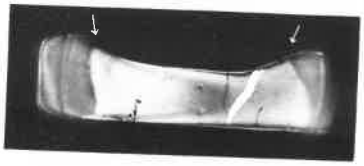

Specimen between crossed polaroids

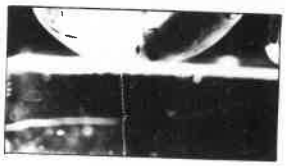

0 secs

10 secs

200 secs

580 secs

1000 secs

1500 secs

1740 secs

2180 secs

3160 secs

Fig.IV.XX Photographic Sequence showing there is little bubble loss during indentation of a Single Crystal (Secs. 49, 412).

no measurable bubble loss took place. This therefore confirms the view that even though mechanism (2) may take place, in general grain boundaries are necessary for enhanced bubble loss. It was hoped that parallel experiments would be performed in which the bubbles in a polycrystalline specimen are photographed during indentation. Because of brittle fracture of the ice specimen and the perspex surround, all these attempts unfortunately failed. However there is no doubt (from the post-indentation examination of polycrystalline ice specimens) that the enhanced bubble loss effect does occur in the presence of crystal grain boundaries.

Since this process occurs only above the pressure melting temperature we assume that the grain boundaries must be in a liquid-like state for bubble loss to occur.

(4) Summary.

To sum up, we conclude that above the pressure melting temperature there are liquid like layers at the grain boundaries. These account for the bubble loss and the formation of large grains. In addition, together with a surface regelation process, this mechanism accounts for the major part of the drop in hardness observed.

D. Additional Discussion

4.13 A Reinterpretation of Glen's Creep Results

The writer has shown (Sec.4.10) that the kinematic hardness equation and Glen's Flow Law may be written in analogous form, viz.

$$p = A_4.(\frac{1}{t})^{1/m} . \exp(\frac{Q}{mRT}) \qquad (4.17)$$

$$\sigma = A_5.(\dot{\epsilon})^{1/m} . \exp(\frac{Q}{mRT}) \qquad (4.18)$$

We can therefore draw plots of $\log \sigma$ against $\frac{1}{T}$ just like the hardness curves. Varying $\dot{\epsilon}$ will give a family of such curves just as in the hardness

no measurable bubble loss took place. This therefore confirms the view that even though mechanism (2) may take place, in general grain boundaries are necessary for enhanced bubble loss. It was hoped that parallel experiments would be performed in which the bubbles in a polycrystalline specimen are photographed during indentation. Because of brittle fracture of the ice specimen and the perspex surround, all these attempts unfortunately failed. However there is no doubt (from the post-indentation examination of polycrystalline ice specimens) that the enhanced bubble loss effect does occur in the presence of crystal grain boundaries.

Since this process occurs only above the pressure melting temperature we assume that the grain boundaries must be in a liquid-like state for bubble loss to occur.

(4) Summary.

To sum up, we conclude that above the pressure melting temperature there are liquid like layers at the grain boundaries. These account for the bubble loss and the formation of large grains. In addition, together with a surface regelation process, this mechanism accounts for the major part of the drop in hardness observed.

D. Additional Discussion

4.13 A Reinterpretation of Glen's Creep Results

The writer has shown (Sec.4.10) that the kinematic hardness equation and Glen's Flow Law may be written in analogous form, viz.

$$p = A_4.\left(\frac{1}{t}\right)^{1/m} . \exp\left(\frac{Q}{mRT}\right) \qquad (4.17)$$

$$\sigma = A_5.(\dot{\epsilon})^{1/m} . \exp\left(\frac{Q}{mRT}\right) \qquad (4.18)$$

We can therefore draw plots of $\log \sigma$ against $\frac{1}{T}$ just like the hardness curves. Varying $\dot{\epsilon}$ will give a family of such curves just as in the hardness

plots for varying loading times (t). We have recalculated Glen's data in this way and the results are plotted in Fig.IV.XXI. It is at once apparent that these results show two striking resemblances to the hardness data. First at temperatures below the pressure melting temperature where plastic flow and creep are occurring, the slopes are very similar. Equations (4.17) and (4.18) show that this similarity is to be expected and is discussed further in Section 4.11.

Secondly at temperatures at or above the pressure melting temperature (i.e. $-0.02^{\circ}C$ for Glen's creep curves, and $-0.08^{\circ}C$ to $-3^{\circ}C$ for the hardness curves) both sets of curves show that the stress for a given strain rate is appreciably smaller than expected. Glen used Riecke's relation (Sec.3.5) to show that pressure melting is impossible at $-0.02^{\circ}C$. However more recently it has become apparent (see Sec.3.5) that Riecke's formula cannot be validly used, seeing that, apart from any other reasons, it predicts a value for ΔT (the depression of the melting point) which is small compared to that obtained using the Clausius-Clapeyron equation (3.1). Using a magnified temperature scale, Glen's $-0.02^{\circ}C$ results have therefore been replotted in Fig.IV.XXII using the pressure melting curves derived from the Clausius-Clapeyron equation. Section 3.5(d) shows that according to the theory of Verhoogen et al. the value $\frac{\sigma}{3}$ should be used for P in equation (3.1), whereas the Gibbs-Kamb theory proposes that it is the value σ that should be used. The two pressure melting curves plotted in Fig.IV.XXII are derived using both these values for P. However for reasons discussed in Section 3.5, only the Gibbs-Kamb value σ is acceptable. Considering therefore the pressure melting curve for $P = \sigma$ only, we see that four of Glen's $-0.02^{\circ}C$ results are at or above the pressure melting temperature; we conclude that the reason for the enhanced creep rates lies in a pressure melting effect rather than the "periodic melting" mechanism proposed by Glen ((1),(2)).

Since the pressure melting effect has been fairly extensively examined in the hardness experiments, we now try and extend these arguments to Glen's $-0.02^{\circ}C$ creep results: from a comparison with the theory outlined for the hardness-behaviour in the pressure melting regime, we see that Glen's enhanced creep rates may be a result of a) the regelation process No.(ii), and/or

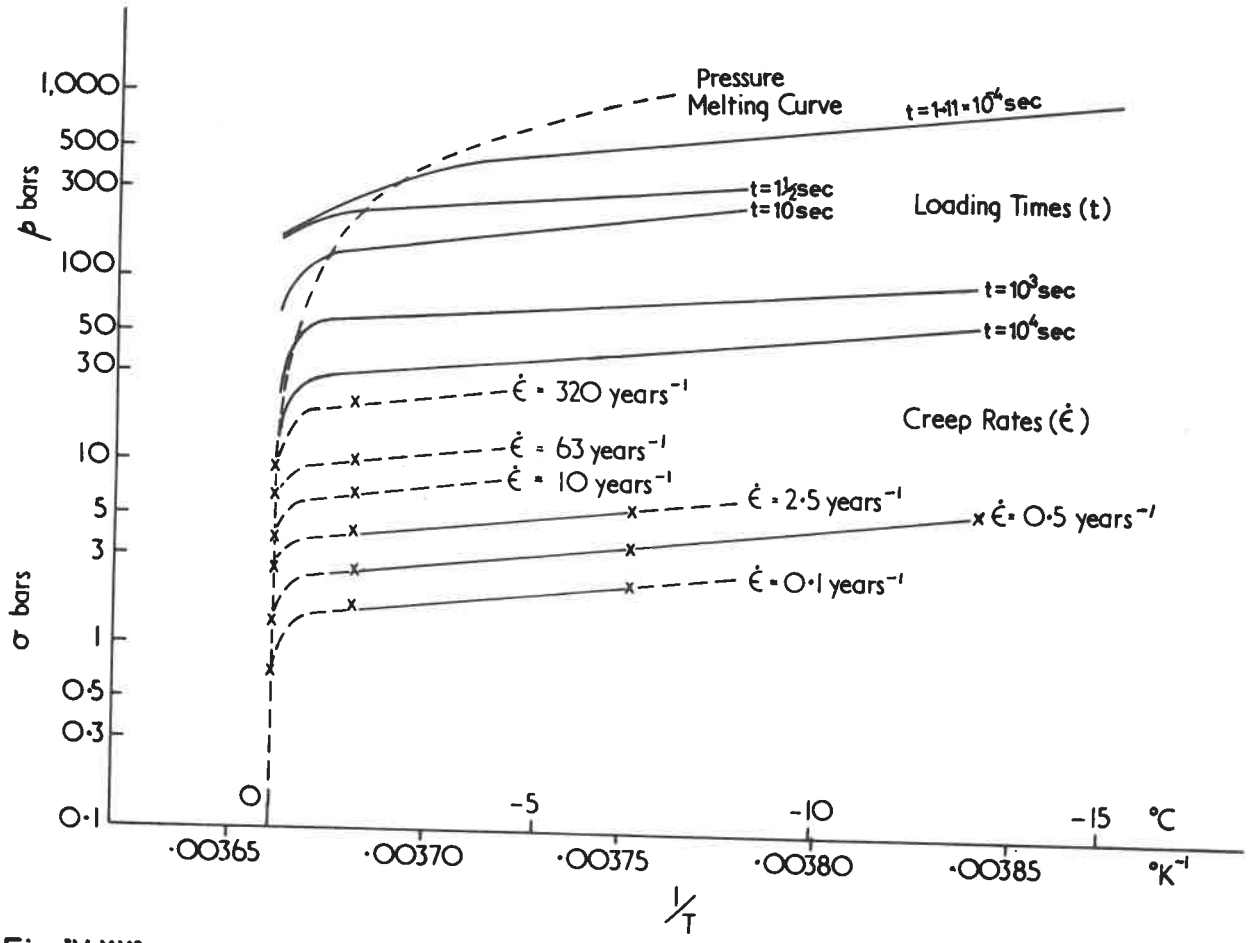

Fig.IV.XXI Comparison of Creep (Glen) and Hardness (Fig.IV.VII) Data.(Secs. 4.11-4.13).

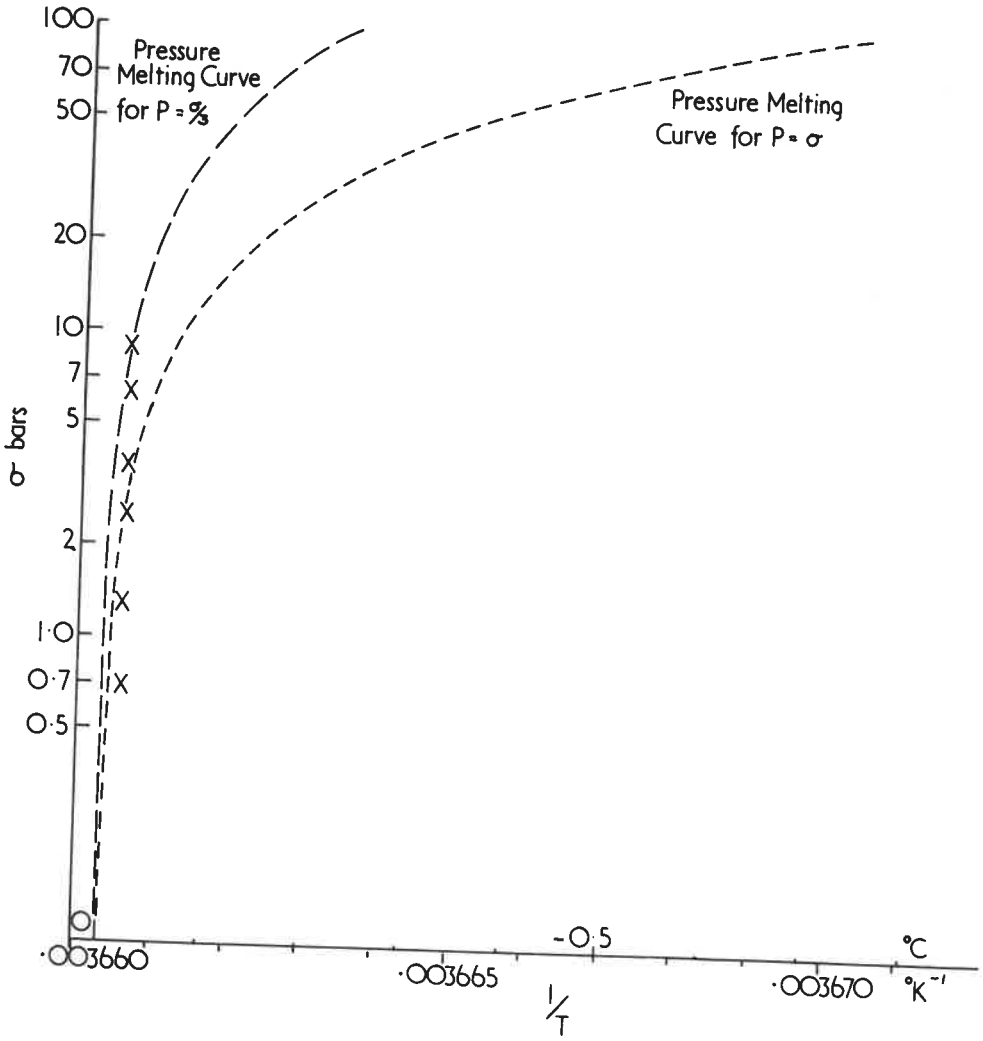

Fig. IV.XXII Glen's Creep Data for −0.02°C (see Fig. IV.XXI) on a Magnified Temperature Scale (only the P=σ Melting Curve is Physically Meaningful).

b) the liquid grain boundary process No.(iii). We discuss these possibilities separately:

(a) Regelation. If a regelation process was present in Glen's -0.02°C tests, one would expect it to take place as a thin liquid layer formed at the top and bottom platten-ice interfaces under the pressure σ. This liquid film would then flow to the sides of the ice specimen where it could refreeze in the absence of the applied pressure σ.

However if this process were to occur, one might expect a regelation lip (as in the hardness experiments) to be formed on the sides of the specimen. Glen (2) did not report any such observation and in addition the photograph taken of one of his specimens after deformation at -0.02°C ((2), Fig.5.3) does not seem to indicate any lip formation. In addition one notes that the plattens used by Glen were good thermal insulators. These creep experiments may therefore be regarded as being analogous to the hardness experiments in which an ebonite indenter was used (Secs.4.6 and 4.12). One would therefore similarly expect the "recycling regelation heat" to be transported through the ice, rather than the platten, thereby reducing the effectiveness of the regelation process to negligible proportions.

It is seen that there are weighty reasons for considering the regelation process to be inactive in Glen's experiments. However in contrast one should note that according to Table IV.VII and Fig.IV.XII the regelation process assumes greater importance for lower strain rates (i.e. longer loading times). As Glen's experiments were conducted using lower strain rates than those in the hardness tests, one may argue that the regelation process may be sufficiently increased so as to become significant even though thermally insulated plattens were used.

Clearly it is not possible, at present, to say with certainty whether or not the regelation process makes any significant contribution to the enhanced flow rates in Glen's experiments. However it is the writer's opinion that the regelation process is unlikely to be of any importance here.

(b) Grain Boundary Melting. By analogy with the hardness experiments one may postulate that in the interior of the ice specimen, many of the grain boundaries are in a liquid like state. The hydrostatic pressures in these

liquid boundaries should be as large as σ. Hence it is proposed that the liquid grain boundary process operates for temperatures at or above the pressure melting curve (for $p = \sigma$) in Fig.IV.XXII.

To avoid any possible confusion to the reader it is pointed out that the grain boundary process (like the regelation process) assumes greater importance at the lower strain rates (or longer loading times). One may have possibly come to a different conclusion after examining Table IV.VII. However it must be realised that this table indicates the relative importance of each process. That the absolute magnitudes of both the regelation and the liquid grain boundary processes increase with loading time (or with decreasing strain rates) is evident from Fig.IV.XXIII. In theory it should be possible to extrapolate the curve in Fig.IV.XXIII to the strain rate (or stress) range involved in Glen's experiments; by using these values one could check whether Glen's $-0.02^{\circ}C$ enhanced creep rates corresponds to those expected when only creep and grain boundary processes are active. However the errors involved in such an extrapolation (of about two orders of magnitude) are too large. It is the opinion of the writer that only when more creep experiments are performed in the pressure melting regime, will it be possible to make any definite conclusions on this matter.

It is interesting to note that the particular grain boundary process called "intergranular regelation" (see footnote in Sec.4.12) may be of importance here. A simple calculation suggests that this mechanism could contribute to Glen's enhanced flow rates at $-0.02^{\circ}C$ particularly if the compressional stress is concentrated on certain grains.

To sum up, it is concluded that Glen's enhanced creep rates at $-0.02^{\circ}C$ are a result of a pressure melting effect. In particular it is believed though not with certainty, that the liquid grain boundary process (as described in Sec.4.12(iii)) is mainly responsible for these enhanced creep rates. In fact Glen's Flow Law, for ice at $-0.02^{\circ}C$, has been extensively used in Glaciological theory without particular regard to pressure melting temperatures of the ice in question. This chapter shows however that the pressure melting temperature is a parameter of utmost importance. Some of the Glaciological implications of these results are discussed in Section 7.2.

liquid boundaries should be as large as σ'. Hence it is proposed that the liquid grain boundary process operates for temperatures at or above the pressure melting curve (for $p = \sigma'$) in Fig.IV.XXII.

To avoid any possible confusion to the reader it is pointed out that the grain boundary process (like the regelation process) assumes greater importance at the lower strain rates (or longer loading times). One may have possibly come to a different conclusion after examining Table IV.VII. However it must be realised that this table indicates the relative importance of each process. That the absolute magnitudes of both the regelation and the liquid grain boundary processes increase with loading time (or with decreasing strain rates) is evident from Fig.IV.XXIII. In theory it should be possible to extrapolate the curve in Fig.IV.XXIII to the strain rate (or stress) range involved in Glen's experiments; by using these values one could check whether Glen's $-0.02^{\circ}C$ enhanced creep rates corresponds to those expected when only creep and grain boundary processes are active. However the errors involved in such an extrapolation (of about two orders of magnitude) are too large. It is the opinion of the writer that only when more creep experiments are performed in the pressure melting regime, will it be possible to make any definite conclusions on this matter.

It is interesting to note that the particular grain boundary process called "intergranular regelation" (see footnote in Sec.4.12) may be of importance here. A simple calculation suggests that this mechanism could contribute to Glen's enhanced flow rates at $-0.02^{\circ}C$ particularly if the compressional stress is concentrated on certain grains.

To sum up, it is concluded that Glen's enhanced creep rates at $-0.02^{\circ}C$ are a result of a pressure melting effect. In particular it is believed though not with certainty, that the liquid grain boundary process (as described in Sec.4.12(iii)) is mainly responsible for these enhanced creep rates. In fact Glen's Flow Law, for ice at $-0.02^{\circ}C$, has been extensively used in Glaciological theory without particular regard to pressure melting temperatures of the ice in question. This chapter shows however that the pressure melting temperature is a parameter of utmost importance. Some of the Glaciological implications of these results are discussed in Section 7.2.

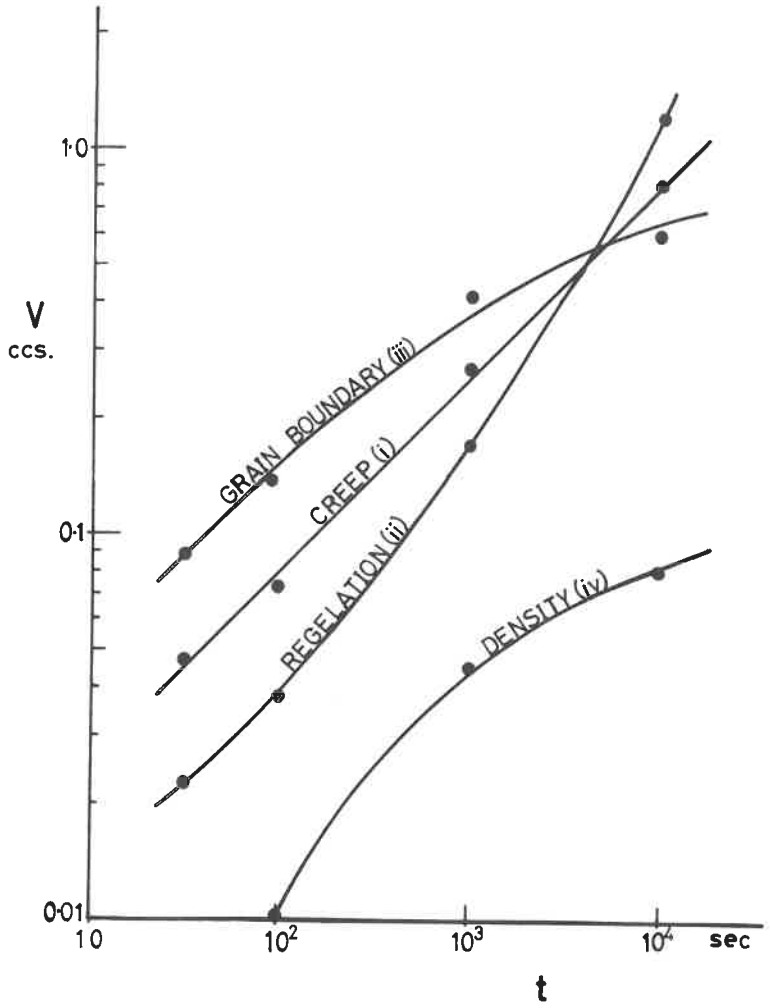

Fig. IV.XXIII Absolute Magnitude of the Mechanisms in Indentation at 0°C - see Table IV.VII (log. scales).

4.14 Comparison with other Work

The hardness curves given in this chapter show approximate agreement with those obtained by other workers ((164), (253), (254)). However in view of the different experimental conditions and analyses involved (see Sec.3.6 for an appreciation of these difficulties) it is felt that further comparison of these absolute values for the hardness of ice is not really worthwhile. It is interesting to note that most of these other results suffer from the mistake of failing to properly divide the data into different regimes of deformation. Specifically Butkovich (164) fails to differentiate between the different activation energies above and below $-7^{\circ}C$ (see Table III.I (9)). King's results (253) fail to differentiate between the creep and pressure melting regimes. It is however evident that King's results, while relatively few in number, can be shown to be consistent with the "two regime model" (for $0^{\circ}C \rightarrow -10^{\circ}C$) outlined in this chapter. For these reasons, the activation energy deduced by Glen ((1),(2)) from King's results can no longer be regarded as very meaningful. In fact Section 4.11 shows that if anything the activation energy for creep Q increases with stress; the opposite conclusion was drawn (1) from King's preliminary results.

4.15 Elastic Recovery

Tabor (239) has noted that the permanent indentation after a hardness test has a larger radius of curvature r than that of the indenting sphere R. However the change in the indentation diameter d after removal of the load is very small and the equations (4.1) and (4.2), which have been used to calculate the hardness values in this thesis, may therefore be regarded as realistic.

This change in the curvature of the indentation after removal of the load has been shown by Tabor to be the result of the release of elastic stresses in the specimen. Using a simplified form of Hertz's classical equations ((255), (256)), this elastic recovery effect may be treated quantitatively using the following equation:

$$d = 2a = k \left\{ \frac{L}{2} \cdot \frac{Rr}{(r-R)} \cdot \frac{1}{E} \right\}^{1/3} \qquad (4.31)$$

where $k \simeq 2.22$

The results obtained from the preliminary hardness experiments (see Sec.4.4(i)) provide sufficient data to test the validity of equation (4.31) when applied to the indentation of ice. However the elastic recovery measurements made in the friction experiments (Chapter V) were more accurate than those of the hardness experiments. Because the stress systems in friction experiments are more complicated, it is difficult to know how much importance can be attached to these determinations.

The hardness and friction (creep regime) results yield values for k in the range 3-5.5. These values are seen to be higher than the theoretical value (2.22). Physically, this means that the indentations recovered by an amount greater than that predicted by the "elastic recovery equation" (4.31).* However these determinations must not be regarded as being accurate. It is interesting to note however that these observations (for hardness and friction experiments) indicate that the elastic recovery in the pressure melting regime is considerably less. This provides additional reasons for believing that the modes of deformation involved in the pressure melting and creep regimes are considerably different.

4.16 Brittle Cracking of Ice Specimens

It was noticed that "fine cracks" sometimes developed in the ice specimens during indentation. These cracks were only observed with the large columnar grained specimens. Because the specimens were constrained during indentation by the metal mould, the width of these cracks was very small - in fact these cracks were noticeable only because they appeared as thin white (or cloudy) interior surfaces extending over areas of several sq.cms. A study of these cracks showed that many of them were coincident with the grain boundary surfaces between adjacent crystals. This can be seen by comparing the optical and

*Alternatively, this means that the effective Young's Modulus E is smaller than the expected value (10^{11} dynes/cm^2).

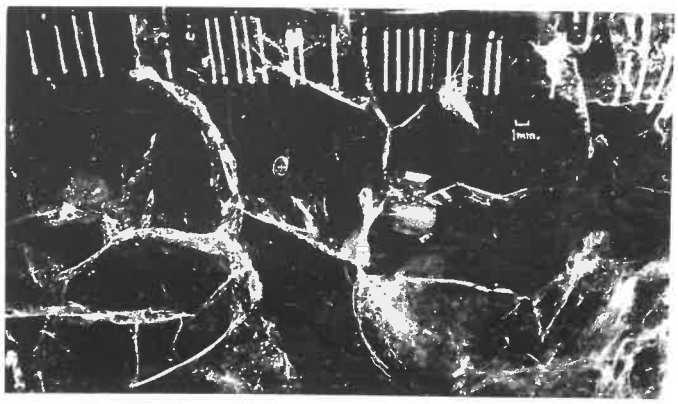

a Optical Examination

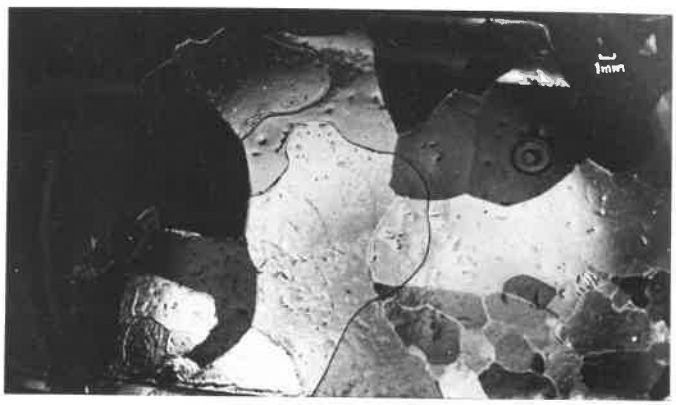

b Crossed-Polaroid Examination

Fig.IV.XXIV Pictures showing that Many of the Cracks (seen in a as White Lines, excluding the array of growth bubbles) are Coincident with the Grain Boundaries (seen in b) - Sec. 4.16.

crossed-polaroid pictures of an ice specimen after indentation (Fig.IV.XXIV)- most of the cracks are coincident with grain boundaries. It is interesting to note that Gold (see Sec.3.6(d)) has observed that when columnar grained ice specimens are subjected to compressions of 4-20 bars, about one quarter of the cracks occur at grain boundaries. While no such statistical study has been made for the hardness experiments, it is almost certain that the proportion of cracks at grain boundaries after indentation is greater than 1/4 as observed by Gold. The reason for these differences may be that, unlike Gold's experiments, the hardness experiments involved (i) mechanical constraining of the specimen by the mould, (ii) penetration in the direction of the long axis of the columnar grains, and (iii) a stress range 1-30 times higher.

Exceptions to grain boundary-crack formation were often evident with very large grain specimens. In one particular specimen several cracks were found in one grain. When viewed along the c axis of this grain, the crack lines were seen to intersect at angles which were discreet multiples of 30°. In view of the six fold symmetry in the basal plane of ice, it is clear that these cracks must have been in definite crystallographic planes. Unfortunately this specimen was accidentally lost by melting before there was any chance to determine the crystallographic directions of the crack lines by standard X-ray methods.

4.17 Unusual Features - "Deformation Bands"

The etchant-replica studies (see Table IV.II) revealed a large number of interesting features. The etch-replicant used in all these studies was a solution of about 6 per cent Formvar in ethylene dichloride. The replicas were usually lifted off the ice using ordinary "sellotape". The replicas were then coated with Gold ($\sim$ 100 Å thick) using ordinary evaporating techniques in order to reduce the reflections off the back face of the replica. The photographs were taken using a metallurgical optical microscope.

In addition to the ordinary and "furrowed" etch pits (as seen for example in Figs.IV.XVI.XVII, see also Bascom et al. (314)) the usual geometrical shaped etch pits expected for a hexagonal structure like ice were seen. "Etch pit

Rosettes" with 4-fold and 6-fold symmetries were common. Sometimes single (or double) rows of etch pits were seen parallel and close to a grain boundary - with a separation of 5-1,000μ. Unusual clusters of etch pits were frequently seen at bubbles, inclusions or imperfections throughout certain grains only. These features apparently bear resemblance to the thermal etching characteristics sometimes observed in metals (Packer (257)). Unfortunately there is not sufficient space to discuss these features in any detail.

One extremely unusual feature that must be briefly discussed here is the common occurrence of "deformation bands" in the replicas of deformed highly polycrystalline ice. "Deformation band" is merely a descriptive name for these bands necessarily coined by the writer because of the apparent lack of similar observations by other investigators. Its characteristics are now discussed: these bands are narrow (10 to 150μ) but extend for several centimetres and terminate usually but not always, at the ice surface. Closer examination shows that these bands consist of 20-60 parallel, sometimes puckered, layers about 1-5μ thick. Typical examples of such bands are shown in Figs.IV.XXV. These deformation bands curve smoothly through the specimen and are usually continuous across the grain boundaries - they cannot therefore be associated with any particular crystallographic direction. While nearly always of smooth continuous shape they sometimes turn very sharply near their termination. Rare occurrences of discontinuity are shown in Figs.IV.XXV. In these photographs the bands appear to have slipped sideways through a distance of 100-700μ. A magnification of this slip region (Fig.IV.XXV) shows an interesting array of lines set at angles of approximately 120°. These bands were only noticed in the ice sections cut perpendicular (vertical) to the plane of the indentation. It is to be noted that the replicas were taken shortly after the vertical sectioning - this may possibly indicate that the reason for the absence of these bands in the horizontal sections is that they were lost by atmospheric evaporation at the ice surface before being covered by the etchant-replicating fluid. These bands were observed in specimens which had been deformed in both the creep and pressure melting regimes, for static and dynamic indentations. The maximum density of bands was found for specimens deformed just below the pressure melting point (-1½°C to -3°C, say) - i.e. the temperatures for which creep regime

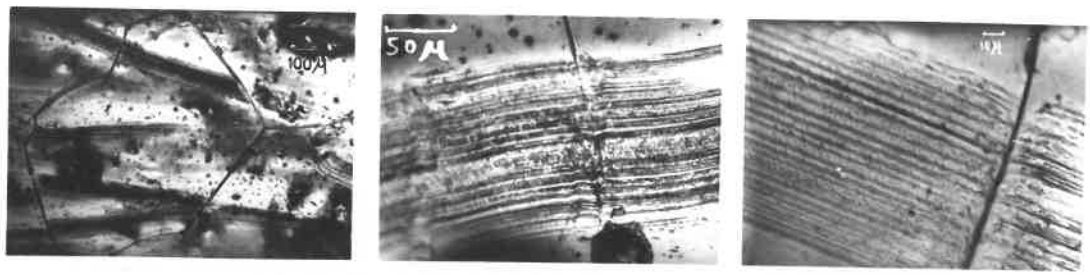

a b c

a-c Examples of Bands Crossing Grain Boundaries.

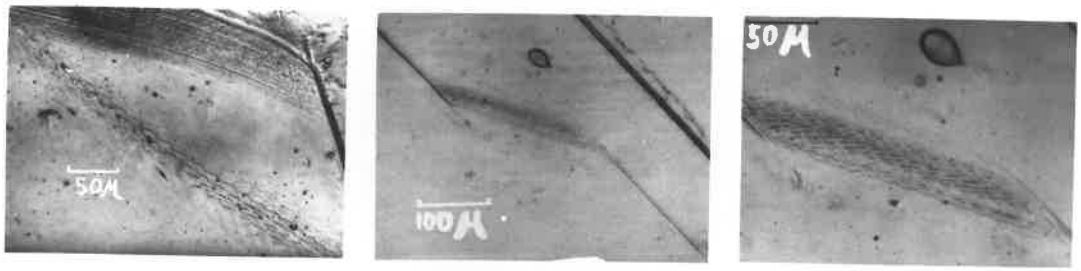

d e f

d-f Examples of "Slipping Bands".

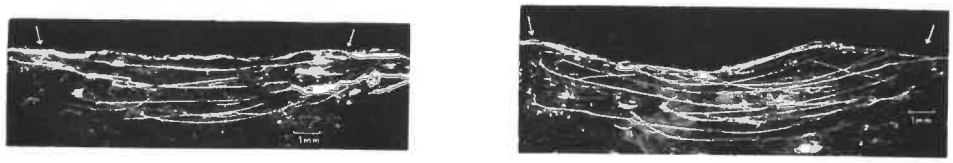

g (t= 2secs) h (t=10⁴secs)

g-h General Morphology of Bands after Indentation (T=-0·7°C).

Fig.IV.XXV Some Characteristics of the "Deformation Bands"-Sec. 4.17.

recrystallization is a maximum. The overall geometrical shape of these bands proved to be most interesting. Because the bands were narrow they had to be normally viewed in high magnification microscopes - this produced a reduction in the field of view and therefore the overall shape of the bands could not be appreciated. However it was found that by altering the direction of the incident light beam with respect to the direction of the bands, it was possible to bring out strong reflections from the thin sublayers in the bands. Using this technique with low magnification microscopy, it was possible to obtain pictures showing the general morphology of the bands as in Figs. IV.XXV$_{g-h}$. It is immediately apparent that the general morphology of these bands is as if they were once horizontal but became displaced into a concave path as a result of the plastic deformation in the ice under the indenter. In this respect the bands appear to be very similar to the post-indentation shapes of the horizontal markers sometimes used in plasticine models. The bands appear to be considerably less curved for indentations in the pressure melting regime. The origin of these bands remains a mystery to the writer. In view of its characteristics described above, it would appear that it cannot be just a feature formed in the preparation of the specimens. Apart from the "slip photographs", the bands appear to have little crystallographic connection. They seem to be more related to the general morphology of indentation - deformation and possibly stress-enhanced - recrystallization. Because these deformation bands are so numerous and phenomenologically consistent, it was felt that some mention ought to be made of them even though their origin and behaviour is uncertain.

4.18 Summary of the Chapter

Studies on the indentation of ice have indicated some anomalies in its deformation properties near the melting point. It is found that above the pressure melting temperature, there is a considerable increase in the flow rate of ice. In addition, the deformed ice is characterised by its large grain size and loss of bubbles. Using various techniques, it has been possible to extend the range of stresses and strain rates in these studies. However it is

found that the same anomalies still occur consistently above the new pressure melting temperatures. It has therefore been found both necessary and convenient to divide the deformation behaviour of ice into two distinct regimes over the temperature range of $0^{\circ}C$ to $-12^{\circ}C$, say.

The lower temperature range ($\leq(0.08\pm3)^{\circ}C$ to $-10^{\circ}C$) is called the "Creep Regime". This is because the hardness values and the recrystallisation habits can be interpreted in terms of the transient, steady-state, and accelerated creep properties of ice as determined by Glen and Steinemann. However these hardness experiments effectively extend the range of study to much higher stresses and strain rates than those used previously. It is noted that certain deviations from Glen's Flow Law are apparent in these experiments. More specifically, it is noted that for stresses above about 300 bars, the stress exponent n and the activation energy Q increase rapidly. An attempt is made to interpret both the normal and deviatory plastic flow in terms of the dislocation models outlined in Section 3.6.

The higher temperature range ($0^{\circ}C$ to $-(0.08\pm3)^{\circ}C$) is called the "Pressure Melting Regime". This is because the anomalies always occur above the pressure melting temperature; this means that any relevant explanations must include some melting phenomenon. Recent experiments shed further light on the mechanisms involved in the pressure melting regime. As a result it has been found that the anomalous behaviour can be interpreted in terms of two other processes in addition to ordinary creep. Both these processes involve melting phenomena and are called the "Regelation" and the "Liquid Grain Boundary" processes. The deformation of ice has now been treated quantitatively in terms of these three processes. In addition the grain growth and bubble loss phenomena may be interpreted in terms of the liquid grain boundary process.

Although a number of unexplained features emerge from these studies, it is probably true to say that, on balance, the subject has been clarified considerably. These explanations have fairly far reaching implications for both the "Physics of Ice" and for Glaciology.

CHAPTER V

THE SLIDING FRICTION OF ICE

5.1 Introduction

A number of investigations have been made of the friction of snow and ice: for instance (a) Bowden et al. ((259)-(261)) have demonstrated the role of frictional heating and melting of ice at high speeds ($\sim$ ms./sec), (b) Jordan et al. (262) have shown the importance of the relative humidity of the atmosphere and the liquid "film concept" in the intermediate velocity range ($\sim 10^{-2}$-1 cm/sec), (c) Ericksson (263) has investigated the dependence of friction on the type of snow surface used at high speeds ($\sim$ ms/sec), and (d) Schulz and Knappwost (315) have studied the low temperate friction peaks at speeds of 0.2-1 cm/sec. In this chapter however we are concerned mainly with the effect of pressure melting on the frictional properties of ice at low speeds ($\sim 10^{-2}$ cm/sec). In order to develop these ideas it is first necessary to outline very briefly some of the more important concepts involved in the study of friction.

Bowden and Tabor ((259),(260)) have shown that in a friction experiment, the real area of intimate contact between the hard indenter and the (softer) material surface is not necessarily as large as the apparent area of contact. The indenter is considered to be supported by a large number of minute asperities. The integral sum of the areas of these asperities constitutes the real area of contact. This real area A is expressed in terms of a Yield Stress Y of the material and the normal Load L applied through the indenter:

$$A = \frac{L}{Y} \qquad (5.1)$$

At these regions of real contact, strong adhesion occurs and the force F_s required to deform and break these asperity-bonds in sliding is known as the adhesion (or shear) component of friction. It is related to the specific shear strength s of the asperities:

$$F_s = s_o A \tag{5.2}$$

If one defines the shear component of the coefficient of friction μ_s in the usual way;

$$\mu_s = \frac{F_s}{L} \tag{5.3}$$

then combining equations (5.1)-(5.3) gives:

$$\mu_s = \frac{s_o A}{Y_o A} = \frac{s}{Y} \tag{5.4}$$

However in the theory of friction, one must also consider the force required to plastically move the material ahead of the indenter. This force F_p is known as the ploughing term. We may then define the total friction force F as:

$$F = F_s + F_p \tag{5.5}$$

and the analogous coefficient of friction equation:

$$\mu = \mu_s + \mu_p \tag{5.6}$$

where generally $\mu_j = \frac{F_j}{L}$ (5.7)

(j, arbitrary suffix)

It has been shown ((264),(265)) that in fact one cannot always consider a simple relation between these friction components (as in equations (5.5), (5.7)) because the ploughing and adhesion effects are not entirely independent. This is particularly so for materials in which μ_s is large, when the adhesion forces produce extra "pile up" in front of the indenter thereby increasing the ploughing effect. However in the treatment which follows it will be assumed that these two terms can be treated independently. This assumption is probably a reasonable one for ice, particularly in the pressure melting regime where the adhesion component F_s is low. However this basic assumption should not be entirely forgotten.

We now attempt to estimate the magnitude of the ploughing term F_p: For a hard spherical indenter (radius, R) being dragged across a smooth specimen of ice, one may estimate the area of the friction track (d = 2a) by assuming that only the front half of the indenter area A_L is supported by the ice. This gives:

$$A_L = \frac{\pi a^2}{2} \tag{5.8}$$

$$\frac{\pi a^2}{2} = \frac{L}{P_L(v)} \tag{5.9}$$

where $P_L(v)$ represents the "mean normal pressure" of the ice for a particular sliding speed v. In order to calculate the ploughing component one needs to consider the projected area of ice ahead of the indenter A_F - i.e. the area of indenter seen below the ice surface when viewed horizontally along the friction track. However the area A_F should in principle include some area above the ice surface due to pile up ahead of the indenter. Even though the shear component of friction F_s for ice is small, there may be appreciable pile up formed as a result of regelation processes (as in the hardness experiments, Sec.4.12). However no measurements of this pile up were made in these friction experiments. In this treatment therefore, the pile up is ignored but obviously future experiments must include these refinements. For $d \ll 2R$, one may approximate:

$$a \ll R, \quad A_F \simeq \frac{2a^3}{3R} \tag{5.10}$$

When the track width becomes comparable with the sphere diameter (i.e. $d \simeq 2R$, $a \simeq R$) one must use the exact equation:

$$\left.\begin{aligned} 0 \leqslant a \leqslant R, \quad A_F &= \frac{R^2}{2}[\theta - \sin\theta] \\ \text{where} \quad \theta &= 2\sin^{-1}\left(\frac{a}{R}\right) \end{aligned}\right\} \tag{5.11}$$

These formulae may then be used to estimate the ploughing force F_p:

$$F_p = P_F(v).\, A_F \tag{5.12}$$

where $P_F(v)$ represents the "mean pressure resisting tangential displacement" for the ice at a sliding speed of v. Substituting equations (5.9), (5.10), (5.11) into equation (5.12) gives:

$$a \ll R, \quad F_p \simeq \frac{P_F(v)}{P_L(v)} \cdot \frac{4a}{3\pi R} \cdot L \qquad (5.13)$$

$$0 < a \lesssim R, \quad F_p = \frac{P_F(v)}{P_L(v)} \cdot \frac{R^2(\theta - \sin\theta)}{\pi a^2} \cdot L \qquad (5.14)$$

We note that $F_p = \mu_p . L$ (equation (5.7)) and make the approximation that $P_F(v) \simeq P_L(v)$. Willis (264) has shown that this is a reasonable approximation for well lubricated metals - in fact it turns out, as might be expected, that for ice:

$$P_L(v) \simeq p(t) \qquad (5.15)$$

where $p(t)$ is the hardness of ice for a loading time t which is characterised by certain experimental parameters (this is discussed further in Sec.5.4 (iii)). Hence we finally obtain:

$$a \ll R, \mu_p \simeq \frac{P_F(v)}{P_L(v)} \cdot \frac{4a}{3\pi R} \simeq \frac{4a}{3\pi R} \qquad (5.16)$$

$$0 < a \lesssim R, \mu_p = \frac{P_F(v)}{P_L(v)} \cdot \frac{R^2(\theta - \sin\theta)}{\pi a^2} \lesssim \frac{R^2(\theta - \sin\theta)}{\pi a^2} \qquad (5.17)$$

This leads to the important result that on this theory, the contribution of ploughing to the coefficient of friction is independent of the material, speed of sliding etc., and is determined solely by the geometry of the track indentation. These equations are used to estimate the magnitude of ploughing in the friction results (Sec.5.4,(iv)). The two approximations ((i)$P_F(v) \simeq P_L(v)$, and (ii) that pile up is negligible) are such that the value of μ_p determined from equations (5.16) and (5.17) is under-estimated.

Similar equations ((5.8)-(5.17)) have been derived independently by others ((264)-(266)).

5.2 List of Experiments

Altogether three series of friction experiments were performed. The first was entirely preliminary in nature so that the appropriate modifications in the experimental arrangement could be made in future experiments - this experiment is not discussed. The main features of the other two experiments are given in Table V.I below:

Table V.I. Details of Friction Experiments

Code No.	Nature of Experiment	Nos. of traversals: Loads	Indenter: μ (measured)	Nature of Specimen: Temperatures (Approx.)	Comments
3M	Speed of sliding = $2.5\text{-}3.5\times10^{-2}$ cm/sec. μ 1-10 traversals determined. Track width for 10 traversals measured.	10	$2\frac{1}{2}$" diam. steel indenter	Highly polycrystalline	(i) μ is temperature dependent with minimum at $\simeq -1^{\circ}C$. (ii) "Ploughing effects" evident. (iii) Creep and Pressure melting regimes evident.
		73 kgs.	0.06-0.14	$0^{\circ}C$ to $-12.6^{\circ}C$	
4N	Speed of sliding = $2.5\text{-}3.5 \times 10^{-2}$ cm/sec. μ 1-10 traversals determined Track width for 1,10 traversals measured.	1,10	$2\frac{1}{2}$" diam steel indenter	Columnar grained	(i) μ values not so reliable as in 3M. (ii) Track widths for 1 traversal confirm 2-regime-model
		73,115, 175 kgs	0.06-0.14	$0^{\circ}C$ to $-10^{\circ}C$.	

The first experiment (3M) yielded good friction curves (Fig.V.I) for the highly polycrystalline ice specimens used. The track widths for 10 traversals only were measured. It was however also required to know the track widths after just one traversal. This was done in the latter experiment (4N) where the track widths for experiments involving both 1 and 10 traversals were measured. Here however the coefficient of friction values were not so consistent. This was obviously a grain orientation effect. (It is shown in Section 2.10 that clear columnar grained ice produces large grains with a certain amount of preferred orientation). In addition the friction force in these experiments behaved somewhat erratically during the traversals - this was presumably the anisotropic behaviour of certain large grains present in the friction track. Such effects were absent in the former experiment (3M) where there were so many grains ($\sim$ 2 mms size) beneath the indenter at any one instant as to completely average out these anisotropy effects. For this reason the friction results of only the highly polycrystalline ice (Fig.V.I) are discussed. Also, because of the bubbles naturally present in the highly polycrystalline ice specimens (3M), it was easy to measure the bubble loss for friction experiments in the pressure melting regime. The highly polycrystalline specimens were not so useful however in the crossed-polaroid studies because the small grains did not contrast strongly with those of recrystallisation - it is the large columnar grained ice specimens (4N) that demonstrate clearly the different recrystallisation habits observed.

We see therefore that these two experiments supplement each other in providing a set of extremely useful data whereas either experiment by itself would have been insufficient. In order to clarify the situation Table V.II shows which experiment is used for each of the various experimental parameters used in this chapter.

Table V.II Classification of Experimental Determinations

Experimental determination	Experiment used
a) μ for 1-10 traversals.	3M (highly polycrystalline ice)
b) d_1, track widths for 1 traversal.	4N (columnar-grained ice)
c) d_{10}, track widths for 10 traversals.	3M, 4N
d) Direct optical observations of bubbles and "cloudy regions".	3M, 4N
e) Crossed-Polaroid observation of Grain structures, recrystallisation.	4N

5.3 Experimental Procedure, Errors

The general experimental set-up used in these friction experiments is as described in Section 2.7. A typical friction trace is shown in Fig.II.IV.

The errors involved in the determination of the track width, effective hardness etc. are similar to those for static hardness (Sec.4.3). Again, the maximum accuracy of measurements is at the warmer temperatures (near $0^{\circ}C$) when the track widths become large. In any one series of experiments, the random errors of observation result in an estimated random error of about $\pm$ 3 per cent in μ. Typically $\mu \sim 0.1$; this means the random error in μ is ~ 0.003. It can be seen from Fig.V.I, that the general scatter of points in the friction curves is consistent with this value. However, as with the hardness curves (see Sec.4.3), there may be errors systematic to all the points in Fig.V.I. Even if such systematic errors do exist, they are unlikely to affect the main conclusions in this chapter as we are mainly interested in the relative changes in μ for different temperatures.

5.4 The Interpretation of the Friction Results

(i) Friction Results.

Fig.V.I shows the results for the coefficient of friction μ against temperature for different numbers of traversals n using highly polycrystalline ice (experiment 3M). It was found more accurate to take the mean value of μ from successive forward and backward traversals - hence the term $(n + \frac{1}{2})$ refers to the mean value obtained from the n^{th} and $(n + 1)^{th}$ traversals. These curves illustrate two important features:

(1) that μ decreases with n.

(2) that μ has a minimum at about $-(1 \text{ to } 2)^{\circ}C$.

(ii) Track Width Results, Effective Hardness.

The track widths (d = 2a) were measured and P_L (the effective hardness) was calculated using equation (5.9). These results are shown in Fig.V.II on an Arrhenius type of plot. This curve illustrates three important features;

(1) that below $-2^{\circ}C$ say, P_L decreases gradually with temperature. This decrease with temperature is very similar to that in the hardness curves (e.g. Fig.IV.I) in Chapter IV - the activation energy, $7\frac{1}{2}$ k.cals/mole, also compares well with the average values, 7.7 and 8.04, obtained for $\frac{Q}{m}$ from Figs. IV.I and IV.III.

(2) that above a temperature of $-1.5^{\circ}C$ to $-2^{\circ}C$ the effective hardness drops markedly. This drop is very similar to those on the hardness curves in the pressure melting range (e.g. Fig.IV.III), and here also the drop occurs at a temperature close to the pressure melting temperature. In fact the drop would seem to occur just a little below the pressure melting temperature. This is to be expected since the pressure melting curve has been calculated taking into account only the vertical(load) stresses; i.e. the smaller tangential (or frictional) stresses have been ignored.

(3) that the drop in the effective hardness occurs in the same temperature range as the increase in μ at the warmer temperatures (Fig.V.I).

(iii) The Two Regime Model for Friction of Ice.

It is clear from (i) and (ii) above, that the friction results show two distinct regimes of behaviour for temperatures below and above $-(1.5 \text{ to } 2)^{\circ}C$.

5.4 The Interpretation of the Friction Results

(i) Friction Results.

Fig.V.I shows the results for the coefficient of friction μ against temperature for different numbers of traversals n using highly polycrystalline ice (experiment 3M). It was found more accurate to take the mean value of μ from successive forward and backward traversals - hence the term $(n + \frac{1}{2})$ refers to the mean value obtained from the n^{th} and $(n + 1)^{th}$ traversals. These curves illustrate two important features:

(1) that μ decreases with n.

(2) that μ has a minimum at about $-(1 \text{ to } 2)^{\circ}C$.

(ii) Track Width Results. Effective Hardness.

The track widths (d = 2a) were measured and P_L (the effective hardness) was calculated using equation (5.9). These results are shown in Fig.V.II on an Arrhenius type of plot. This curve illustrates three important features;

(1) that below $-2^{\circ}C$ say, P_L decreases gradually with temperature. This decrease with temperature is very similar to that in the hardness curves (e.g. Fig.IV.I) in Chapter IV - the activation energy, 7½ k.cals/mole, also compares well with the average values, 7.7 and 8.04, obtained for $\frac{Q}{m}$ from Figs. IV.I and IV.III.

(2) that above a temperature of $-1.5^{\circ}C$ to $-2^{\circ}C$ the effective hardness drops markedly. This drop is very similar to those on the hardness curves in the pressure melting range (e.g. Fig.IV.III), and here also the drop occurs at a temperature close to the pressure melting temperature. In fact the drop would seem to occur just a little below the pressure melting temperature. This is to be expected since the pressure melting curve has been calculated taking into account only the vertical(load) stresses; i.e. the smaller tangential (or frictional) stresses have been ignored.

(3) that the drop in the effective hardness occurs in the same temperature range as the increase in μ at the warmer temperatures (Fig.V.I).

(iii) The Two Regime Model for Friction of Ice.

It is clear from (i) and (ii) above, that the friction results show two distinct regimes of behaviour for temperatures below and above $-(1.5 \text{ to } 2)^{\circ}C$.

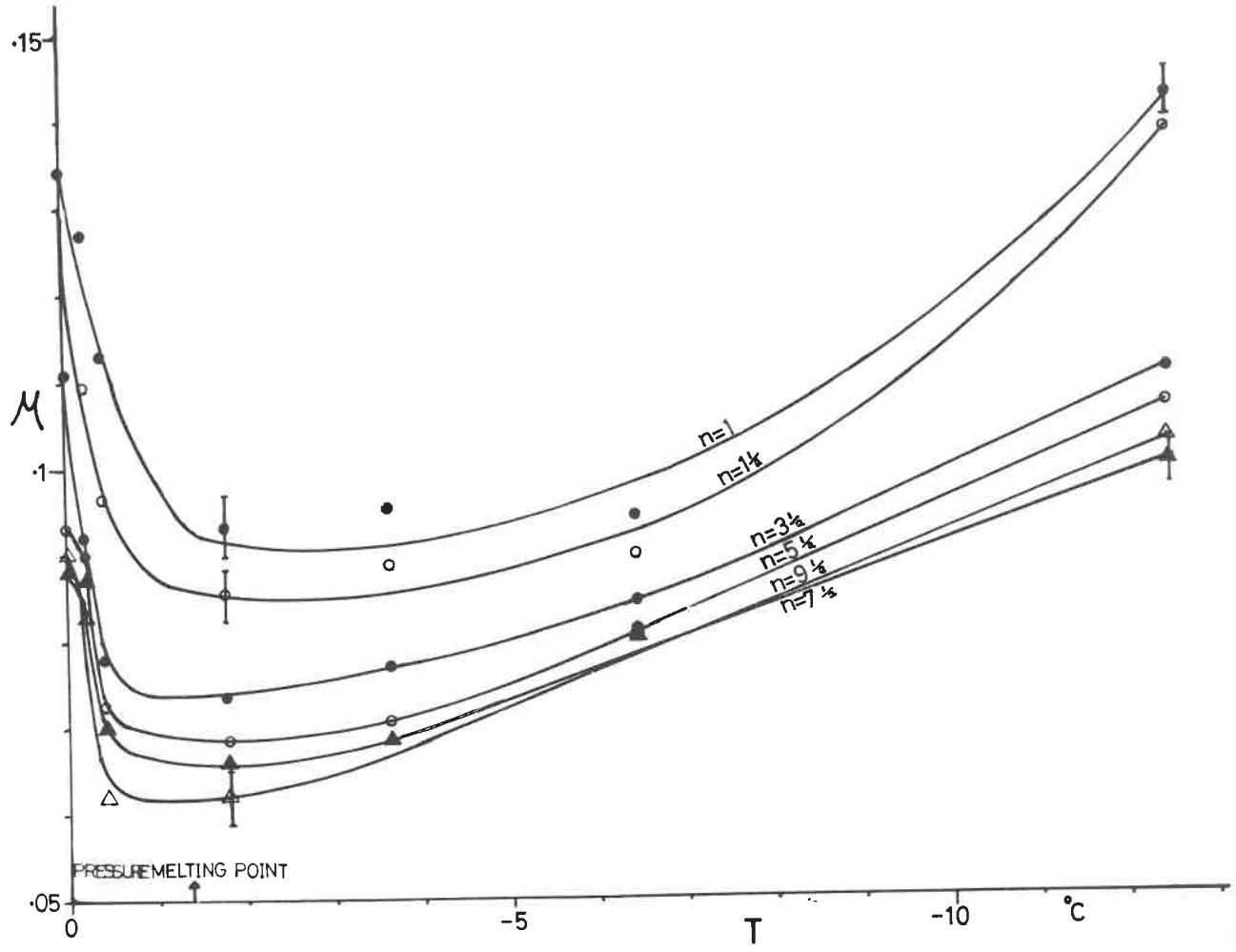

Fig.V.I Friction of Steel on Ice for many (n) Traversals (Secs. 5.2-5.4).

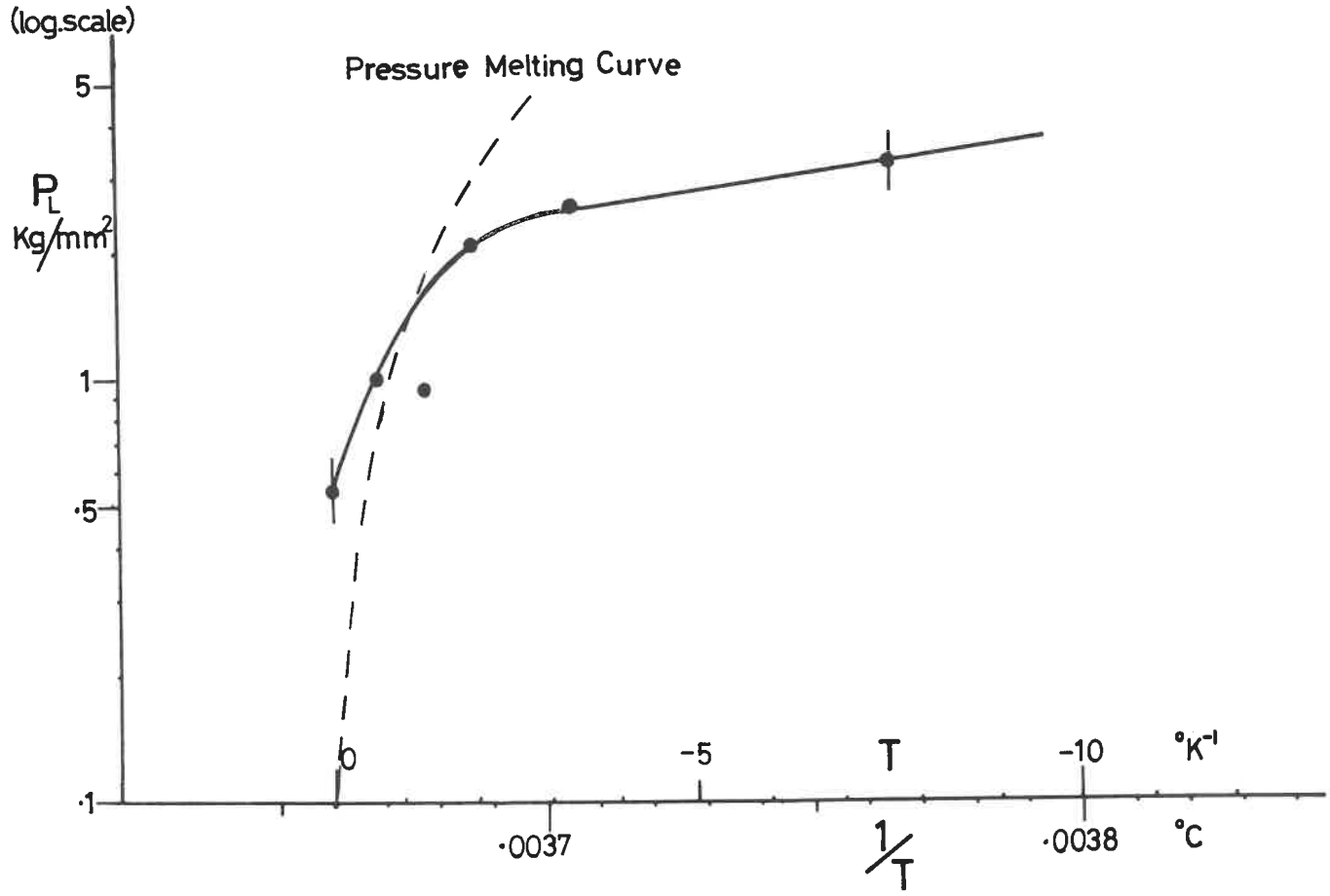

Fig.V.II Effective Hardness calculated from the Friction Tracks (Arrhenius Plot) (Sec. 5.4, ii).

These two regimes bear a close correspondence with the two regimes of hardness given in Chapter IV - accordingly the same nomenclature is used for the two regimes of friction behaviour. However it is important to note that the two regime model is illustrated by an additional parameter in the friction results, viz. the coefficient of friction μ. The fact that this additional parameter μ also falls in line with the two regime model, must be considered as strong confirmation of the two regime model. Altogether the friction results illustrate the two regimes in four somewhat independent ways; (A) the drop in effective hardness P_L, (B) Crossed-Polaroid studies of recrystallisation, (C) visual examination of the bubbles and cloudy regions, and (D) the variation of μ with temperature. These four features are discussed below:

(A) The similarity between the drop in P_L and the drop in the hardness curves (Ch.IV) above the pressure melting temperature has already been noted in (ii) above. It is interesting to note that the P_L curves compare with the hardness curves (Fig.IV.I) for a loading time of $t \sim$ 10-100 secs. For the sliding speeds used in the friction results, this time range corresponds to a distance of traverse of 0.3-3 cms. This distance range corresponds roughly to the range of track diameters found for these friction experiments. This is a reasonable result; it means that the parameter $P_L(v)$ may be considered as an "effective hardness" parameter where the "effective loading time" corresponds approximately to the time taken for the indenter to traverse its "own length 2a of indentation". The variation of P_L with temperature gives a similar activation energy to those obtained from the hardness results below the pressure melting temperature; above the pressure melting temperature P_L drops rapidly also in agreement with the hardness curves. This indicates that the "sinking in of the indenter" in the friction experiments is governed mainly by creep and plastic flow below the pressure melting temperature $\sim(1.5 \rightarrow 2)^{\circ}C$, and by pressure melting effects above $\sim(1.5 \rightarrow 2)^{\circ}C$. The identification of $P_L(v)$ with a corresponding hardness loading time (t = 10-100 secs.) may be important. This is because in the hardness Section (4.12), the magnitude of the three composite mechanisms involved in the pressure melting regime have been estimated for different

loading times. If one is correct in assuming that these proportions are approximately similar for the friction experiments, then one concludes that for these friction experiments at 0°C; 29 per cent creep, 12-15 per cent regelation, and 52-58 per cent liquid grain boundary are the approximate magnitudes of each pressure melting mechanism.

(B) The crossed-polaroid pictures (experiment 4N) show very beautifully the different recrystallisation habits of the deformed ice in the two regimes. This is because (1) large columnar grain specimens are used, and (2) the size of the recrystallisation zones are larger than those in the hardness indentations on account of the additional stresses involved (the tangential or frictional stresses) and also because many traversals are made.

In the creep regime (below - (1.5 to 2)°C), the size of the recrystallised grains are small, $\sim \frac{1}{2}$ mm. (see Fig.V.IV), and the size of the recrystallised zone increases with temperature. Fig.V.IV(b) gives an example of one of the colour print pictures obtained - these prints were made from colour slides and are therefore not so good as the original transparencies.

However in the pressure melting regime (above -(1.5 to 2)°C), the size of the recrystallised grains are larger, being 2 mms to cms (see Fig.V.III). Fig.V.III(b) also shows a colour print picture of V.III(a).

The mechanisms for these recrystallisations are believed to be "accelerated flow-stress enhanced recrystallisation" (creep regime) and "liquid grain boundary-grain growth" (pressure melting regime). These mechanisms are discussed in more detail in Secs.4.11(iii) and 4.12(2).

(C) Visual examination of the deformed ice confirms the results obtained from the Crossed-Polaroid studies. For the same reasons, the effects are more pronounced in these friction experiments than in the hardness experiments.

In the creep regime (below -(1.5 to 2)°C), the aggregate of small-grain ice appears white in contrast to the relatively transparent surrounding ice. (see Fig.V.VI.)

The behaviour of the ice in the pressure melting regime (above -(1.5 to 2)°C) is shown most clearly by using ice specimens deliberately prepared with inclusions of fine air bubbles (Experiment 3M). The undeformed regions

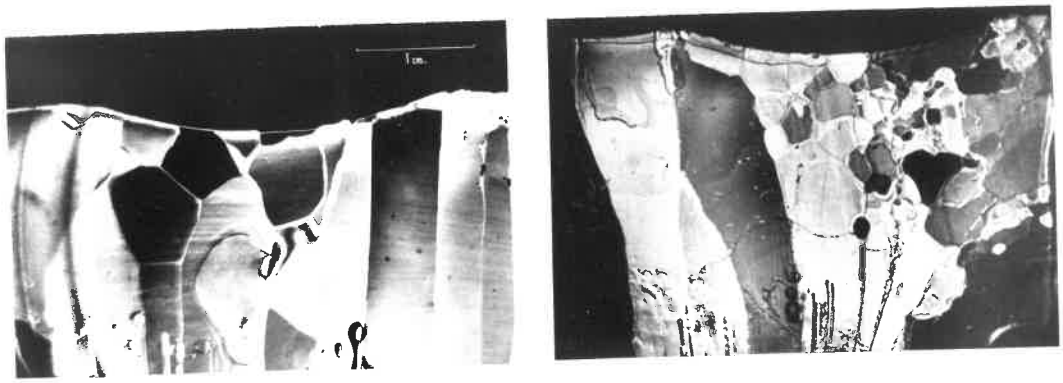

Fig.V.IIIa (i) 0°C PRESSURE MELTING REGIME (ii) -1½°C

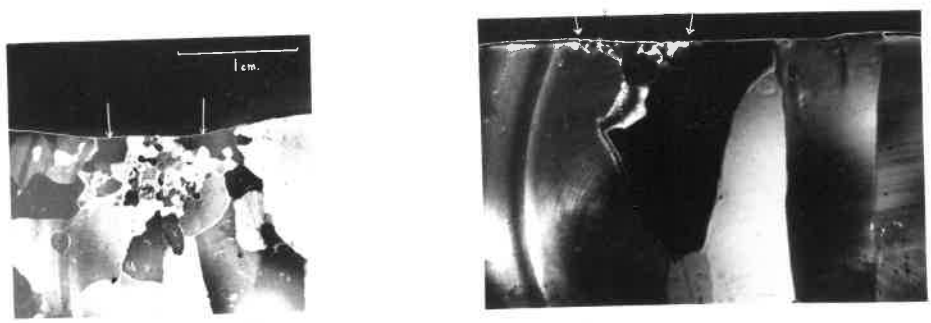

Fig.V.IVa (i) -1·9°C CREEP REGIME (ii) -10°C

"Crossed Polaroid" Examination of deformed zones for different temperatures of indentation (Sec. 5.4(iii)).

Fig.V.III.b. (reverse colour print of a(i))

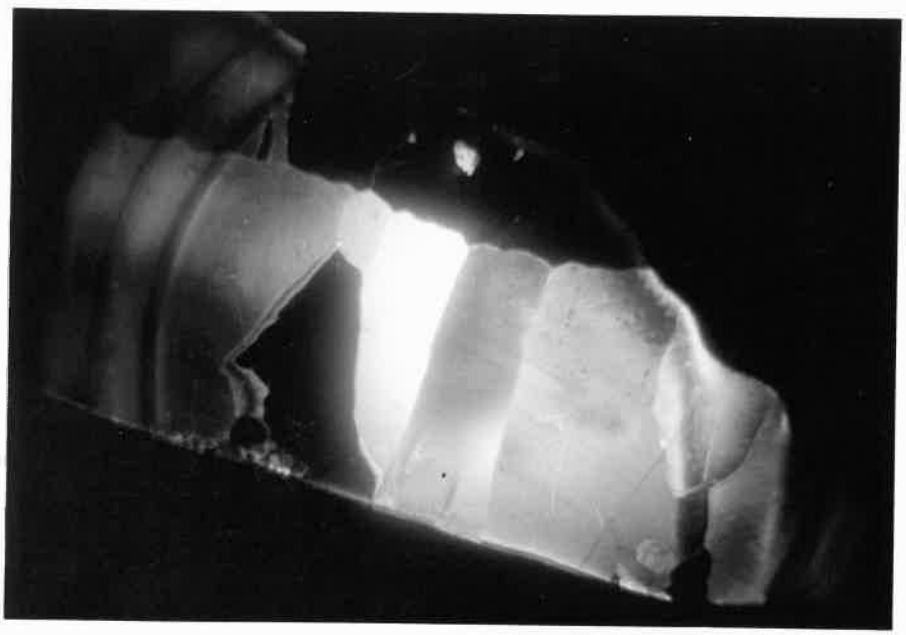

Fig.V.IV.b. (reverse colour print of a (ii))

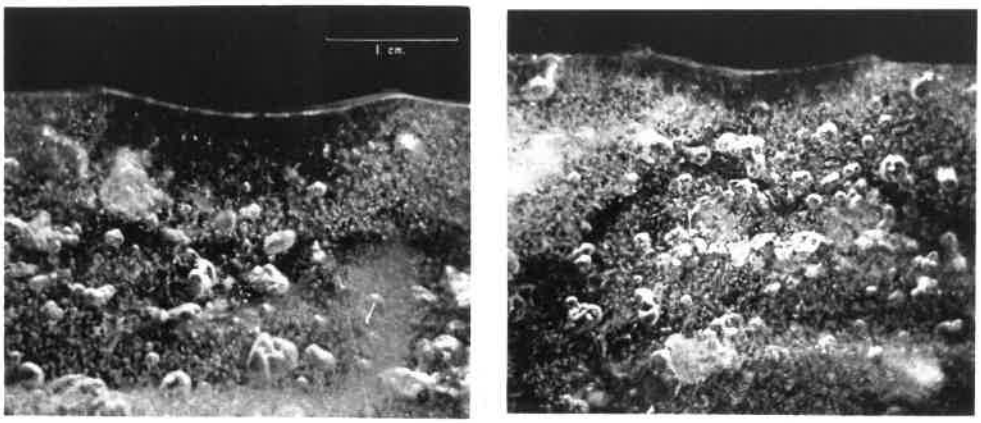

Fig.V.V (using bubbly ice)

-0·2°C PRESSURE MELTING REGIME -0·4°C

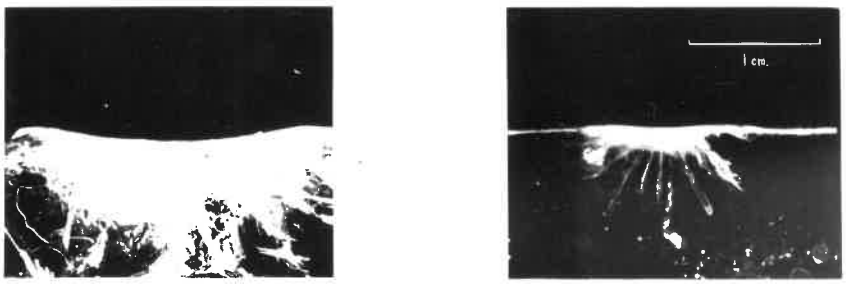

Fig.V.VI (using clear ice)

-3·4°C CREEP REGIME -10°C

Photographs showing the nature of the deformed zone for different temperatures of indentation (Sec. 5.4, iii).

appear "cloudy". After frictional grooving, the contact zone becomes clear (Fig.IV.V). The mechanism for this bubble loss is believed to be the migration, annihilation or aggregation of the bubbles at the liquid grain boundaries. This mechanism is discussed in more detail in Sec.4.12(3).

(D) It is seen that the coefficient of friction μ increases rapidly above the pressure melting temperature (see Fig.V.I). This sudden change in μ is attributed to a pressure melting phenomenon. One might at first have expected the coefficient of friction to decrease rather than increase sharply above the pressure melting temperature. However one must allow for ploughing effects - in fact it turns out that the ploughing term becomes increasingly more important above the pressure melting point. A quantitative treatment of this effect is given in (iv) below - this enables the separate coefficients μ_p and μ_s to be calculated. These are shown in Fig.V.VII. It can be seen that both μ_p and μ_s change rapidly above the pressure melting temperature. The increase in μ_p and the decrease in μ_s are both attributed to pressure melting effects and are discussed further below ((iv) and (vi)).

(iv) The Ploughing Effect.

It is pointed out in Section 5.1 that the separation of the ploughing and adhesion effects in friction (using equations (5.5) - (5.7)) is only really valid when either μ_s or μ_p is small. It is well known that the adhesion term μ_s for ice is very small near $0^{\circ}C$. This means that the study of the friction of ice at temperatures close to $0^{\circ}C$ offers an excellent opportunity to check the validity of the ploughing equations (5.12)-(5.17).

Using equations (5.16) and (5.17), the ploughing term μ_p has been calculated from the friction results at different temperatures. By subtracting μ_p from the coefficient of friction μ one obtains a value for the adhesion term μ_s (see equation (5.6)). The results of these calculations are shown in Fig.V.VII.

It is seen that, as might be expected, the adhesion term μ_s decreases from the relatively large value of 0.097 at $-12.55^{\circ}C$ to the very small value of 0.01 at $0^{\circ}C$. The ploughing term however increases from 0.046 at $-12.55^{\circ}C$ to 0.124 at $0^{\circ}C$. About 75 per cent of this increase occurs in the temperature range (of only $1.9^{\circ}C$) above the pressure melting point. The

appear "cloudy". After frictional grooving, the contact zone becomes clear (Fig.IV.V). The mechanism for this bubble loss is believed to be the migration, annihilation or aggregation of the bubbles at the liquid grain boundaries. This mechanism is discussed in more detail in Sec.4.12(3).

(D) It is seen that the coefficient of friction μ increases rapidly above the pressure melting temperature (see Fig.V.I). This sudden change in μ is attributed to a pressure melting phenomenon. One might at first have expected the coefficient of friction to decrease rather than increase sharply above the pressure melting temperature. However one must allow for ploughing effects - in fact it turns out that the ploughing term becomes increasingly more important above the pressure melting point. A quantitative treatment of this effect is given in (iv) below - this enables the separate coefficients μ_p and μ_s to be calculated. These are shown in Fig.V.VII. It can be seen that both μ_p and μ_s change rapidly above the pressure melting temperature. The increase in μ_p and the decrease in μ_s are both attributed to pressure melting effects and are discussed further below ((iv) and (vi)).

(iv) The Ploughing Effect.

It is pointed out in Section 5.1 that the separation of the ploughing and adhesion effects in friction (using equations (5.5) - (5.7)) is only really valid when either μ_s or μ_p is small. It is well known that the adhesion term μ_s for ice is very small near 0°C. This means that the study of the friction of ice at temperatures close to 0°C offers an excellent opportunity to check the validity of the ploughing equations (5.12)-(5.17).

Using equations (5.16) and (5.17), the ploughing term μ_p has been calculated from the friction results at different temperatures. By subtracting μ_p from the coefficient of friction μ one obtains a value for the adhesion term μ_s (see equation (5.6)). The results of these calculations are shown in Fig.V.VII.

It is seen that, as might be expected, the adhesion term μ_s decreases from the relatively large value of 0.097 at -12.55°C to the very small value of 0.01 at 0°C. The ploughing term however increases from 0.046 at -12.55°C to 0.124 at 0°C. About 75 per cent of this increase occurs in the temperature range (of only 1.9°C) above the pressure melting point. The

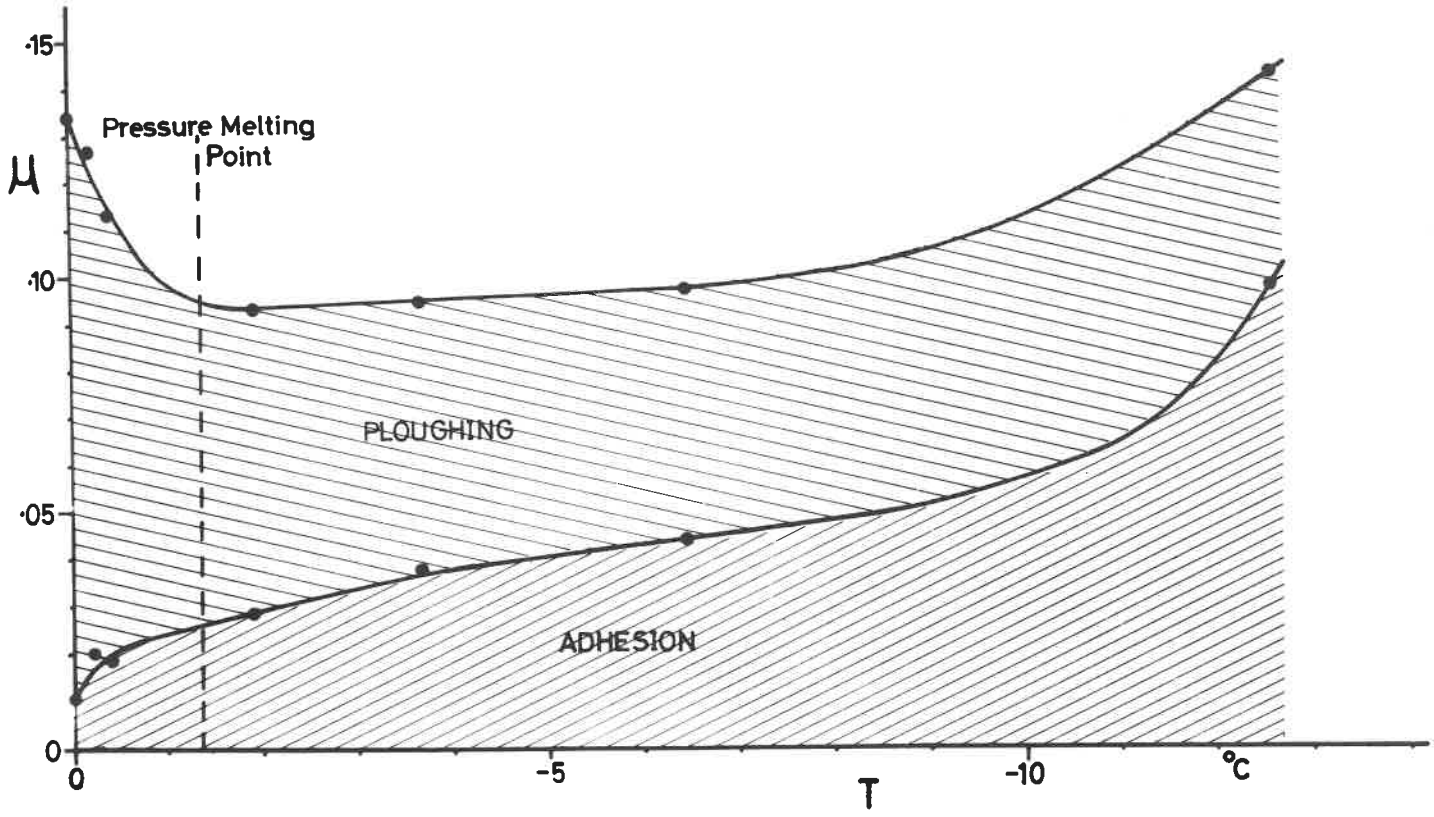

Fig.V.VIIa Components of Sliding Friction - Steel on Ice (Sec.5.4).

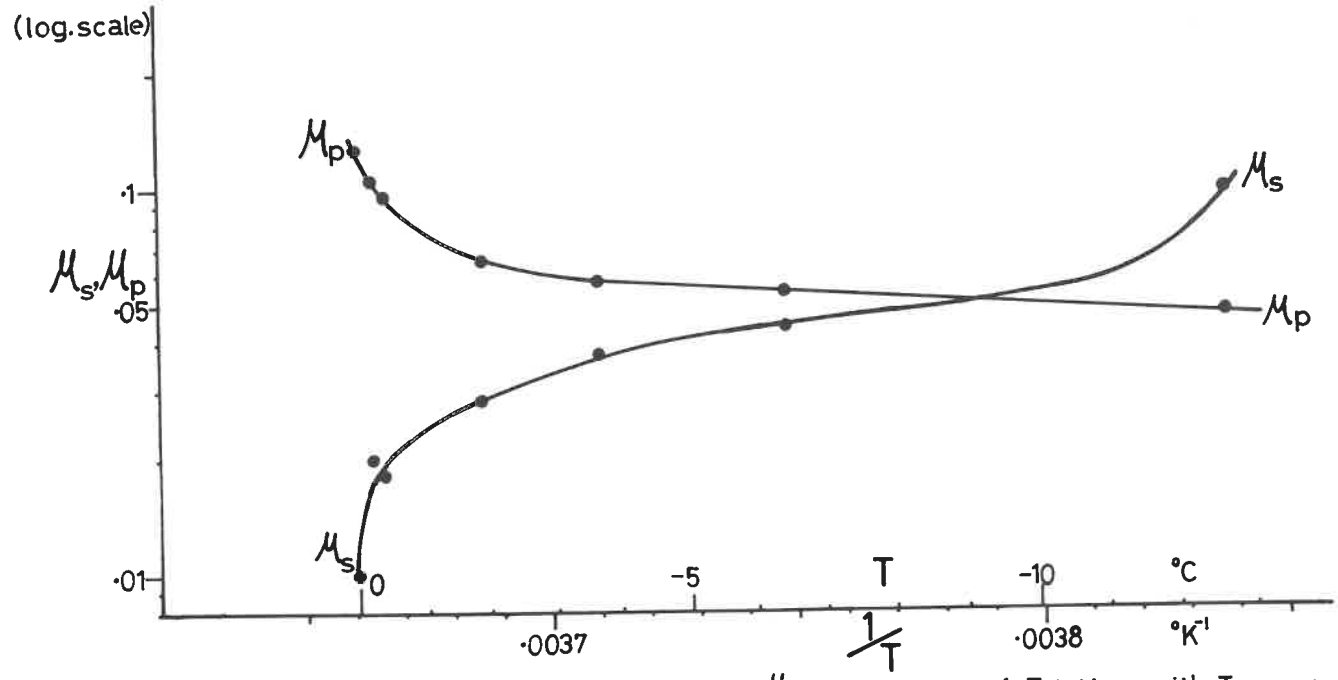

Fig.V.VII b Variation of Ploughing μ_p and Adhesion μ_s components of Friction with Temperature -Sec.5.4.

reason for this sudden increase in ploughing is a pressure melting phenomenon; because the ice sinks so much further into the ice when the temperature is above the pressure melting point, the indenter has to "plough through" a much larger projected area of ice. With the spherical indenter used, this area effect increases more rapidly than the drop in hardness and therefore the ploughing force increases.

We note that at $0^{\circ}C$ the friction, as expected, arises almost entirely ($92\frac{1}{2}$ per cent) from ploughing because the adhesion (in contrast to the ploughing) becomes extremely small.

It is seen therefore that these results are remarkably consistent with those expected for ice displaying pressure melting effects. This agreement is taken as a substantial confirmation of the ploughing theory developed in Section V.I. It is hoped that future experiments (in which an "ice indenter" is dragged over a flat steel surface, thereby almost completely eliminating the ploughing effect) will be performed to check this explanation. It is interesting to note that Ericksson's experiments, which involve hard sliders, (263) also show a similar increase in friction above $-(1 \text{ to } 2)^{\circ}C$. The reason for this increase now becomes apparent as a ploughing effect following pressure melting.

Before leaving this subject we briefly consider two interesting manifestations of ploughing in these friction results:

(1) If one examines a typical friction trace (for example, Fig.II.IV) it is seen that there is an increase in friction (called a "friction hump") at the end of all traversals except the first. This effect increases with the number of traversals and is a striking demonstration of the ploughing process: Each time the indenter commences a new traversal it ploughs beneath the track produced by the previous traversal. However the indenter is deeper in the ice in the new traversal, and it therefore has to plough an additional volume at the far end of the track where the indenter passes over the terminus of the previous track. This additional ploughing volume increases with each traversal and hence the "hump" in the friction traces (Fig.II.IV) becomes progressively larger.

(2) Fig.V.I shows that for any given temperature, μ decreases with the number of traversals. We wish to calculate the ploughing effect for

each traversal. This is defined as F_p^n where n is the number of traversals. From equation (5.12)

$$F_p^n = P_F . \Delta A_F^n \qquad (5.18)$$

where A_F^n is the relevant ploughing area for the n^{th} traversal. Clearly, this is given by:

$$\Delta A_F^n = A_F^n - A_F^{n-1} \qquad (5.19)$$

where A_F^n is the total horizontally projected area after n traversals (see Sec.5.1). Using equation (5.10)

$$F_p^n = P_F . \Delta A_F^n = \frac{2}{3R} [a_n^3 - a_{n-1}^3] . P_F \qquad (5.20)$$

where a_n is the ½-diameter of the track after n traversals. In view of the lack of work hardening in ice (Sec.3.6), P_F may be conveniently considered to be a constant. Using this equation and the experimental values for a_n, the writer has performed some calculations which show that the rate of decrease of μ with n (Fig.V.I) is in good numerical agreement with equations (5.18)-(5.20). It is therefore concluded that the decrease of μ with n is mainly a result of the decrease in ploughing. Similar observations for metals have been made, for example, by Eldredge and Tabor ((214),(260)).

(v) The Specific Shear Strength.

In order to avoid confusion on the subject of adhesion, it is necessary to consider the specific adhesion (or specific shear strength) of ice s as derived from a friction result. In this treatment we consider only the numerical values of s and not the physical processes which are involved in the shearing of the steel-ice interface - these processes are dealt with later in this Section ((vi), The Adhesion Component). The specific shear strength s is defined in Section 5.1 by the equation:

$$\mu_s = \frac{F_s}{L} = \frac{s . A}{Y . A} = \frac{s}{Y} \qquad (5.1)-(5.4)$$

or

$$s = \mu_s . Y = \mu_s . \frac{L}{A} \qquad (5.22)$$

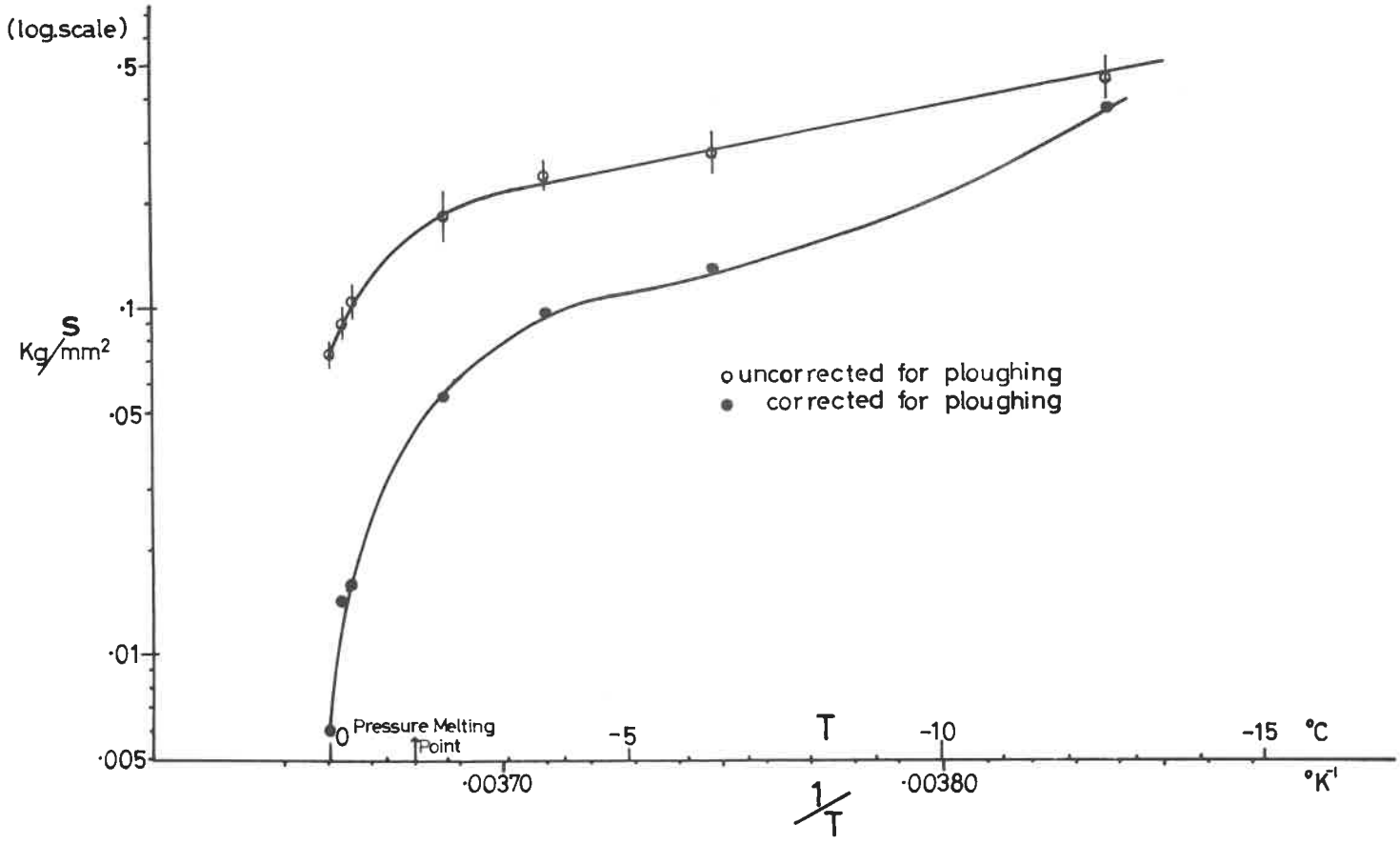

Fig.V.VIII Variation of Shear Strength (Steel on Ice) with Reciprocal Temperature (Sec. 5.4,v).

This quantity is a measure of the shear strength of a unit area of true indenter-ice contact. The difference between this parameter s and the adhesion coefficient of friction μ_s illustrates one important feature of a friction experiment which is not present in many other experimental situations. The area of contact A varies with temperature in the friction experiments. The quantity μ_s measures the shear resistance of the total contact region. In many other physical situations, e.g. an adhesion experiment or the sole (or portion of the sole) of a glacier on its bed, it is more expedient to have a knowledge of the shear strength of a specified area of true contact. This quantity F_s may be directly calculated from the shear strength value and the area of contact:

$$F_s = s.A \qquad (5.23)$$

(equation (5.23) is obtained from equations (5.3) and (5.19))
For these purposes, Fig.V.VIII has been plotted showing the variation of s (calculated from equation (5.22) using the values of μ_s given in (vi) below) with temperature. A curve is also given showing the values of s that would be obtained if μ was used instead of μ_s in the calculations i.e. if ploughing was neglected. There is considerable difference between the curves above $-12^{\circ}C$.

The friction curve (Fig.V.I) agrees well with that given by Bowden et al. ((260), P.141) for steel on ice. However there is considerable difference between the specific adhesion curve (Fig.V.VIII) and that of Bowden et al. ((260), P.142). This difference presumably arises because no allowance was made for ploughing in the latter curve. However, there is good agreement between Fig.V.VIII (for s) and the specific adhesion curves of Raraty and Tabor for ice on clean steel ((216), (260)).

(vi) The Adhesion Component

It is shown in (iv) above that the adhesion component of friction may be estimated by making a theoretical ploughing correction to the coefficient of friction μ. The results are shown in Fig.V.VII. It is seen that, (1) μ_s decreases from the relatively large value of 0.097 at $-12.55^{\circ}C$ to about 0.03 just below the pressure melting temperature, and (2) μ_s

decreases fairly rapidly from about 0.03 at the pressure melting temperature to 0.01 at 0°C. It must be remembered that these values must not be taken too seriously as they are derived from the difference between two other parameters (μ and μ_p). It is hoped that the future experiments, mentioned in (iv) above, may furnish more direct and accurate determinations of μ_s. However in spite of these limitations, some interesting deductions may be made. These are discussed below:

(1) The variation of μ_s with temperature can be explained in two ways: (a) the change in shear strength of the ice-steel interface, or (b) the change in viscous properties of a surface liquid film. If (a) is the dominant mechanism one should expect the shear strength of this interface to be of the same order of magnitude as the effective hardness P_L. However a comparison of Figs. V.II and V.VIII (or alternatively the specific adhesion results of Raraty and Tabor (216), (260)) shows that the shear strength is 30-300 times smaller than P_L between -7°C and 0°C - the discrepancy is less at -12½°C (a factor of 10). This therefore indicates that the shear strength of an ice-steel interface is not an important factor at these temperatures. A similar conclusion may be drawn if one analyses the adhesion (Raraty and Tabor (216),(260)) and friction data in terms of Glen's Creep Law: If one were to suppose that the adhesion-friction forces result from the plastic-creep resistance offered by a certain depth of ice near the interface, then using Glen's law a calculation can be made to determine the thickness of this zone. The value thus obtained is enormous - $>10^4$cms! Clearly, the adhesion-friction forces cannot be associated with interfacial or bulk shear in the ice specimens. The decrease of $\frac{s}{P_L}$ at -12½°C however suggests that the interfacial shear strength may well be important at lower temperatures. We now consider the alternative explanation (b) in the light of the literature reviewed in Section 3.4.

In order to exclude pressure melting effects, we consider only the friction results below the pressure melting temperature. In particular we consider the value $\mu_s = 0.044$ at $T = -6.44$°C as it is close to Jellinek's (Sec.3.4,(iv)) working temperature (-5°C). We now suppose that in this friction experiment the indenter is supported on its contact

region (area, A) by a liquid film of thickness δ and viscosity η. Using simple viscosity theory we may relate these parameters to the adhesion friction force F_s and the speed of sliding v;

$$\frac{F_s}{A} \simeq \eta \cdot \frac{v}{\delta} \qquad (5.21)$$

Substituting the experimental parameters for $T = -6.44^{\circ}C$ yields:

$$\left(\frac{\eta}{\delta}\right)_{-6.44^{\circ}C} \sim 4 \times 10^{8} \text{ poise.cm}^{-1}.$$

This compares with the stainless steel-ice adhesion values obtained by Jellinek (Sec.3.4,(iv))

$$\left(\frac{\eta}{\delta}\right)_{-5^{\circ}C, \text{ Jellinek, adhesion}} \sim 0.7 \times 10^{8} \text{ poise.cm}^{-1}$$

In view of the approximations and different experimentations involved in this comparison, the similarity in these two values is considered remarkably close. We make this comparison a little more specific by using Jellinek's estimations for the value of δ :

(Jellinek) adhesion ($-5^{\circ}C$), η = 70 → 700 poise for δ = 100 → 1,000 Å
(Barnes) friction ($-6.44^{\circ}C$) η = 400 → 4,000 poise for δ = 100 → 1,000 Å
(or alternatively, η = 70 → 700 poise for δ = 18 → 180 Å)

Similar calculations for other temperatures yield for example:

friction, $\left(\frac{\eta}{\delta}\right)_{-1.9^{\circ}C} \sim 1.8 \times 10^{8}$ poise. cm^{-1}

friction, $\left(\frac{\eta}{\delta}\right)_{-12.55^{\circ}C} \sim 12 \times 10^{8}$ poise. cm^{-1}.

The latter values indicate that an increase of temperature is accompanied by either (or both) an increase in the film thickness or a decrease in its viscosity - both effects are, of course, what would be expected. Fig.V.VII indicates that below some temperature between -6.5 and $-12.5^{\circ}C$, the value

of μ_s, and therefore η/δ also, must start to increase rapidly. This effectively means that at these lower temperatures ($\sim -12^{\circ}C$) the identity of a surface liquid film is being rapidly lost. It may be significant that the friction runs were not quite so smooth or consistent at these lower temperatures.

The writer wishes to make it clear that he is not using these friction results in an attempt to substantiate the "ordered surface film" theory of ice. These calculations are merely meant to show that the friction results may be interpreted in terms of this film theory, and that such an interpretation gives very good agreement with the surface film parameters calculated from adhesion results. A more general conclusion is also suggested - that friction and adhesion forces arise from a common cause. However it should be noted that, in addition, similar values for η/δ can be obtained from experiments of a completely different nature (e.g. the grain boundary - internal friction peak - see Sec.6.4, (i)).

(2) We now wish to make a similar analysis for the adhesion component of friction in the pressure melting regime. Fig.V.VII suggests that μ_s decreases fairly rapidly with temperature in the pressure melting regime. The writer believes that this decrease is due to the formation of a continuous film of water between the ice and the indenter. It is believed that this film possesses similar characteristics to that of the regelation film proposed to explain the indentation hardness results (Sec.4.12). By performing calculations similar to those in (1) above, it is found that

$$\text{friction}, \left(\frac{\eta}{\delta}\right)_{0^{\circ}C} < 0.17 \times 10^{8} \text{ poise.cm}^{-1}.$$

This value is more than an order of magnitude smaller than those calculated for the creep regime. This leads to an important point: the manner of creation of this film is completely different from that of any film formed in the creep regime. Whereas the latter probably exists, if at all, as a result of surface ordering effects over a wider temperature range, the film in the pressure melting regime suddenly forms when the temperature-pressure conditions are conducive to surface regelation (or pressure melting). One therefore expects that this film is much larger than any formed in the

creep regime. By analogy with the admittedly simpler case of hardness (Sec.4.12,(1)), one may postulate that the film thickness is of the order of microns. The literature (Secs.3.3 and 3.4) suggests that even with these sort of thicknesses, this water film would possess a viscosity considerably greater than that of ordinary bulk water.

5.5 Summary

Results have been obtained for the coefficient of friction μ of a stainless-steel hemispherical slider on ice over a temperature range of $0^{\circ}C$ to $-12\frac{1}{2}^{\circ}C$ and with a sliding speed of $\sim 3 \times 10^{-2}$ cm.sec.

It is found that, like in the hardness experiments, it is possible to divide the friction behaviour into two distinct temperature regimes. These two regimes are likewise denoted as "creep" (below the pressure melting point) and "pressure melting" (above the pressure melting point). These two regimes are reflected in the experimental observations of (1) the track width (or effective hardness), (2) the grain structure of the ice (revealed by polarised light), (3) the general appearance of the ice (revealed by ordinary light), and (4) the friction force. The friction force measurements provide an extra parameter (compared to the hardness experiments) with which to illustrate the existence of the two regimes. In particular, it appears that the two ploughing and adhesion components of the friction force both clearly illustrate the two regime model.

By developing a simple theory of ploughing, it has been possible to calculate separately the ploughing and adhesion components of friction. These results explain a number of unusual features in the friction of ice, viz: (a) the increase in μ above the pressure melting point, (b) the increase in μ at the end of a friction track, and (c) the decrease in μ with the number n of traversals.

Also by using this theory it is demonstrated that the adhesion component of friction μ_s decreases (as expected) with increasing temperature with a marked drop above the pressure melting effect. It is shown that, for the sliding speeds used (3×10^{-2} cm/sec): (a) the values of μ_s below the

pressure melting point may be interpreted in terms of a "surface liquid layer" rather than the alternative concept of "shearing of the ice-steel junctions". The viscosity-thickness characteristics of this layer are in good agreement with those obtained from adhesion (Jellinek) and internal friction (Sec.6.4,(i)) experiments. The increase of the specific shear strength at still lower temperatures (below $-12\frac{1}{2}^{o}C$) suggests that the alternative "shearing of junctions" model may predominate at low temperatures.

(b) the values of μ_s (and s) above the pressure melting point have implications for glaciology - these are discussed in Chapter VII (in particular Sec.7.2,(ii)).

CHAPTER VI

THE MECHANICAL RELAXATION OF ICE

6.1 Introduction

Tabor ((260),(268)) has shown that, neglecting interfacial slip processes, the rolling friction of a hard cylinder or sphere on a flat solid is primarily due to hysteresis losses in the solid itself. Ludema ((269) (316)) has verified this theory for certain polymeric solids by showing that there is a strong correlation between the primary and secondary rolling friction peaks and the peaks observed for example in torsion pendulum experiments.

This chapter is concerned with a similar comparison between data on the rolling and internal friction of ice. Because the available data on the internal friction of ice is for a much higher frequency range than that corresponding to the rolling friction experiments, the comparison obtained is not so clear as that obtained by Ludema. Until internal friction measurements are made at lower frequencies, this comparison must only be considered as preliminary. However some interesting conclusions can be drawn from these results.

It is assumed that the amplitudes An of the damped oscillations in these experiments are given by:

$$An = Ao \exp -(n\Lambda) \qquad (6.1)$$

where Ao is the initial amplitude, n the integral number of oscillations, and Λ the logarithmic decrement. The phase lag ϕ is defined in the usual way:

$$\tan \phi = \frac{\Lambda}{\pi} \qquad (6.2)$$

The value of tan ϕ at a friction peak is denoted by tan ϕ_{max}. It is

found that the temperature at which a particular friction peak occurs depends on the frequency ∂ of oscillation. This variation is assumed to be of the form:

$$\partial = \partial_{o} \cdot \exp - \left(\frac{Q}{RT}\right) \qquad (6.3)$$

It is also assumed that the region of elastic-intimate contact between the hard roller and the ice surface may be calculated from the equations of Hertz ((255),(256)). For a cylinder on a flat surface, the width b of the rectangle of contact is given by:

$$b = 2\sqrt{\frac{4LR}{\pi}\left(\frac{1-\gamma^2}{E}\right)} \qquad (6.4)$$

Using this equation, the average pressure P beneath the roller may be estimated as

$$P = \frac{L}{b.\ell} \qquad (6.5)$$

where ℓ is the axial length of the cylinder. Corresponding equations can be derived for spherical rollers.

6.2 Experimental Details

The apparatus used for the determination of rolling friction was developed by Ludema (269) and is shown schematically in Fig. VI.1. The ice specimen is housed in a small brass surround and can be initially cooled to -180°C in 3 to 4 hours by means of an air circulation system in which the air is cooled by liquid nitrogen. The temperature was measured using a thermocouple embedded in the specimen. The energy losses per cycle during rolling friction were measured as a function of temperature with the cooling system switched off. The total warming up procedure would usually take 5-6 hours. By constantly removing thermal insulation the warming up rate was maintained constant, the specimen temperature variation being less than 1°C during each determination. The amplitude of the oscillations of the pendulum pointer were read off a circular scale. The base of the pendulum comprised

found that the temperature at which a particular friction peak occurs depends on the frequency ∂ of oscillation. This variation is assumed to be of the form:

$$\partial = \partial_{o} \exp -\left(\frac{Q}{RT}\right) \qquad (6.3)$$

It is also assumed that the region of elastic-intimate contact between the hard roller and the ice surface may be calculated from the equations of Hertz ((255),(256)). For a cylinder on a flat surface, the width b of the rectangle of contact is given by:

$$b = 2\sqrt{\frac{4LR}{\pi}\left(\frac{1-\delta^2}{E}\right)} \qquad (6.4)$$

Using this equation, the average pressure P beneath the roller may be estimated as

$$P = \frac{L}{b.\ell} \qquad (6.5)$$

where ℓ is the axial length of the cylinder. Corresponding equations can be derived for spherical rollers.

6.2 Experimental Details

The apparatus used for the determination of rolling friction was developed by Ludema (269) and is shown schematically in Fig. VI.1. The ice specimen is housed in a small brass surround and can be initially cooled to -180°C in 3 to 4 hours by means of an air circulation system in which the air is cooled by liquid nitrogen. The temperature was measured using a thermocouple embedded in the specimen. The energy losses per cycle during rolling friction were measured as a function of temperature with the cooling system switched off. The total warming up procedure would usually take 5-6 hours. By constantly removing thermal insulation the warming up rate was maintained constant, the specimen temperature variation being less than 1°C during each determination. The amplitude of the oscillations of the pendulum pointer were read off a circular scale. The base of the pendulum comprised

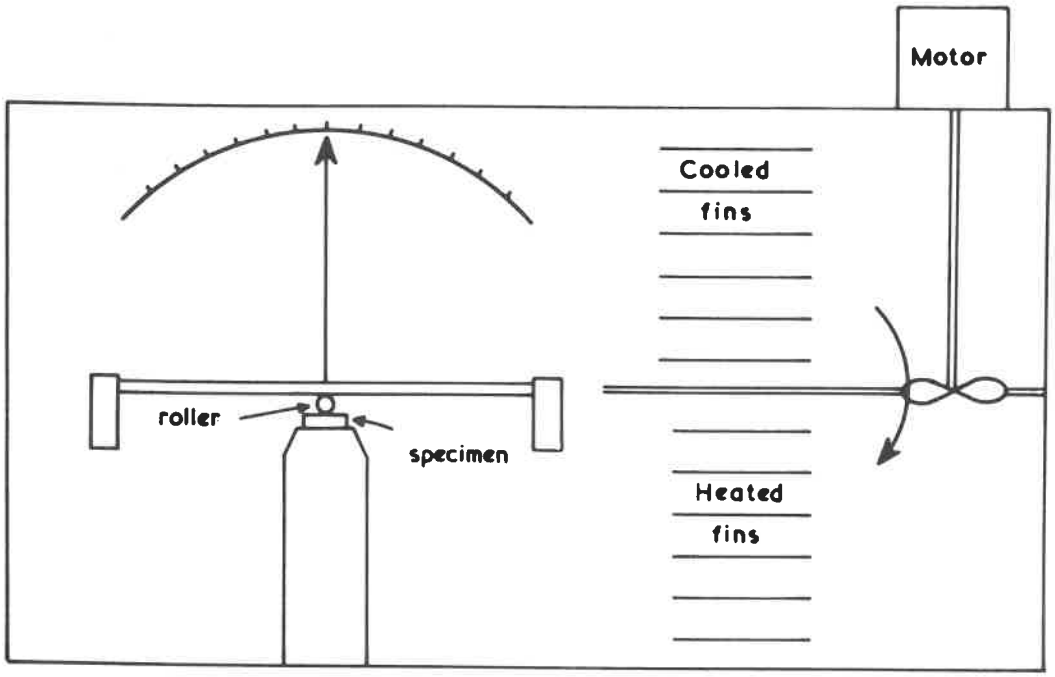

Fig. VI.I The Pendulum Rolling Friction Apparatus
- after Ludema (Sec. 6.2)

of a steel cylinder (or alternatively, two steel spheres) which was lowered on to the specimen surface after the cooling procedure (and specimen cover removal) had been completed. The rolling friction determinations were made for a total amplitude of swing of 25-30°.

Unfortunately, there exists, in rolling friction experiments, an ambiguity in the value of the effective frequency of the oscillations. For example, the frequency of the cylinder-pendulum used in these experiments is about 1/8 c.p.s. However if one considers the equation of Hertz (6.4) it can be shown that the width of intimate contact ($\simeq$ .02 mm) is about 80 times smaller than the total distance traversed by the pendulum in one half swing. It can therefore be argued that, on average, the effective frequency of (intermittent) oscillation of the elemental ice volumes are about 80 times higher than that of the pendulum, i.e. about 10 c.p.s. This is an average value, and it is important that the frequency ambiguity should be borne in mind while comparing the internal and rolling friction data.*

Table VI.I gives a list of the rolling friction experiments performed in this preliminary project.

The purpose of using the 2-Sphere-Pendulum (in No.12.0.2) was to investigate the effect of hydrostatic pressure on the rolling friction of ice. Because the load was concentrated over two small regions beneath each sphere, the average hydrostatic pressure P was about 20 times higher than that obtained with the Cylinder-Pendulum.

Measurements at temperatures above -20°C. have not been included here since their interpretation was complicated by the presence of a thin water film formed by heat transport from the roller - there were however no large fluctuations of temperature in the bulk specimen. Although this film was very thin, calculations have shown that surface tension forces are too large to be ignored.

It is likely that during the first few cycles at the lowest temperatures some plastic deformation occurs to give rise to the groove formed in the region of traversal. This means that we must expect higher losses at first than those due to the relaxation effects alone. For this reason, the lowest temperature points have been omitted in Figs.VI.III-V.

---

* It is, in principle, possible to resolve this ambiguity by studying the variation of damping with amplitude.

Table VI.I Rolling Friction Experiments

Code No.	Nature of Specimen	Type of Pendulum	Temperature Range	Comments
12.0.1	Highly Polycrystalline ice (see Sec.2.9)	Cylinder §i,ii, iv,vi	-177°C upwards §viii	(i) Results shown in Fig.VI.III
12.0.2	Highly Polycrystalline ice	2-sphere §i,iii, v,vii	-127° (upwards) §viii	(i) Results not shown in detail (ii) Measurements not very accurate
12.0.3	Highly Polycrystalline ice doped with Na.OH (~ 0002 mole)	Cylinder §i,ii, iv,vi	-177°C (upwards) §viii	(i) Results shown in Fig.VI.IV. (ii) Measurements more accurate than those in 12.0.1. (iii) A crack developed during cooling but should not influence results because it was situated well away from the roller
12.0.4	Mendenhall Single Crystal (see (270)), Surface approximately Parallel to Basal Plane	Cylinder §i,ii, iv,vi	-181°C (upwards) §viii	(i) Results shown in Fig.VI.V, (ii) Measurements more accurate than those in 12.0.1. (iii) Some cracks developed during cooling - may possibly affect results

§ i - Weight L of both pendulums is 270 gms.
§ ii - Cylinder-Pendulum, radius R = 1/8 inch, axial length ℓ = 1 inch.
§ iii - 2-Sphere-Pendulum, radii R = 1/8 inch.
§ iv - Cylinder-Pendulum, Frequency of Swing = 1/8 c.p.s., effective frequency of elemental oscillations ~ 10 c.p.s.
§ v - 2-Sphere-Pendulum, Frequency of Swing ≃ 1/20 c.p.s., effective frequency of elemental oscillations ~ ½ c.p.s.
§ vi - Cylinder-Pendulum, Calculated pressure (from equation (6.4) and (6.5)) P = 54 bars.
§ vii - 2-Sphere-Pendulum, P = 1,000 bars.
§viii - Measurements above -20°C not possible because of surface melting (see below).

6.3 The Internal Friction of Ice

In this section, we consider the available data on the internal friction of ice (Kneser et al. (271), Schiller (272), (273), Kuroiwa (274)). In particular Kuroiwa has made thorough investigations in the 100-1,000 c.p.s. frequency range using many different ice specimens. Some of the results obtained by him are shown in Fig.VI.II. The curves exhibit three distinct internal friction peaks which we will consider separately.

(i) The High Temperature (Grain Boundary) Peak.

This has been attributed to grain boundary sliding because of the absence of any such peak with single crystal specimens. The increase of tan ϕ near $0^{\circ}C$ is clearly seen in Fig.VI.II but no actual peaks exist in any of Kuroiwa's curves. Although Kuroiwa has assumed that this increase of tan ϕ represents the low temperature side of a grain boundary peak, it has not been shown definitely to be a relaxation process. In the course of the writer's work it was hoped to show whether or not this effect is a relaxation process by demonstrating that a true peak exists (since rolling friction experiments involve lower frequencies and one would therefore expect the peak, if it exists, to shift to lower temperatures). Because of the complicating effect of the surface melting phenomenon (Sec.6.2), this aim has not, so far, been achieved.

By observing the shift of the low temperature side of this "peak" with different frequencies, Kuroiwa was able to estimate an activation energy of about 65 k.cal/mole.

(ii) The Intermediate (Proton) Peak.

This peak, which occurs at $-20^{\circ}C \rightarrow -40^{\circ}C$ in Kuroiwa's curves, is generally known as a "proton peak". It is well known that measurements of the dielectric losses in ice crystals can be explained in terms of proton reorientations formed by migration of Bjerrum defects through the lattice (see Granicher et al (275), and Sec.3.2). The excellent correlation between the internal friction and dielectric relaxation ((275)-(279)) strongly suggest that the two relaxation processes arise from a common mechanism. Kuroiwa has demonstrated that the peak exists in single and polycrystalline ice, and in ice specimens doped with various impurities. The activation energy for this peak is found to be 13.1 k.cal/mole for the pure ice specimens.

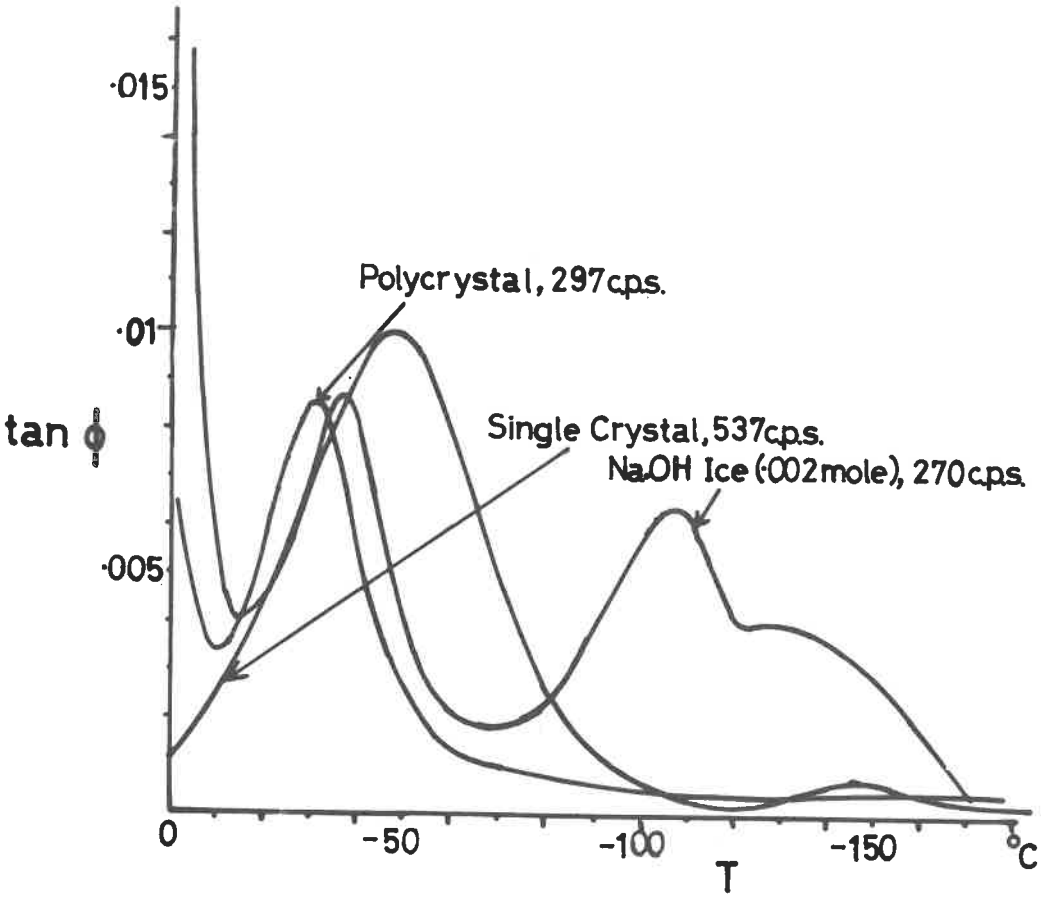

Fig.VI.II Internal Friction of Ice I - after Kuroiwa (Sec. 6.3).

(iii) The Low Temperature (Impurity) Peak.

This peak is attributed to impurities. Pure ice specimens do not show any internal friction peaks at low temperatures. Those doped with certain impurities exhibit this third peak for temperatures usually in the range of ~100°C to ~170°C. Fluorine atoms which occupy interstitial positions in the ice lattice (see Kopp et al. (90), (170)) give rise to an extremely small peak. However crystals doped with impurities which form clusters (NaCl, HCl, and NaOH) give rise to peaks which are orders of magnitude larger. This difference indicates that the low temperature peak is associated with the local clustering rather than interstitial occupation of impurities in the ice lattice. In none of these cases was it possible to detect any temperature shifts with changes of frequency.

Since (from Kuroiwa's data) the NaOH doped ice specimens give characteristically large and broad peaks, they were thought to be particularly suitable for the present work. Experiments on the rolling friction of NaOH doped ice are considered in the next Section.

6.4 The Interpretation of the Rolling Friction Results

The rolling friction curves for ice are shown in Figs. VI.III-V. Although preliminary in nature, these results show some interesting features:

(i) The Grain Boundary Peak.

The general rise of tan ϕ at the warmer temperatures in the internal friction curves is partly attributed to the grain boundary effect described by Kuroiwa. Because the frequencies associated with these experiments are much lower than those of Kuroiwa, it is to be expected that the onset of the grain boundary process should be located at a lower temperature. Kuroiwa's curves indicate that this onset occurs at ~20°C to ~30°C for a frequency of 180 c.p.s. By using the appropriate activation energy ($\simeq 65 \pm 15$ k.cal/Mole, see Sec. 6.3,(i)) we estimate that for a frequency of 10 c.p.s. this onset ought to occur at about ~40°C. (If one were to incorrectly consider the frequency of the pendulum (1/8 c.p.s.) one would obtain an "onset temperature" of about ~250°C.) It can be seen from Figs. VI.III and IV that the

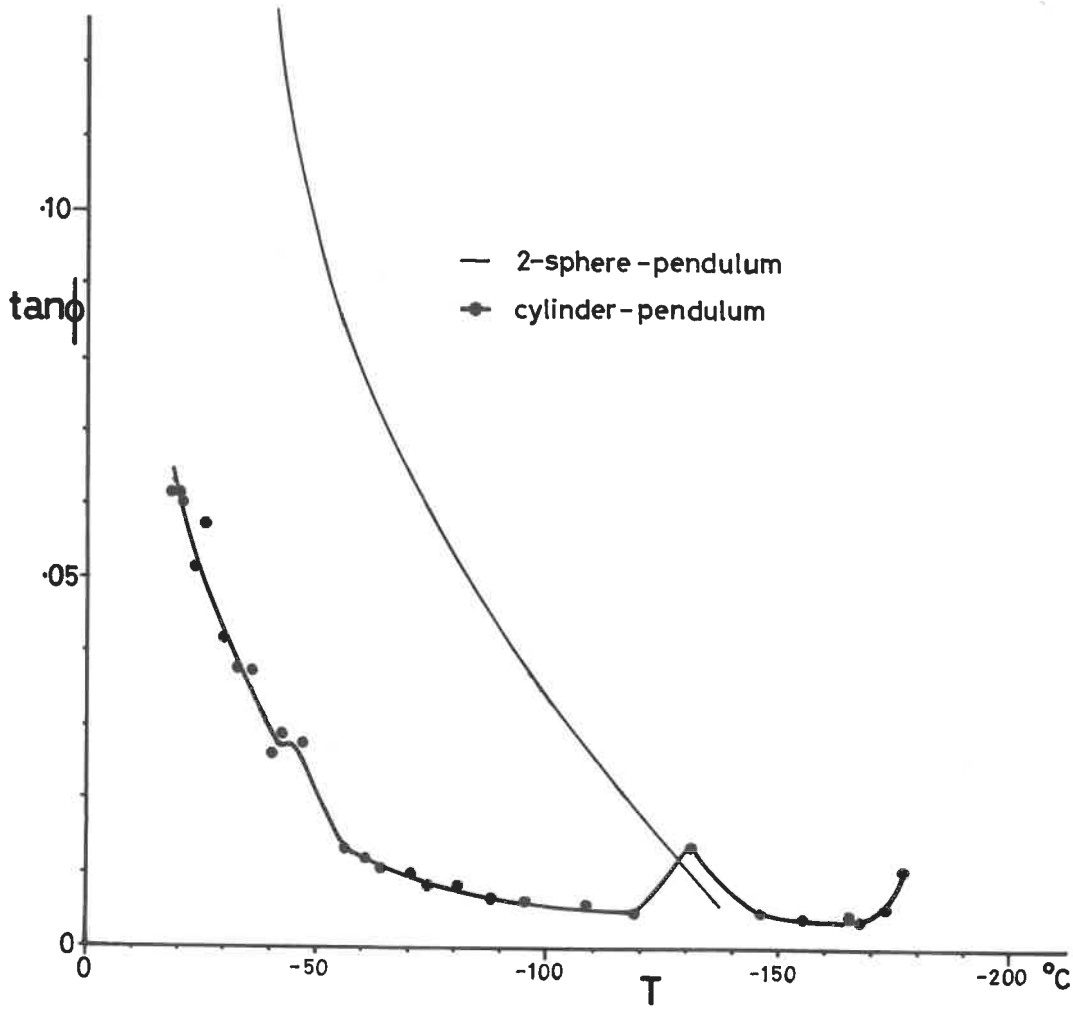

Fig.VIII Mechanical Relaxation of Polycrystalline Ice (from Rolling Friction data) -Secs.6.2, 6.4.

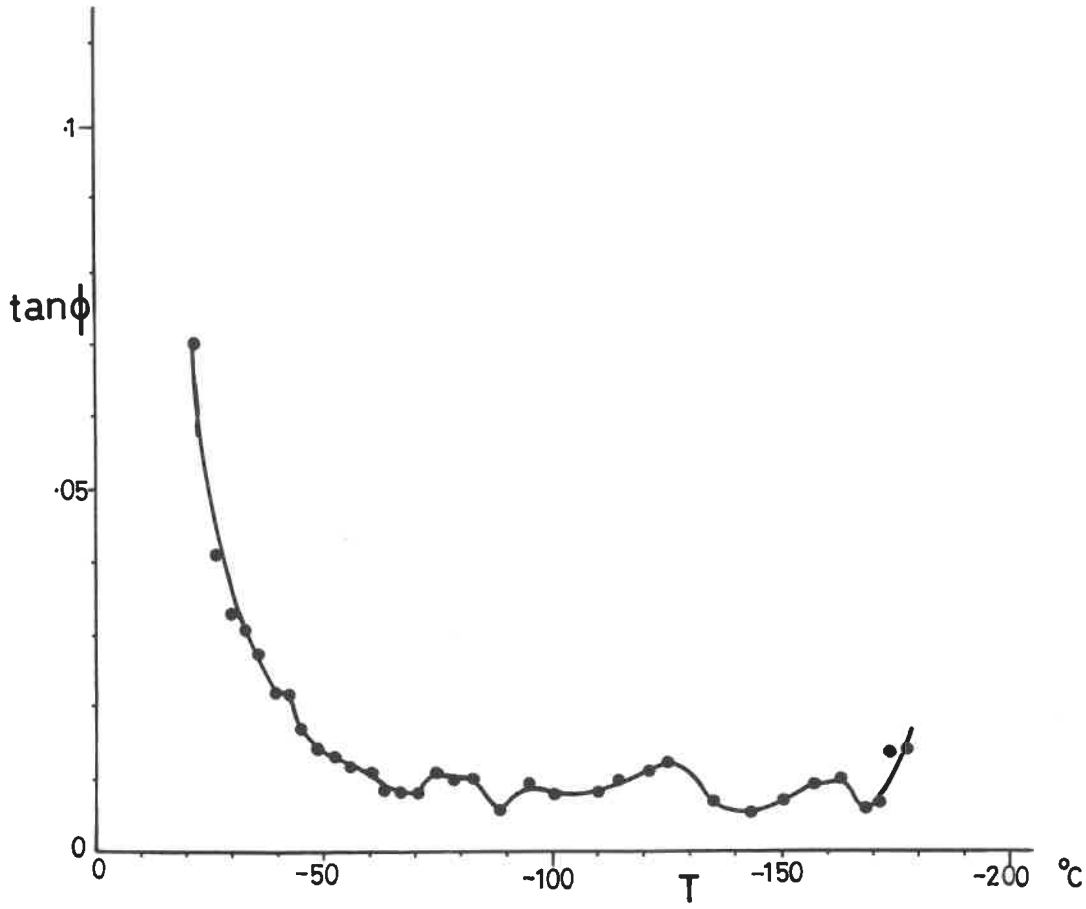

Fig.VI.IV Mechanical Relaxation of Na.OH(·0002mole) Polycrystalline Ice (from Rolling Friction data) - Secs. 62, 64.

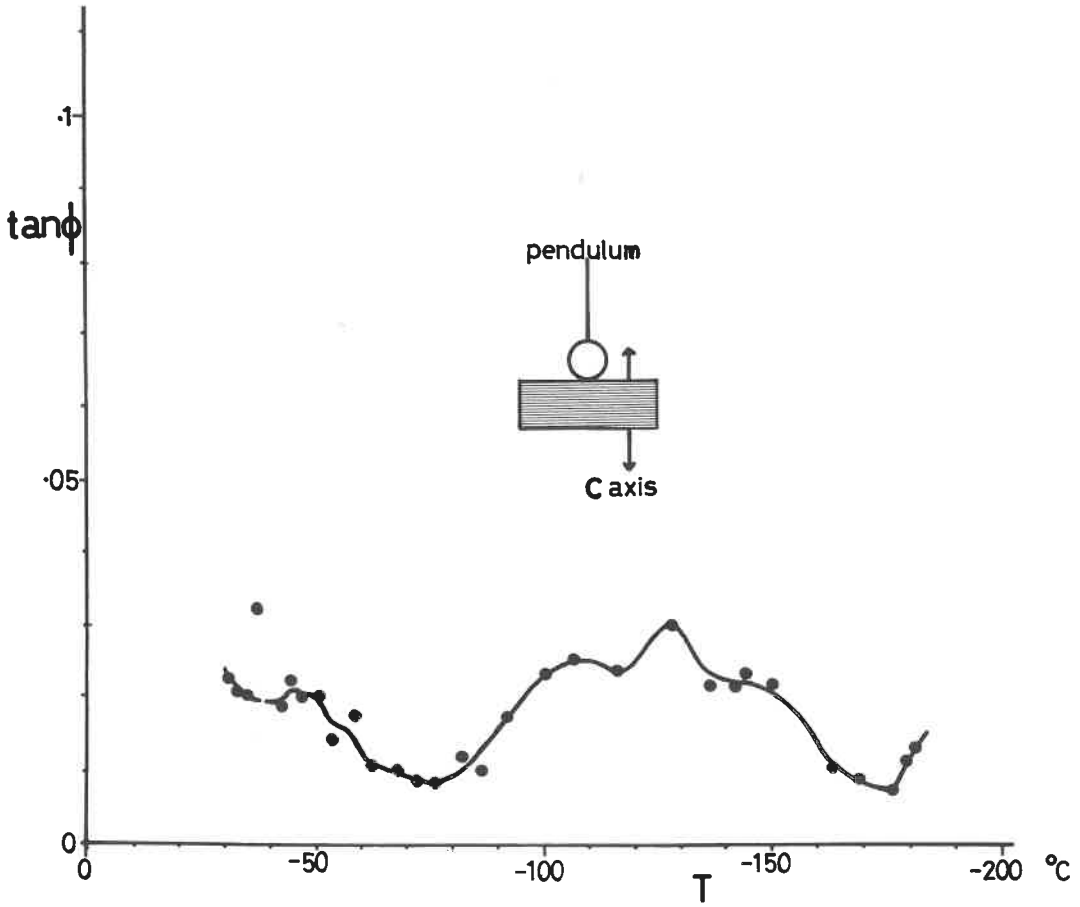

Fig. V Mechanical Relaxation of a Single Crystal of Ice (from Rolling Friction data) -Secs. 6.2, 6.4.

onset temperatures obtained lay between -40°C and -70°C. Estimates, such as these, based on the onset (rather than the peak) of the grain boundary process are very rough, and the above correlation is therefore considered as reasonable agreement between the two sets of data.

The identification of the rise of tan ϕ (above -70°C) with a grain boundary process is supplemented by the two-sphere pendulum experiment (No.12.0.2.). This experiment, while not being a very accurate one, shows a genuine shift to lower temperatures (see Fig.VI.III). The onset temperature in this case is much lower (about -100°C). If we consider the grain boundary losses to be associated with viscous "liquid like" shearing at the grain boundaries (see below) then this result might be expected; in view of the pressure melting properties of bulk ice, it is possible that the effect of hydrostatic pressure is to extend the viscous shearing properties of the grain boundaries to a lower temperature regime. This concept must however be treated with extreme caution particularly when one considers that the viscosity of ordinary cold water also shows an unusual dependence on hydrostatic pressure (see (38), (280)-(282)).

Kuroiwa's curves show that near the melting point tan ϕ rises extremely rapidly to values in excess of 0.02. However the incompleteness of these curves make it impossible to estimate the peak value tan $\phi_{max.}$. It was originally hoped that the lower frequency rolling friction experiments would provide a near complete picture of this grain boundary peak. The curves obtained (Figs.VI.III and IV) indeed indicate that for temperatures above -20°C, tan ϕ increases to values of at least 0.2-0.4. These values are at least an order of magnitude greater than the maximum values in Kuroiwa's curves. However it is difficult to estimate how much of this increase can be attributed to the surface melting phenomenon described in Section 6.2. The fact that the Single Crystal curve (Fig.VI.V) also shows an increase in tan ϕ at the upper temperatures, indicates that the surface melting phenomenon is appreciable above -20°C. However for the present purposes it is sufficient to note that tan $\phi_{max.}$ must be much larger than the "cold-side-values" of Kuroiwa. It is hoped that future rolling friction experiments will yield accurate values for tan $\phi_{max.}$.

We now wish to make a more detailed study of the grain boundary peak in ice by extending the equations formerly used successfully for the grain boundary viscosity of several metals (e.g. Al., Sn., Cu., Ag., see McLean (283), Ch.X; Mo., Ta., see Murray (284), Ch.V). Whereas for metals it is assumed that the viscous shear takes place over just a few molecular layers at the grain boundary, we will generalise the case for ice by denoting δ as the film width in the formulae below. Extending the ideas of Kê (285), McLean (283) has developed a formula for the viscosity η of the grain boundary layers:

$$\eta = \frac{Gu \cdot \delta}{wd(Gu/Gr-1)} \qquad (6.6)$$

where $w = 2\pi\nu$, d is the grain size, Gu and Gr are the relaxed and unrelaxed Moduli of rigidity. Zener (318) has shown theoretically that the elastic Modulus Gu should relax to a lower value Gr when the temperature is increased to values warmer than that of peak. In particular, if grain boundary sliding is the cause of this peak, this relaxation is related to Poisson's ratio γ by the formula:

$$\frac{Gr}{Gu} = \frac{2(7+5\gamma)}{5(7-4\gamma)} \qquad (6.7)$$

We now proceed to use these formulae to evaluate η/δ and discuss the experimental validity of the calculations: Substituting $\gamma_{ice} = 0.365$ (see (286), P.446) in equation (6.7) yields:

$$\frac{Gu}{Gr} \sim 1.57$$

Assuming that $Gu \simeq \frac{Eu}{(1+\gamma)2}$ (see for example (287)), and substituting the experimental values { $Eu \sim 10^{11}$ dynes.cm^{-2} (see (286), P.445), grain size $d \sim 0.2$ cm, frequency ~ 10 c.p.s. } for a grain boundary peak at $\sim 0^{\circ}$C into equation (6.6), we get:

$$\eta/\delta \sim 5 \times 10^{9} \text{ poise.cm}^{-1}$$

We do not know the width δ of the grain boundary film, but assuming it

to be of molecular dimensions, we obtain

$\delta = 100$ Å, $\eta = 5{,}000$ poise

$\delta = 10$ Å, $\eta = 500$ poise

$\delta > 2.7$ Å (bond length for ice), $\eta > 140$ poise

Although these viscosity values are considerably greater than those of bulk water (0.02 poise), they are far too low too be compared with those of ice ($> 10^{14}$ poise). However if we consider the grain boundary layers to behave as confined rather than bulk water (see Secs.3.3 and 3.4) the following interesting comparison may be made with friction and adhesion data:

(i) Grain boundary peak, near 0°C, $\eta_\delta \sim 5 \times 10^9$ poise.cm^{-1}

(ii) Adhesion data, -5°C (Jellinek, Sec.3.4, (iv)), $\eta_\delta \sim (0.15\text{-}0.7) \times 10^8$ poise.cm^{-1}

(iii) Sliding Friction, -6°C -13°C (Sec.5.4, (v)), $\eta_\delta \sim (4\text{-}12) \times 10^8$ poise.cm^{-1}

It is significant that three such different experiments give good (order of magnitude) agreement for this parameter. This confirms our view that, under the rolling friction-experimental conditions, the grain boundaries exhibit mechanical-viscous properties (above say -(20 to 50)°C) which are closer to those of "confined" rather than "bulk" water.

It is now necessary to consider other implications of this semi-theoretical estimate:

(1) If a grain boundary peak exists near 0°C then one should expect a relaxation of the rigidity modulus near this temperature by an amount $\sim \frac{1}{1.57}$ the (equation (6.7)). The writer has made a very brief study of some of published data ((286),(288)-(290)) on the elastic moduli of ice: The static measurements of the rigidity of ice are unreliable near 0°C. The dynamic measurements, while inherently more accurate, also show considerable experimental scatter. However it seems to the writer that there is a definite trend in the literature of a sudden decrease in the dynamic moduli of ice within 10 or 20°C of the melting point. The exact onset temperature is of

course frequency sensitive and it is therefore hoped that future experiments, using an internal friction-rigidity-apparatus developed at this laboratory, will extend the frequency range to values as low as those in the rolling friction experiments ($\sim$ 10 c.p.s.).

(2) According to the theory of Zener (291) the modulus relaxation should be related to the height of the internal friction peak by the following equation:

$$\tan \phi_{max} = \tfrac{1}{2} \frac{Gu-Gr}{Gav.} \qquad (6.8)$$

Substituting our value of 1.57 for $\frac{Gu}{Gr}$ in equation (6.8), we obtain

$$\tan \phi_{max} \sim 0.2$$

This is an interesting result; while Kuroiwa's curves cannot give any indication of tan ϕ values as large as this the rolling friction experiments, in spite of the somewhat misleading surface melting phenomenon, indicate that tan ϕ may well increase up to values comparable with 0.2.

We conclude that the high temperature rolling-internal friction data for ice is consistent with the phenomenological theories of grain boundary relaxation provided the viscous layers between the grains have the properties of confined rather than bulk water.

(ii) The Low Temperature Peaks.

Figs.VI.III to V show that a number of peaks are evident below the grain boundary sliding regime as in the case of Kuroiwa's work. While his curves show just two peaks (proton and impurity), the number of individual low temperature peaks in the rolling friction curves may be as high as 4 or 5. One would expect, using Kuroiwa's data, that the proton peak should occur between -60°C and-90°C for the rolling friction experiments. Figs.VI.III-V show that the majority of the peaks occur below -90°C.

On the grounds that the impurity peaks are insensitive to frequency changes (Sec.6.3,(iii)), one may tentatively suggest that some of the following peaks may represent impurity effects:

a) polycrystalline ice, below -175°C (Fig.VI.III),

b) Na.OH ice, -125°C, or -163°C, or below -175°C (Fig.VI.IV),

c) Single crystal ice, -144°C, or below -180°C (Fig.VI.V),

In particular the characteristic "double hump" (-125°C and -163°C) for the Na.OH ice bears some resemblance to that in Kuroiwa's curve (Fig.VI.II). Future experiments, at frequencies intermediate between those used by Kuroiwa and the writer, will help to analyse these peaks with more certainty. It is therefore not, at present, worthwhile to make a detailed conjectural study of them.

One important point however does emerge; that the proton effect, if it still exists at these temperatures, exhibits two or more peaks with each one having an activation energy different to that of Kuroiwa's proton peak.* The possibility of appreciable proton ordering in ice below about -170°C has been discussed in Sec.3.2. One may therefore tentatively argue that these low frequency rolling friction experiments cause the proton peaks to shift to lower temperatures than that expected. The migrating protons then experience a different system of electric fields as a result of this ordering. This perturbation is then manifested in these low temperature peaks - the different peaks presumably correspond to different activation energies of proton movement in the different systems of electric fields present.

6.5 Summary

The rolling friction results have been interpreted assuming that they illustrate the characteristic hysteresis (rather than the sliding friction) losses of the bulk ice specimen. The results have not been used to illustrate the correlation between the internal friction and rolling friction of ice - rather it has been assumed that this correlation has been *a priori* proven, and the results are therefcre used to demonstrate the mechanical relaxation properties of ice at low frequencies ($\lesssim 10$ c.p.s.).

---

* It is interesting to note that Schulz and Knappwost (315) also obtain some unusual low temperature peaks for the sliding friction of ice. Unfortunately at present the relation between Internal and Sliding Friction is not well understood.

Three difficulties emerge in the analysis:

(a) the internal friction peaks shift (with frequency) at different rates. This makes it a little difficult to compare these results with those of Kuroiwa where the frequencies are 100-1,000 c.p.s.

(b) the surface melting phenomenon which existed with the present experimental arrangement. This masked the viscoelastic effects above -20°C.

(c) the ambiguity in attributing an "effective" (or average) frequency value to the rolling friction.

It is thought that with certain future experiments these problems will be resolved.

The interesting features that emerge from this study are:

(a) It has been found that the high temperature rolling-internal friction data for ice is consistent with the phenomenological theories of grain boundary relaxation provided the viscous layers between the grains have the properties of confined rather than bulk water.

(b) The low temperature data indicates departures from the single relaxation proton peak observed at high temperatures by other workers. An explanation may lie in the proton ordering effects that are believed to exist in ice at low temperatures.

CHAPTER VII

SUMMARY AND CONCLUSIONS

7.1 Experimental Results - Summary and Conclusions

The results of this thesis can be divided into two complementary main parts, (a) the Hardness and Friction Results (Chapters IV and V), and (b) the Mechanical Relaxation Results (Chapter VI).

(a) Hardness and Friction Results.

It has been found necessary to divide the hardness and friction behaviour of ice into two distinct temperature regimes: The lower temperature regime ($\simeq(0.08 \rightarrow 3)^{\circ}C$ to $\simeq 12^{\circ}C$) is called the "Creep Regime", the higher temperature regime ($0^{\circ}C$ to $\simeq(0.08 \rightarrow 3)^{\circ}C$) is called the "Pressure Melting Regime". It is convenient to illustrate these two regimes by reference to Glen's Flow Law for ice:

$$\dot{\epsilon} = A' \cdot \sigma^{m} \cdot \exp - \left(\frac{Q}{RT}\right) \qquad (3.3)$$

This equation describes the rate of plastic flow $\dot{\epsilon}$ of ice when subjected to a stress σ, at a temperature T. By using a kinematic theory of hardness, it has been possible to analyse the hardness data in terms of this equation. Generally speaking:

(1) At high temperatures when the stresses are sufficiently high to initiate "pressure melting" in certain regions of the specimen, the ice flows more easily. In terms of equation (3.3) this is equivalent to stating that the "pre-exponential constant" A' suddenly increases when the ice specimen becomes superheated (i.e. temperature above the pressure melting point) under the effect of the applied stress. However the stress exponent m does not change significantly in the pressure melting regime.

(2) At low temperatures the stresses are not sufficient to produce pressure melting within the ice specimen - the ice therefore deforms as an

ordinary plastic material. For hardness experiments therefore, the flow law (equation (3.3)) is obeyed in this regime: Indeed the values of Q and m obtained from these studies agree well with those obtained by Glen.

A previous paper (141) pointed out the complexity of deformation behaviour in Ice. This paper emphasised that deviations occurred only above the pressure melting point. It was therefore concluded that these deviations were the result of some melting phenomena. More recent experiments have confirmed this view; various techniques (prolonged static, dynamic methods) have extended the range of stresses and strain rates of the former studies. The present results cover a strain rate range of about 10^8, and a stress range of about 10^3, and the original conclusions still hold. This thesis (Chapter IV, see also (294)) gives a fuller explanation of the mechanisms involved in the pressure melting regime. The data obtained from several experiments strongly suggest that two major processes are responsible for the enhanced flow rate in the pressure melting regime. These two processes are called "regelation" and "the grain boundary process". While the term "regelation" is in common use, the "grain boundary process" is an innovation and is considered to be one of the most significant outcomes of this research. In particular this process assumes that there are liquid like layers at most of the grain boundaries in the pressure melting regime whose widths may be several microns. This description is required because the process operates only above the pressure melting point and must therefore involve a melting phenomenon. Additional evidence for grain boundary melting is presented in Section 4.12, and some suggestions are offered to explain how this process causes the enhanced flow rates observed.

In parallel with the two regimes of hardness behaviour, it is found that there is also a marked change in the general nature of the deformed ice over the entire range (10^{-4} to 10^4 sec) of loading times. Optical studies, polarised light and etchant-replica techniques all help to reveal the grain structure properties of these deformed zones. The recrystallization habits displayed in the creep regime are interpreted in terms of the transient,

steady-state, and accelerated creep properties of ice as determined by Glen and Steinemann. However the deformation zones in the pressure melting regime are strikingly different; they are characterised by the loss of bubbles and considerable grain growth. The grain boundary process is also used to account for these deviations. Again it is required that these grain boundaries are in a liquid state. Additional evidence is presented to confirm this view (Sec.4.12).

These results prove useful in reinterpreting previous work on the creep of ice. (1) The low temperature creep results of Glen and Steinemann are considered; it is found that there are considerable deviations from their flow laws at higher stresses (> 300 bars). An attempt is made to interpret the entire plastic behaviour in terms of current dislocation models (Sec.4.11). (2) The warm (-0.02°C) temperature results of Glen are also reinterpreted in terms of the "regelation" and "liquid grain boundary" processes (Sec.4.13). The glaciological implications of this reinterpretation are discussed in Section 7.2.

It is interesting to note that the stress-temperature treatment of the pressure melting regime is basically different to that normally used with pressure melting effects. Regelation theories commonly assume a "stress-temperature compatibility condition" by equating the temperature of the ice-water interfaces to that of their pressure melting points - see for example Nye (87), Weertman (140). The writer believes that this is not necessarily the case (see for example, the interface-temperature study by James and Sekerka (295)) and that the discrepancy between experiment and regelation theory rests on this assumption. There are even stronger reasons for disregarding this condition in the interpretation of the hardness results as measurements show that the temperature of the deformed ice usually remains very close to its pre-indentation value. In addition a simple conductivity-calculation shows that in view of the low rates of heat flow inherent in these experiments, the bulk ice beneath the indenter must remain in a superheated state throughout the indentation.

In friction experiments (Ch.V), an additional confirmation of the two regime model is obtained from a study of the two component coefficients of

friction. In particular (i) the adhesion component is interpreted in terms of a liquid film on the surface of ice rather than the conventional model of interfacial plastic flow; and (ii) the ploughing component is used to reinterpret previous work on the friction of ice. Indeed as a result of its behaviour near the melting point, ice presents itself as a suitable material for the study of the adhesion and ploughing components of Friction.

(b) Mechanical Relaxation Results.

A simple rolling friction apparatus has been used to study the mechanical relaxation effects of ice at frequencies of 10 c.p.s. and less. The temperature range used was -20°C to -180°C. While the results are of a preliminary nature, they suggest some interesting interpretations of the structure of ice at low temperatures.

The results at the warmer temperatures illustrate the grain boundary effect of Kuroiwa and are interpreted as arising from the viscous sliding properties of the grain boundaries in ice. Using such an interpretation, the viscosity-width characteristics of these layers were estimated-they compared well with those values deduced from adhesion (Jellinek) and friction (Ch.V) experiments. The implication here is that, in its manner of formation and mechanical behaviour at low strain rates, the viscous grain boundary layer bears a certain resemblance to the "surface liquid layer" proposed for ice. It is important that one is aware of how the behaviour of the viscous layer differs in the hardness and the mechanical relaxation experiments. The latter effect is concerned with a gradual change in size and viscosity of grain boundaries over a wide range of temperatures; the former effect involves the sudden increase in size of these viscous layers when their hydrostatic pressure reaches the critical pressure melting value. Thus the former effect applies only at temperatures above the pressure melting point, while the latter applies to temperatures lower than this as well. The former effect is illustrated by the response of these liquid layers to a continuous indentation load; the latter effect is assessed from the rate of energy dissipation produced by the "viscous-hysteresis" losses of these layers when under an alternating stress.

friction. In particular (i) the adhesion component is interpreted in terms of a liquid film on the surface of ice rather than the conventional model of interfacial plastic flow; and (ii) the ploughing component is used to reinterpret previous work on the friction of ice. Indeed as a result of its behaviour near the melting point, ice presents itself as a suitable material for the study of the adhesion and ploughing components of Friction.

(b) Mechanical Relaxation Results.

A simple rolling friction apparatus has been used to study the mechanical relaxation effects of ice at frequencies of 10 c.p.s. and less. The temperature range used was $-20^{\circ}C$ to $-180^{\circ}C$. While the results are of a preliminary nature, they suggest some interesting interpretations of the structure of ice at low temperatures.

The results at the warmer temperatures illustrate the grain boundary effect of Kuroiwa and are interpreted as arising from the viscous sliding properties of the grain boundaries in ice. Using such an interpretation, the viscosity-width characteristics of these layers were estimated-they compared well with those values deduced from adhesion (Jellinek) and friction (Ch.V) experiments. The implication here is that, in its manner of formation and mechanical behaviour at low strain rates, the viscous grain boundary layer bears a certain resemblance to the "surface liquid layer" proposed for ice. It is important that one is aware of how the behaviour of the viscous layer differs in the hardness and the mechanical relaxation experiments. The latter effect is concerned with a gradual change in size and viscosity of grain boundaries over a wide range of temperatures; the former effect involves the sudden increase in size of these viscous layers when their hydrostatic pressure reaches the critical pressure melting value. Thus the former effect applies only at temperatures above the pressure melting point, while the latter applies to temperatures lower than this as well. The former effect is illustrated by the response of these liquid layers to a continuous indentation load; the latter effect is assessed from the rate of energy dissipation produced by the "viscous-hysteresis" losses of these layers when under an alternating stress.

7.2 Implications for Glaciology

The hardness and friction results of Chapters IV and V are considered in relation to glaciological studies. In particular, the experiments performed close to the melting point are seen to have important implications for glaciology. For convenience, we divide this discussion into two main sections:

(i) Ambiguity in Glen's $-0.02^{\circ}C$ Results.

The enhanced flow results of Sections 4.12 and 5.4 suggest new explanations for the similar enhanced flow rates observed by Glen at $-0.02^{\circ}C$. This reinterpretation is discussed in more detail in Section 4.13. In order to give a clearer picture of the ambiguities involved, the temperature variation of the term $A' \exp -\left(\frac{Q}{RT}\right)$ (equation (3.3)) from Glen's data is shown by the line AOB in Fig. VII.1. If the $-0.02^{\circ}C$ result is ignored, extrapolation of the low temperature data gives the straight line AOC. The discrepancy between these two lines near the melting point gives rise to ambiguity; Section 4.13 argues that this discrepancy is the result of either (or possibly both) a regelation or liquid grain boundary process - the grain boundary process is the preferable choice. It must however be emphasised that while this is probably true, this assumption has yet to be tested experimentally. The use of Glen's data near the melting point has been used in glaciological theory without regard to these ambiguities. Four particular examples are given below:

(1) Glacier Sliding Theory. A number of theories have been proposed for the sliding of a temperate glacier over its bed (Weertman (140),(300), Lliboutry (301),(302),(303), Kamb and LaChapelle (298),(299)). It is usual to consider the sliding as arising from two distinct causes: (a) a plastic type of flow due to stress concentrations around bedrock obstacles, and (b) the regelation of ice around the bedrock obstacles. These two causes are analogous to the processes (i) and (ii) (creep and regelation) described for the indentation experiments. However the important implication from these experiments is that a third term should be considered in the theory of bed sliding of glaciers, i.e., the enhanced flow rate due to grain boundary effects as in process (iii). In particular Weertman's theory gives a

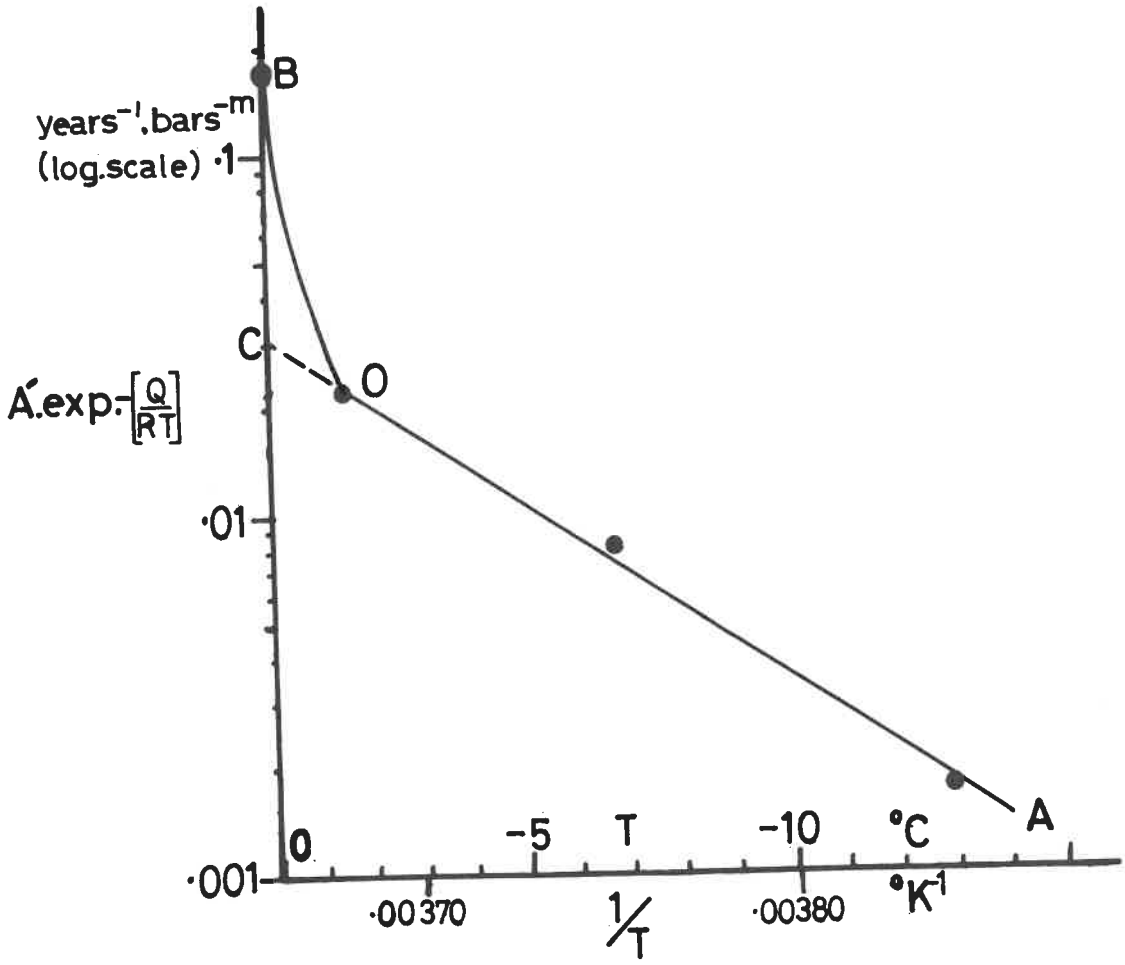

Fig.VII.1 Variation of Creep Factor with Reciprocal Temperature -Glens data (Sec. 7.2).

very clear picture of the effects of creep and regelation alone on sliding. In order to calculate the effects of plastic flow (i.e.(a) above), Weertman has to assume a particular value for the flow rate $A' \exp-\left(\frac{Q}{RT}\right)$. In fact Weertman uses a value which is equivalent to that indicated by B in Fig.VII.I. However we do not know which processes are responsible for the increased flow-rate observed in Glen's - 0.02^{o}C results. For example, if the increase in Glen's flow rate at -0.02^{o}C is due to the grain boundary process (iii) alone, then Weertman's usage of this particular flow rate value would mean that the grain boundary process is inadvertently incorporated into his theory. On the other hand if this is not the case, then Weertman's theory does not fully include the grain boundary process. Because of this uncertainty Weertman's treatment may need to be qualified. (Weertman (304) has independently also noted some of these complications). It is also pointed out (Barnes and Robin (305), see also (ii) below) that the stress concentrations in Weertman's theory may be as large as 50 bars. If this is the case then there are additional reasons for believing that the flow of ice around bed rock obstacles would be more accurately represented by the hardness curves (for say $t = 10^{3} - 10^{4}$ secs) than by Glen's results which were obtained from experiments at the lower stress range of about 1-11 bars. It is interesting to note that for $t = 10^{3}-10^{4}$ secs the three processes (creep, regelation and grain boundary) occur in roughly equal amounts.

Even if Weertman's theory gives the correct answers, it is still necessary to emphasise the importance of the liquid grain boundary process so that a more complete picture of the physical processes occurring at the bed may be obtained; for example, see ((ii),(2)) below.

(2) General Glacier Flow. Meier (236) has made a stress-strain rate analysis for the flow of the Saskatchewan Glacier (Canada), and compared his results to the -0.02^{o}C laboratory results (i.e. point B in Fig.VII.I) of Glen. He concludes, on the basis of this comparison, that there is a change in nature of the flow of ice at a stress of about 1 to 10^{-1} bars. However it is now evident that this comparison is only meaningful provided the bulk of this glacier is at the melting point. In view of the present ideas on temperate glaciers, this would seem to be unlikely. Hence the quantitative

(and possibly qualitative also) conclusions drawn from this comparison must now be questioned.

(3) Tunnel Closure in Glaciers. Attempts have been made (Nye (207), Paterson and Savage (306)) to relate the flow law of ice obtained from the rate of Glacier tunnel closures to that obtained in the laboratory. Comparisons with Glen's $-0.02^{\circ}C$ results are now seen to be dubious unless the bulk ice surrounding the tunnel is at the pressure melting point. One can use value B (Fig.VI.I) provided the ice is near the pressure melting point but otherwise some value along OC should be used. For these reasons the comparison made by Nye (207,Fig.2) and the temperature deductions made by Paterson and Savage may need to be qualified.

However the determinations of the stress exponent m from tunnel closure measurements are meaningful - the results of Section 4.5 show that, unlike $A' \exp -\left(\frac{Q}{RT}\right)$, m does not change very much in the pressure melting regime.

(ii) The Enhanced Flow Rates at (or above) the Pressure Melting Point.

It must be remembered that the pressures involved in the hardness (and friction) experiments are of the order of 10-200 bars near the melting point. Such pressures are not typical of the main ice bulk of temperate glaciers; however, Weertman's model of sliding involves stress concentrations proportional to the relative areas of obstacle and intervening glacier bed. For a mean shear stress on bedrock of 1 bar, the stress concentration factor could produce stresses up to 50 bars near the obstacles. (Direct measurements of such stress concentrations have not been made). It would seem that the hardness (and friction) results have particular relevance to the conditions existing near the bed-rock obstacles of a glacier. These "enhanced flow rate" results are now therefore used to interpret certain characteristics of the sole of a glacier. It is again necessary to invoke the liquid grain boundary process for this study. Glen's results (Fig.VII.I) imply that this grain boundary process can increase the strain rates by a factor of > 500 per cent. Similarly the ebonite hardness results (Figs.IV.IV and V) imply the stress for a given strain rate may be reduced by as much as 25 per cent. This liquid grain boundary process is therefore considered to be of prime importance for this study. Five particular examples are discussed below:

(1) Weertman's Stress Concentration Effect.

Weertman's assumption, that the glacier sliding is retarded mainly by obstacles projecting into the basal ice, rests on the ability of the remaining bed rock surface to offer little resistance to the basal movement. Weertman argues that this is possible if the ice is supported on a thin film of water giving low frictional resistance. This model gives rise to the stress concentration effect described above (ii). The adhesion-friction curve (Fig. V. VII) and specific-shear-strength curve (Fig. V. VIII) indicate that for ice near $0^{\circ}C$, the frictional resistance is indeed low. It is also interesting to note that this confirmation of Weertman's assumptions does not require the presence of a water film possessing macroscopic dimensions. It should be noted, however, that Figs. V. VII and V. VIII are for a steel-ice interface. It is hoped that these experiments will be repeated using rock-ice interfaces.

(2) The Sole of the Glacier.

It is emphasised (in (i), (1)) above, the importance of the liquid grain boundary process in explaining the characteristics of the sole. The sole of the glacier is a layer of relatively clear ice, sometimes containing debris, and about 0.5m thick. Kamb and LeChapelle's comments ((298), (299)) on this zone are:

(a) "The lowermost 0.5 m of ice above the regelation layer was relatively bubble-poor and appeared unfoliated. Above this zone, typical bubble foliation was prominent."

(b) "A stake anchored in the ice a distance of 10 cm above bedrock showed an average motion of 1.6 cm.day^{-1} parallel to the bed. A stake 150 cm above bedrock moved 12 per cent faster. By means of a vertical profile of marker pegs spaced 10 cm apart, it was found that most of this 12 per cent differential motion occurred within the lowermost 50 cm of ice, as shear uniformly distributed except for two irregularities suggestive of 'shear zones', which, however, had only intermittent activity. In any case essentially all the motion of 1.6 cm day^{-1} took place as slip at the bedrock-ice interface."

Observations recorded by McCall (307) on the 30-cm thick sole of Skauthoe cirque glacier in Norway are broadly similar to the observations of Kamb and LaChapelle. McCall suggests that the bubble-free nature of the sole "probably originated" by meltwater percolating down the headwall of the glacier and freezing against the base of the ice. Such an explanation is unlikely to apply to the tunnel in which Kamb and LaChapelle worked.

The bubble-free nature of the ice and the relatively rapid strain rates observed in the sole of the Blue Glacier and Skauthoe both suggest strongly that the liquid grain boundary process is occurring in the same manner as in the hardness and friction experiments. The large crystal size in Fig.5 of Kamb and LaChapelle's paper also suggests the liquid grain boundary process, as the relatively rapid shear in this layer would otherwise be expected to produce smaller crystal sizes.

More recently it has been suggested (309) that, in addition to the - grain boundary process, all three pressure melting regime processes (i.e. (i) creep, (ii) regelation, and (iii) liquid-grain boundary) are evident in Kamb and LaChapelle's observations. It is suggested that:

(a) The bottom ~1 cm "regelation layer" illustrates the regelation process No.(ii). This layer is presumably formed by regelation from the up-stream to the down-stream side of the bedrock protuberance.

(b) The layer ~(1-50) cms from the bed illustrates the liquid grain boundary process No.(iii). This is because of the similarity in the texture of this layer and that the deformation zones in the hardness experiments. In addition this layer deformed far more rapidly than the bulk glacier ice above.

(c) The remaining ice (50 cms from the bed to the top surface of the glacier) illustrates the creep process No.(i). In Kamb and LaChapelle's observations the amount of deformation here is much less than in the other two layers (a) and (b).

If this interpretation is correct then Kamb and LaChapelle's observations suggest that, in glacier sliding, the three processes are in order of importance; regelation, liquid grain boundary, and creep. The limited stake measurements suggest that the regelation process is, at the most, 7 times

more effective than the grain boundary process in producing glacier movement - it may however be much less effective than this value. The hardness measurements indicate that, for a steel indenter and an indentation size ~ cms, the three processes occur in roughly equal amounts at $0^{o}C$. However until more stake measurements (of the sort carried out by Kamb and LaChapelle) are made in the region 0-10 cms from the bed, one cannot really quantitatively discuss this comparison.

It is necessary to point out that, in a previous paper (305), Barnes and Robin effectively termed the liquid grain boundary process as "regelation-deformation". It has been agreed (308) that in future only the term "liquid grain boundary process" (or the abbreviated form, "grain boundary process") will be used in this context.

(3) Catastrophic Advances of Glaciers.

The proposal that temperature effects may be responsible for triggering off glacier surges in sub-polar glaciers (310) receives further support from the hardness and friction results. The slow warming of the basal ice of a glacier into the temperature range in which the grain boundary process and regelation against bedrock protuberances can occur is likely to produce an instability which could lead to rapid basal sliding and a catastrophic glacier advance. The relative roles of such processes and of the sub-glacial water film of Weertman in explaining the rapid rate of flow once an instability develops need further investigation.

With regard to catastrophic advances of temperate glaciers, the results are suggestive but the answer is not clear. The time effect indicates greater apparent hardness values for shorter time intervals, which in terms of sliding would mean more resistance for higher rates of sliding, as is also indicated from the results of Glen. However, in contrast to this, higher rates of sliding imply greater stress concentrations and increased flow rates due to the onset of the grain boundary process. It is not clear which of these two processes is the more important, but the fact that some temperate glaciers, such as the relatively flat lobes of the Vatnajökull ice cap (311), undergo catastrophic advances suggests that the onset of accelerated flow may be due to the processes shown to exist in the hardness and friction experiments.

more effective than the grain boundary process in producing glacier movement - it may however be much less effective than this value. The hardness measurements indicate that, for a steel indenter and an indentation size $\sim$ cms, the three processes occur in roughly equal amounts at $0^{o}C$. However until more stake measurements (of the sort carried out by Kamb and LaChapelle) are made in the region 0-10 cms from the bed, one cannot really quantitatively discuss this comparison.

It is necessary to point out that, in a previous paper (305), Barnes and Robin effectively termed the liquid grain boundary process as "regelation-deformation". It has been agreed (308) that in future only the term "liquid grain boundary process" (or the abbreviated form, "grain boundary process") will be used in this context.

(3) Catastrophic Advances of Glaciers.

The proposal that temperature effects may be responsible for triggering off glacier surges in sub-polar glaciers (310) receives further support from the hardness and friction results. The slow warming of the basal ice of a glacier into the temperature range in which the grain boundary process and regelation against bedrock protuberances can occur is likely to produce an instability which could lead to rapid basal sliding and a catastrophic glacier advance. The relative roles of such processes and of the sub-glacial water film of Weertman in explaining the rapid rate of flow once an instability develops need further investigation.

With regard to catastrophic advances of temperate glaciers, the results are suggestive but the answer is not clear. The time effect indicates greater apparent hardness values for shorter time intervals, which in terms of sliding would mean more resistance for higher rates of sliding, as is also indicated from the results of Glen. However, in contrast to this, higher rates of sliding imply greater stress concentrations and increased flow rates due to the onset of the grain boundary process. It is not clear which of these two processes is the more important, but the fact that some temperate glaciers, such as the relatively flat lobes of the Vatnajökull ice cap (311), undergo catastrophic advances suggests that the onset of accelerated flow may be due to the processes shown to exist in the hardness and friction experiments.

(4) Cavity Formation

Weertman (300) has developed a theory for cavity formation behind bedrock obstacles. He concludes that, for most glaciers, the length l of this cavity is given by

$$l = \frac{\Lambda \cdot (\text{sliding velocity})}{(\text{cavity closure rate})} = \Lambda \left(\frac{Yr^2}{k}\right)^m / (\mu_b \rho g h)^m \quad (7.1)$$

where Λ is the obstacle height, $(\rho g h)$ is the overburden pressure, $\frac{Yr^2}{k}$ is the effective lonitudinal stress which causes the sliding around the obstacle and μ_b is unity except for fast moving glaciers where the cavities interfere with each other. It should be noted that equation (7.1) is derived using a sort of dimensional analysis - two constants of proportionality (which are related to the longitudinal and vertical movement of the cavity roof) are equated. In the opinion of the writer, there is no real reason why these two constants should be equal. If this is so, equation (7.1) should be modified using a constant which can be derived from the equations of sliding (Weertman) and tunnel closure (Nye).

The phenomenon of cavity closure provides an interesting example for using the concept of the liquid grain boundary process. It is perfectly conceivable that whereas ice on the upstream is at or above the pressure melting point because of the high longitudinal compressive stresses, on the downstream side where the compressive stresses are lower the ice is at or below the pressure melting point. On this reasoning we therefore have two regions of ice with different "plastic properties". The uppermost ice is affected by the grain boundary process; the ice on the downstream side of the obstacle is not affected by the liquid grain boundary process. Weertman in his treatment assumes these two ice regions to be identical in their plastic behaviour. Equation (7.1) effectively shows that the cavity length is proportional to the flow rate of the upstream ice and inversely proportional to the (vertical) flow rate of the downstream ice. We now treat this quantitatively: We note that in ((i),(1)) above, it is argued that Weertman probably uses the correct value of $A' \exp - \left(\frac{Q}{RT}\right)$ in his computation of the glacier sliding speed. However

by using the same value for the rate of cavity closure, this computation is overestimated by a certain factor. Using Glen's data (Fig.VII.I) this factor is determined as $\left\{A' . \exp - \left(\frac{Q}{RT}\right)\right\}_B \Big/ \left\{A' . \exp - \left(\frac{Q}{RT}\right)\right\}_C \simeq 5.7$. If one uses the ebonite hardness data (Fig.IV.IV) a similar value can be obtained. This means that the cavity length predicted by Weertman is > 5 times too short. (It must be remembered, however, that the writer believes that Weertman's formula, equation (7.1), is uncertain for other reasons as well - see above)

It should be interesting to see if this increase in cavity length is sufficient to affect Weertman's sliding theory. One basic difference between the theories of Weertman and Lliboutry (312) is that, unlike the former, the latter theory effectively assumes the cavities to be as long as the distance of separation between comparable obstacles.

7.3 Future Experiments

Through writing this thesis it has become apparent that certain important experiments should be performed in the future. Most of these have been outlined in the relevant Sections; they are briefly enumerated here:

(i) "Creep of ice" experiments over the temperature range $-1^{\circ}C$ to $-20^{\circ}C$ with single and poly ice crystals. These experiments would provide better data for the variation of the activation energy for creep with temperature and stress.

(ii) Compressional "creep of polycrystalline ice" experiments in the pressure melting regime with the view to studying the importance of the liquid grain boundary process.

(iii) Experiments designed to compare the creep rates of samples with different simple and complex stress systems. These experiments would help to clarify the difficulties involved when making comparisons between (a) glaciological studies and laboratory experiments, and (b) different laboratory experiments.

(iv) Dynamic hardness experiments using widely differing impact times (a difficult experiment). These results would be invaluable for a further

study of the deformation of ice at high strain rates.

(v) More experiments involving the photography of air or vapour bubbles in ice during indentation.

(vi) The hardness of single ice crystals in the pressure melting and creep regimes.

(vii) Friction experiments involving ice sliders and steel (or rock) surfaces. These results would be useful for (a) testing current theories of friction, (b) glaciological theories of sliding.

(viii) Friction and Hardness experiments of ice at lower temperatures ($\sim -10^{\circ}C$ to $\sim -20^{\circ}C$, say).

(ix) Friction experiment over a range of velocities. These experiments would be useful for testing the "surface layer concept" developed in Section 5.4.

(x) The role of "brittle fracture" in the deformation of single and polycrystalline ice specimens.

(xi) Mechanical Relaxation experiments on single, polycrystals of ice over (a) the temperature range $0^{\circ}C$ to $-180^{\circ}C$, (b) range of hydrostatic pressure of 0 to a few k.bars, (c) range of frequencies of say < 1 to 20 c.p.s. These experiments would give a clearer picture of the physical processes responsible for the internal friction peaks in ice.

SYMBOLS

General

$\sim$	of the order of
$\simeq$	approximately equal to
$\propto$	proportional to

- other conventional mathematical symbols used

ρ	density
μ	micron = 10^{-4} cm (also coefficient of friction)
δ	theoretically; thickness of supposed special film on water or ice, experimentally; measurements concerned with this film e.g. separation of parallel plates
η	effective viscosity of above film
Q	an activation energy - usually of creep. Suffix s.d. refers to self-diffusion.
R	Gas Constant $\simeq$ 2 cal/mole. (Also experimental radius)
T	Temperature
Tm	Melting Point
ΔT	Change in melting point
Tc	Critical Temperature (kinks etc.)
t	time
n	integral number of events
d	grain size (Ch.VI.) or diameter
S	Entropy
V	volume (e.g. of indentation)
h	height
b, l	width, length

Mechanical

σ, σ_{ij}	stress
ϵ, ϵ_{ij}	strain
$\dot{\epsilon}, \dot{\epsilon}_{ij}$	strain rate
P	hydrostatic pressure

τ	octahedral shear stress
τ_{ij}	shear stress
$\dot{\delta}$	octahedral shear strain rate
δ	Poisson's Ratio
m	Stress Exponent
$A^{sup.}$	pre-exponential constant for creep or hardness equations
E	Young's Modulus
$G_{sub.}$	Rigidity Modulus, subscripts u,r,av., refer to the unrelaxed, relaxed, or geometric mean value
∂ ,w	frequency, angular frequency

Experimental

p	hardness (1 Kg/mm^2 ≃ 100 bars ≃ 1,420 p.s.i. ≃ 10^8 $dynes/cm^2$)
	subscripts: dyn. - dynamic experiment stat.- static (or gradual change) load l.r. - load rate
A	area of indentation
d	diameter of indentation
a	radius of indentation
r	radius of curvature of recovered indentation
D	diameter of indenter
R	radius of indenter
L	load
t	loading time, impact time
μ	coefficient of friction
	subscripts p and s refer to ploughing and adhesion components
s	specific shear strength
F	force of friction, subscripts as with μ
v	speed of sliding
$P_L(v)$	effective hardness or "mean normal pressure"
$P_F(v)$	"mean pressure resisting tangential displacement"

E'	energy of impact
M	mass of projected indenter
Λ	logarithmic decrement of damping
tan ϕ	phase angle, subscript max. refers to maximum value

REFERENCES

(1) Glen, J. W., Proc. Roy. Soc., A, 228, 519 (1955).

(2) Glen, J. W., Ph.D. Thesis, Cambridge (1953).

(3) Roos, D. V. D., J. Glac., 6, 411 (1966).

(4) Hobbs, P. V., private communication, to be published.

(5) Ragle, R. H., C.R.R.E.L. Res. Rep.No.107, (1963).

(6) Bader, H., J. Geol., 59, 519 (1951).

(7) Kamb, B., Sci., 150, 205 (1965).

(8) Honjo, G., and Shimaoka, Acta Cryst., 10, 710 (1957).

(9) Blackman, M., and Lisgarten, N. D., Adv. Phys., 7, 189 (1958).

(10) Bridgman, P. W., Proc. Am. Acad. Arts Sci., 47, 441 (1912).

(11) Tamman, G., Ann. Phys., 2, 1 (1900).

(12) Lonsdale, K., Proc. Roy. Soc., A, 247, 424 (1958).

(13) Owston, P. G., Adv. Phys., 7, 171 (1958).

(14) Bragg, W. H., Proc. Phys. Soc. Lond., 34, 98 (1921).

(15) Peterson, S. W., and Levy, H. A., Acta Cryst., 10, 70 (1957).

(16) Bernal, J. D., and Fowler, R. H., J. Chem. Phys., 1, 515 (1933).

(17) Pauling, L., J. Amer. Chem. Soc., 57, 2680 (1935).

(18) Nagle, J. F., J. Math. Phys., 7, 1484 (1966).

(19) Suzuki, Y., Cont. Inst. Low Temp. Sci., Ser. A21, 1 (1966).

(20) Giaque, W. F., and Stout, J. W., J. Amer. Chem. Soc., 58, 1144 (1936).

(21) Kamb, B., Acta Cryst., 17, 1437 (1964).

(22) Hobbs, M. E., Jhon, M. S., and Eyring, H., Proc. Nat. Acad. Sci., U.S.A., 56, 31 (1966).

(23) Truby, F. K., J. App. Phys., 26, 1416 (1955).

(24) Teichmann, I., and Schmidt, G., Physica Status Solidi, 8, 145 (1945). - see also (92), (319), (320).

(25) Dengel, O., Eckener, U., Plitz, H., and Riehl, N., Phys. Letters, 9, 291 (1964).

(26) Bjerrum, N., Kgl. Danske Videnskab. Selskab. Mt.-fys.Medd. 27, No.1, 56 p (1951).

(27) Bjerrum, N., Sci., 115, 385 (1952).

(28) Evans, S., J. Glac., 5, 773 (1965).

(29) Nemethy, G., and Scheraga, H. A., J. Chem. Phys., 36, 3382, 3401 (1962).

(30) Frank, H. S., Fed. Proc., 24(2), Supp.No.15, p.5-1 (1965).

(31) Wicke, E., Angew. Chem. Internat. Edit., 5, 106 (1966).

(32) Kavanau, J. L., "Water and Solute-Water Interactions", (Holden-Day Inc., San Francisco, 1964).

(33) Luck, W., Fortsch. Chem. Forsch., 4, (1964).

(34) Drost-Hansen, W., "The Water-Ice Interface As Seen From The Liquid Side", (ACS Symposium on Interfacial and Surface Properties of Ice, 151st Meeting, American Chemical Society, Pittsburg, 1966).

(35) Drost-Hansen, W., First International Symposium on Water Desalination, (Wash., D.C., 1965).

(36) Drost-Hansen, W., Symp. Equilibrium Concepts in Natural Water Systems, Adv. in Chem. Series, ACS, to be published.

(37) Marchi, R. P., and Eyring, H., J. Phys. Chem., 68, 221 (1964).

(38) Jhon, M. S., Grosh, J., Ree, T., Eyring, H., J. Chem. Phys., 44, 1465 (1966).

(39) Bernal, J. D., and Fowler, R. H., J. Chem. Phys., 1, 518 (1933).

(40) Pople, J. A., Proc. Roy. Soc., A, 205, 163 (1951).

(41) Wall, T. F., and Hornig, D. F., J. Chem. Phys., 43, 2079 (1965).

(42) Wonham, J., Proc. Inst. Mech. Eng., 180, Pt.3J, (1965-6). - See also (280).

(43) Horne, R. A., and Johnson, D. S., J. Phys. Chem., 70, 2182 (1966).

(44) Cappi, J. B., Ph.D. Thesis, Univ. London, (1964). - See also (282).

(45) Vand, V., and Senior, W. A., J. Chem. Phys., 43, 1869-1887 (1965).

(46) Frank, H. S., and Wen, W. Y., Disc.Far.Soc., 24, 133 (1957).

(47) Stewart, G. W., Phys. Rev., 37, 9 (1931).

(48) Griffith, J. H., and Scheraga, H. A., see Abstract I 43, 150th. Meeting ACS (1965).

(49) Pauling, L., "Hydrogen Bonding", (Hadzi, ed., Pergamon Press, London, 1959).

(50) Frank, H. S., and Quist, A. S., J. Chem. Phys., 34, 604 (1961).

(51) Mak, T. C. W., J. Chem. Phys., 43, 2799 (1965).

(52) Röntgen, W. K., Ann. Phys. Chim. (Wied.), 45, 91 (1892).

(53) Grjotheim, K., and Krogh-Moe, J., Acta Chem. Scand., 8, 1193 (1954).

(54) Wada, G., Bull. Chem. Soc. (Jap.), 34, 955 (1961).

(55) Samoilov, O. Ya., "Structure of Aqueous Electrolyte Solutions and the Hydration of Ions", (trans., D. J. G. Ives), (Consultants Bureau, N.Y., 1965).

(56) Jamin, J., Compt. Rend., 43, 1191 (1856).

(57) Erréra, J., quoted in (58), P.27.

(58) Drost-Hansen, W., Ind. Eng. Chem., 57, 18 (1965).

(59) Drost-Hansen, W., N.Y. Acad. Sci., Annals, Conf. Monograph, 125 (Art.2), 471 (1965).

(60) Koefoed, J., Disc. Far. Soc. 24, 216 (1957).

(61) Morgan, J., and Warren, B. E., J. Chem. Phys., 6, 666 (1938).

(62) Schufle, J. A., and Venugopalan, M., J. Geophys. Res., 72, 3271 (1967).

(63) Narsingh Dass, and Gilra, N. K., J. Phys. Soc. Jap., 21, 2039 (1966).

(64) Fletcher, N. H., Phil. Mag., 7, 255 (1962).

(65) Watts-Tobin, R. J., Phil. Mag., 8, 333 (1963).

(66) Hori, T., S.I.P.R.E. Transl. No.62,(1960).

(67) Swinzow, G., private correspondence (1967).

(68) Fedyakin, N. N., "Research in Surface Forces", edited by Acad. B. V. Deryagin, 126 (authorised trans. from the Russian, Consultants Bureau, N.Y., 1963).

(69) Derjaguin, B. V., Fedjakin, N. N., and Talayev, M. V., J. Colloid and Interface Sci., 24, 132 (1967).

(70) Derjaguin, B. V., Fedjakin, N. N., and Talayev, M. V., Dokl. Akad. Nauk SSSR, 167, 376 (1966).

(71) Derjaguin, B. V., Fedjakin, N. N., and Talayev, M. V., Dokl. Akad. Nauk SSSR, 165, 878 (1965).

(72) Derjaguin, B. V., and Greene-Kelly, R., Trans. Faraday Soc., 60, 449 (1964).

(73) Derjaguin, B. V., Disc. Faraday Soc. No.42, 109 (1966).

(74) Palmer, L. S., Cunliffe, A., and Hough, J. M., Nature, 170, 796 (1952).

(75) Chalmers, J. A., and Pasquill, F., Phil. Mag., 23, 88 (1937).

(76) Arabadzi, V. I., S.I.P.R.E. Transl.No.1., (1950). - See also other references given in (34) and (321).

(77) Tyndall, J., Proc. Roy. Soc., A, 9, 141 (1858).

(78) Thompson, W., Proc. Roy. Soc., A, 9, 761 (1858).

(79) Thompson, J., Proc. Roy. Soc., A, 10, 152 (1859).

(80) Faraday, M., Phil. Mag., 17, 162 (1859).

(81) Faraday, M., Proc. Roy. Soc. Lond., 10, 440 (1860).

(82) Bottomley, J. T., Nature, 5, 185 (1872).

(83) Kamb, B., and LaChapelle, E., J. Glac., 5, 166 (1964).

(84) Nunn, K. R., and Rowell, M. M., Phil. Mag., 16, 1281 (1967).

(85) Townsend, D. W., and Vickery, R. P., Phil. Mag., 16, 1275 (1967).

(86) Drake, L. D., and Shreve, R. L., quoted in (87).

(87) Nye, J. F., Phil. Mag., 16, 1249 (1967).

(88) Telford, J. W., and Turner, J. S., Phil. Mag., 8, 527 (1963).

(89) Weyl, W. A., J. Colloid Sci., 6, 389 (1951).

(90) Kopp, M., Res. Rep. No.3, "An NMR Study of the Diffusion of Hydrofluoric Acid in Ice", MS. thesis, (*, 1965).

(91) Kopp, M., Prog. Rep. No.19, "Diffusion and Relaxations in the Lattice of Ice," (*, 1966-7).

(92) Kopp, M., Prog. Rep. No.C, "A Transitional Film on the Surface of Ice", (*, 1962).

(93) Kopp, M., Prog. Rep. No.B., "Processes on the Surfaces of Ice", (*, 1961-2).

(94) Kopp, M., Surface Sci., 7, 82 (1967).

(95) Barnes, P., "The Surface Structure of Water and Ice"; A report based on a lecture given by P. Barnes at Dr.Tabor's Surface Physics Internal Colloquia, Cavendish Laboratory, Cambridge, July 1967.

(96) Bullemer, B., and Riehl, N., Solid State Communications, 4, 447 (1966).

(97) Kopp, M., Z. Angew. Math. Phys., 13, 431 (1962).

(98) Jaccard, C., Int. Conf. Low Temp. Sci., Hokkaido University, Sapporo, Japan, (1966).

(99) Bradley, R. S., Trans. Faraday Soc., 53, 687 (1957).

(100) Latham, J., Nature, 200, 1087 (1963).

(101) Kingery, W. D., J. App. Phys., 31, 833 (1960).

(102) Kuroiwa, D., S.I.P.R.E. Res. Rep. No.86, (1962).

(103) Kuroiwa, D., Low Temp. Sci., A, 19, 1 (1960).

(104) Hobbs, P. V., and Mason, B. J., Phil. Mag., 9, 181 (1964).

(105) Hosler, C. L., Jensen, D. C., and Goldshlak, L., J. Met., 14, 415 (1957).

(106) Hosler, C. L., and Hallgren, R. E., Disc. Faraday Soc., No.30, 200 (1960).

---

* Kopp, M., Mellon Institute, 4400 Fifth Avenue, Pittsburgh, PA 15213.

(107) Hosler, C. L., and Hallgren, R. F., "Ice Crystal Aggregation", presented at the Int. Cong. Phys. of Clouds (Hailstorms) at Verona 9-13 (1960).

(108) Nakaya, U., and Matsumoto, H., S.I.P.R.E. Res. Pap. No.4, (1953).

(109) Hobbs, P. V., and Radke, L. F., J. Glac., 6, 879 (1967).

(110) Nichols, F. A., and Mullins, W. W., J. App. Phys., 36, 1826 (1965).

(111) Jellinek, H. H. G., S.I.P.R.E. Res. Rep. No.23, (1957).

(112) Jellinek, H. H. G., S.I.P.R.E. Res.Rep. No.38, (1957).

(113) Jellinek, H. H. G., S.I.P.R.E. Res. Rep. No.62, (1960).

(114) Evans, S., and Paren, J., private communication (1967).

(115) Nakamura, T., private communication (1967), to be published, Int. Conf. Low Temp.Sci., Hokkaido University, Sapporo, Japan (1966).

(116) Hoekstra, P., and Miller, R. D., C.R.R.E.L. Res.Rep. No.153, (1965).

(117) Maeno, N., "Air Bubble Formation in Ice Crystals", a paper presented at the International Conf. on Low Temp. Sci., Inst. Low Temp. Sci., Hokkaido Uni., Sapporo, Japan (1966), in press. (Parts of this paper to be found in Low Temp. Sci., Ser.A, 24., English Summary P.109).

(118) Nakaya, U., Hanajima, M., and Muguruma, J., J. Fac. Sci., Hokkaido Uni., Ser II, V, 3, 97-106 (1958).

(119) Hallet, J., Phil. Mag., 6, 1073 (1961).

(120) Hobbs, P. V., et al., private communication (1967).

(121) Fletcher, N. H., Phil. Mag., 8, 1425 (1963).

(122) Butkovich, T. R., Trans. Amer. Geophys. Un., 39, 305 (1958).

(123) Jellinek, H. H. G., J. Coll. Sci., 14, 268 (1959).

(124) Nakaya, U., S.I.P.R.E. Res.Rep. No.58, (1959).

(125) Hobbs, P. V., J. Geophys. Res., 70, 3903 (1965).

(126) Ramseier, R. O., and Sander, G. W., C.R.R.E.L. Res.Rep. No.189, (1966).

(127) Ramseier, R. O., and Keeler, C. M., J. Glac., 6, 421 (1966).

(128) Hobbs, P. V., and Radke, L. F., J. Glac., 6, 893 (1967).

(129) Moser, H., Ann. d. Physik, 1, 341 (1929).

(130) Poynting, J. H., Phil. Mag., 12, 32 (1881).

(131) Riecke, E., Ann. d. Phys. und Chem., 54, 731 (1895).

(132) Gibbs, J. W., On the equilibrium of heterogeneous substances, in "Collected Works of J. Willard Gibbs"(Yale Uni. Press, New Haven, Conn., 1906).

(133) Kamb, W. B., J. Geophys. Res., 66, 259 (1961).

(134) Kamb, W. B., J. Geophys. Res., 66, 3985 (1961)

(135) Kamb, W. B., J. Geol., 67, 153 (1959).

(136) Goranson, R. W., "Thermodynamic relations in multicomponent systems", (Carnegie Inst. Wash. Publ., 1930).

(137) Verhoogen, J., "The chemical potential of a stressed solid", 251 (Trans. Am. Geophys. Un., 32, 1951).

(138) MacDonald, J. F., Geol. Soc. Am. Mem., 79, 1 (1960).

(139) Steinemann, S., Int. Un. Geod. Geophys., Int. Ass. Sci. Hydrology, Symposium of Chamonix, Physics of Ice Movement, 254 (1958).

(140) Weertman, J., J. Glac., 3, 33 (1957).

(141) Barnes, P., and Tabor, D., Nature, 210, 878 (1966).

(142) Damien, B. C., Ann. Sci. École Norm. Sup. (2), 10, 233-304 and 272-278 (1881).

(143) Damien, B. C., J. de Phys. (1), 10, 198 (1881).

(144) Itagaki, K., Int. Conf. Low Temp. Sci., Hokkaido University, Sapporo, Japan (1966).

(145) Glen, J. W., and Perutz, M. F., J. Glac., 2, 397 (1954).

(146) Steinemann, S., J. Glac., 2, 404 (1954).

(147) Steinemann, S., U.G.G.I., Ass. Int. Hyd. Sci., Gen. Ass. Rome, 4, 449 (published 1956).

(148) Steinemann, S., Beiträge zur geologischen karte der Schweiz, geotechnische Series Hydrologie, No.10, (1958). (Res.Trans., Amer. Met. Soc. Trans. Service, Air Force Cambridge Res. Labs., Office of Aerospace Res., U.S.A.F., L. G. Hanscom Field, Mass.).

(149) McConnel, J. C., Proc. Roy. Soc., 49, 323 (1891)

(150) Nakaya, U., S.I.P.R.E. Res. Rep.No.28, (1958).

(151) Nakaya, U., S.I.P.R.E. Res. Rep. No.13, (1956).

(152) Nakaya, U., Symposium de Chamonix, U.G.G.I. (I.A.S.H), "Physics of the Movement of the Ice", 229 (Braamstraat 61, Gentbrugge, Belgique, 1958).

(153) Tamman, G., and Salge, N., Neues Jb. Min. Geol. Paläont., Beil. Bd., A, 57, 117 (1928).

(154) Kamb, B., J. Glac., 3, 1097 (1961).

(155) Walker, J. C. F. W., private communication (1966).

(156) Jones, S. J., and Glen, J. W., paper submitted to "Commission des Neiges et Glaces", Ass. Int. Hyd. Sci., Assemblee Générale de Berne, (1967).

(157) Readey, D. W., and Kingery, W. D., Acta Met., 12, 171 (1964).

(158) Higashi, A., Koinuma, S., and Mae, S., Jap. J. App. Phys., 3, 610 (1964).

(159) Higashi, A., Int. Conf. Low Temp. Sci., Hokkaido Uni., Sapporo, Japan, (1966).

(160) Griggs, D. T., and Coles, N. E., S.I.P.R.E. Rep. No.11, (1954), (some of this data has been replotted against 1/kT by Steinemann, P.16 (148)).

(161) Butkovich, T. R., and Landauer, J. K., Symposium de Chamonix, U.G.G.I. (I.A.S.H.), "Physics of the Movement of the Ice, 318 (Braamstraat 61, Gentbrugge, Belgique, 1958).

(162) Butkovich, T. R., and Landauer, J. K., S.I.P.R.E. Res. Rep. No.56, (1959).

(163) Higashi, A., and Sakai, N., J. Fac. Sci., Hokkaido Uni., Sapporo, Japan, Ser II, V, No.5, 221 (1961).

(164) Butkovich, T. R., S.I.P.R.E. Res. Paper No.9, (1954).

(165) Itagaki, K., C.R.R.E.L. Res. Rep. No.178, (1966).

(166) Itagaki, K., J. Phys. Soc. Jap., 22, 427 (1967).

(167) Itagaki, K., J. Phys. Soc. Jap., 19, 1081 (1964).

(168) Dengel, O., and Riehl, N., Phys. Kondens. Materies, 1, 191 (1963).

(169) Onsager, L., and Runnels, L. K., Proc. Natl. Acad. Sci. U.S., 50, 208 (1963).

(170) Kopp, M., Branaal, D. E., and Lowe, I. J., J. Chem. Phys., 43, 2965 (1965).

(171) Kuhn, W., and Thürkauf, M., Helv. Chim. Acta, 41, 938 (1958).

(172) Lytton, J. L., Shepard, L. A., and Dorn, J. E., Trans. Met. Soc. A.I.M.E., 212, 220 (1957).

(173) Atkins, A. G., and Tabor, D., Proc. Roy. Soc., A, 292, 441 (1966).

(174) Flinn, J. E., and Munson, D. E., Phil. Mag., 10, 861 (1964).

(175) Garofalo, F., "Fundamentals of Creep and Creep-Rupture in Metals" (Collier-Macmillan Ltd., London, 1965).

(176) Wakahama, G., "Low Temperature Science", Series A, Physical Sciences, 57 (Ed. by Inst. Low Temp. Sci., Hokkaido Uni., Japan, 1962).

(177) Wakahama, G., "ibid"., Ser.A, 77 (1962).

(178) Wakahama, G., "ibid"., Ser. A, 101 (1962).

(179) Wakahama, G., "ibid"., Ser. A, 117 (1962).

(180) Yosida, Z. and Wakahama, G., "ibid", Ser.A, 29 (1962).

(181) Glen, J. W., Physik Der Kondensierten Materie, in press.

(182) Weertman, J., J. App. Phys., 26, 1213 (1955).

(183) Weertman, J., J. App. Phys., 28, 362 (1957).

(184) Weertman, J., J. App. Phys., 28, 1185 (1957).

(185) Weertman, J., "Ice and Snow", 28 (ed. by W. D. Kingery, The M.I.T. Press, Cambridge, Mass., 1963).

(186) Servi, I. S., and Grant, N. J., J. Metals, 3, 909 (1951).

(187) Schoeck, G., Phys. Rev., 102, 1458 (1956).

(188) Eshelby, J. D., Phil. Mag., 6, 953 (1961).

(189) Higashi, A., Koinuma, S., and Mae, S., Jap. J. App. Phys., 4, 575 (1965).

(190) Bartlett, J. L., and Readings, C. J., paper submitted to "Commission des Neiges et Glaces", Ass.Int.Hyd.Sci., Assemblee Générale de Berne, (1967).

(191) Tegart, W. J. McG., J. Glac. 5, 251 (1964).

(192) Friedel, J., "Dislocation interactions and internal strains.", 220 (In Rassweiler, G. M., and Grube, W. L., ed. "Internal stresses and fatigue in metals.", Amsterdam, Elsevier Pub. Co., 1959).

(193) Higuchi, K., Acta Met., 6, 636 (1958).

(194) Bryant, G. W., and Mason, B. J., Phil. Mag., 5, 1221 (1960).

(195) Muguruma, J., J. Electron Microscopy, 10, 246 (1961).

(196) Muguruma, J., and Higashi, A., J. Phys. Soc. Jap., 18, 1261 (1963).

(197) Muguruma, J., and Higashi, A., Nature, 198, 573 (1963).

(198) Muguruma, J., Nature, 190, 37 (1961).

(199) Muguruma, J., Nature, 208, 180 (1965).

(200) Hayes, C. E., and Webb, W. W., Sci., 147, 44 (1965).

(201) Hayes, C. E., and Webb, W. W., Phil. Mag., 16, 909 (1967).

(202) Andrade, E. N. da C., Proc. Roy. Soc., A, 84, 1 (1910).

(203) Andrade, E. N. da C., Proc. Roy. Soc., A, 90, 329 (1914).

(204) Mott, N. F., Phil. Mag., 44, 742 (1953).

(205) Cottrell, A. H., "Dislocations And Plastic Flow in Crystals", 210 (Clarendon Press, Oxford, 1953).

(206) McQueen, H. J., Wong, W. A., and Jonas, J. J., Can. J. Phys., 45, 1225 (1967).

(207) Nye, J. F., Proc. Roy. Soc., A, 219, 477 (1953).

(208) Nye, J. F., Proc. Roy. Soc., A, 239, 113 (1957).

(209) Glen, J. W., Un. Geod. Geophys. Int., Ass. Int. d'Hydrologie Sci., Symposium de Chamonix, 171 (1958).

(210) Rigsby, G. P., S.I.P.R.E. Res. Rep. No.32 (1957).

(211) Rigsby, G. P., J. Glac., 3, 273 (1958).

(212) Haefeli, R., Jaccard, C., and Quervain, M. de, paper submitted to "Commission des Neiges et Glaces", Ass. Int. Hyd. Sci., Assemblee Générale de Berne, (1967).

(213) Nye, J. F., Symposium de Chamonix, U.G.G.I. (I.A.S.H.), "Physics of the Movement of the Ice", 139 (1958).

(214) Eldredge, K. R., and Tabor, D., Proc. Roy. Soc., A, 229, 181 (1955).

(215) Nayar, H. S., Ph.D. Thesis, Rensslaer Polytech. Inst., Dept. Mat. Eng., Troy, N.Y., (1966).

(216) Raraty, L. E., and Tabor, D., Proc. Roy. Soc., A, 245, 184 (1958).

(217) Butkovich, T. R., and Landauer, J. K., S.I.P.R.E. Res. Rep. No.72, (1960).

(218) Mellor, M., and Smith, J. H., C.R.R.E.L. Res.Rep. No.220 (1966).

(219) Landauer, J. K., J. App. Phys., 26, 1493 (1955).

(220) Jellinek, H. H. G., and Brill, R., J. App.Phys., 27, 1198 (1956).

(221) Dillon, H. B., and Andersland, O. B., paper submitted to Int. Conf. on Phys. Snow and Ice, Inst. Low Temp. Sci., Hokkaido Uni., Sapporo, Japan (1966).

(222) Higashi, A., S.I.P.R.E. Res. Rep. No.51, (1959).

(223) Jellinek, H. H. G., S.I.P.R.E. Res. Rep. No.63, (1960).

(224) Taylor, G. I., J. Inst. Metals, 62, 307 (1938).

(225) Gold, L. W., "Ice and Snow", 8 (ed. by W. D. Kingery, The M.I.T. press, Cambridge, Mass., 1963).

(226) Shoumsky, P. A., Symposium de Chamonix, U.G.G.I. (I.A.S.H.), "Physics of the Movement of the Ice", 244 (1958).

(227) Glen, J. W., Adv. Phys., 7, 254 (1958).

(228) Glen, J. W., "Ice and Snow", 3 (ed. by W. D. Kingery, The M.I.T. press, Cambridge, Mass., 1963).

(229) Ivanov, K. E., and Lavrov, V. V., S.I.P.R.E. Transl. No.10, (1951).

(230) Gold, L. W., Can. J. Phys., 44, 2757 (1966).

(231) Gold, L. W., Can. J. Phys., 38, 1137 (1960).

(232) Gold, L. W., Can. J. Phys., 41, 1712 (1963).

(233) Gold, L. W., Can. J. Phys., 43, 1414 and 1423 (1965).

(234) Gold, L. W., Int. Conf. Low Temp. Sci., Hokkaido Uni., Sapporo, Japan (1966).

(235) Butkovich, T. R., S.I.P.R.E. Res. Paper No.11, (1954).

(236) Meier, M. F., "Mode of Flow of Saskatchewan Glacier", Geol. Survey Prof. Paper No.351, (U.S. Government Printing Office, Washington, 1960).

(237) Tabor, D., Proc. Roy. Soc., A, 192, 247 (1948).

(238) Tabor, D., Engineering, 165, 289 (1948).

(239) Tabor, D., "The Hardness of Metals", 115 (Clarendon Press, Oxford, 1951), out of print.

(240) Tabor, D., J. Inst. Metals, 79, Part I, 1 (1951).

(241) Tabor, D., Endeavour, XIII, 27 (1954).

(242) Tabor, D., "The Physical Meaning of Indentation Hardness", a paper presented at the conference on "Hardness Testing", Sheffield, October,(1953).

(243) Tabor, D., Brit. J. App. Phys., 7, 159 (1956).

(244) Atkins, A. G., Silvério, A., and Tabor, D., J. Inst. Metals, 94, 369 (1966).

(245) Bader, H., J. Glac., 1, 443 (1950).

(246) Silvério, A., Ph.D. Dissertation, (Cambridge University, 1963).

(247) McLean, D., "Mechanical Properties of Metals", (N.Y. and London, John Wiley, 1962).

(248) Kuroiwa, D., C.R.R.E.L. Res. Rep. No.142, (1965).

(249) Weertman, J., to be published in J. Glac.

(250) Nakaya, U., S.I.P.R.E. Paper No.13, (1956).

(251) Stehle, N. S., U.S. Naval Civil Engineering Laboratory, Tech. Rep. No.R421 (Port Heuneme, California, 1965).

(252) Stehle, N. S., Int. Conf. Low Temp. Sci., Hokkaido University, Sapporo, Japan (1966).

(253) King, R. F., Ph. D. Thesis, Cambridge, (1952).

(254) Kruschov, M. M., and Berkovich, Ye.S., Izucheniye tverdosti l'da (A Study of the Hardness of Ice), Izdatel'stvo Akademii Nauk S.S.S.R., (1960).

(255) Hertz, H., J. reine angew. Math., 92, 156 (1881).

(256) Hertz, H., "Miscellaneous Papers", (London, 1896).

(257) Packer, M. E., private communication, Cambridge (1967).

(258) Muguruma, J., J. Fac. Sci., Hokkaidô Uni., Japan, Ser.II, VI, 11 (1963).

(259) Bowden, F. P., and Tabor, D., "The Friction and Lubrication of Solids", Part I (Clarendon Press, Oxford, 1954).

(260) Bowden, F. P., and Tabor, D., "The Friction and Lubrication of Solids", Part II (Clarendon Press, Oxford, 1964).

(261) Bowden, F. P., Proc. Roy. Soc., A, 217, 462 (1953).

(262) "Friction of Snow and Ice", S.I.P.R.E. Rep. No.17, (a report compiled by R. C. Jordan on a joint research project at the University of Minnesota, 1955).

(263) Ericksson, R., S.I.P.R.E. Transl. No.44, (1955).

(264) Willis, R. F., Ph.D. Thesis, (Cambridge University, 1967).

(265) Bowden, F. P., and Tabor, D., Brit. J. App. Phys., 17, 1521 (1966).

(266) Goddard, J., and Wilman, H., Wear, 5, 114 (1962).

(267) Camp, P. R., Kiszenick, W., and Arnold, D. A., C.R.R.E.L. Res. Rep. No.198, (1967).

(268) Tabor, D., Proc. Roy. Soc., A, 229, 198 (1955).

(269) Ludema, K. C., Ph.D. Thesis, Cambridge (1964).

(270) A Mendenhall Glacier single crystal obtained from C.R.R.E.L., U.S.A., with the kind help from Messrs R. O. Ramseier, J. Paren,

and J. C. F. Walker. The properties of this crystal must be similar to those for the other crystals obtained by CRREL [(296)(297)]: The melted conductivity lies between 1 and 7 x 10^{-6} mhos.cm, and the Fluorine concentration is about 10^{-8} mole.

(271) Kneser, H. O., Magun, S., and Zeigler, G., Naturwissenschaften, 42, 437 (1955).

(272) Schiller, P., Zeitschrift für Physik, 153, 1 (1958).

(273) Schiller, P., National Research Council, Canada, Tech. Transl. No.TT-890 of (272).

(274) Kuroiwa, D., C.R.R.E.L. Res. Rep. No.131, (1965).

(275) Gränicher, H., Jaccard, C., Scherrer, P., and Steinemann, A., Disc. Faraday Soc., No.23, 50 (1957).

(276) Auty, R. P., and Cole, R. H., J. Chem. Phys. 20, 1309 (1952).

(277) Eder, F. X., Ann. Physik, 1, 381 (1947).

(278) Smyth C. P., and Hitchcock, C. S., J. Amer. Chem. Soc., 54, 4631 (1932).

(279) Paren, J., private communication, (1968).

(280) Wonham, J., Nature, 215, 1053 (1967).

(281) Horne, R. A., et al., - Refs. given in (43).

(282) Bett, K. E., and Cappi, J. B., Nature, 207, 620 (1965).

(283) McLean, D., "Grain Boundaries in Metals", (Clarendon Press, Oxford, 1957).

(284) Murray, M. J., Ph.D. Thesis, Cambridge, (1966).

(285) Kê, T. S., J. App. Phys., 22, 274 (1949).

(286) Dorsey, N. E., "Properties of Ordinary Water - Substance", (Reinhold Publishing Corporation, New York, 1940).

(287) Timoshenko, S., and Goodier, J. N., "Theory of Elasticity", 9 (McGraw-Hill Book Co. Inc., 1951).

(288) Robin, G. de Q., "Seismic Shooting And Related Investigations", 80-81 (Norsk Polarinstitutt, Oslo, 1958).

(289) Robin, G. de Q., Endeavour, XXIII, 102 (1964).

(290) Lotze, V. W., Zeitschrift für Geophysik, 23, 243 (1957).

(291) Zener, C., "Elasticity and Anelasticity of Metals", 47 (The University of Chicago Press, 1948).

(292) Runnels, L. K., Scientific American, 215, No.6, 118 (1966).

(293) Belyshkin, D. V., Glass and Ceramics (transl. from Russian, Consultants Bureau), XXIII, 523 (1966).

(294) Barnes, P., and Tabor, D., paper submitted to "Commission des Neiges et Glaces", Ass.Int.Hyd.Sci., Assemblee Générale de Berne, (1967).

(295) James, D. W., and Sekerka, R. F., J. Crystl. Growth, 1, 67 (1967).

(296) Ramseier, R. O.,C.R.R.E.L. Res. Rep. No.232, 25-28 (1967).

(297) Paren, J., private communication, (1968).

(298) Kamb, B. and LaChapelle, E., J. Glac., 5, 159 (1964).

(299) Kamb, B., and LaChapelle, E., private communication,(1967), to be published.

(300) Weertman, J., J. Glac., 5, 287 (1964).

(301) Lliboutry, L., "Traité de Glaciologie", Tome II (Glaciers, Variations du Climat, Sols Gelés), (Masson et Cie., Paris, 1965).

(302) Lliboutry, L., paper submitted to "Commission des Neiges et Glaces", Ass.Int.Hyd.Sci., Assemblee Générale de Berne, (1967).

(303) Lliboutry, L., J. Glac., 7, 21 (1968).

(304) Weertman, J., "Present Understanding of Conditions at Bottom of Ice Sheets", A talk given to the Glaciological Society Meeting at Hanover, N.H., October 1st, 1966.

(305) Barnes, P., and Robin, G. de Q., Nature, 210, 882 (1966).

(306) Paterson, W. S. B., and Savage, J. C., J. Geophys. Res., 68, 4537 (1963).

(307) McCall, J. G., "Norwegian Cirque Glaciers", 39 (Roy. Geograph. Soc. Res. Ser.No.4) (William Clowes and Sons, Ltd., London and Beccles, 1960).

(308) Barnes, P., and Robin, G. de Q., private discussion, (1967).

(309) Barnes, P., Nye, J. F., and Walker, J. C. F., private discussion, (1968).

(310) Robin, G. de Q., J. Glac., 2, 523 (1955).

(311) Thorarinsson, S., "Jökull (Reykjavik)", III, 14, AR, 76 (1964).

(312) Lliboutry, L., Annales de Géophysique, Tom 15, No.2, 250 (1959).

(313) Weertman, J., U.G.G.I., Ass.Int.Hyd.Sci., Commission des Neiges et Glaces, Colloque d'Obergurgl, 10-9-18-9, 31 (1962).

(314) Bascom, W. D., Cottington, R. L., Singleterry, and Jones, R. L., NRL Rep. No.6350 (U. S. Naval Res. Lab., Washington, D.C., 1966).

(315) Schulz, H. H., and Knappwost, A., Wear, 11, 3 (1968).

(316) Ludema, K. C., and Tabor, D., Wear, 9, 329 (1966).

(317) Owston, P. G., Quart. Rev. Chem. Soc. V, 344 (1951).

(318) Zener, C., Phys. Rev. 60, 906 (1941).

(319) Tippe, A., Naturwissenschaften, 54, 95 (1967).

(320) Deubner, A. Heise, R. and Wenzel, K., Naturwissenschaften, 47, 600 (1960).

(321) Jindal, B. K., and Tiller, W. A., Surface Sci., 9, 137 (1968).